(2)

NAVAL POSTGRADUATE SCHOOL

Monterey, California

THESIS

FLOW VISUALIZATION OF THE EFFECT OF PITCH RATE ON THE VORTEX DEVELOPMENT ON THE SCALE MODEL OF A F-18 FIGHTER AIRCRAFT

by

Park,Sung-Nam

June 1989

Thesis Advisor — M.F. Platzer
Co-Advisor — S.K. Hebbar

REPORT DOCUMENTATION PAGE

1a Report Security Classification: Unclassified			1b Restrictive Markings
2a Security Classification Authority			3 Distribution Availability of Report: Approved for public release; distribution is unlimited.
2b Declassification/Downgrading Schedule			
4 Performing Organization Report Number(s)			5 Monitoring Organization Report Number(s)
6a Name of Performing Organization: Naval Postgraduate School	6b Office Symbol (if applicable): 33		7a Name of Monitoring Organization: Naval Postgraduate School
6c Address (city, state, and ZIP code): Monterey, CA 93943-5000			7b Address (city, state, and ZIP code): Monterey, CA 93943-5000
8a Name of Funding/Sponsoring Organization	8b Office Symbol (if applicable)		9 Procurement Instrument Identification Number
8c Address (city, state, and ZIP code)			10 Source of Funding Numbers: Program Element No / Project No / Task No / Work Unit Accession No

11 Title (include security classification): FLOW VISUALIZATION OF THE EFFECT OF PITCH RATE ON THE VORTEX DEVELOPMENT ON THE SCALE MODEL OF A F-18 FIGHTER AIRCRAFT

12 Personal Author(s): Park,Sung-Nam

13a Type of Report	13b Time Covered	14 Date of Report (year, month, day)	15 Page Count
Master's Thesis	From To	June 1989	145

16 Supplementary Notation: The views expressed in this thesis are those of the author and do not reflect the official policy or position of the Department of Defense or the U.S. Government.

17 Cosati Codes			18 Subject Terms (continue on reverse if necessary and identify by block number)
Field	Group	Subgroup	High angle of attack aerodynamics, Effect of pitch rate and yaw, Vortex development and breakdown, Flow visualization by dye injection, Water tunnel studies, F-18 fighter aircraft.

19 Abstract (continue on reverse if necessary and identify by block number)

Experiments were performed in a water tunnel to visualize the vortex bursting phenomenon on a $\frac{1}{48}$ th scale model of the F-18 fighter aircraft.

Photographs were taken to investigate the effect of pitch rate and yawing on bursting locations of vortices shed from the forebody and the strake during simple pitch up and simple pitch down maneuvers in the angle of attack range up to 50°.

It was found that the vortex burst point moves upstream with increasing pitch rate. At the same pitch rate, vortex bursting was usually found to occur earlier for the pitch-down than for the pitch-up maneuver. Aircraft yawing generated significant vortex asymmetries due to earlier vortex bursting on the windward side thus leading to undesirable side forces and yawing moments.

20 Distribution Availability of Abstract	21 Abstract Security Classification	
☒ unclassified/unlimited ☐ same as report ☐ DTIC users	Unclassified	
22a Name of Responsible Individual: M.F. Platzer	22b Telephone (include Area code): (408) 646-2059	22c Office Symbol: 67Pl

DD FORM 1473,84 MAR 83 APR edition may be used until exhausted
All other editions are obsolete

Approved for public release; distribution is unlimited.

Flow Visualization of the Effect of Pitch Rate on the Vortex Development on the scale model of a F-18 Fighter Aircraft

by

Park,Sung-Nam
Major, Korean Air Force
B.S., Air Force Academy, 1978

Submitted in partial fulfillment of the
requirements for the degree of

MASTER OF SCIENCE IN AERONAUTICAL ENGEERING

from the

NAVAL POSTGRADUATE SCHOOL
June 1989

Author: _____
Park,Sung-Nam

Approved by: _____
M.F. Platzer, Thesis Advisor

_____
S.K. Hebbar, Co-Advisor

_____
for E.Roberts Wood, Chairman,
Department of Aeronautics and Astronautics

_____
Gordon E. Schacher,
Dean of Science and Engineering

ABSTRACT

Experiments were performed in a water tunnel to visualize the vortex bursting phenomenon on a $\frac{1}{48}$ th scale model of the F-18 fighter aircraft.

Photographs were taken to investigate the effect of pitch rate and yawing on bursting locations of vortices shed from the forebody and the strake during simple pitch up and simple pitch down maneuvers in the angle of attack range up to 50°.

It was found that the vortex burst point moves upstream with increasing pitch rate. At the same pitch rate, vortex bursting was usually found to occur earlier for the pitch-down than for the pitch-up maneuver. Aircraft yawing generated significant vortex asymmetries due to earlier vortex bursting on the windward side thus leading to undesirable side forces and yawing moments.

TABLE OF CONTENTS

LIST OF TABLES

LIST OF FIGURES

ACKNOWLEDGEMENTS

My gratitude goes to my thesis advisor, Professor M. F. Platzer, and co-advisor, Professor S. K. Hebbar, for their guidance and encouragement throughout the months of preparation and data collection required to complete this thesis. This work was sponsored by the Naval Air System Command and the Naval Postgraduate School.

I would also like to thank the R.O.K. Air Force for the opportunity to study.

I would also like to thank the many people at the Naval Postgraduate School who provided the services and expertise necessary for this research. In particular:

Mr. Al McGuire, Aero Lab

Mr. Mitch Nichols, Photo Lab

Finally, I acknowledge the sacrifices made by my wife In-Ok and two daughters and son in their support of my efforts.

I. INTRODUCTION

The high angle of attack characteristics of a fighter aircraft are highly configuration dependent and vortex dominated. High angle of attack flight is limited by the vortex breakdown phenomenon and by the onset of vortex asymmetry. As a result large undesired forces and moments can occur which may lead to departure from controlled flight and therefore attention must be paid to high-rate pitch-up problems, lateral and directional instability problems, and roll and yaw control problems. The forebody of the fuselage and the LEX or strakes or canards have a strong influence on the vortex development and on the lateral and directional stability.

A knowledge of the unsteady structure of the vortices, including the occurrence of vortex breakdown (or bursting) is therefore crucial in optimizing the maneuverability of a fighter aircraft. During the vortex breakdown process an abrupt transition from a jet-like to a wake-like core occurs, accompanied by a marked increase in the level of turbulence. Vortex breakdown usually occurs in one of two modes. In the axisymmetric mode a dye line of rotating and recirculating fluid forms in the viscous core of the vortex. In the spiral mode there is a cork screw like distortion to the vortex core. Vortex breakdown on stationary wings has been investigated extensively, and is assessed by Wedemeyer [Ref. 1]. However, experimental studies related to vortex breakdown on pitching wings aircraft have been somewhat limited to date. Of the more recent studies, [Ref. 2] examines in detail the response of vortex breakdown on a pitching delta wing, undergoing various classes of ramp motion including simple pitch up and simple pitch down. In particular, the study focusses on both global control (involving pitching motions) and local control (in the form of suction or blowing) of leading-edge vortices on a delta wing. The unsteady response of leading-edge vortex flows over a delta wing has been described for high angle of attack conditions in [Ref. 3]. This study focusses on the response of vortex development and breakdown due to large amplitude transient pitching motion of a sharp-edged delta wing and demonstrates the occurrence of a long time-scale response associated with vortex breakdown.

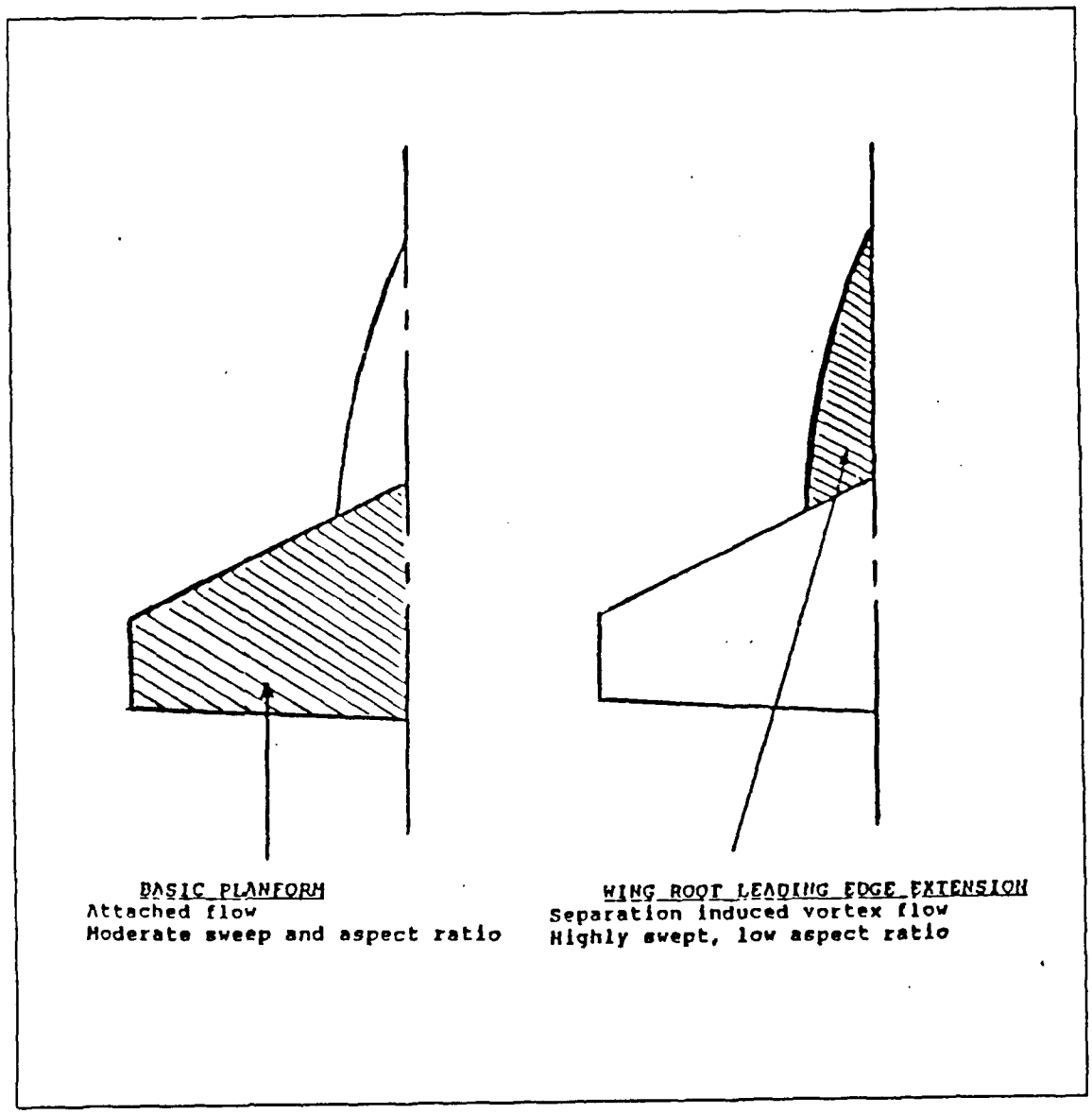

Figure 1. Hybrid wing containing LEX

The present investigation was undertaken to characterize the vortex flow field around a maneuvering fighter aircraft model, specifically the F-18. As is well known, this aircraft has achieved superior high angle of attack performance by incorporating the hybrid wing concept which results from the combining of a conventional wing with moderate sweep-back and aspect ratio with a wing root leading edge extension (LEX), also known as strake. Figure 1 illustrates these two

concepts in their combined form. The conventional wing maintains attached flow up to moderate angles of a attack but eventually produces buffet and stall. However, the LEX induces a vortex flow which increases in strength with increasing angle of attack. The vortex flow creates an area of high negative pressure on the wing upper surface which increases the lift and delays the flow separation on the basic planform. Unfortunately, at a certain angle of attack this vortex flow becomes unstable and starts to burst into a highly irregular and turbulent flow which causes a rapid loss of lift and severe buffeting loads on the vertical tails. For this reason a detailed knowledge of the vortex burst mechanism and location is highly desirable, especially during maneuvering flight conditions.

The goal of this thesis therefore was to study the effects of pitch rate on the vortex development on the F-18 aircraft model in the NPS water tunnel using dye-injection for flow visualization with particular emphasis on visualization, documentation and interpretation of vortices generated from the forebody and the strakes at high angles of attack, with and without yaw.

II. THE DYNAMIC STALL PHENOMENON

A. DESCRIPTION

The words " dynamic stall " are used to describe the flow phenomenon that occurs on a wing in unsteady motion which experiences flow separation.

B. DYNAMIC STALL EVENTS

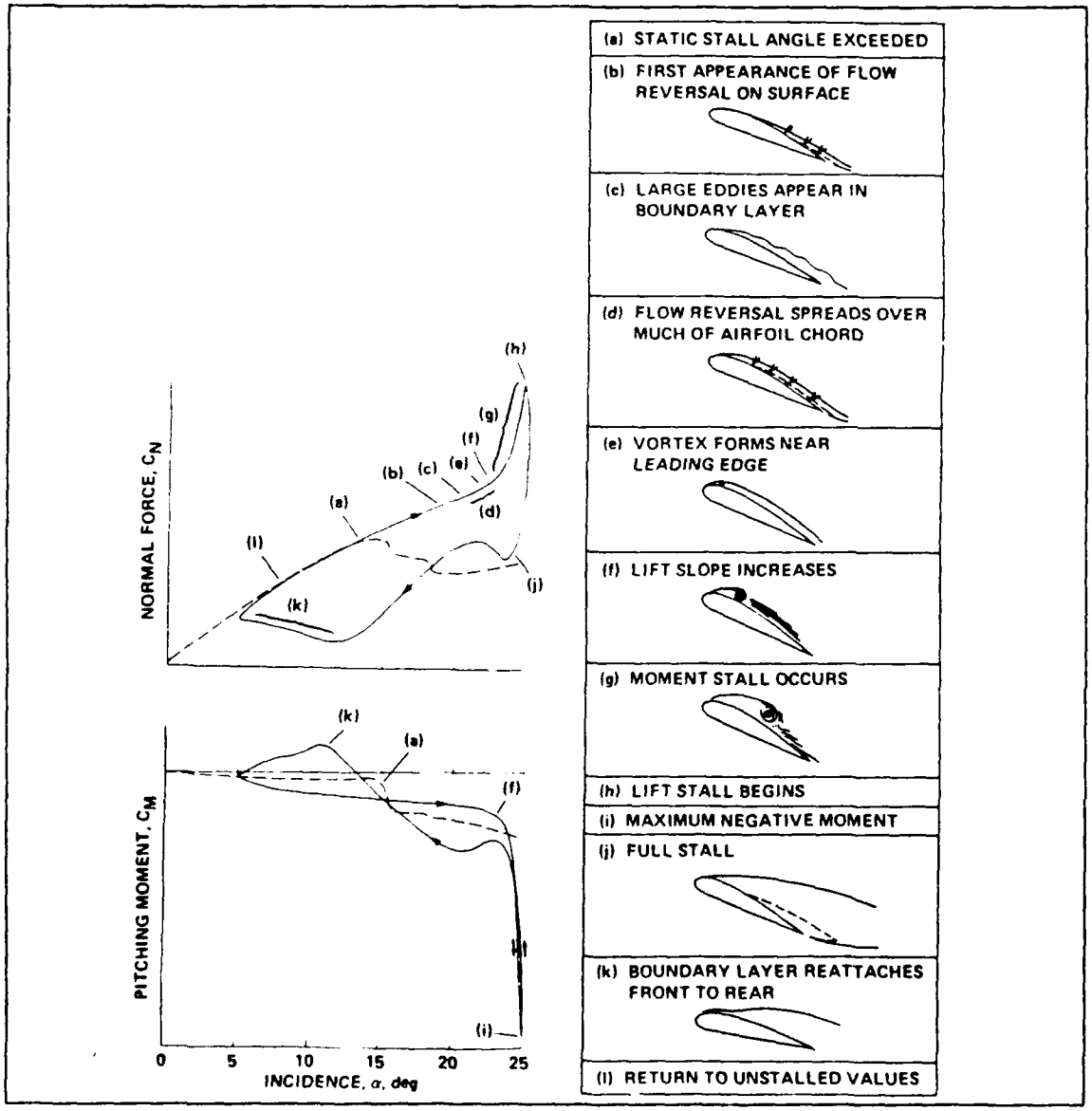

Figure 2. A chronology of dynamic stall events[Ref. 5]

Figure 2 [Ref. 4] describes the development of the normal force and pitching moment versus angle of attack and the corresponding boundary layer behavior for a dynamically stalling NACA 0012 airfoil.

A chronology of dynamic stall events should start at point (a) in Fig.2 , where the pitching airfoil passes the static stall angle without any discernible change in the viscous or inviscid flow around the airfoil. At point (b) , the first indication of disturbance in the viscous flow appears , when the flow reverses near the trailing edge of the airfoil . At point (e) , a vortex forms near the leading edge of the airfoil, inducing strong pitching moment effects on the airfoil (point (f) and (i)), producing the phenomenon known as dynamic stall.

C. STALL REGIMES

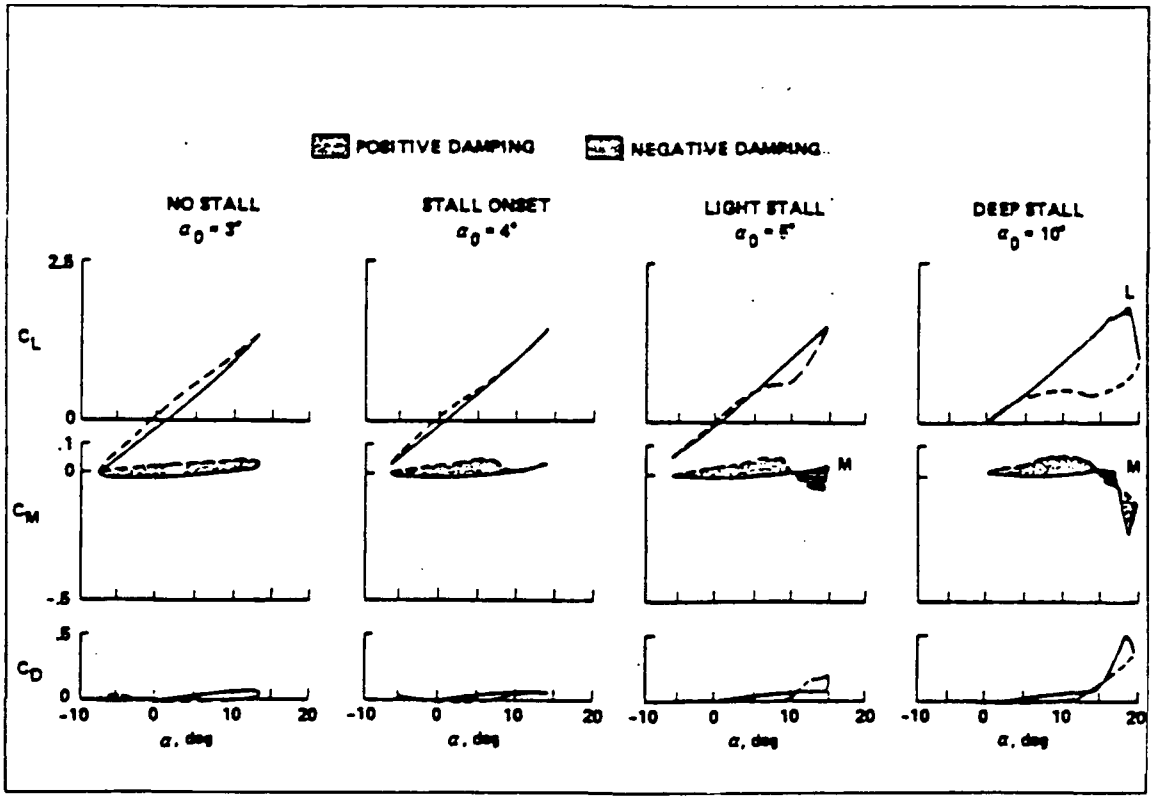

Figure 3. Dynamic stall regimes, NACA 0012 airfoil

Figure 3 [Ref. 5] illustrates the different stall regimes which may be encountered. For small maximum angles of attack only light stall will be

encountered. In this case, a significant drag increase and loss of lift compared to the theoretical attached flow values will be found. Another distinguishing feature of the light dynamic stall is the scale of the interaction. The vertical extent of the viscous zone tends to remain on the order of the airfoil thickness, generally less than for static stall. The quantitative behavior of light stall is sensitive to airfoil geometry, reduced frequency, maximum incidence and Mach number.

Further increases in α_{max} lead to the deep dynamic stall regime. This regime is dominated by the vortex-shedding phenomenon. Figure 3 illustrates some of the qualitative and quantitative differences between light and deep stall. The qualitative features of deep stall are less sensitive to the details of the airfoil geometry, motion, Reynolds number, and Mach number. The quantitative air loads depend on the time history of the angle of attack for the portion of the cycle when the static stall angle is exceeded.

D. EFFECT OF VARIOUS PARAMETERS

Table 1 [Ref. 5], gives a summary of the most important parameters which affect dynamic stall.

Table 1. IMPORTANCE OF DYNAMIC STALL PARAMETERS.

STALL PARAMETERS	EFFECT
Airfoil shape	Large in some cases
Mach number	Small below $M_\infty = 0.2$, Large above $M_\infty = 0.2$
Reynolds number	Small at low Mach number, Unknown at high Mach number
Reduced frequency	Large
Mean angle, Amplitude	Large
Type of motion	Virtually unknown
3-D effects	Virtually unknown
Tunnel effects	Vitually unknown

1. Airfoil Geometry

In the light dynamic stall regime, the leading edge geometry of an airfoil is an important factor in determining the boundary layer separation characteristics. The leading edge stall produces a relatively concentrated vortex and abrupt changes in lift, pitching moment and drag coefficient during the development of the dynamic

stall event. This contrasts with trailing edge stall, which is more common on airfoils with relatively blunt noses or a large amount of leading edge camber. Boundary layer separation which progresses forward from the trailing edge tends to occur more gradually. Also, the more gradual the trailing edge separation, the less negative the resulting aerodynamic damping.

2. Reduced Frequency

The reduced frequency of the oscillation is an important parameter affecting dynamic stall, but its influence depends on the stall regime and the type of boundary layer separation. For example, Fig. 4 and Fig. 5 [Ref. 5] show opposite trends in the light stall regime for leading edge and trailing edge stalling airfoils tested under identical conditions.

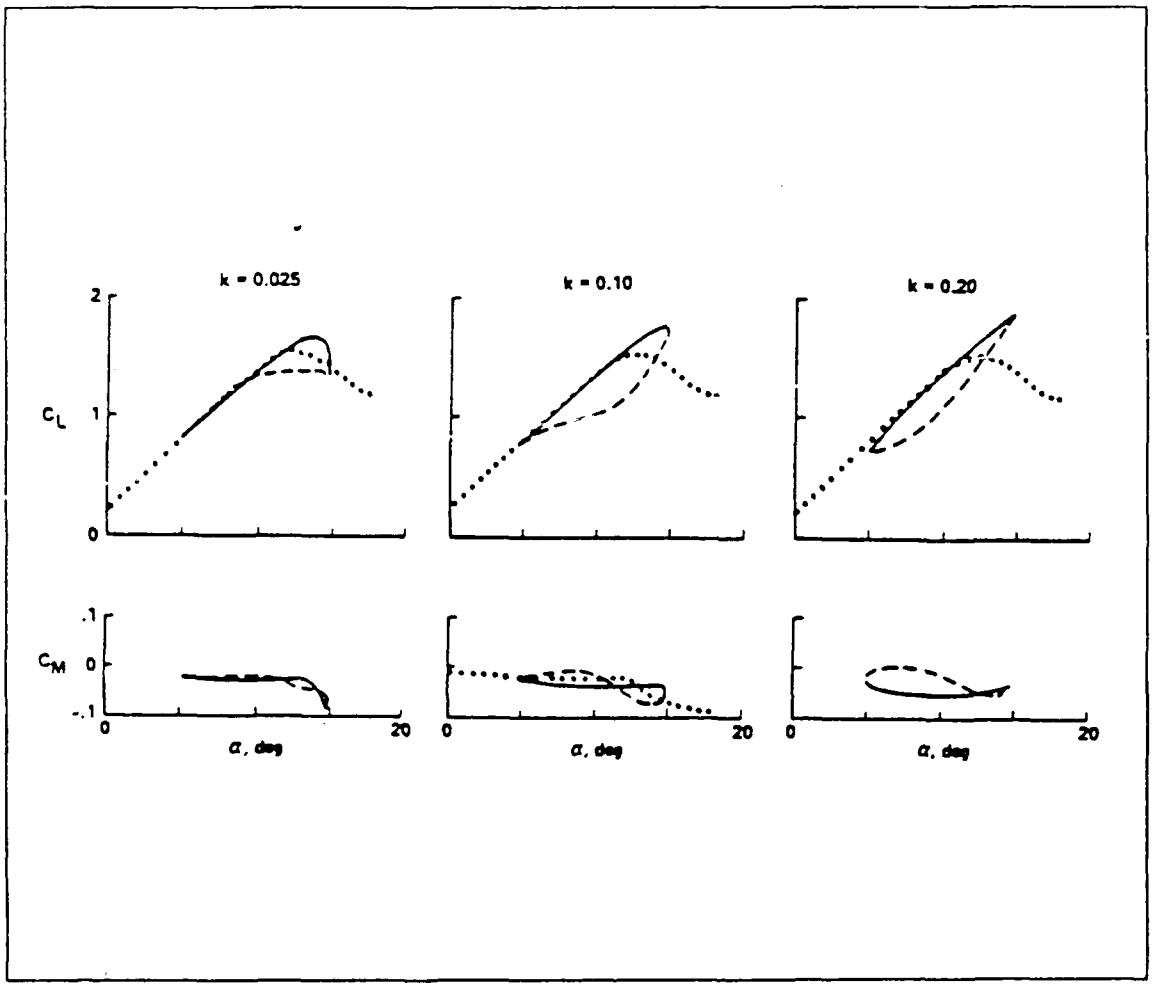

Figure 4. The effect of reduced frequency on the VR-7 airfoil at $M_\infty = 0.3$ and $\alpha = 10^0 + 5^0 \sin \omega t$ [Ref. 5]

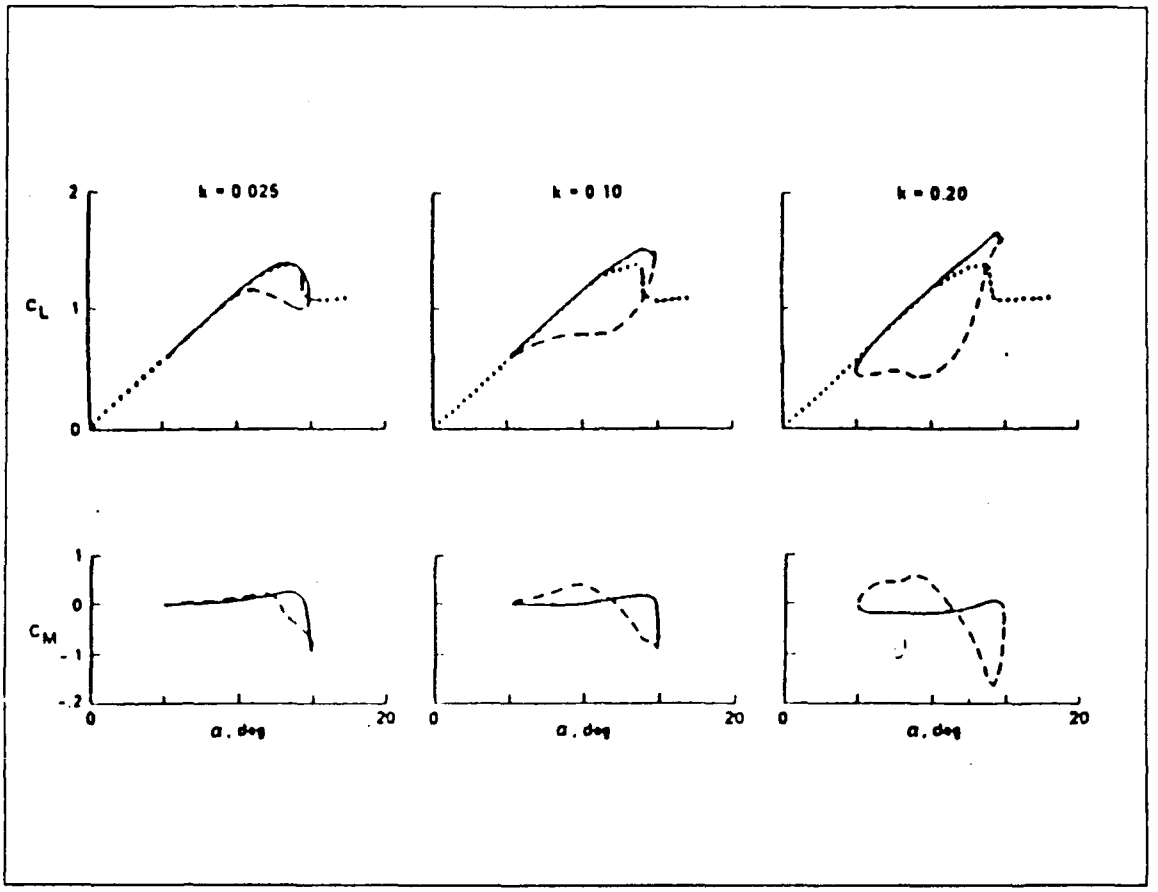

Figure 5. The effect of reduced frequency on the NACA 0012 airfoil at $M_\infty = 0.3$ and $\alpha = 10^0 + 5^0 \sin \omega t$ [Ref. 5]

Fig. 6 [Ref. 5] is more illustrative of the trends in deep dynamic stall. The reduced frequency is defined by:

$$k = \frac{\omega c}{2U_\infty}$$

where, k : reduced Frequency
ω : rotational frequency, rad/s
c : chord length of airfoil,ft
U_∞ : free stream velocity, ft/s

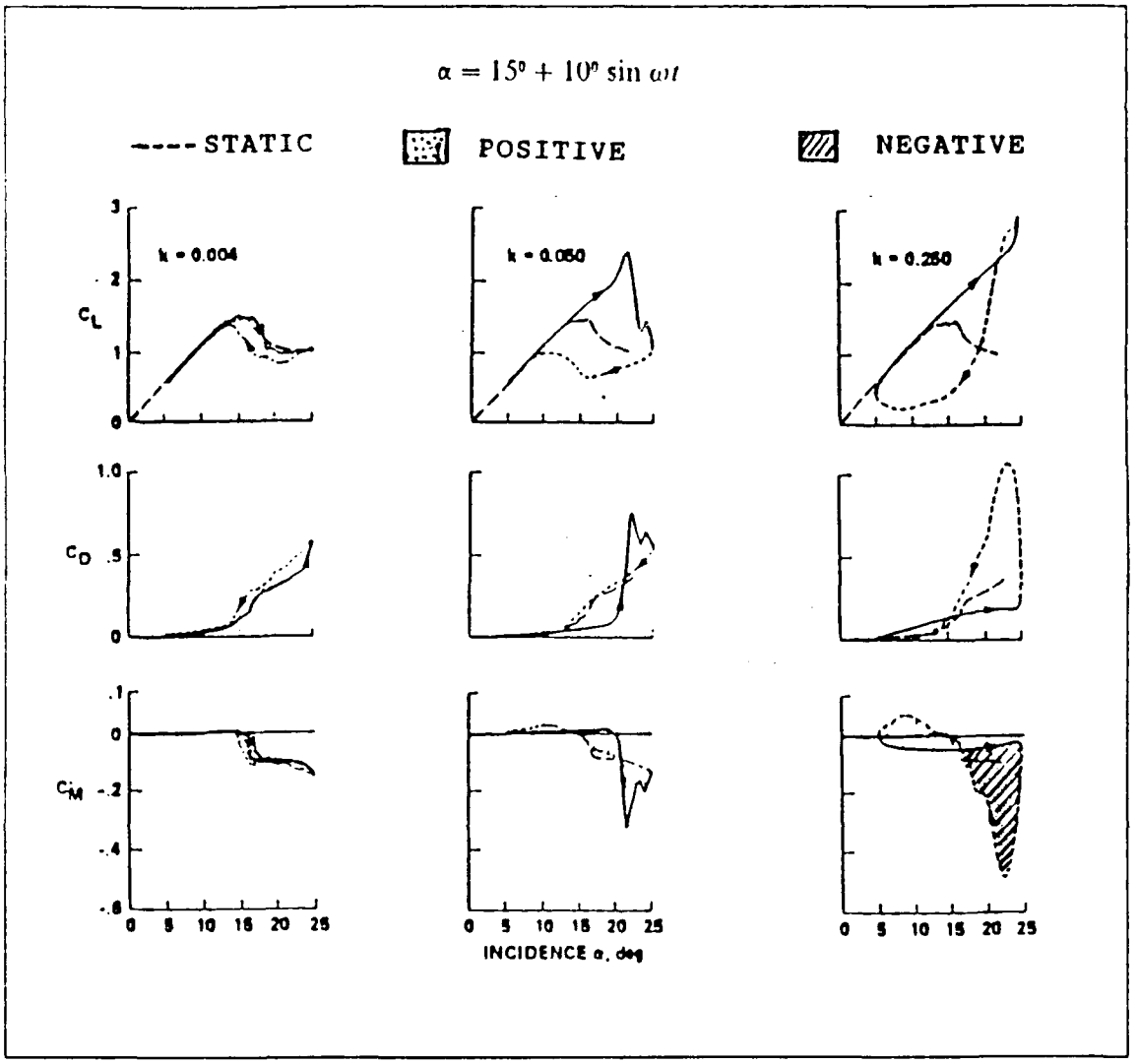

Figure 6. The effect of reduced frequency in the deep stall regime. NACA 0012, $M_\infty = 0.1$[Ref. 5]

3. Amplitude and Mean angle

Dynamic stall effects depend significantly on the amplitudes of oscillation. Fig. 7 [Ref. 5] presents the lift and pitching moment for three test conditions each of which has the same mean angle.

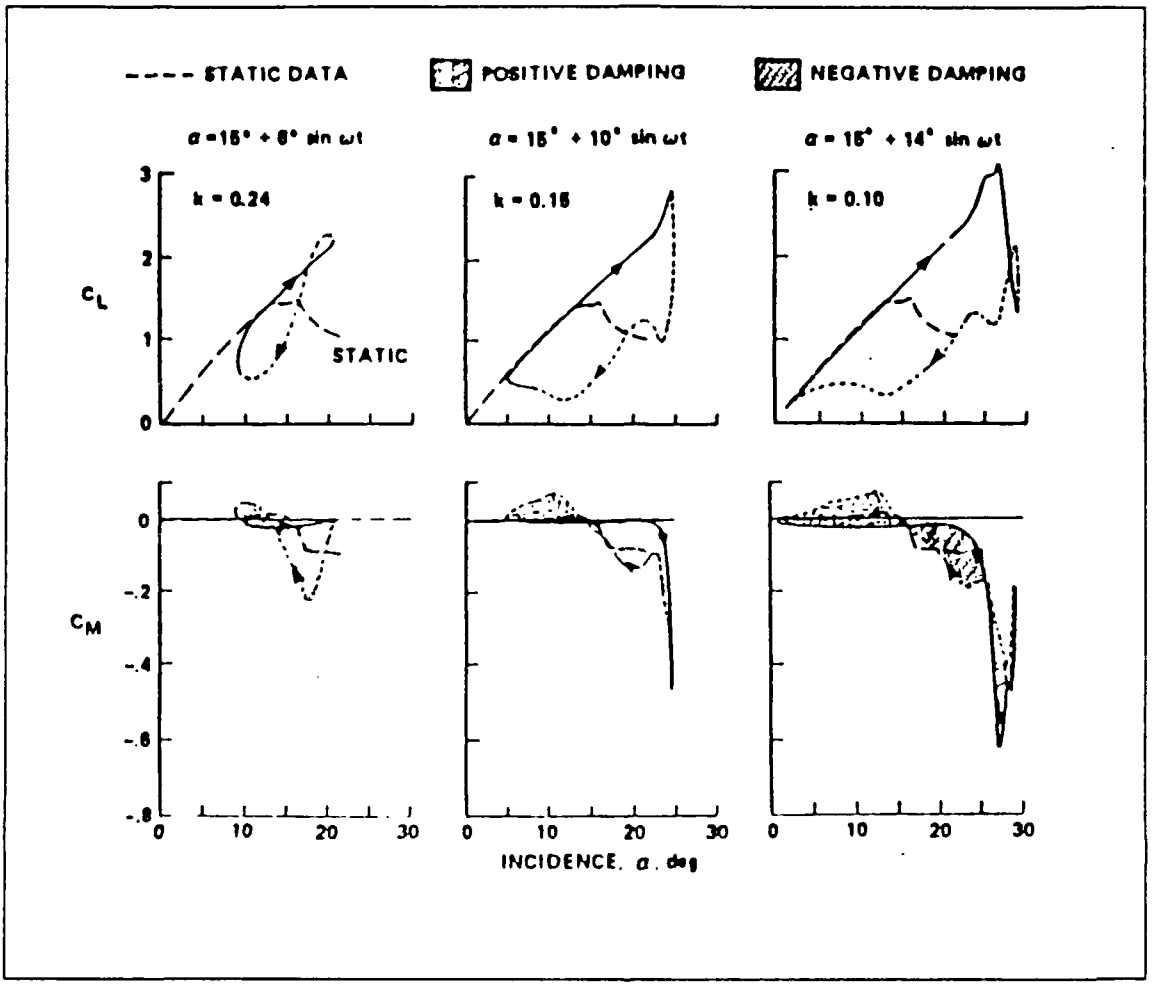

Figure 7. The effect of amplitude at $\frac{\alpha_{max} C}{U_\infty} = 0.05$ [Ref.5]

4. Mach Number

McCroskey [Ref. 5] has shown that the dynamic stall behavior of an airfoil is also dependent on Mach number. This effect has recently been investigated in some detail by Chandrasekhara and Carr [Ref. 6], who found that an increase in Mach number tends to decrease the dynamic lift effect.

5. Reynolds Number

High Reynolds number dynamic stall tests were recently completed by Lorber and Carta [Ref. 7] for a Sikorsky airfoil, thus giving for the first time an assessment of the influence of this important parameter.

6. Three Dimensional Effects

The three dimensional aspects of the dynamic stall phenomena on wings and complete aircraft are still insufficiently understood and explored. Therefore, they present important challenges for future experimental and computational dynamic stall research.

E. CALCULATION METHODS

As summarized by McCroskey [Ref. 5], a number of methods were developed in the 1960's and 1970's to predict two-dimensional dynamic stall. These methods were based on discrete potential vortex modelling, on direct empirical correlation techniques, such as the Boeing-Vertical Gamma Function Method, the MIT method, or time delay methods. These methods all have serious limitations because of the empirical or questionable assumptions underlying them.

Very recently, however, encouraging progress has been made to analyze the dynamic stall phenomenon by means of Navier-Stokes computations using supercomputers. Ekaterinaris [Ref. 8] and Patterson and Lorber [Ref. 9] achieved good agreement with the experimental results of Lorber and Carta. It needs to be emphasized, however, that such calculations are limited to two-dimensional flows. The dynamic stall and vortex breakdown phenomena occuring on the F-18 aircraft, which is the subject of this thesis, are still inaccessible to direct computation.

III. FLOW VISUALIZATION TECHNIQUES

Flow visualization is one of many available tools in experimental fluid mechanics. It differs from other experimental methods in that it renders certain properties of a flow field directly accessible to visual perception. Flow visualization techniques offer a useful tool to establish an overall picture of the steady and unsteady flow field.

The methods of flow visualization can be classified roughly into three groups [Ref. 10]. These are:

1. addition of foreign materials into gaseous and liquid flows
2. optical flow visualization
3. flow field marking by heat and energy addition

In this thesis only dye injection technique was used. Therefore only the techniques in the first group are discussed below.

A. DYE VISUALIZATON TECHNIQUES

Dye visualization techniques involve addition of a foreign material into gaseous and liquid flows. Commonly employed methods are the classical dye injection method and the dye layer method.

1. The Dye Injection Method

The marking of lines of contours in a flowing liquid by means of dye can be achieved by introducing the dye into the liquid from outside (direct injection), or by generating it with an appropriate chemical reaction in the liquid.

The injection of dye has long been a popular method for visualizing water flows. In 1883, Reynolds was the first to demonstrate the transition from laminar to tubulent flow by injecting a thin thread of liquid dye into a flow of water through a glass tube. The dye is usually introduced to the flow from small holes or slots provided in the model under consideration or from a source external to the body, such as a small hypodermic tube or syringe. The tube from which the dye is dispersed must be placed far enough upstream of a test model, so that interference of the tube with the flow pattern to be studied will be minimized.

The rate at which the dye is released has to be matched with the velocity of the liquid. If the injection rate from the injector tube is allowed to become too large, the

issuing dye might behave like a jet, and vortices appear along the interfaces between the jet and the mainflow. If the dye is released from small holes in the surface of a rigid test model, the number of holes must be minimized; otherwise the flow of the injected dye would interfere with the main flow around the model, and particularly would alter the body wall boundary layer due to the injected mass and momentum.

The dye filaments may be stabilized by mixing the dye with milk (Werle', 1960, see Ref.10) and it is presumed that the fattiness of the milk retards diffusion of the dyed solution into the main bulk of water. At the same time, due to its high reflective properties, milk also meets the condition of good visibility, so that the use of milk in a dye mixture combines two advantages: that of high contrast of dye lines and that of stabilized filaments with respect to rapid diffusion. The dyed portion of the fluid should be illuminated from behind with a diffuse source or banks of fluorescent tubes.

The choice of dye depends on the particular conditions of a flow experiment, but apparently also on such arbitrary circumstances as rapid availability or cost. Food coloring mixed with milk appears to be the most popular dye in pure and salt water. This mixture can be diluted with the water from the operating channel to minimize density gradients, and filaments of different colors can be generated in order to facilitate the identification of the spatial flow structure, for example, in a swirling flow.

Table 2, reproduced from Ref.10, lists a number of dyes, which have been used for flow experiments, together with the working fluid and the respective references. Injection of dye is a standard technique for water tunnel experiments. The dye ejected into a recirculating tunnel remains in the system and gradually contaminates the water. Dumas et al. (1982, see Ref.10), who worked with different fluorescent dyes, report that it takes about 25 minutes of continuous dye injection before 5 cubic meter of water of the recirculating system have to be replaced. For the same unit Reynolds number and model scale the velocity in water is $\frac{1}{15}$ of that in air so that flow characteristics can be observed at a relatively low speed.

Table 2. DYE INJECTION METHODS

WORKING FIELD	DYE	REFERENCES
Water	Milk and food coloring	Werle'(1960f.f)
Salt water	Milk	Simpson(1972)
Water	Food coloring	Han and Patel(1972)
Salt water	Food coloring	Hunt and Snyder(1980)
Polymer solution	Food coloring	Donahue et al.(1972)
Water	Ink	Faler and Leibovich(1977)
Polyethylene	Ink	Masliyah(1972)
Water	Printer's white	Martin and Lockwood(1964)
Salt water	Blue Dextran dye	Delisi and Orlanski(1975)
Water	Fluoresceine	Dumas et al.(1982)
Water	Methylene blue dye	McNaughton and Sinclair(1966)
Water	Fluoresceine ink	Masliyah(1980)

2. The Dye Layer Technique

Flow visualization by the classical dye or smoke injection method runs into difficulties when there is a time dependent pressure field associated with an unsteady flow. In these circumstances, it is not only difficult to release the tracer uniformly into the flow due to the fluctuating pressure field but it is alsodifficult to interpret the observed patterns. The dye layer technique described by Gad-el-Hak (1981) overcomes some of these difficulties. This visualization method can be used in a water towing tank facility.

The dye layer technique has been particularly useful in investigating the complex, time dependent flow fields around three-dimensional lifting surfaces undergoing large amplitude pitching harmonic oscillations. Sheets of laser light are projected in the desired plane to excite the fluorescent dye layers. The alternating horizontal sheets of different color dyes remain quiescent until disturbed by the moving lifting surface. Unlike conventional dye injection techniques, the dye layers mark the flow in the separation regior., the flow in the wake region, and the potential flow away from the surface. This is particulary useful for observing the irrotational motion induced by the leading and trailing edge vortices associated with changing the angle of attack of the lifting surface.

IV. FACILITIES AND PROCEDURES

A. FACILITY

The equipment required to complete the experimental portion of this thesis included:

1. A flow visualization water tunnel.
2. A F-18 fighter aircraft model and necessary support structures.
3. A flow visualization system.
4. A flow recording system (Still camera, Video camera, VCR, TV monitor)

1. Water Tunnel Facility

The experiments were performed in the Naval Postgraduate School flow visualization water tunnel facility [Ref. 11].

The flow visualization water tunnel is a continuous flow tunnel [Fig. 8]. It is built principally of glass to allow maximum viewing of the model. It has provision for viewing from the rear which is especially advantageous when studying flow structures in the cross flow plane. Although the flow velocity can be varied from 0 to 1.0 ft sec, the entire test was performed at an average 0.5 ft sec, since this velocity provides the optimum conditions for visualization.

The test section is nominally 15 inches wide, 20 inches high, and 60 inches long. It has slight divergence in the sidewalls to compensate for boundary layer growth and thus maintains uniform flow velocity across the test section.

The level of flow quality (measured outside the wall boundary layer) over the test section is as follows:

Turbulence intensity level : < 1.0 % RMS

Velocity uniformity : $< \pm 2.0$ %

Mean flow angularity : $< \pm 1.0$ % in both pitch and yaw angle

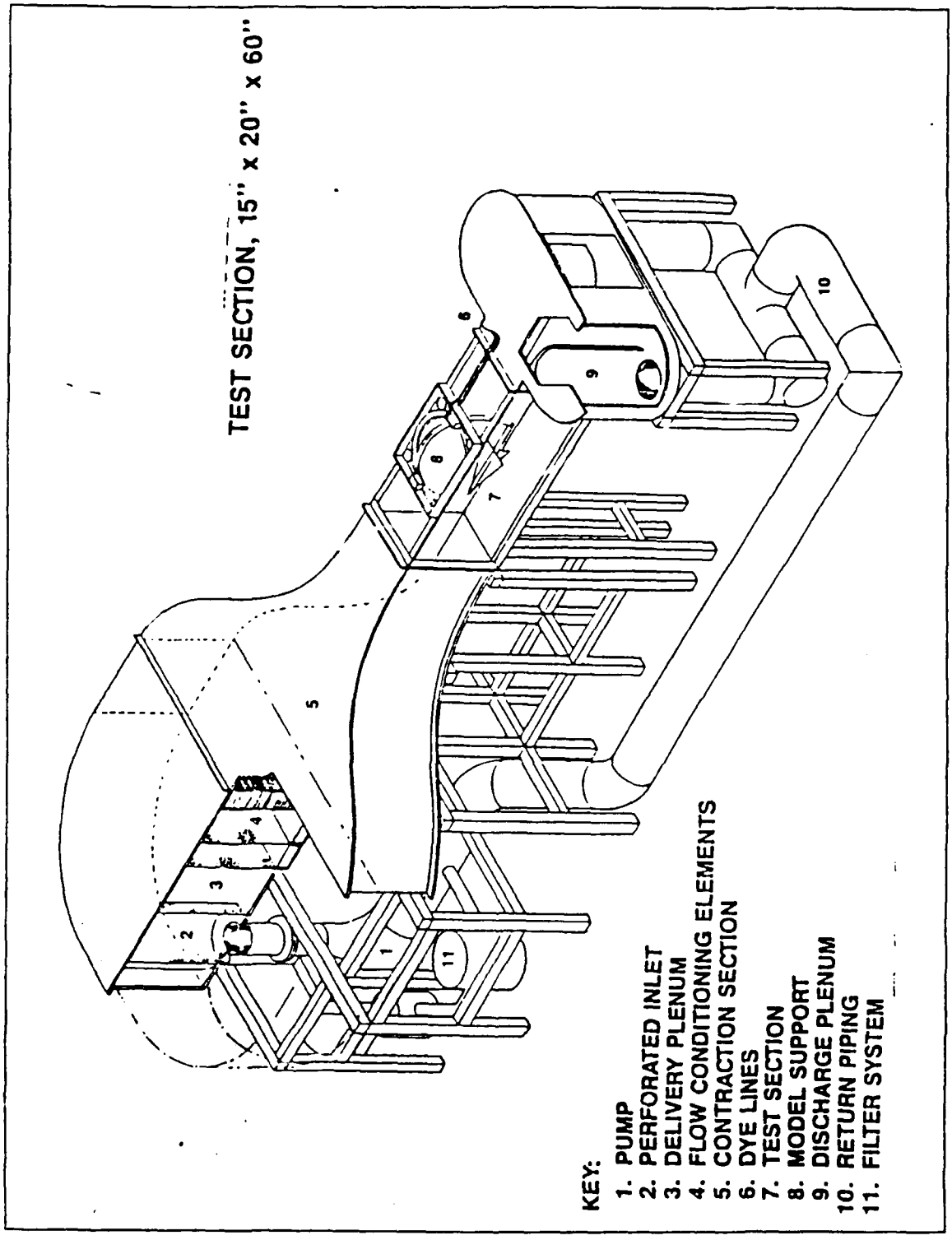

Figure 8. Water Tunnel Facility at the Naval Postgraduate School.

The dye supply system consists of six pressurized color dyes using water soluble food coloring. It is provided with individually routed lines from the dye reservoirs to the model support system. The dye canisters are pressurized with air using a small compressor and a pressure regulator to control the pressure level.

The model support system utilizes a C - strut to vary the pitch angle travel up to 50 degrees between the limits of -10 and 110 degrees, and a turntable to provide yaw variations up to $\pm$ 20 degrees.

The model attitude control system can control two axes. The pitch and yaw directional control switch has plus and minus directions. A plus command will increase the pitch and yaw angle of the model. A minus command will decrease the pitch and rotate the yaw axis in a clockwise rotation when viewed from the top. Each axis has a high / low rate switch which permits the operator to move quickly through large angles. The high rate and low rate correspond to 4.4 deg / sec and 1.4 deg / sec, respectively. Each axis has a limit switch for each direction of travel. These switches are intended to prevent the operator from exceeding the travel limitations of the model support and thus save the model from accidental damage.

2. Fighter Model

The fighter model is a $\frac{1}{48}$ th scale model of the McDonnell Douglas corporation's F-18 fighter aircraft [Fig. 9]. Key dimensions of the model are listed below:

1. Total length = 14.25 in
2. Wing span = 9.375 in
3. Wing chord = 3.5 in(root), 1.5 in (tip)
4. Wing area = 24.97 in^2

The longitudinal axis scaling in Fig. 9 is included to provide a visual reference for discussion of the flow visualization results.

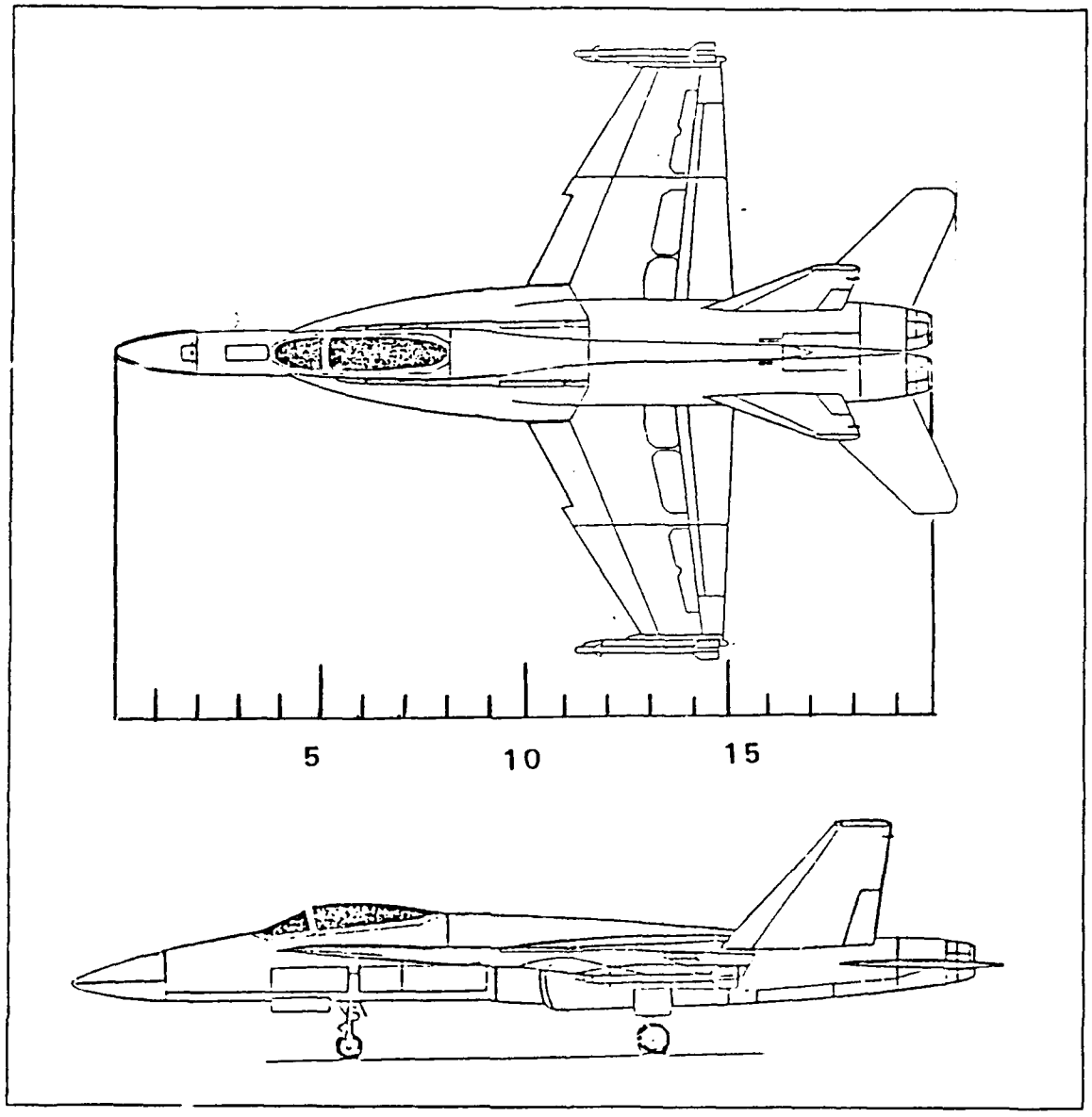

Figure 9. Views of the F-18 Navy Fighter Aircraft.

3. Injection Ports

The aircraft model was equipped with several dye injection ports. Fig. 10 illustrates the locations of these dye ports. The dyes are drawn from the pressurized dye supply system mentioned earlier and injected through the ports on the model. The injection rate of each dye line can be individually controlled by a fine needle valve. Table 3 lists different colors and their locations.

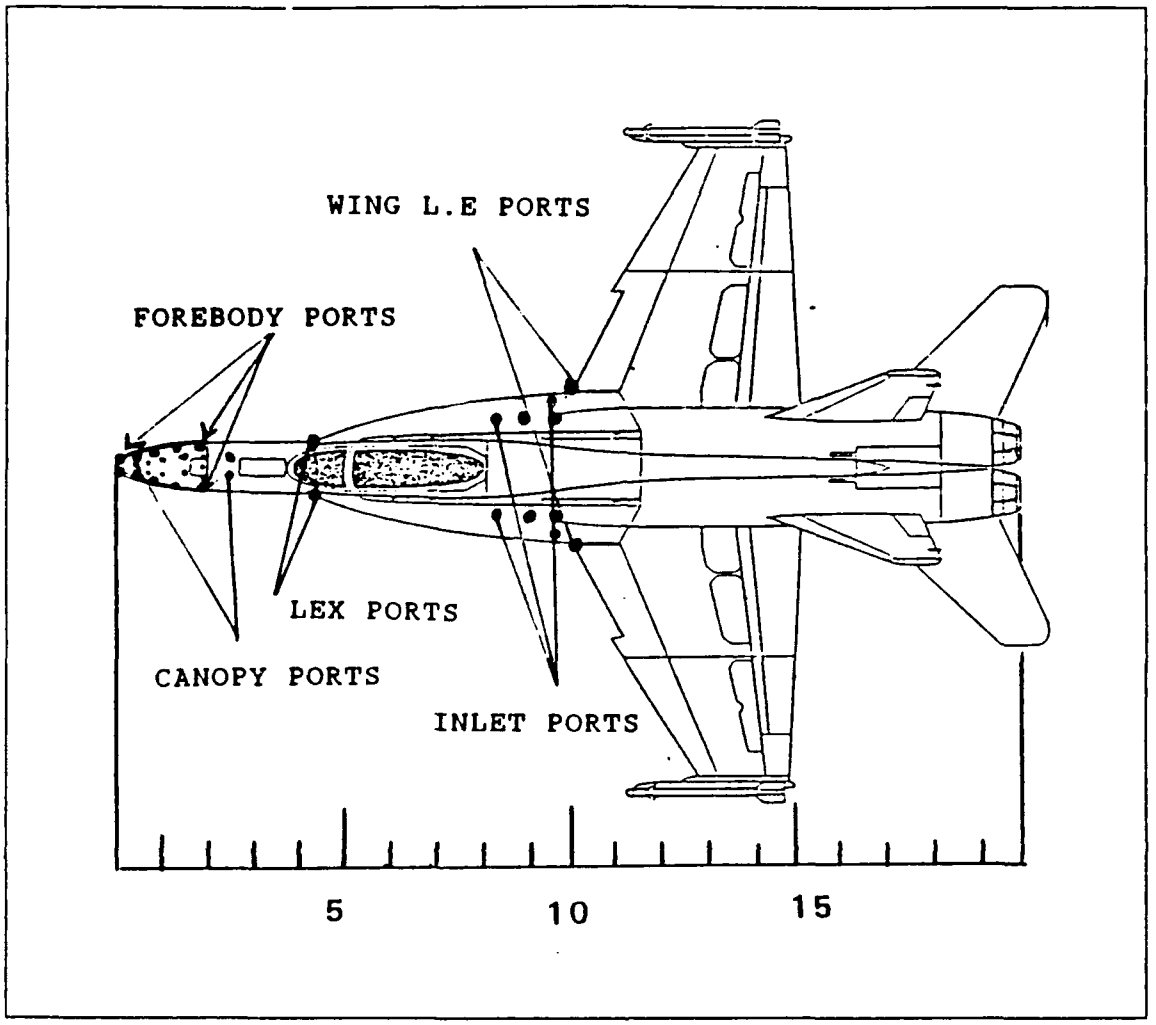

Figure 10. Dye port locations on F-18 model.

Table 3. DYE COLORS AND THEIR INJECTION LOCATION

LOCATION	COLOR(S)
Forebody	Red , Blue
Canopy	Pink
Leading Edge Extension	Black
Wing leading edge	Green
Inlet flow	Yellow

B. EXPERIMENTAL PROCEDURE

The overall goal of the investigation was flow visualization and documentation of the effects of pitch rate on the vortex development and bursting locations on the F-18 aircraft in the low speed, high angle of attack regime, with and without yaw. The focus of this thesis project has been the study of the forebody vortices and strake vortices during simple pitch up and simple pitch down motions, with and without yaw.

To meet this goal, the experiment was carried out in two phases. The first phase involved the forebody vortex flow visualization on the model for two pitch rates, with angle of attack varying from 0 degree to 50 degrees (simple pitch up motion) and 50 degrees to 0 degree (simple pitch down motion). This phase was carried out for yaw angles of 0 deg, + 5 deg, + 10 deg, and + 20 degrees. The flow velocity in the water tunnel was nearly constant at 0.5 ft/sec through the experiment. The second phase involved the LEX (leading edge extension or strake) vortex flow visualization on the model for the same pitch and yaw configurations and flow conditions of the first phase.

1. Model mounting

Before starting any experiment, it is very important to insure that the model is mounted horizontally in the water tunnel with zero pitch, zero yaw and zero roll. The center line of the model (say fuselage) is aligned with the center line of the tunnel. A level check is then performed on both wing tips so that they are located at the same height from a reference plane (say from the tunnel floor). The model symmetry is then checked by observing the symmetry in the shed vortices. Although this is subject to some visual error, the method was found to be reasonably satisfactory.

2. Reduced frequency simulation

From the fomula for reduced frequency, $k = \frac{\omega c}{2U_\infty}$, one can estimate the reduced frequency at various conditions. Table 4 lists these values for the model and the actual aircraft and shows that the water tunnel facility is capable of simulating full scale values of this unsteady parameter in the F-18 aircraft.

Table 4. REDUCED FREQUENCY

PITCH RATE	ω (rad/sec)	Length(ft)	U_∞ (ft/sec)	k(reduced frequency)
Low pitch rate model	0.024	1.12	0.5	0.0273
High pitch rate model	0.0751	1.12	0.5	0.0841
Actual F-18 aircraft(typical flight condition)	1.0472	56	608	0.04823

3. Forebody vortex flow visualization

Table 5 illustrates the test conditions during forebody vortex visualization experiments. It should be mentioned here that although negative yaw angles were covered during the experiment, the corresponding data is neither presented nor discussed in this thesis because of its close similarity with the data for positive yaw angles.

Table 5. FOREBODY VORTEX FLOW VISUALIZATION

AOA(degrees)	YAW(degrees)	CONDITION	PITCH RATE	REMARKS
0 to 50(every 10 deg)	0, +5, +10, +20	Static		Side view,Planform view,Still pictures,Video tape recording
		Dynamic	Low pitch rate up	
			Low pitch rate down	
			High pitch rate up	
			High pitch rate down	

4. LEX vortex flow visualization

Table 6 shows the test conditions during LEX vortex flow visualization experiments. Again negative yaw angles were covered during the experiment, but for reasons mentioned earlier, the data is not presented here.

Table 6. LEX VORTEX FLOW VISUALIZATION

AOA(degrees)	YAW(degrees)	CONDITION	PITCH RATE	REMARKS
0 to 50(every 10)	0, +5, +10, +20	Static		Side view,Planform view,Still pictures,Video tape recording
		Dynamic	Low pitch rate up	
			Low pitch rate down	
			High pitch rate up	
			High pitch rate down	

5. Data acquisition

Data consist of 35mm photographs of the model flowfield in both planform and side views. Although they were not taken simultaneously, in most cases they were taken only a few seconds or minutes apart with one camera. In a few cases, the two views were taken at much different times, but this was not considered to be a problem since the flow at most attitudes was resonably repeatable. Video tapes were also made (with emphasis on planform and side views) to record the observed flow phenomena during static and dynamic conditions.

V. RESULTS AND DISCUSSION

The results of this investigation are presented and discussed below.

In excess of 800 frames of 35 mm black and white film were exposed and over 8 hours of video tape recorded during the investigation. The results of the 35 mm photography are presented in a series of 6 numbered photographic sequenses which are presented as Figures 11 through 183 in Appendix A. Figures 184 through 195 included in Appendix B represent the bursting location data deduced from these photographs. With utmost care and consistency the bursting locations were visually determined from these photographs and scaled for nondimensionalization. Some arbitrariness may still be present in the reduced data but this should not unduly affect the interpretation of the data.

The results will be discussed below in three parts:

1. Forebody vortex flow visualization data.
2. LEX vortex flow visualization data.
3. Bursting location plots.

Each sequence of photographs is referred to in the discussion along with the corresponding figure numbers, followed by an analysis of the observed flow phenomena. Table 7 lists some prominent stations and model feartures at these locations. Port locations are shown in Figure 10 which is scaled for visual reference.

Table 7. STATION IDENTIFICATION ON THE MODEL.

STATION	DISCRIPTION
0	Tip of nose
3.8	Foreward most edge of canopy
4.3	Foreward most edge of LEX
10	Intersection of LEX and Wing leading edge
14.2	Foreward most edge of vertical stabilizer
15.2	Trailing edge of wings
20	Exhaust nozzle end

A. FOREBODY VORTEX FLOW VISUALIZATION DATA

The results of the forebody vortex flow visualization experiments are presented as photographic Sequence Numbers 1 to 3 in Appendix A (Figures 11 through 97) and in the form of bursting location plots in Appendix B (Figures 184 through 189). This data is analyzed below for the effects of pitch rate on bursting location with and without yaw, and the results for the model in dynamic (pitch) motion compared with these for the corresponding stationary model in static (equilibrium) condition.

1. Effects of pitch rate

Sequence Number 1, Figures 11 through 35, shows the development and or bursting of forebody generated vortices for the static case and for simple pitch up and simple pitch down motions at two reduced frequencies (dimensionless pitch rates) with the model at zero yaw. The bursting location plots deduced from these photographs are shown in Figure 184.

Figures 11 through 15 which were taken at intervals of 10° angle of attack indicate that at low angles of attack the forebody flow field is practically vortex-free. Increasing the angle of attack to 20° results in the development of a pair of symmetric nose generated vortices depicted in Figures 16 through 20. As the angle of attack is increased further, Figures 21 through 35, these vortices grow and the vortex burst location moves forward, indicating that the separated flow region increases at higher angle of attack, i.e., flow separation occurs earlier at higher angles of attack. Figures 16 and 31 illustrate typical forebody vortex flow patterns for the static case in low and high angle of attack conditions (20° and 50°), respectively. A careful study of the photographs for the pitch up and pitch down motions and / or the replay of video tape recordings of the flow visualization events show at what angle of attack the transition from symmetric to asymmmetric flow takes place and at what location the asymmetric vortex separates and crosses the model centerline. Furthermore, they clearly highlight what is frequently referred to as aerodynamic hysteresis effects during unsteady motion, causing a different angle of attack for reestablishment of symmetric flow as the angle of attack is reduced (during pitch down motion). It is currently unknown exactly what causes the asymmetric vortex shedding to tend to favor one side.

2. Effects of yaw

Sequence Number 2, Figures 36 through 49 and Sequence Number 3, Figures 50 through 97 show forebody vortex flow patterns obtained for two reduced frequencies at various model yaw angles, for static and dynamic cases, respectively. The corresponding bursting location plots are shown in Figures 184 through 189. These photographs clearly indicate the pronounced effects of even small yaw angles on the vortex development and breakdown. As can be seen in these photographs, the dye line injected from the windwardside of the forebody crosses over to the leeward side, leading to an asymmetric vortex field. They also indicate the effects of yaw on vortex bursting at both the windward and leeward sides.

B. LEX VORTEX FLOW VISUALIZATION DATA

All the results of the LEX vortex flow visualization experiments are presented as photographic Sequence Numbers 4 through 6 in Appendix A (Figures 98 through 183) and in the form of bursting location plots in Appendix B (Figures 190 through 195). This data is analysed below for the effects of pitch rate on bursting location with and without yaw, and the results for the model in dynamic (pitch) motion compared with those for the corresponding stationary model in static (equilibrium) condition. It must be mentioned here that the vortices shed from the forebody are very weak compared to LEX generated vortices and are more viscous dominated. Compared to the forebody vortex flow patterns, the LEX vortex flow patterns were better defined and consequently identification of burst location and scaling was less demanding in this case.

1. Effects of pitch rate

Sequence Number 4, Figures 98 through 118, shows the development and or bursting of LEX generated vortices for the static case and for simple pitch up and simple pitch down motions at two reduced frequencies (dimensionless pitch rates) with the model at zero yaw. The bursting location plots deduced from these photographs are shown in Figure 190.

A careful study of these photographs and the flow visualization events recorded on the video tape indicate the same effects described earlier for the forebody visualization experiments. However, these results show up very dramatically in this case as LEX generated vortices are strong and thus clearly visible.

2. Effects of yaw

Sequence Number 5, Figures 119 through 127 and Sequence Number 6, Figures 128 through 183, show LEX generated vortex flow patterns obtained for two reduced frequencies at various model yaw angles, for the static and dynamic cases, respectively. The corresponding bursting location plots are shown in Figures 191 through 195. As before, the yaw effects discussed earlier for the forebody visualization experiments show up dramatically in this case.

C. BURSTING LOCATION PLOTS

Quantitative documentation of burst response location to varying pitch rates during pitch up and pitch down motions at zero yaw angle is presented in Figure 184 and Figure 190 for forebody and LEX experiments, respectively. It is clear that during both pitch up and pitch down motions in the angle of attack range considered, the burst location always occurred earlier relative to the static case, higher pitch rate implying earlier bursting. Thus for both pitch up and pitch down motions, the burst location curves consistently undershoot the corresponding static curve. The undershoot increases with pitch rate and is greater for the pitch down motion. The vortex breakdown response observed here for the pitch down motion is similar to the one observed by Magness et al. [Ref. 2] in their experimental investigation of leading edge vortices on a pitching delta wing. However, in their study, during the simple pitch up motion the bursting occurred later relative to the static case in the high angle of attack range, i.e., there was overshoot in the bursting location curve for the pitch up motion. No overshoot was observed during the present investigation for the zero yaw case.

The effects of yaw on bursting locations of the forebody vortex and LEX vortex are shown in Figures 184 through 189 and Figures 191 through 195, respectively. Note that in these figures bursting location refers to the bursting of the vortex on the leeward side. It is clear from Figure 184 that for the static case the effect of yaw is to delay bursting, i.e., to cause the forebody vortex bursting to occur later for angles of attack greater than 15°. Similar yaw effects are observed in the case of LEX vortex bursting but only in the 20° to 40° angle of attack range, the yaw effects reversing outside this angle of attack range (Figure 191). During the pitch up and pitch down motion, similar "delay effects" of yaw are observed both on forebody vortex burst locations (Figures 186 through 189) and LEX vortex burst locations (Figures 192 through 195). In the latter case,

these delay effects are present throughout the angle of attack range 10^0 to 50^0. It should also be noted here that at higher angles of attack, the LEX vortex burst location tends toward the leading edge.

VI. CONCLUSION AND RECOMMENDATIONS

A low speed Flow Visualization investigation was initiated into the high angle of attack aerodynamics of a 2% scale model of the F-18 fighter aircraft using dye injection in the NPS water tunnel. The main focus was on the effects of pitch rate on the development bursting of vortices generated from the forebody and the strakes in the high angle of attack range, with and without yaw. The following conclusions are drawn from the results of the experimental investigation:

1. Pitch effects : Steady asymmetric vortices exist at high angle of attack range. At much higher angles of attack, wake like flow is observed.
2. Pitch rate effects : Relative to the static case, bursting occurrs earlier during pitch up motion, and much earlier during the pitch down motion.These effects increase with pitch rate.
3. Yaw effects : In the presence of model yaw, bursting occurs later on the leeward side, but earlier on the windward side. The presence of yaw causes asymmetric vortex bursting, leading to undesirable side forces and yawing moments.

The following recommendations are made based on the results of this investigation:

1. The flow visualization experiments should be extended to higher angles of attack beyond 50°.
2. The experimental results obtained here were based on laborious visual analysis. An automated computer controlled system for carrying out dynamic flow visualization experiments and for data acquisition and analysis is highly recommended.

APPENDIX A. EXPERIMENTAL RESULTS(PHOTOGRAPHS)

FIGURES 11 THROUGH 183

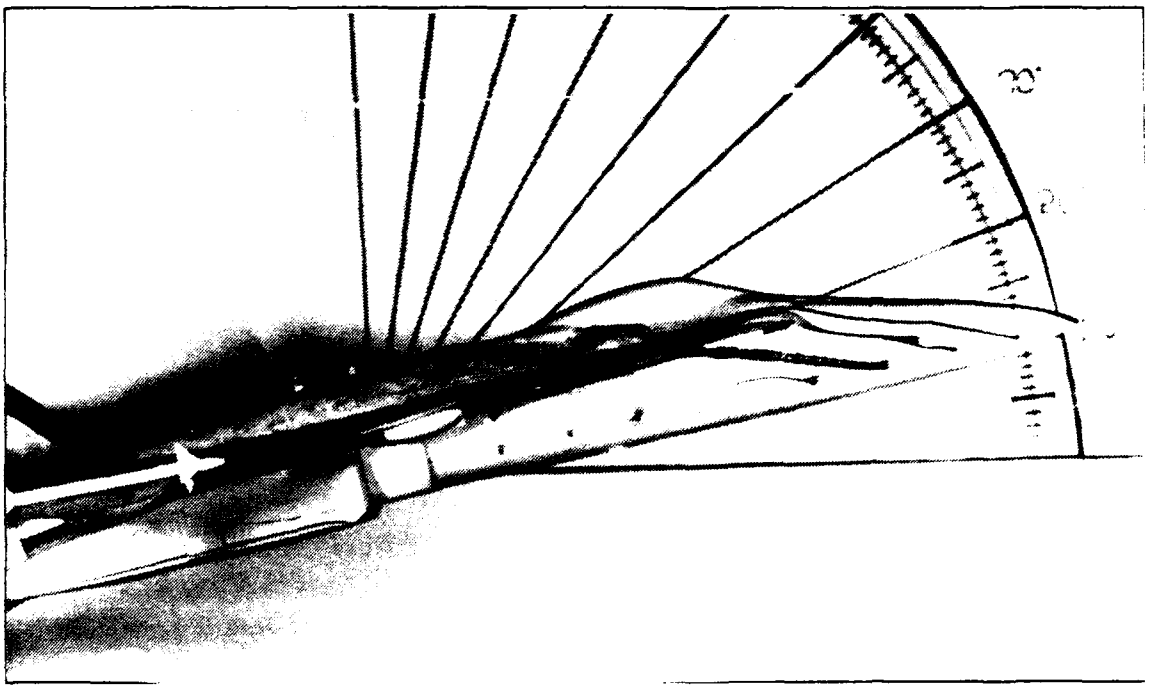

Figure 11. Forebody, Static, AOA = 10 deg , YAW = 0 deg.

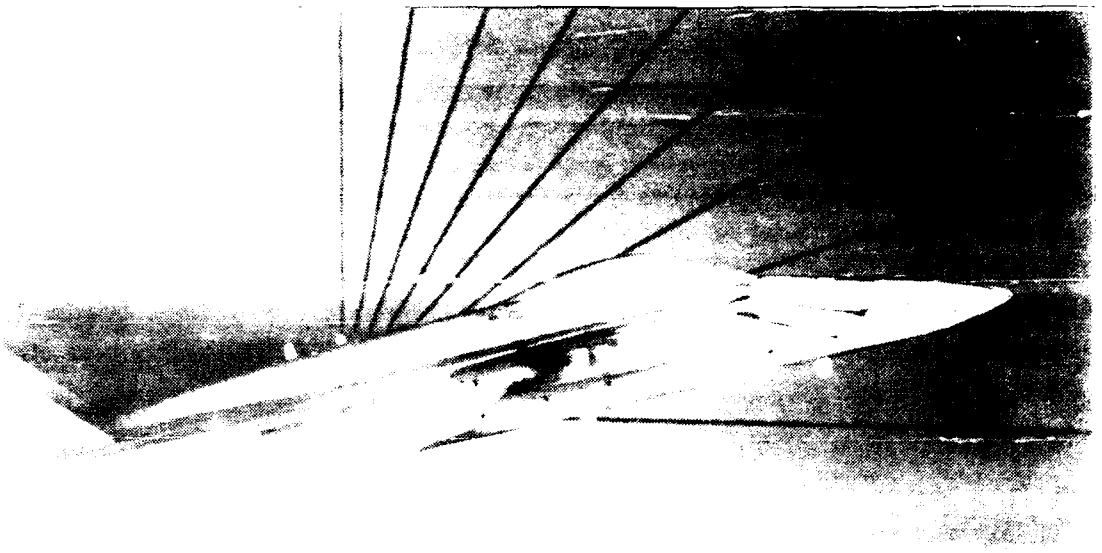

[illegible] AOA [illegible] deg., YAW [illegible] deg.

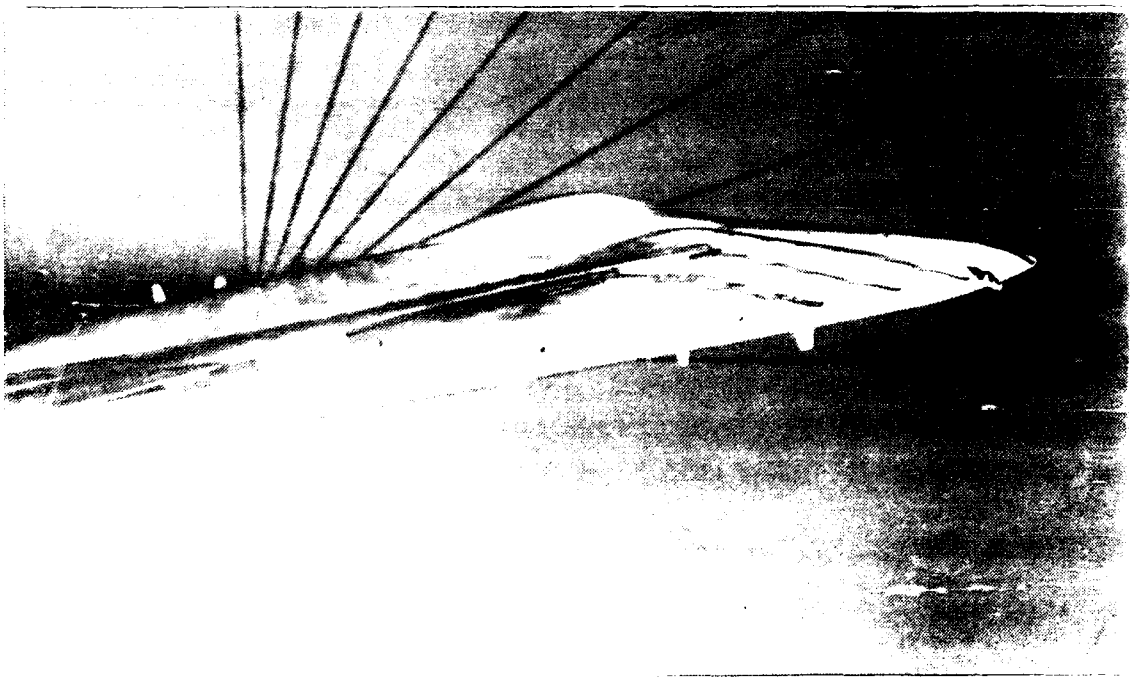

[illegible] AOA [illegible] deg., YAW [illegible] deg.

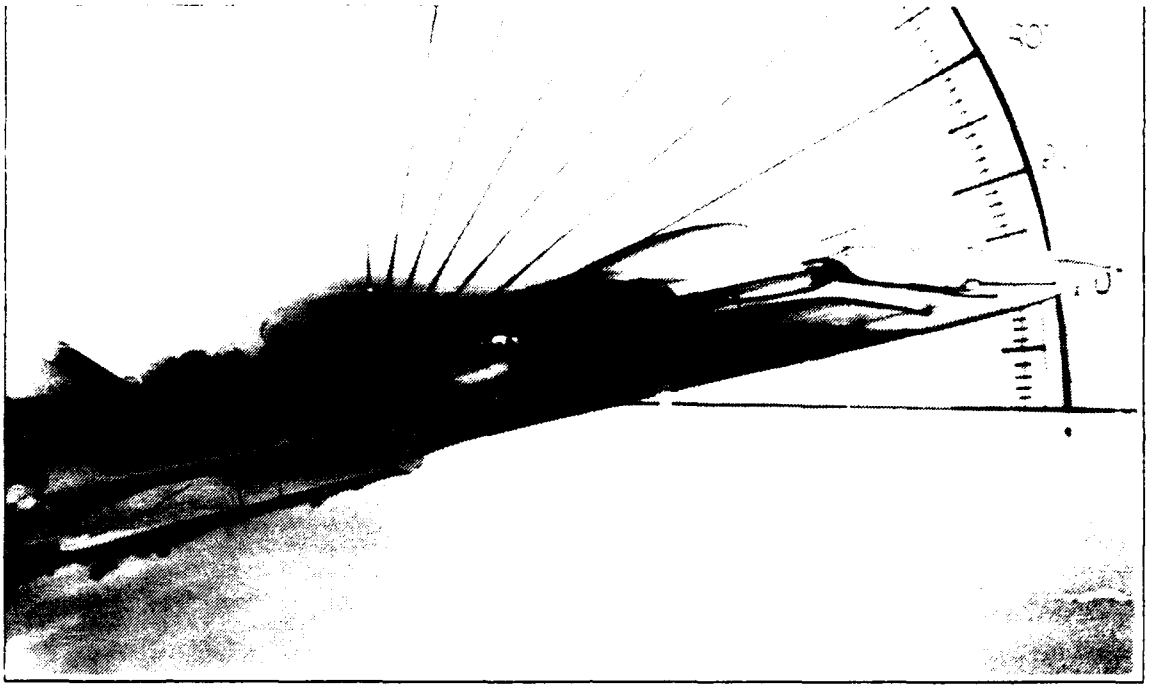

Figure 14. Forebody, High Pitch Up, AOA = 10 deg , YAW = 0 deg.

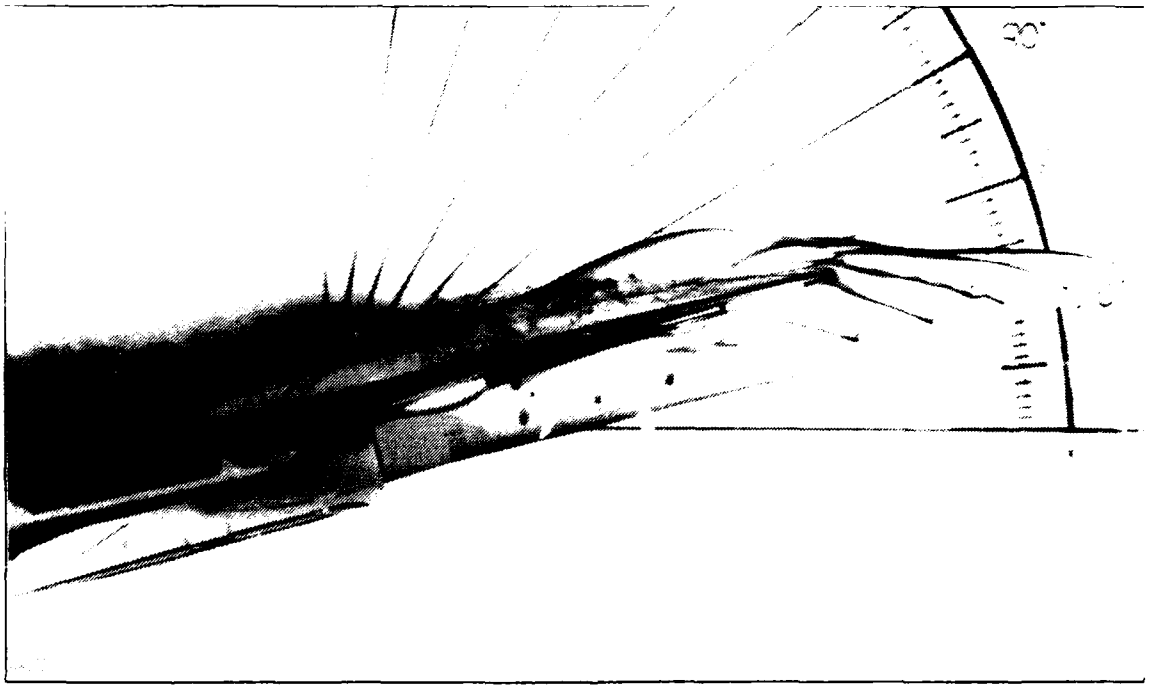

Figure 15. Forebody, High Pitch Down, AOA = 10 deg , YAW = 0 deg.

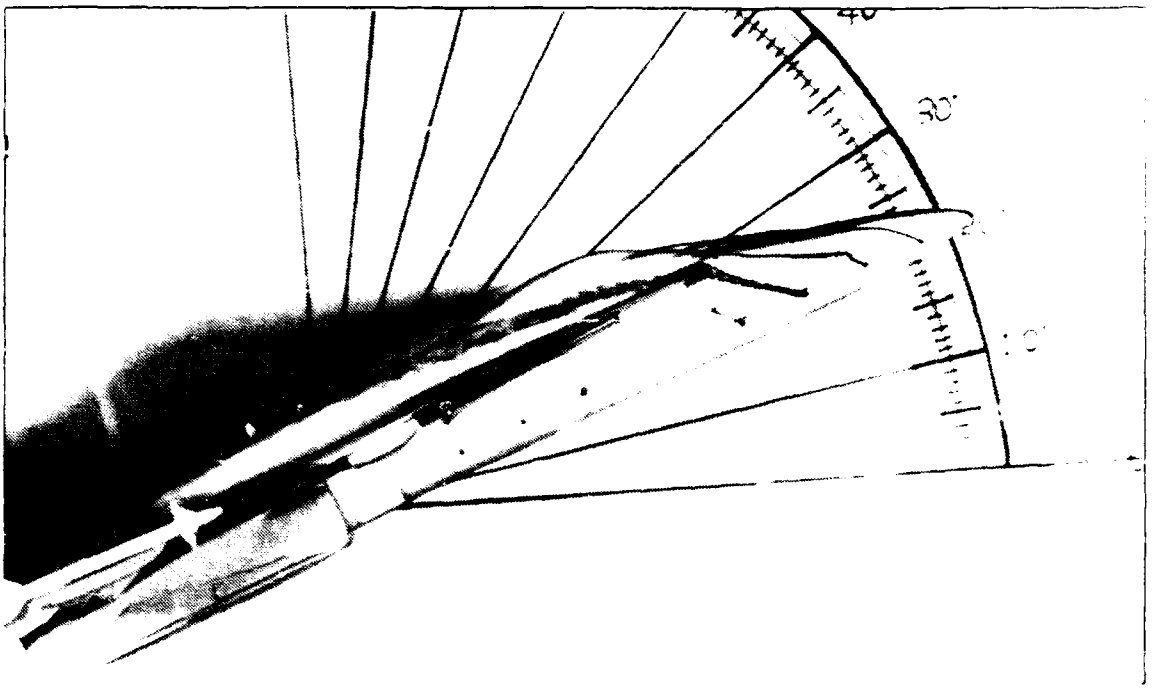

Figure 16. Forebody, Static, AOA = 20 deg , YAW = 0 deg.

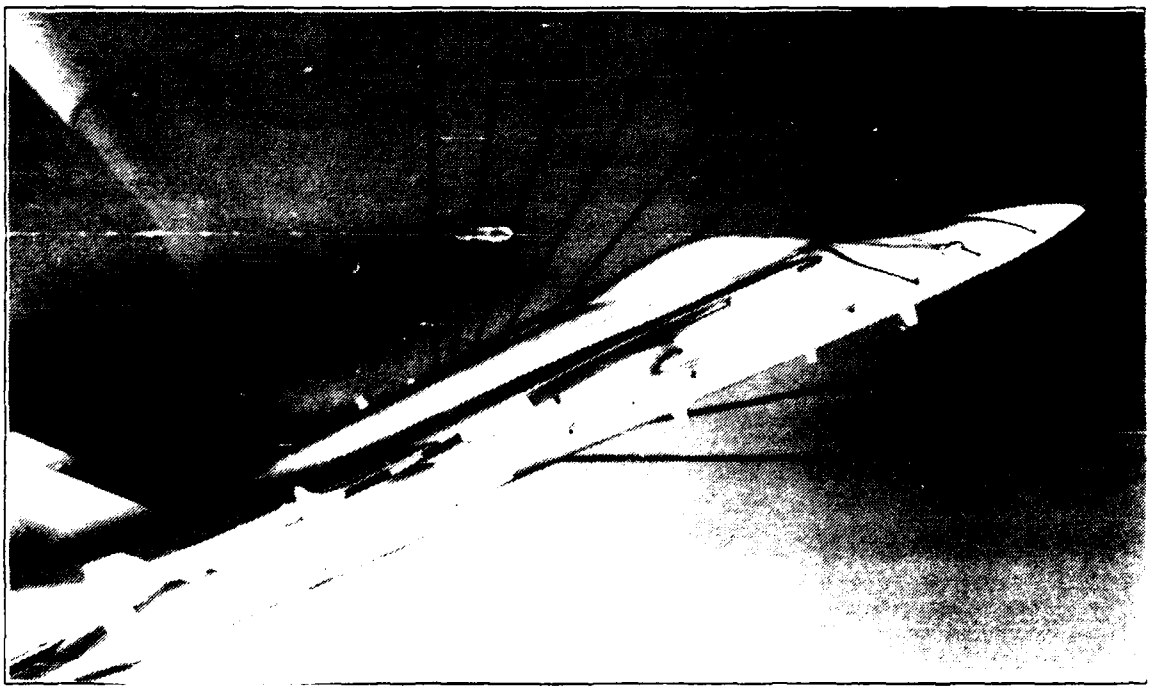

Figure 17. Forebody, Low Pitch Up, AOA = 20 deg , YAW = 0 deg.

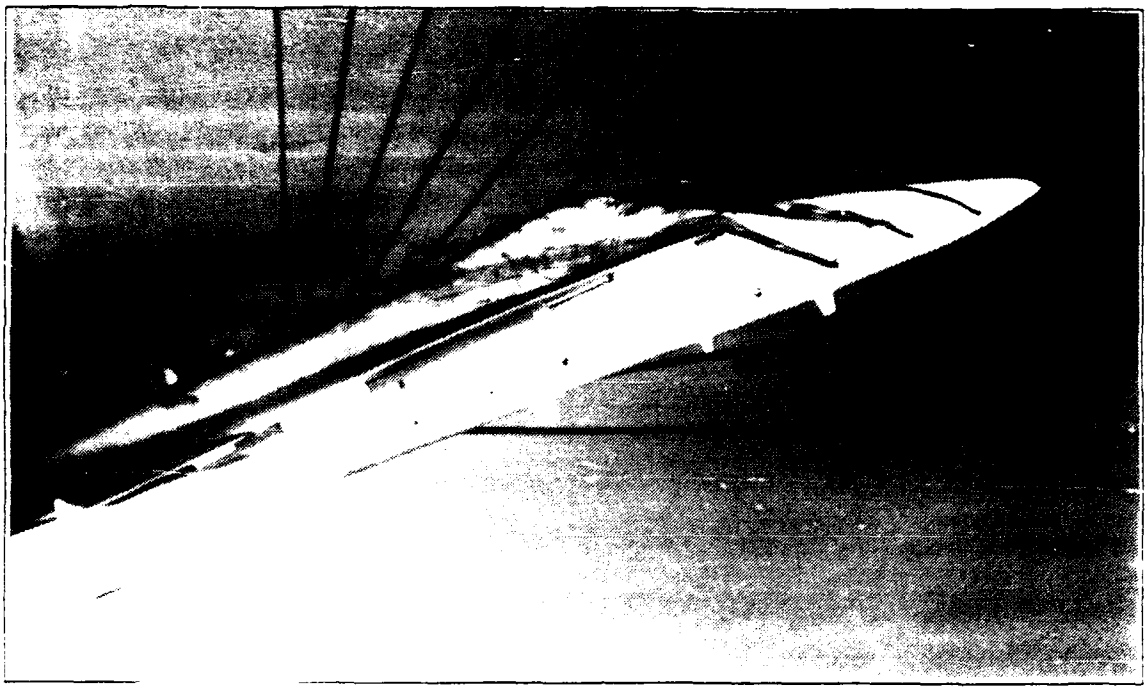

Figure 18. Forebody, Low Pitch Down, AOA = 20 deg , YAW = 0 deg.

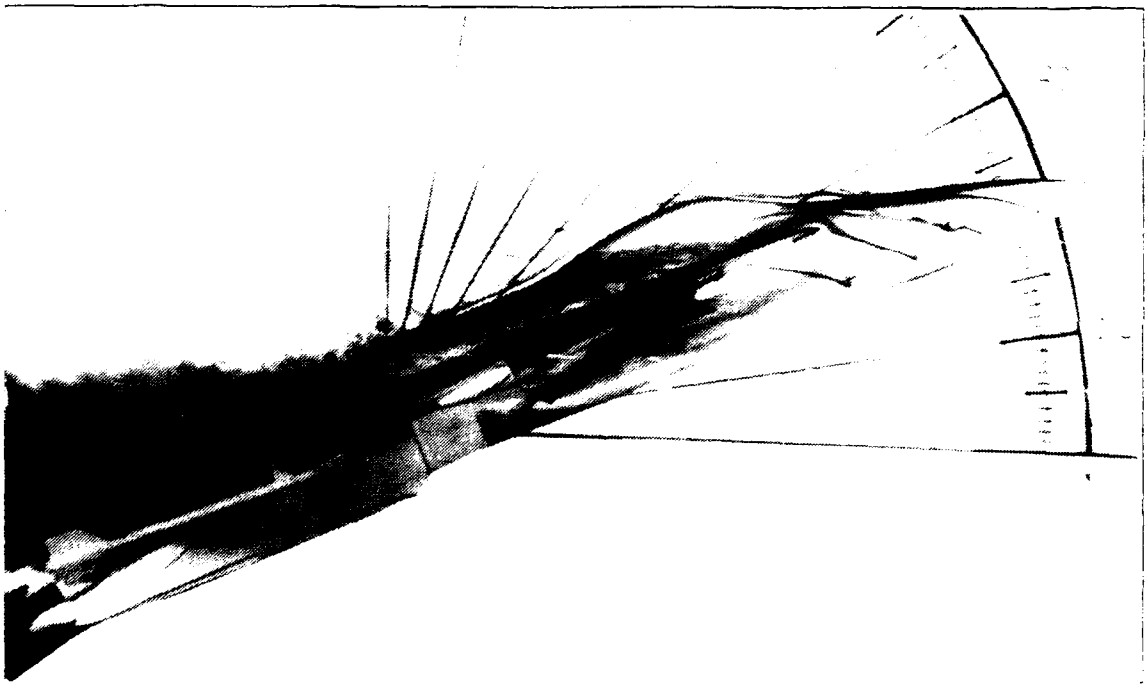

Figure 19. Forebody, High Pitch Up, AOA = 20 deg , YAW = 0 deg.

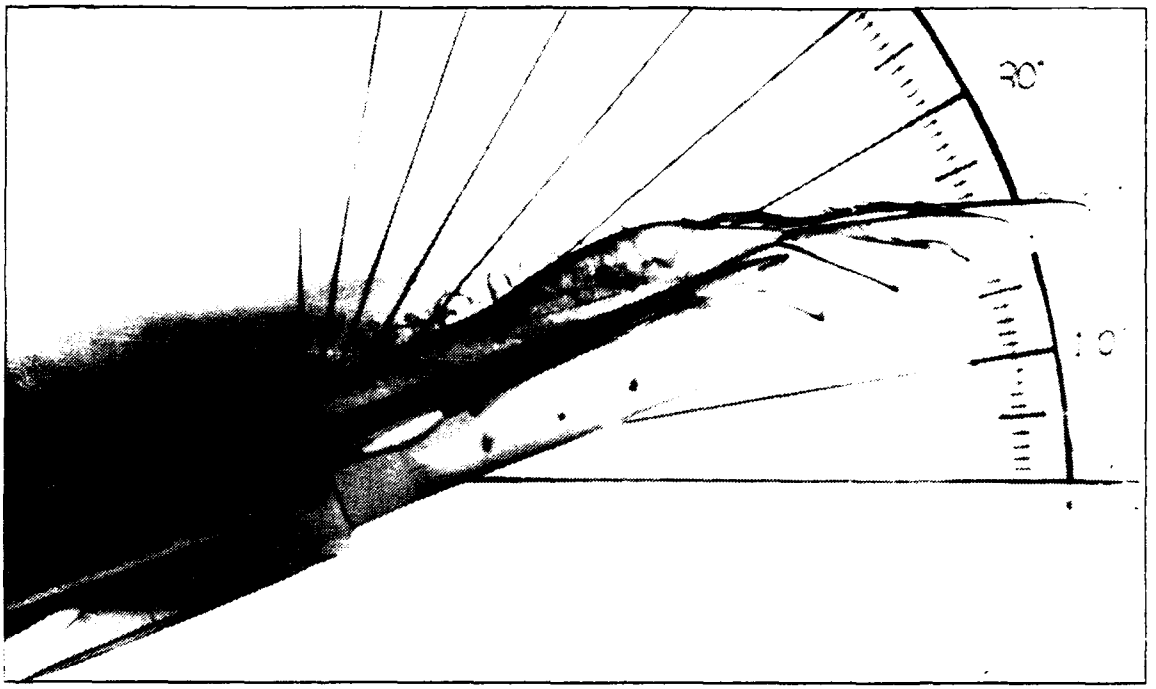

Figure 20. Forebody, High Pitch Down, AOA = 20 deg , YAW = 0 deg.

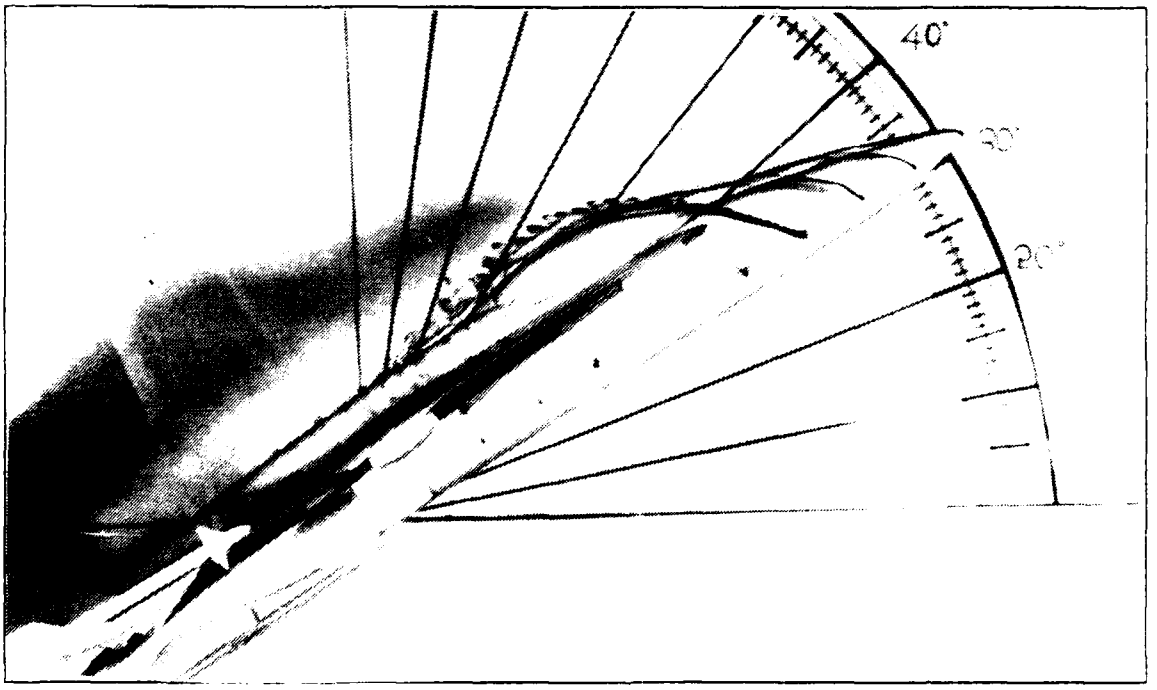

Figure 21. Forebody, Static, AOA = 30 deg , YAW = 0 deg.

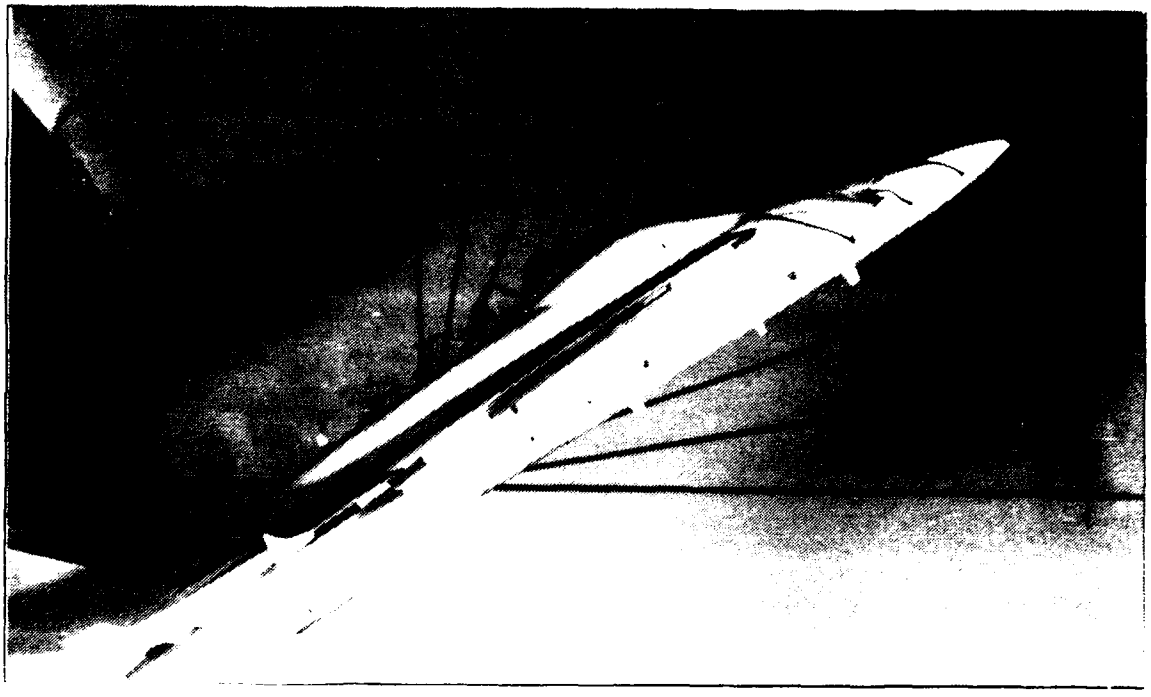

Figure 22. Forebody, Low Pitch Up, AOA = 30 deg , YAW = 0 deg.

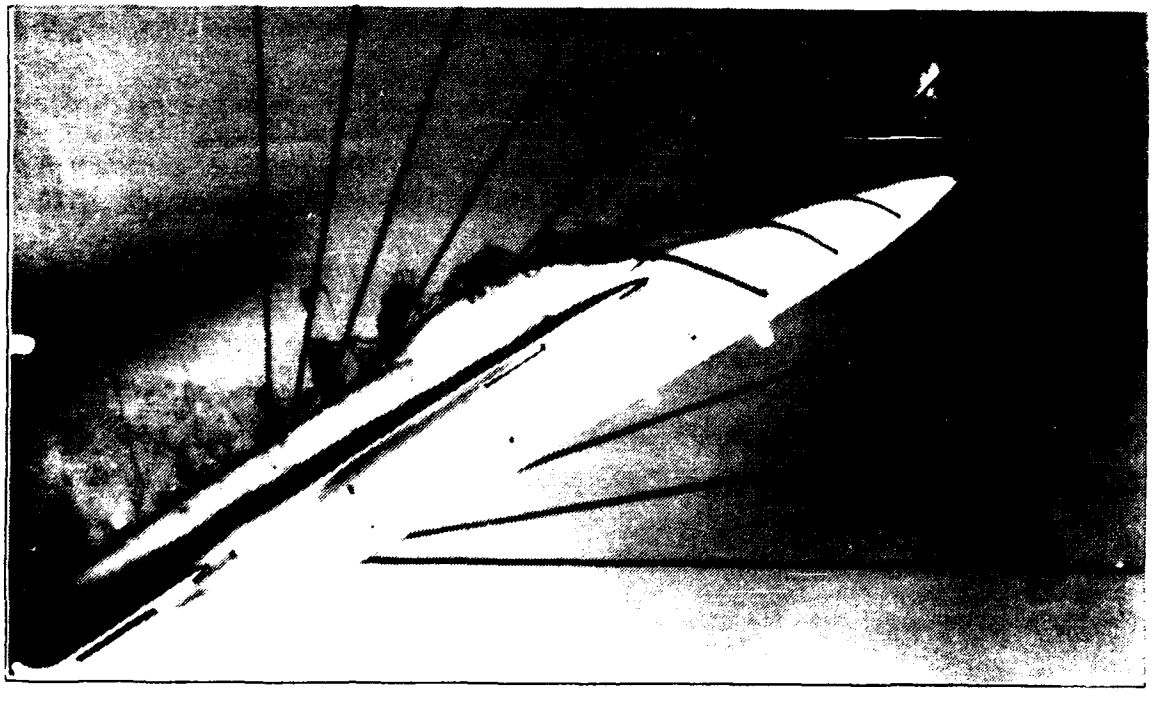

Figure 23. Forebody, Low Pitch Down, AOA = 30 deg , YAW = 0 deg.

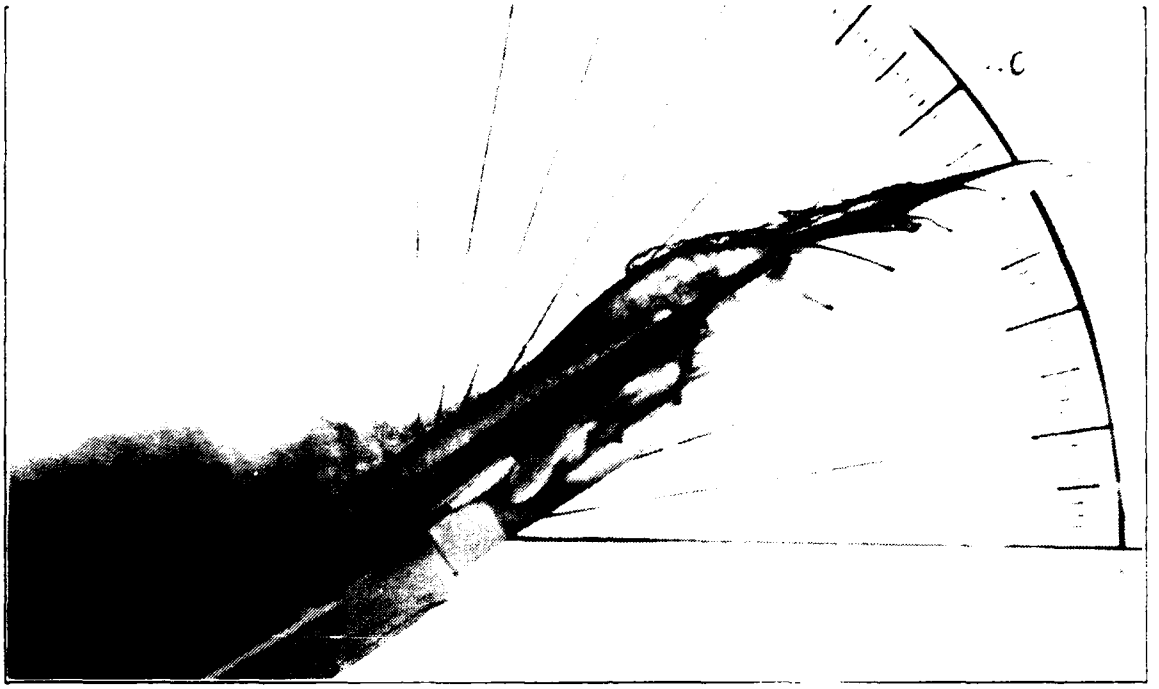

Figure 24. Forebody, High Pitch Up, AOA = 30 deg , YAW = 0 deg.

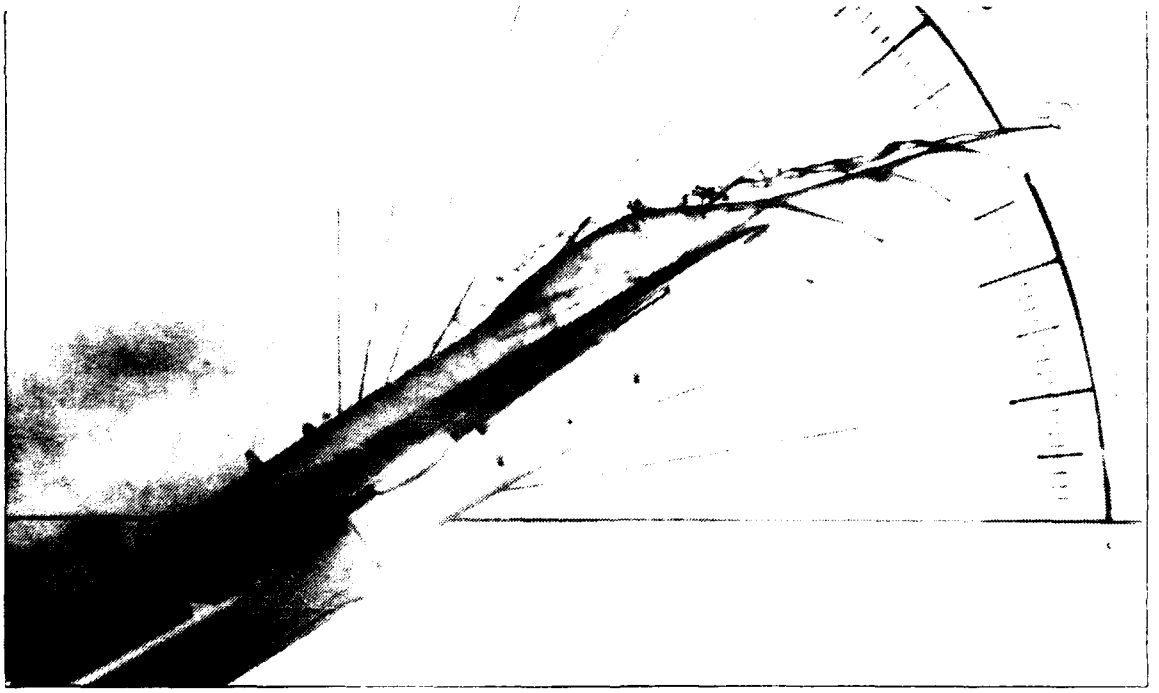

Figure 25. Forebody, High Pitch Down, AOA = 30 deg , YAW = 0 deg.

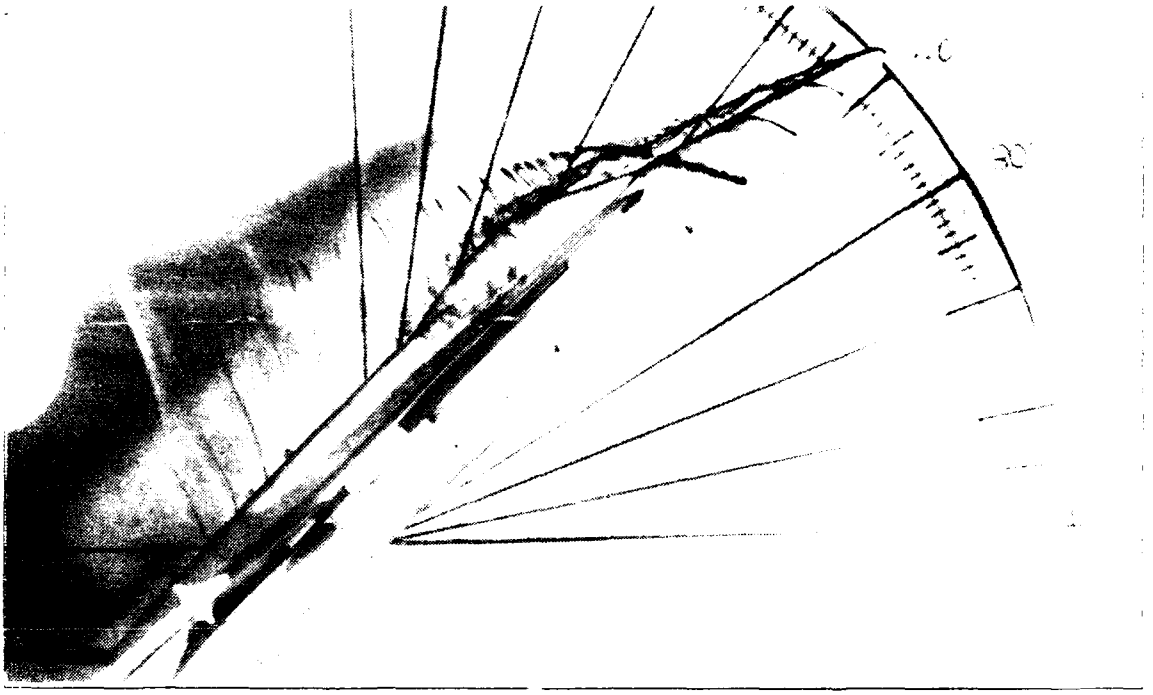

Figure 26. Forebody, Static, AOA = 40 deg , YAW = 0 deg.

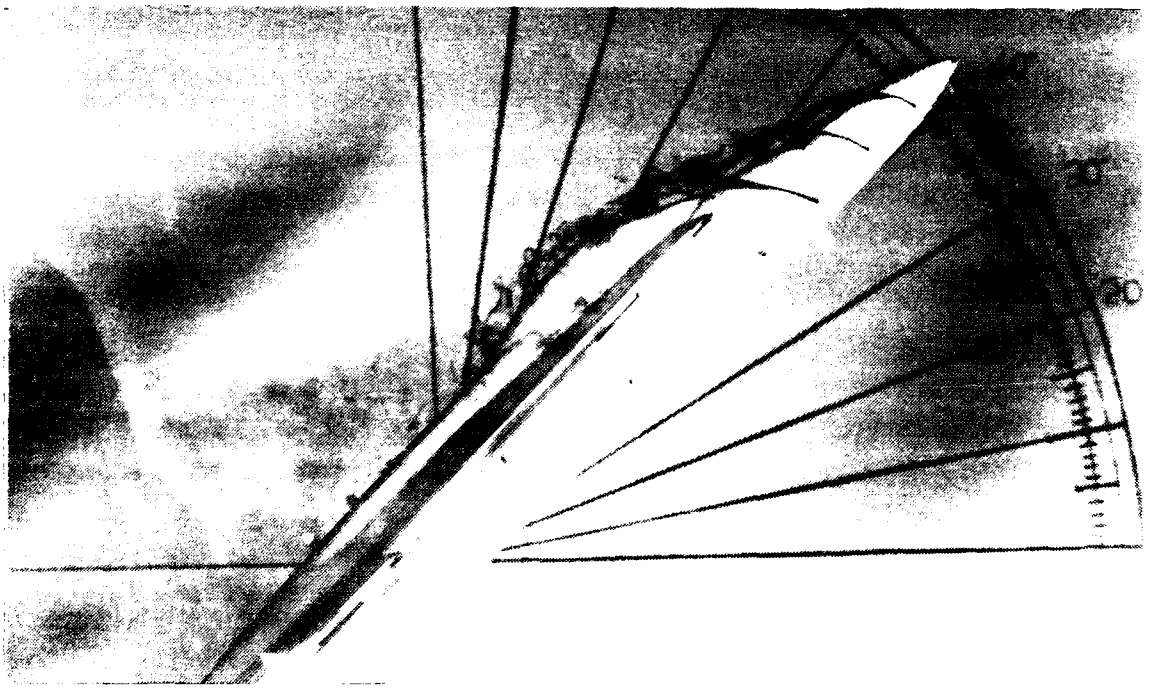

Figure 27. Forebody, Low Pitch Up, AOA = 40 deg , YAW = 0 deg.

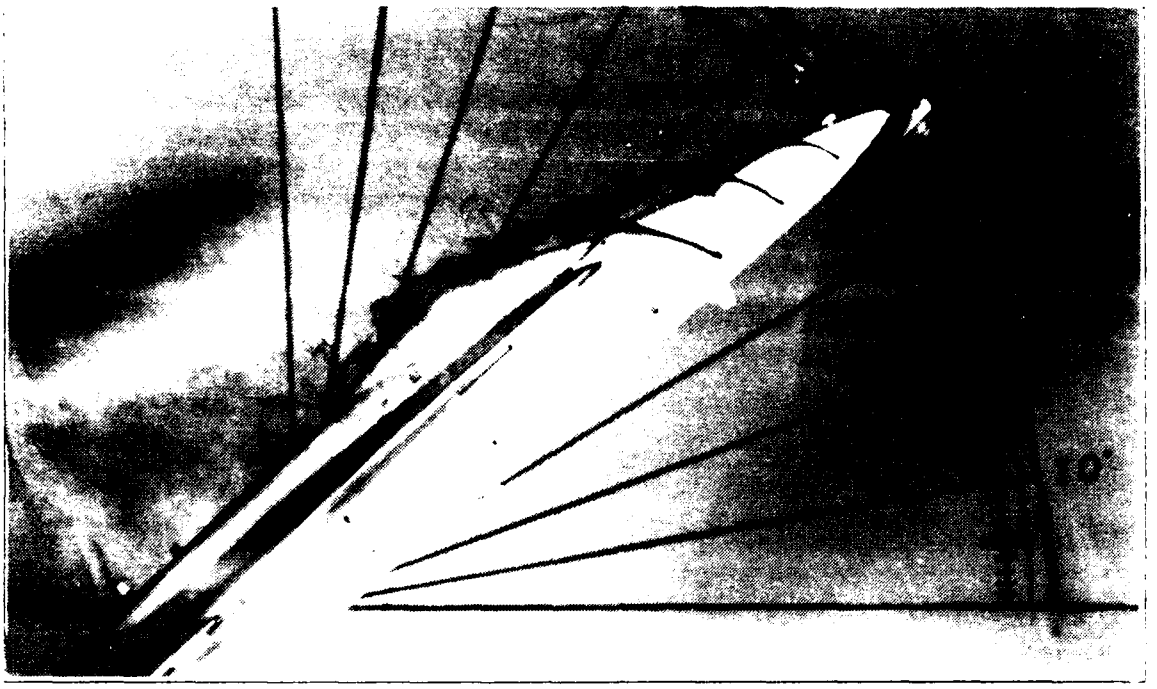

Figure 28. Forebody, Low Pitch Down, AOA = 40 deg , YAW = 0 deg.

Figure 29. Forebody, High Pitch Up, AOA = 40 deg , YAW = 0 deg.

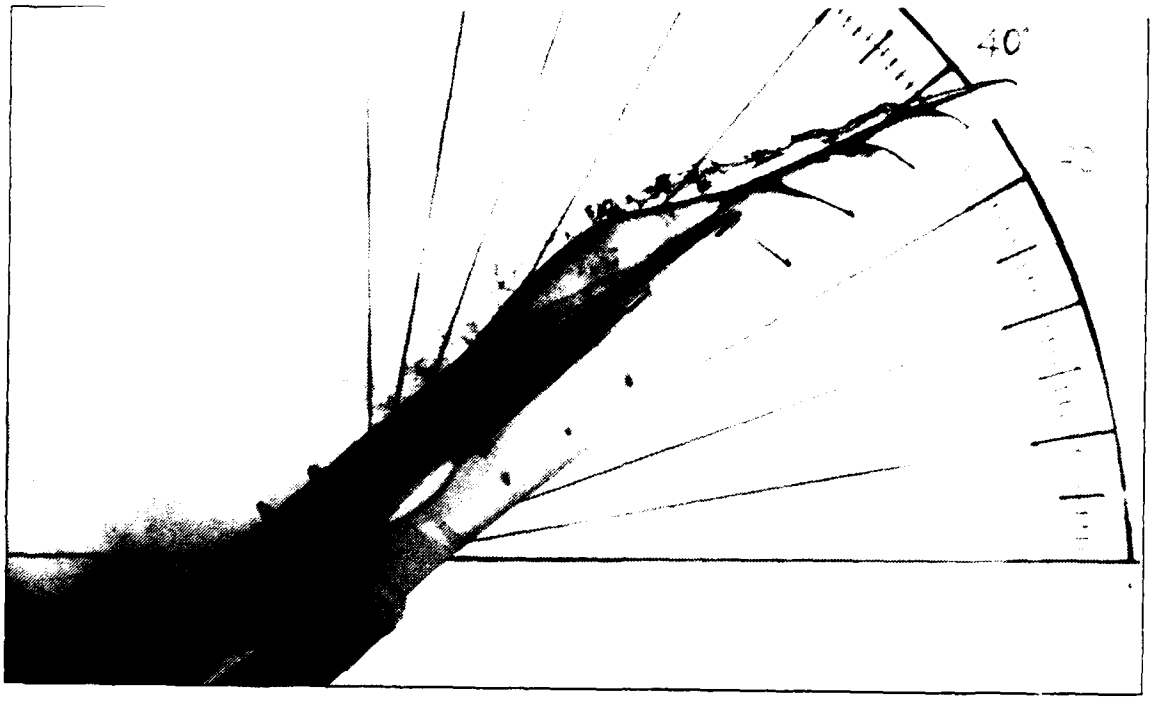

Figure 30. Forebody, High Pitch Down, AOA = 40 deg , YAW = 0 deg.

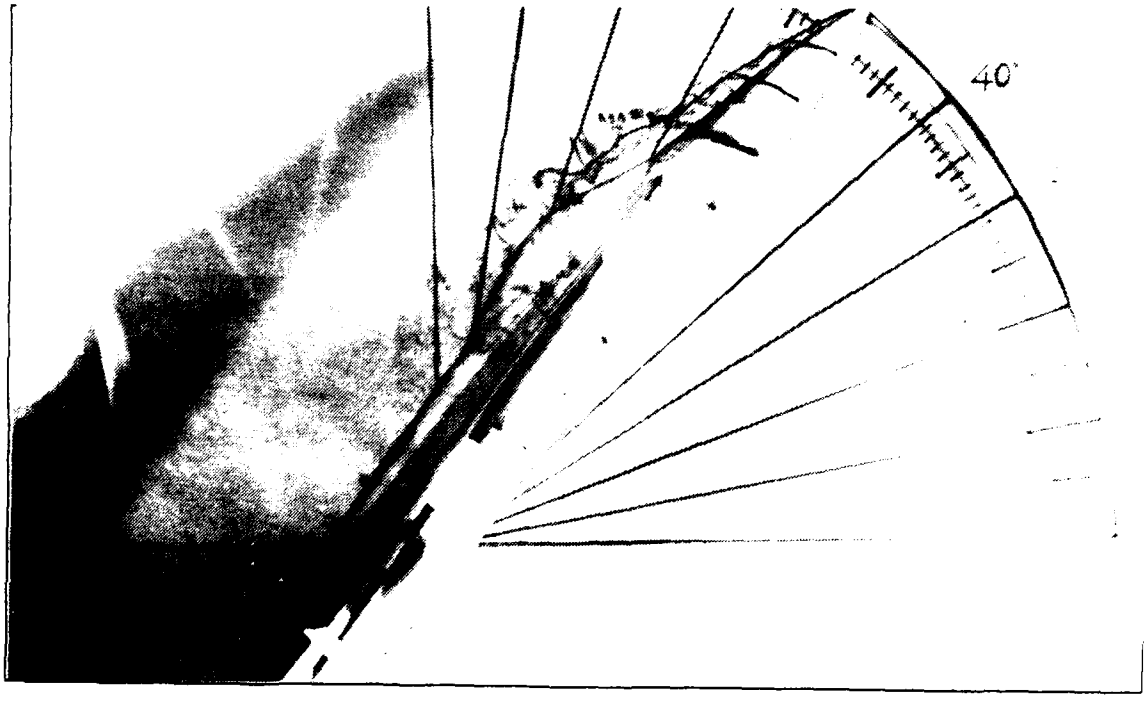

Figure 31. Forebody, Static, AOA = 50 deg , YAW = 0 deg.

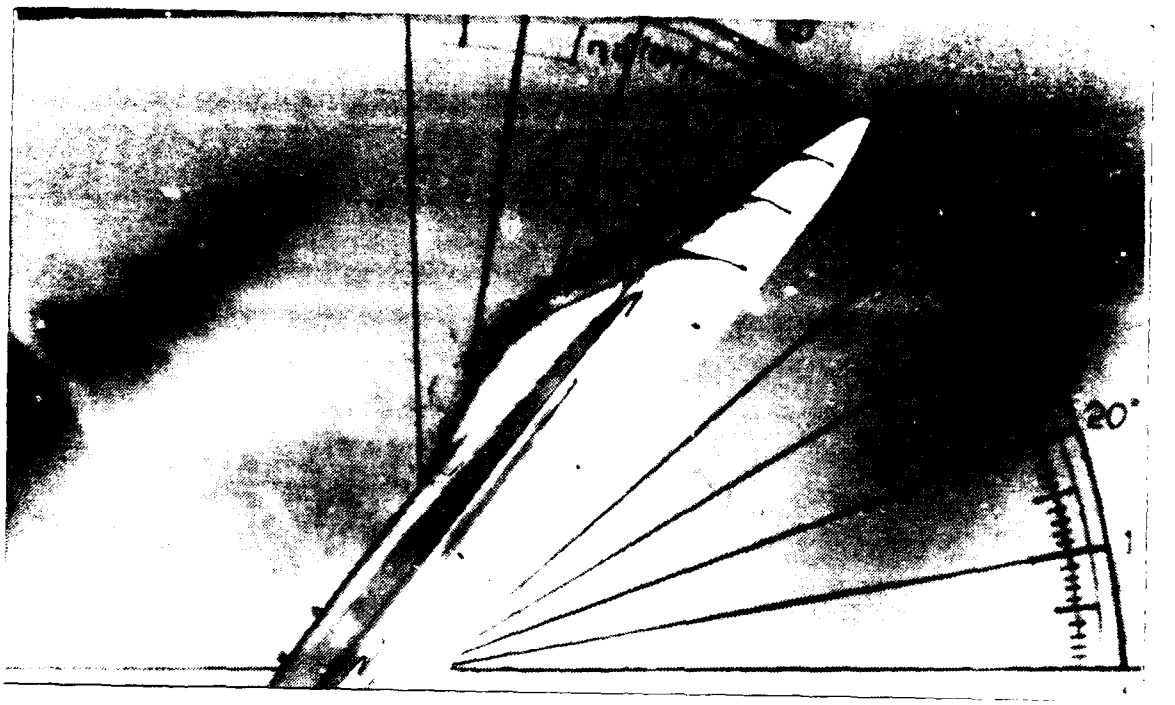

Figure 32. Forebody, Low Pitch Up, AOA = 50 deg , YAW = 0 deg.

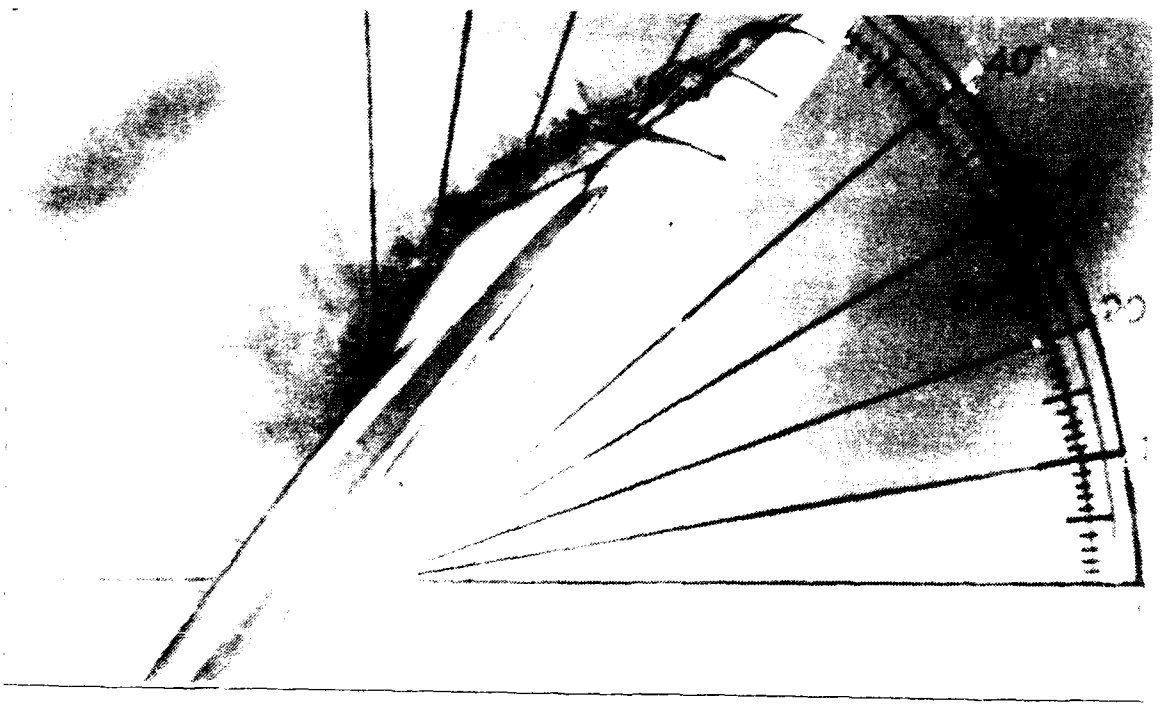

Figure 33. Forebody, Low Pitch Down, AOA = 50 deg , YAW = 0 deg.

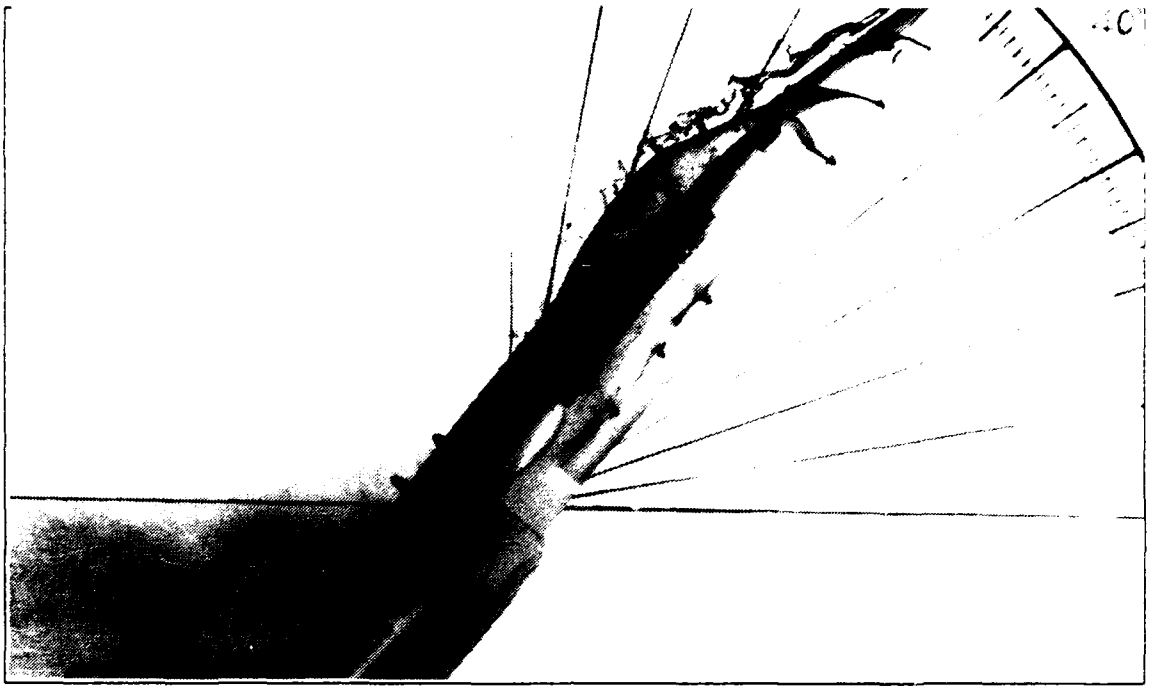

Figure 34. Forebody, High Pitch Up, AOA = 50 deg , YAW = 0 deg.

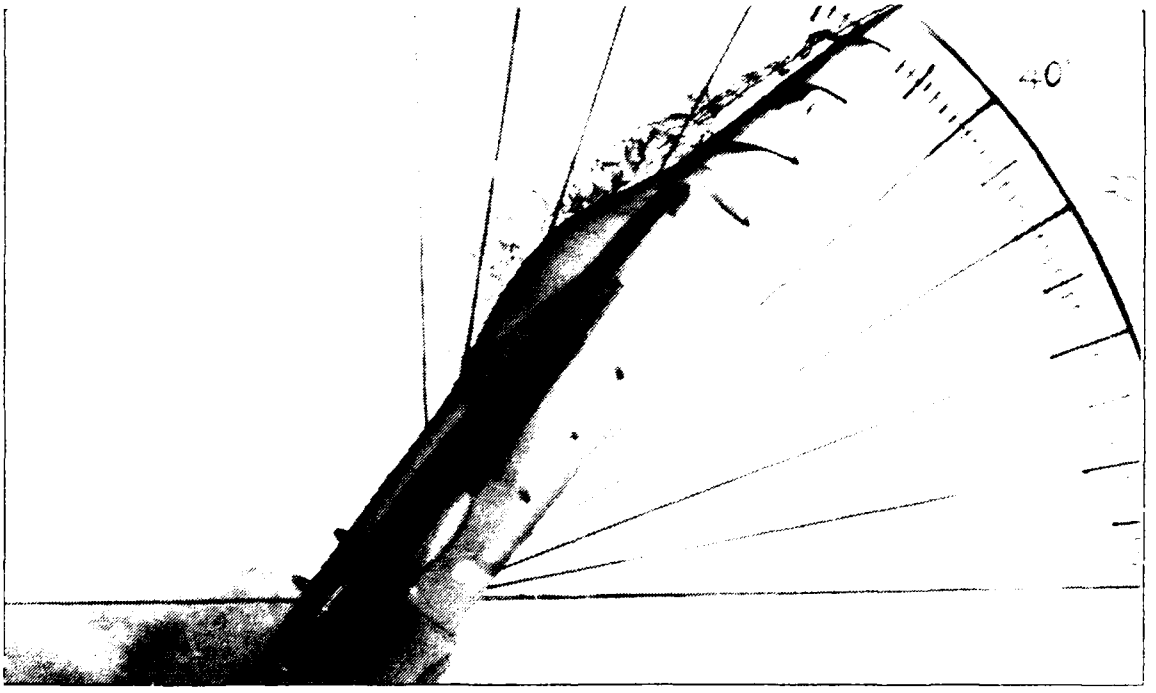

Figure 35. Forebody, High Pitch Down, AOA = 50 deg , YAW = 0 deg.

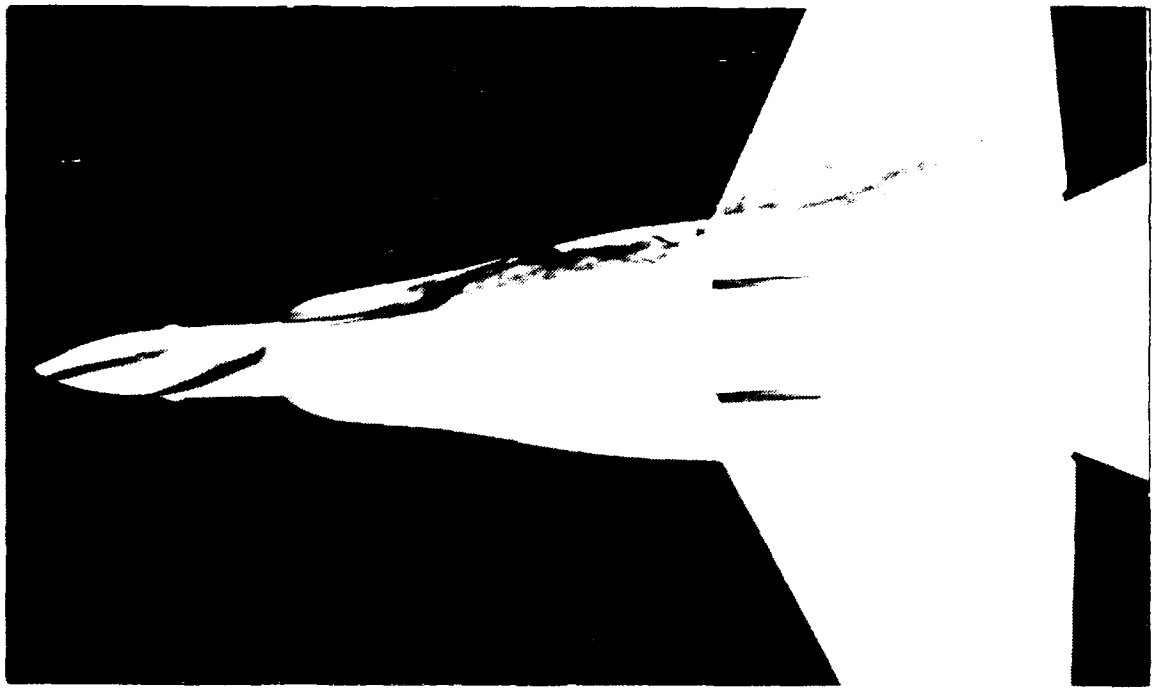

Figure 36. Forebody, Static, AOA = 10 deg, YAW = 5 deg.

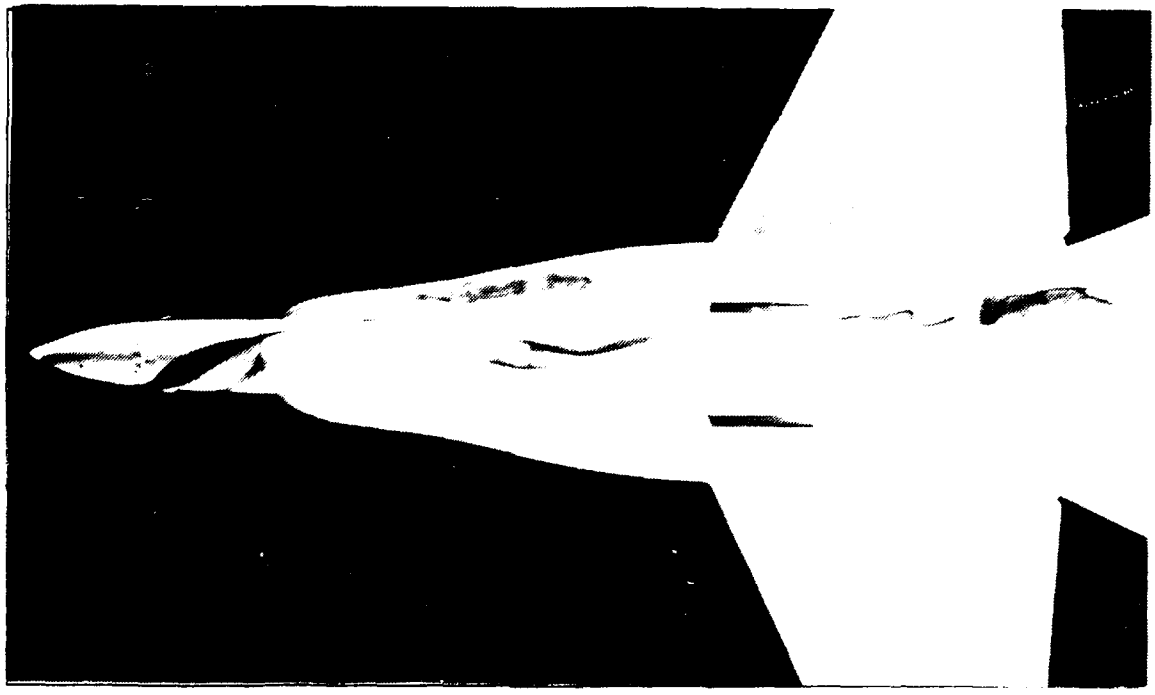

Figure 37. Forebody, Static, AOA = 10 deg, YAW = 10 deg.

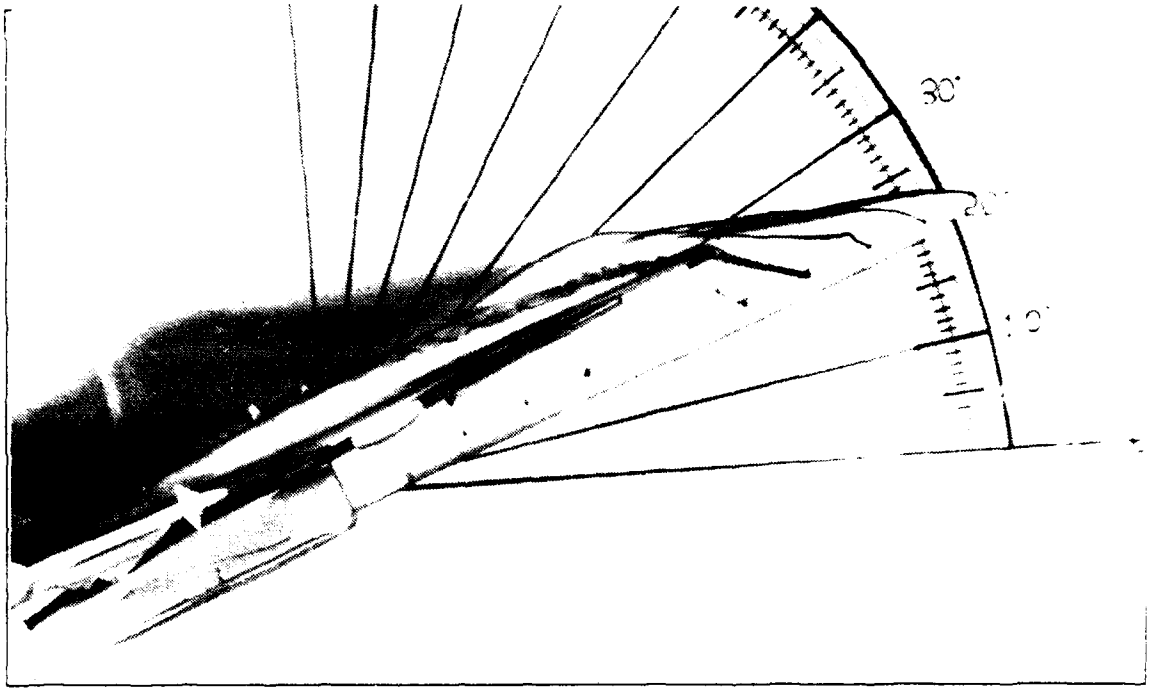

Figure 38. Forebody, Static, AOA = 20 deg, YAW = 0 deg.

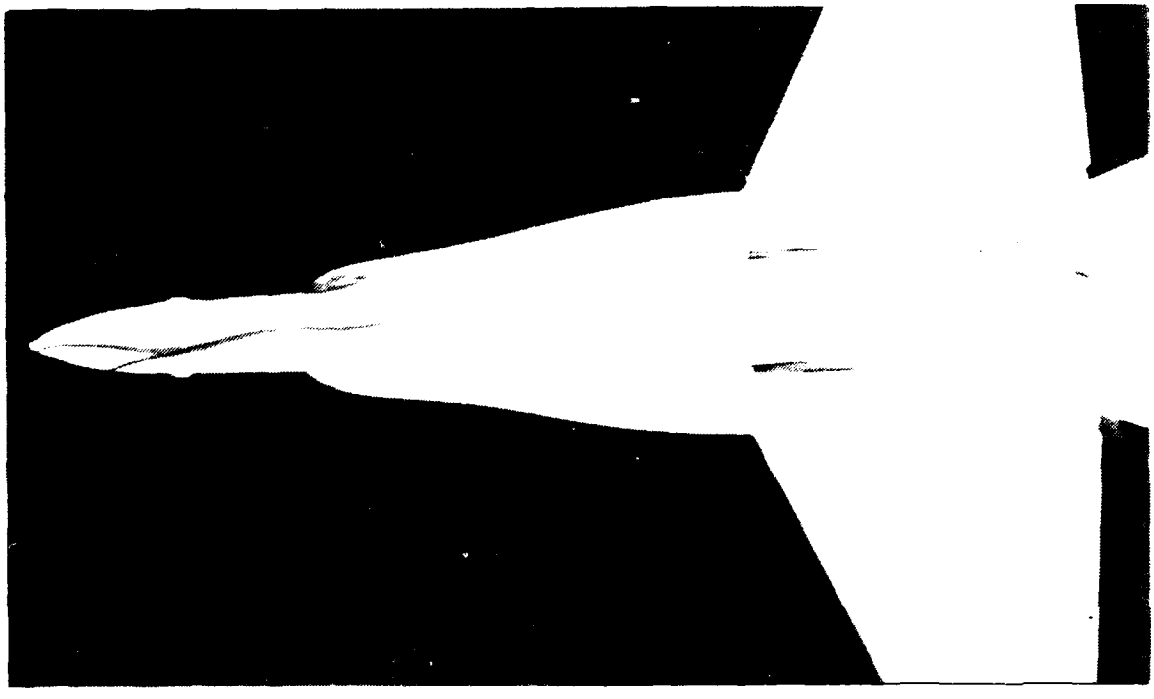

Figure 39. Forebody, Static, AOA = 20 deg, YAW = 5 deg.

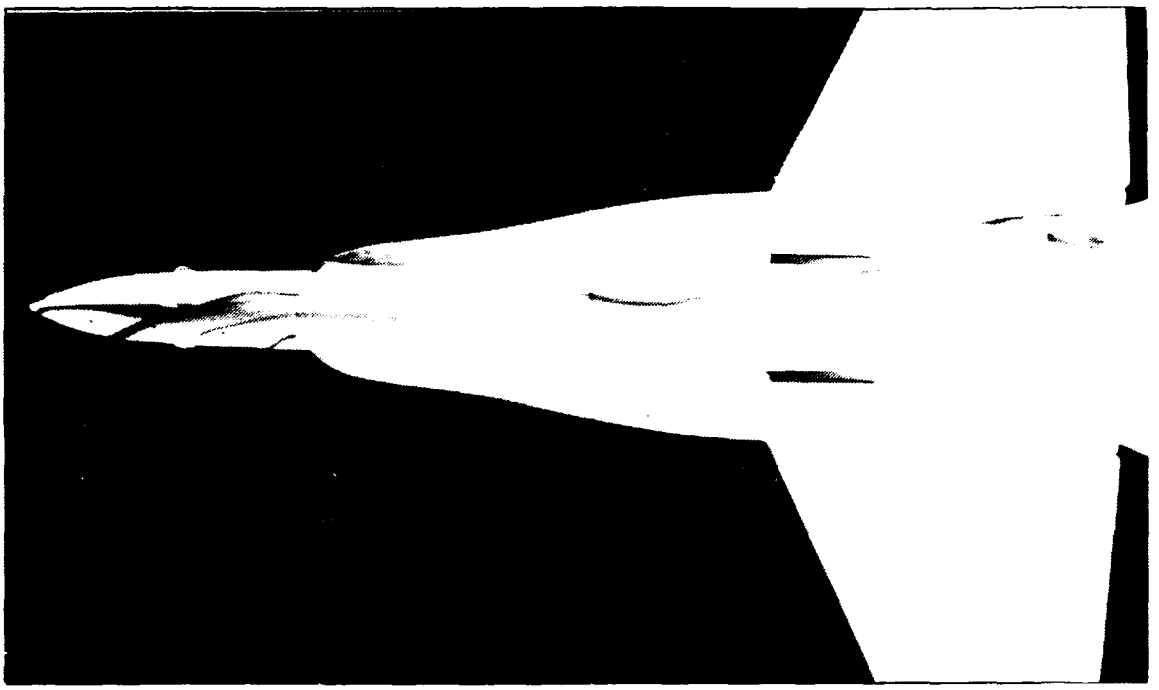

Figure 40. Forebody, Static, AOA = 20 deg , YAW = 10 deg.

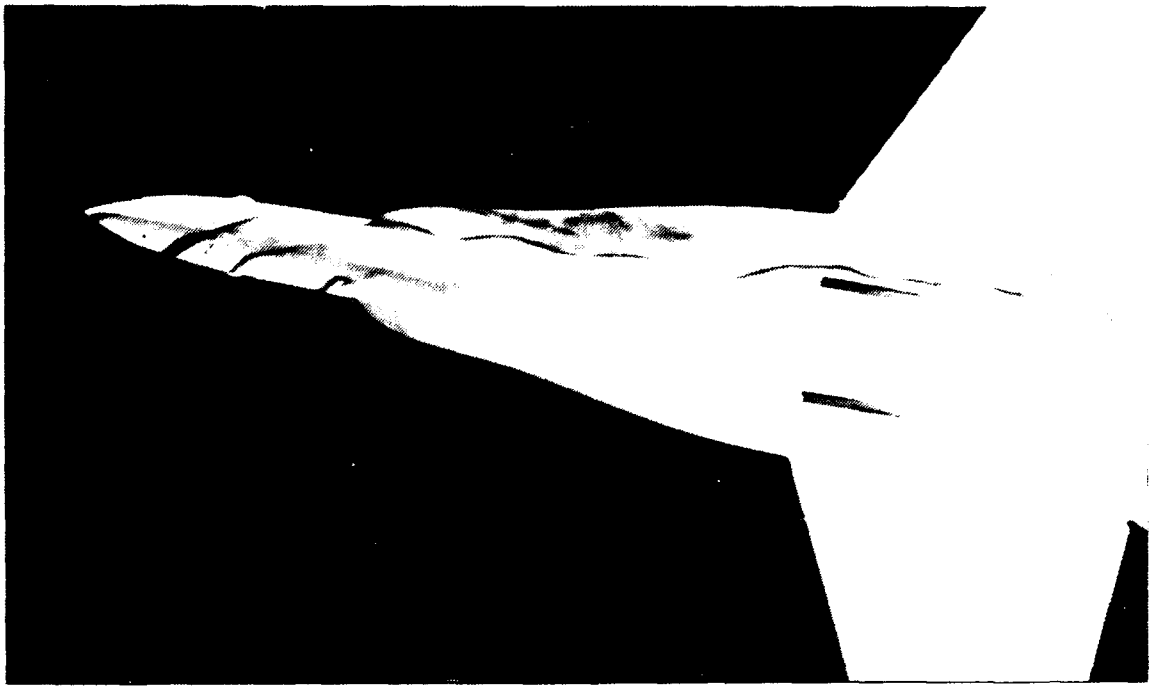

Figure 41. Forebody, Static, AOA = 20 deg , YAW = 20 deg.

Figure 42. Forebody, Static, AOA = 40 deg , YAW = 0 deg.

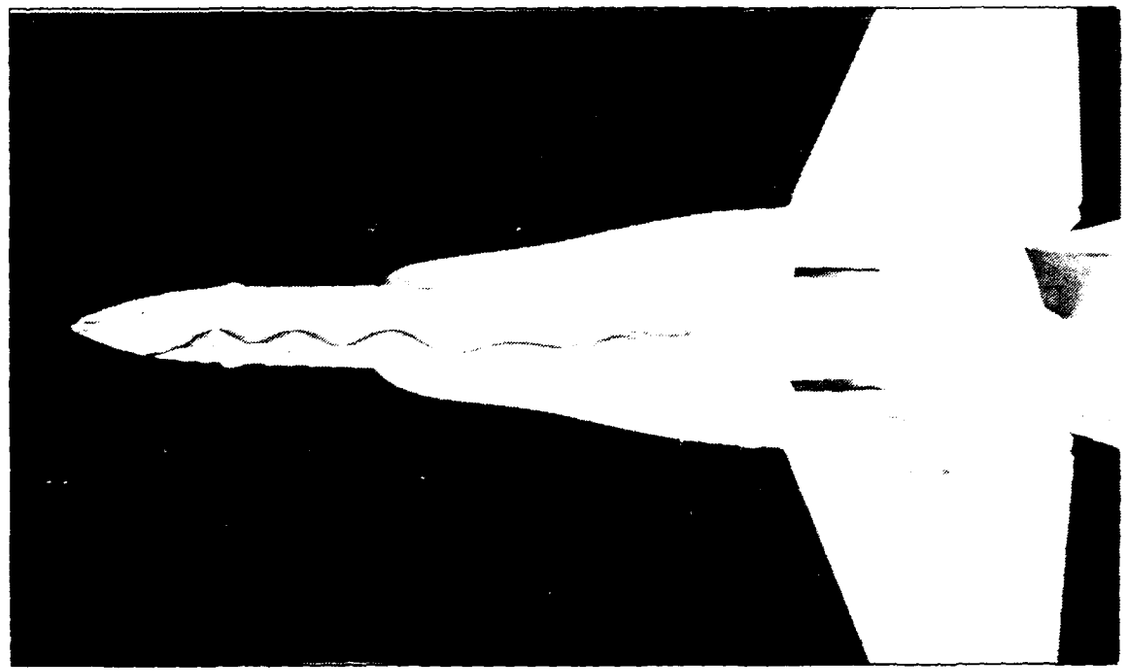

Figure 43. Forebody, Static, AOA = 40 deg , YAW = 5 deg.

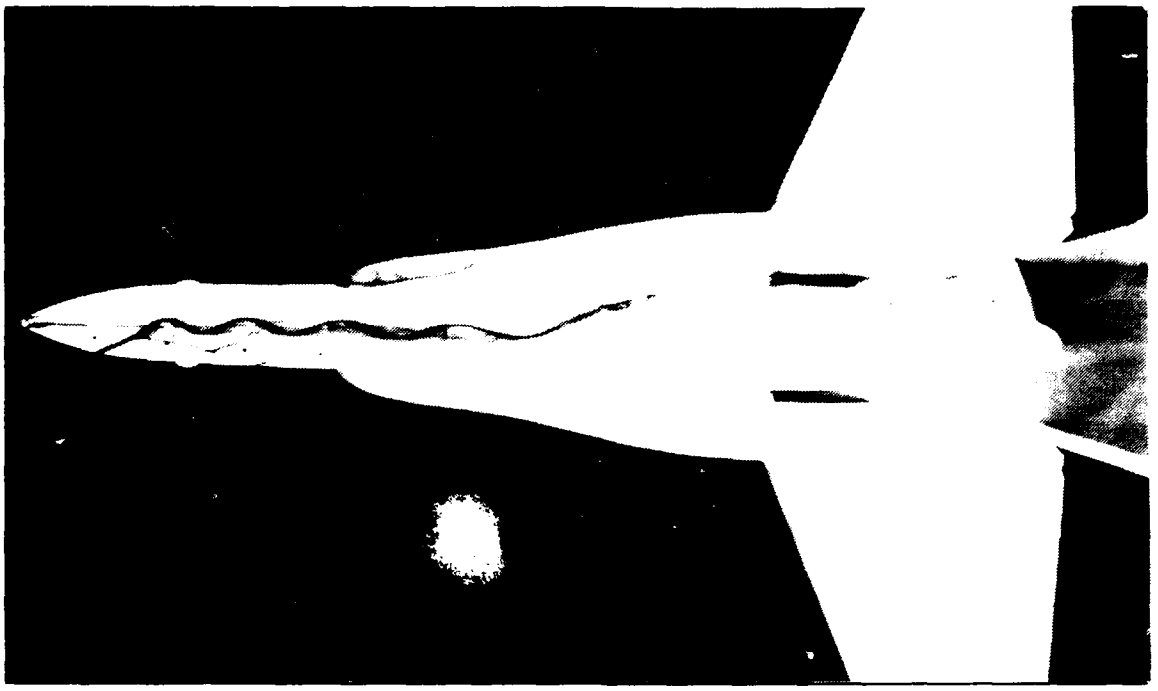

Figure 44. Forebody, Static, AOA = 40 deg , YAW = 10 deg.

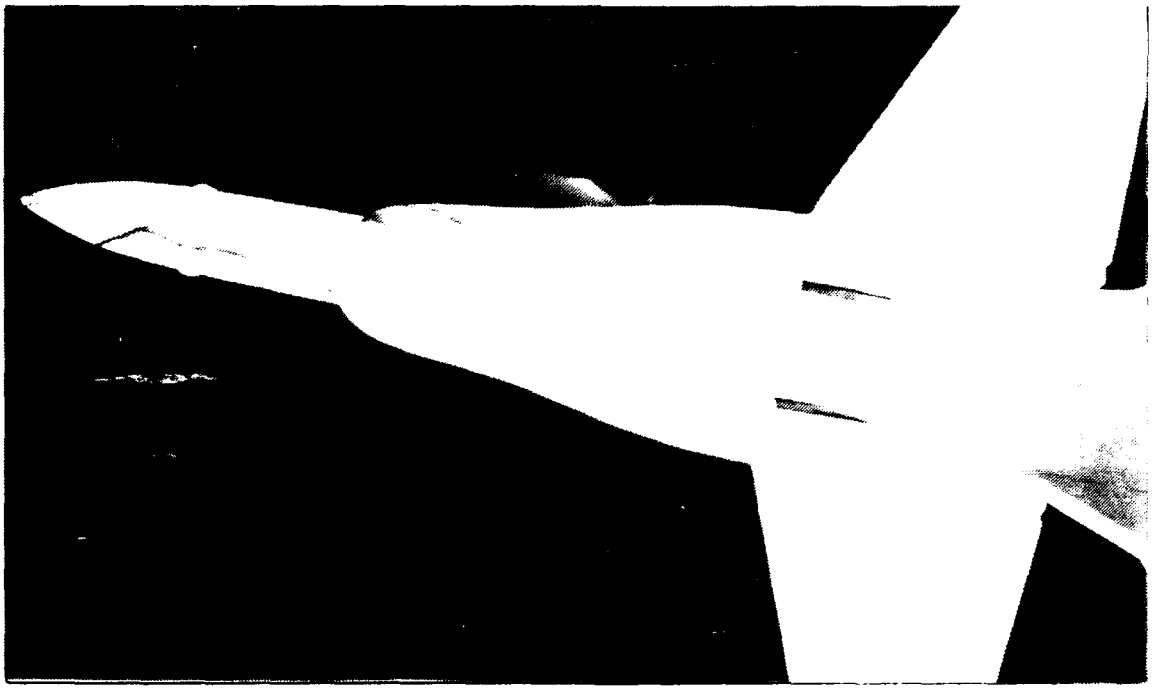

Figure 45. Forebody, Static, AOA = 40 deg , YAW = 20 deg.

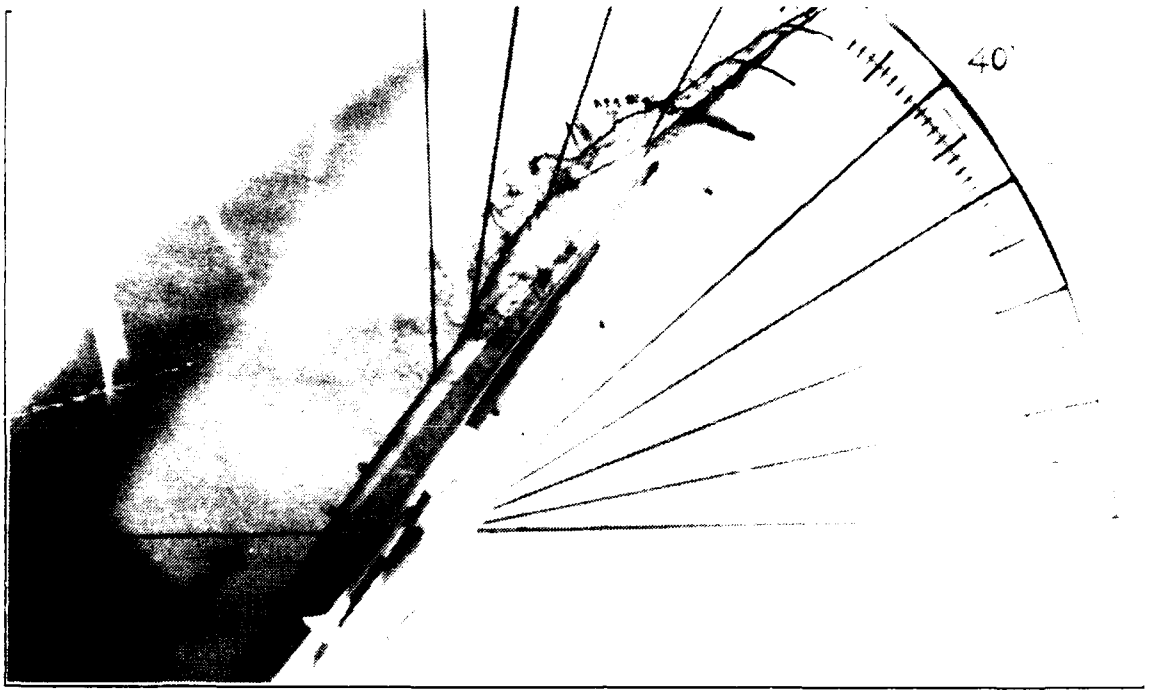

Figure 46. Forebody, Static, AOA = 50 deg , YAW = 0 deg.

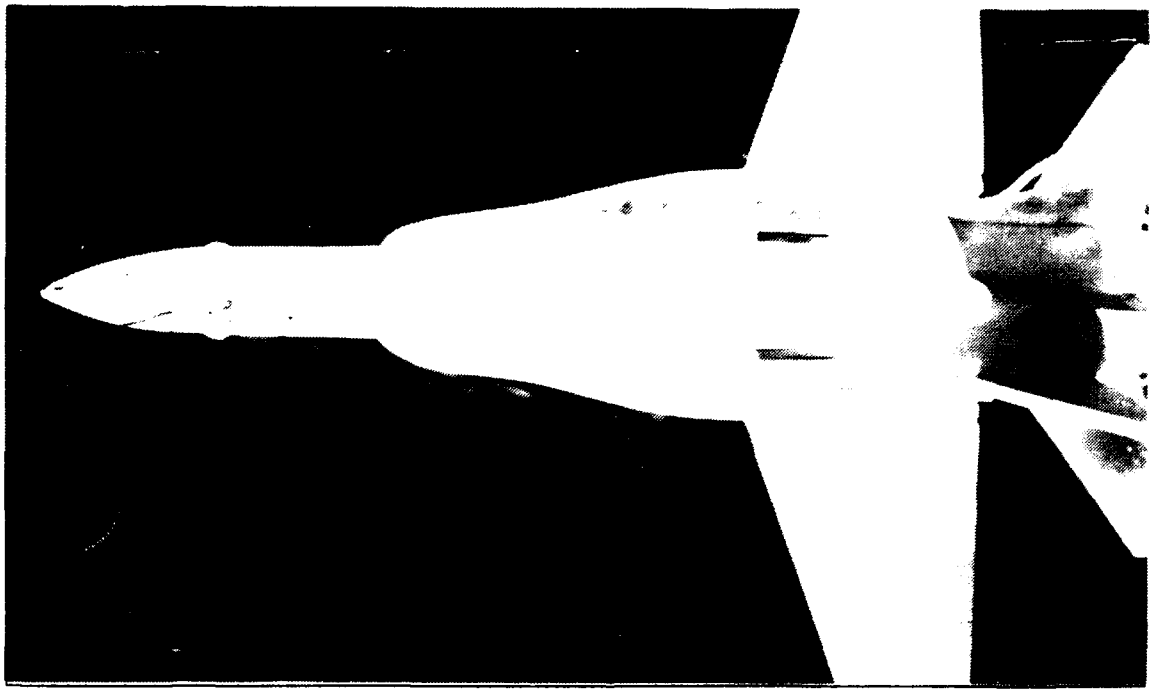

Figure 47. Forebody, Static, AOA = 50 deg , YAW = 5 deg.

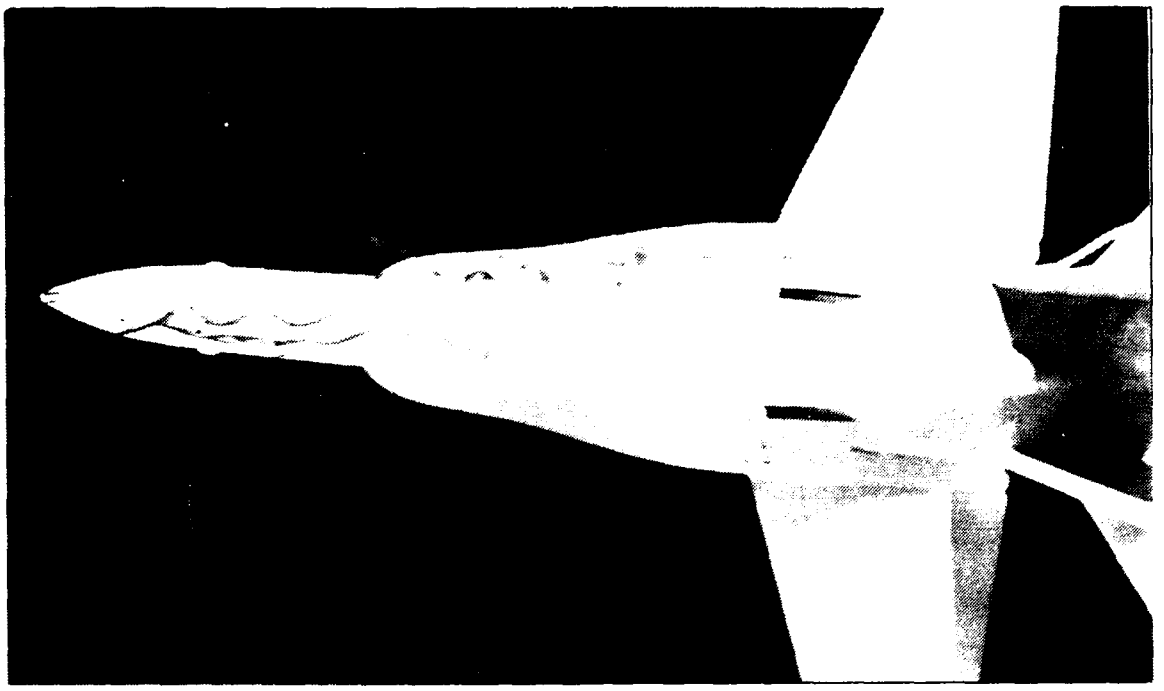

Figure 48. Forebody, Static, AOA = 50 deg , YAW = 10 deg.

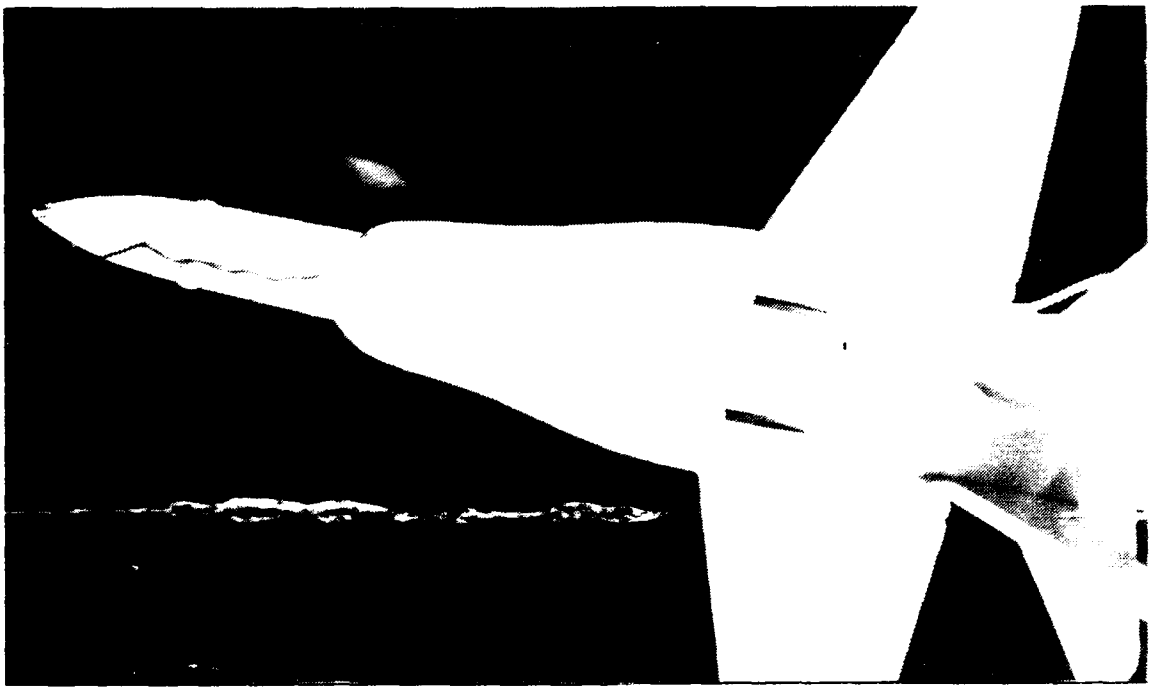

Figure 49. Forebody, Static, AOA = 50 deg , YAW = 20 deg.

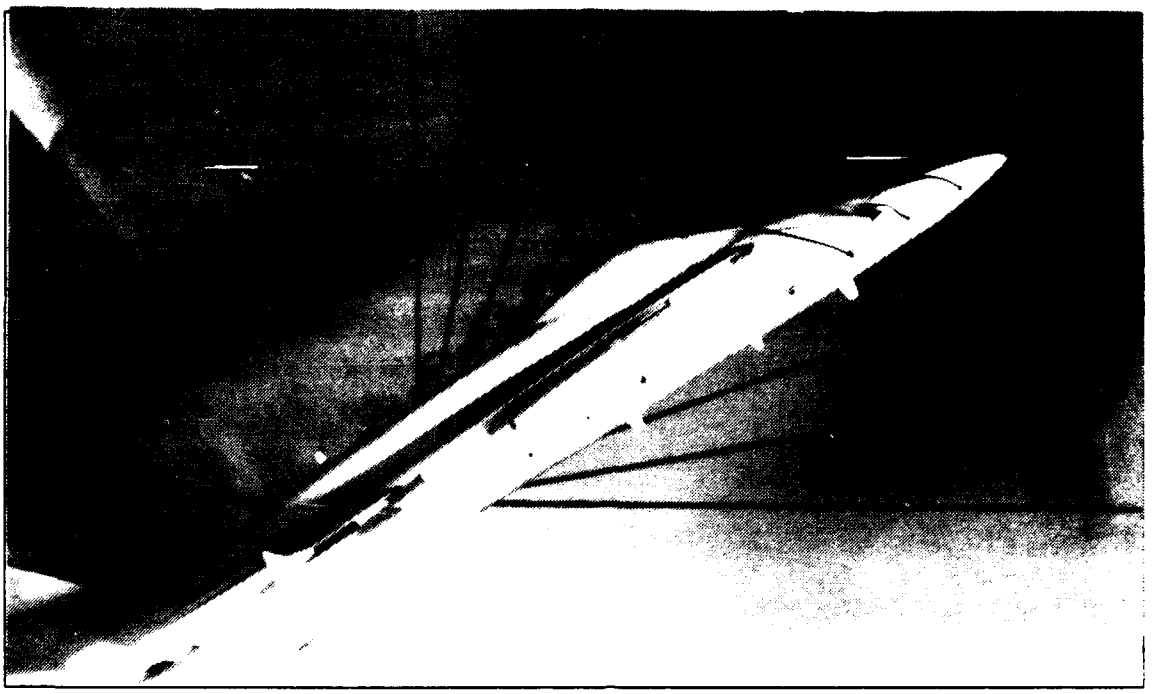

Figure 50. Forebody, Low Pitch Up, AOA = 30 deg , YAW = 0 deg.

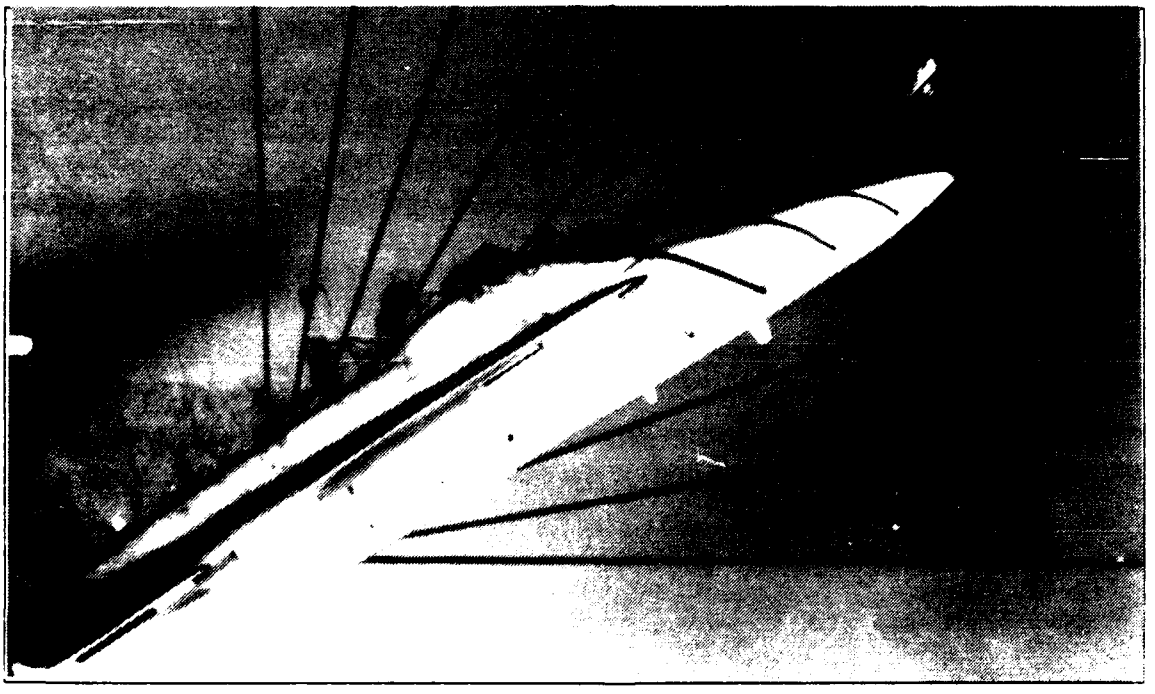

Figure 51. Forebody, Low Pitch Down, AOA = 30 deg , YAW = 0 deg.

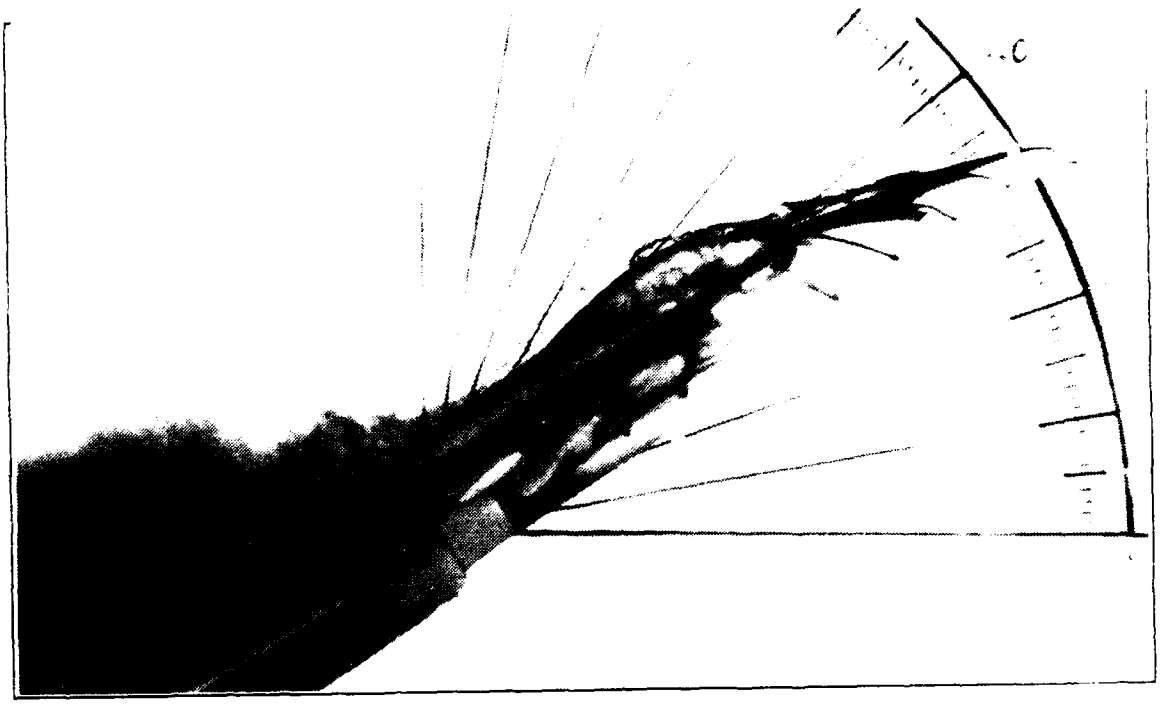

Figure 52. Forebody, High Pitch Up, AOA = 30 deg , YAW = 0 deg.

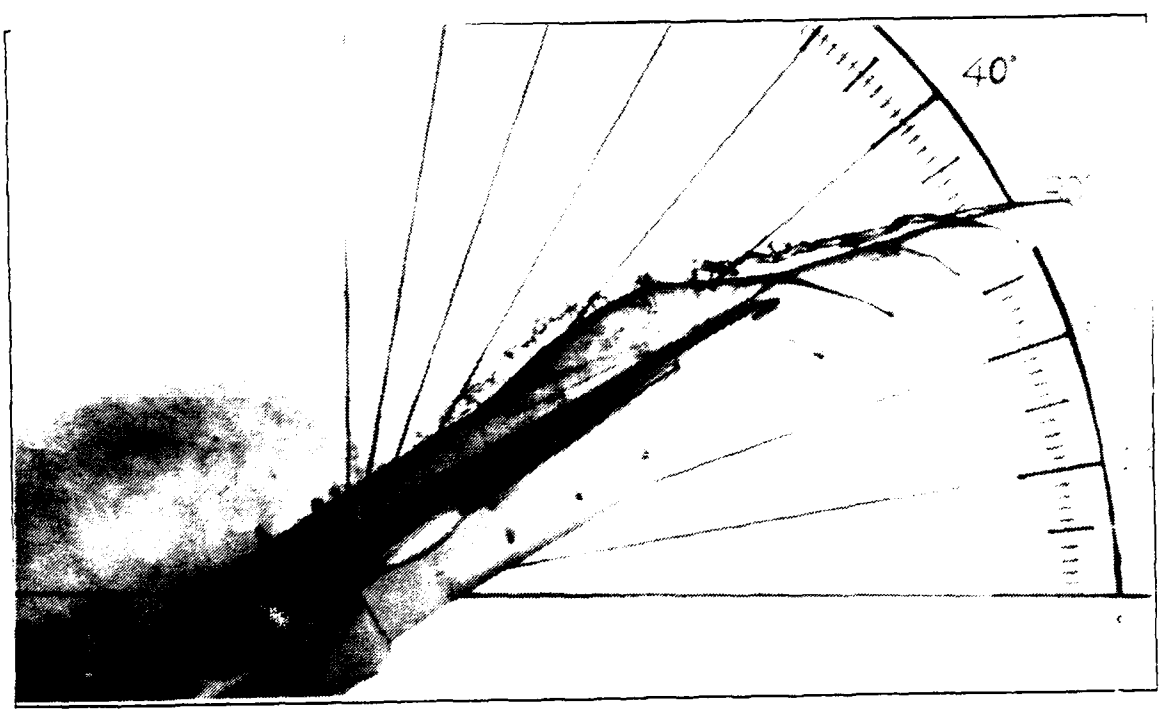

Figure 53. Forebody, High Pitch Down, AOA = 30 deg , YAW = 0 deg.

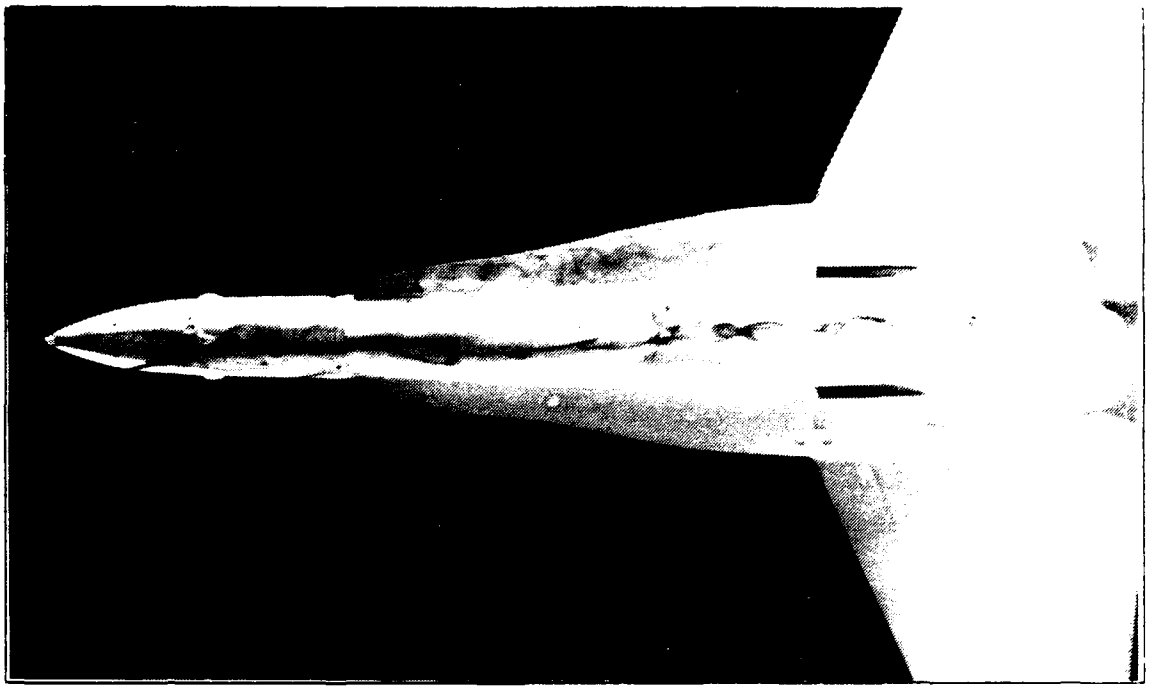

Figure 54. Forebody, Low Pitch Up, AOA = 30 deg , YAW = 5 deg.

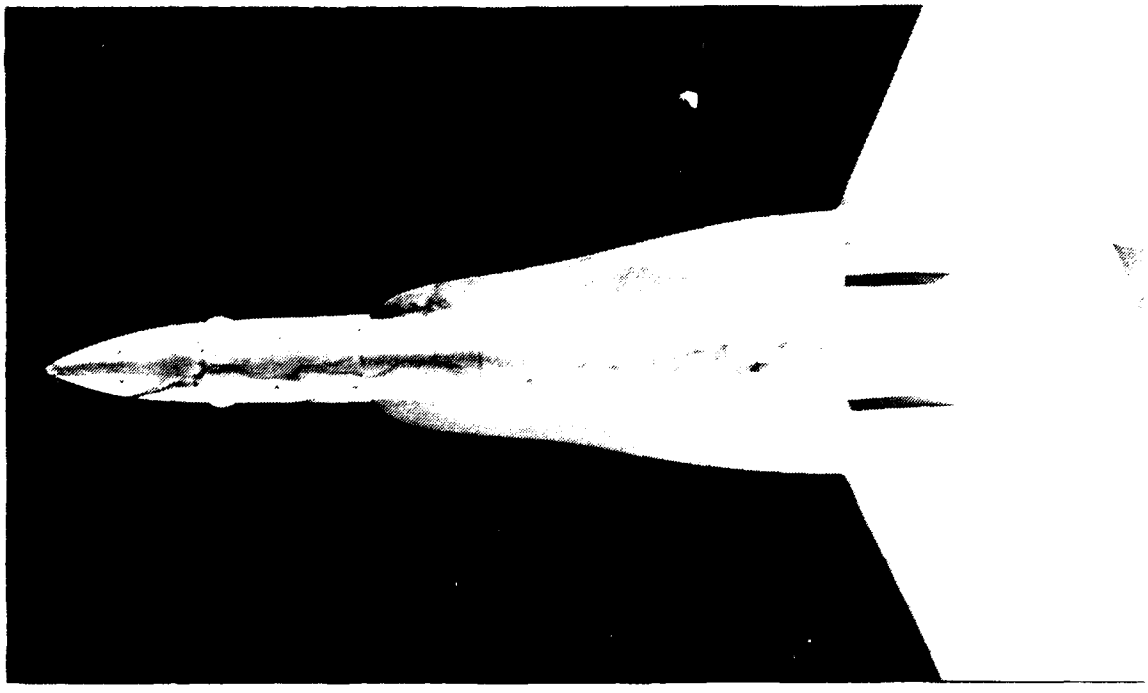

Figure 55. Forebody, Low Pitch Down, AOA = 30 deg , YAW = 5 deg.

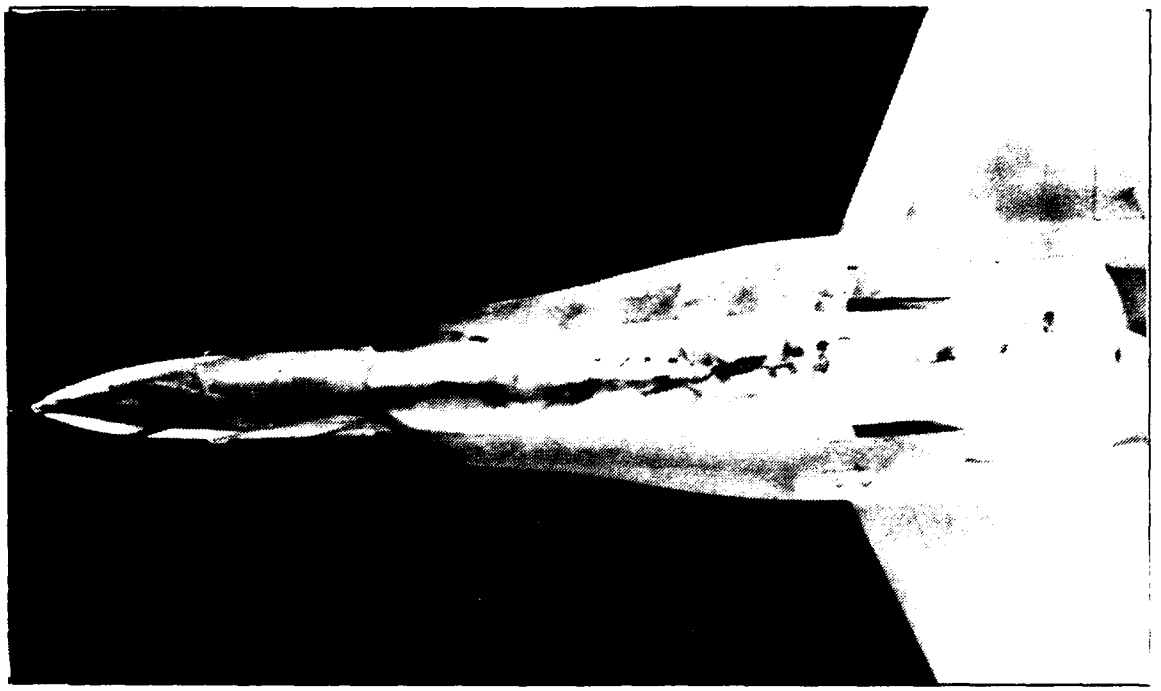

Figure 56. Forebody, High Pitch Up, AOA = 30 deg , YAW = 5 deg.

Figure 57. Forebody, High Pitch Down, AOA = 30 deg , YAW = 5 deg.

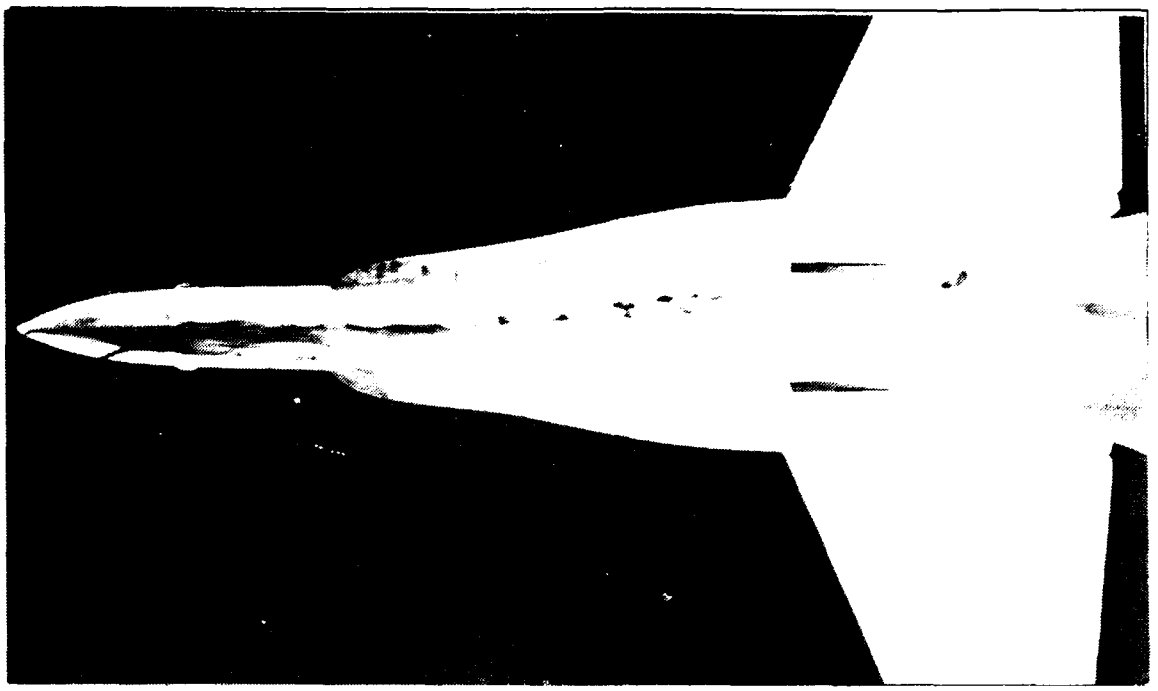

Figure 58. Forebody, Low Pitch Up, AOA = 30 deg , YAW = 10 deg.

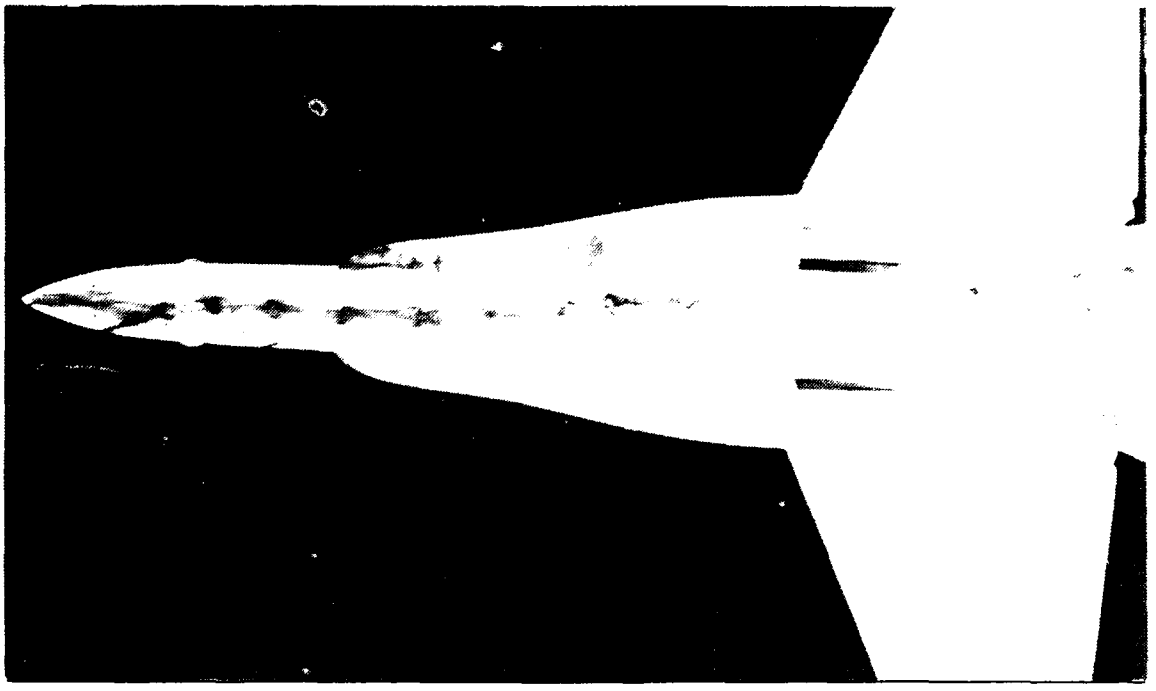

Figure 59. Forebody, Low Pitch Down, AOA = 30 deg , YAW = 10 deg.

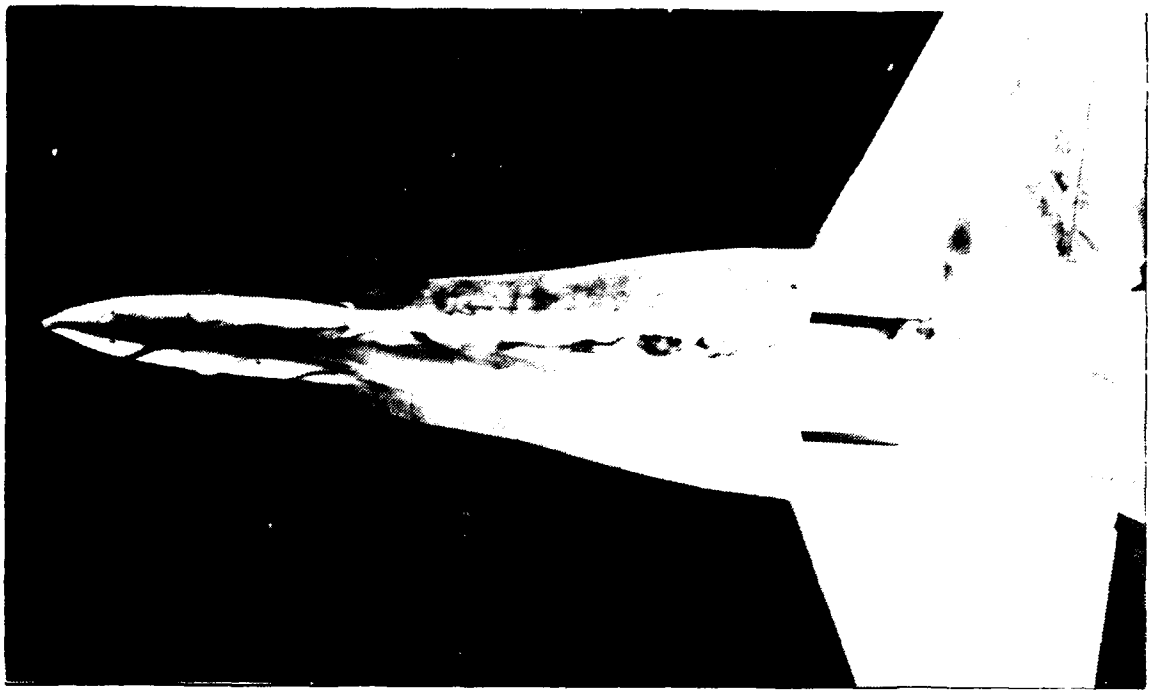

Figure 60. Forebody, High Pitch Up, AOA = 30 deg , YAW = 10 deg.

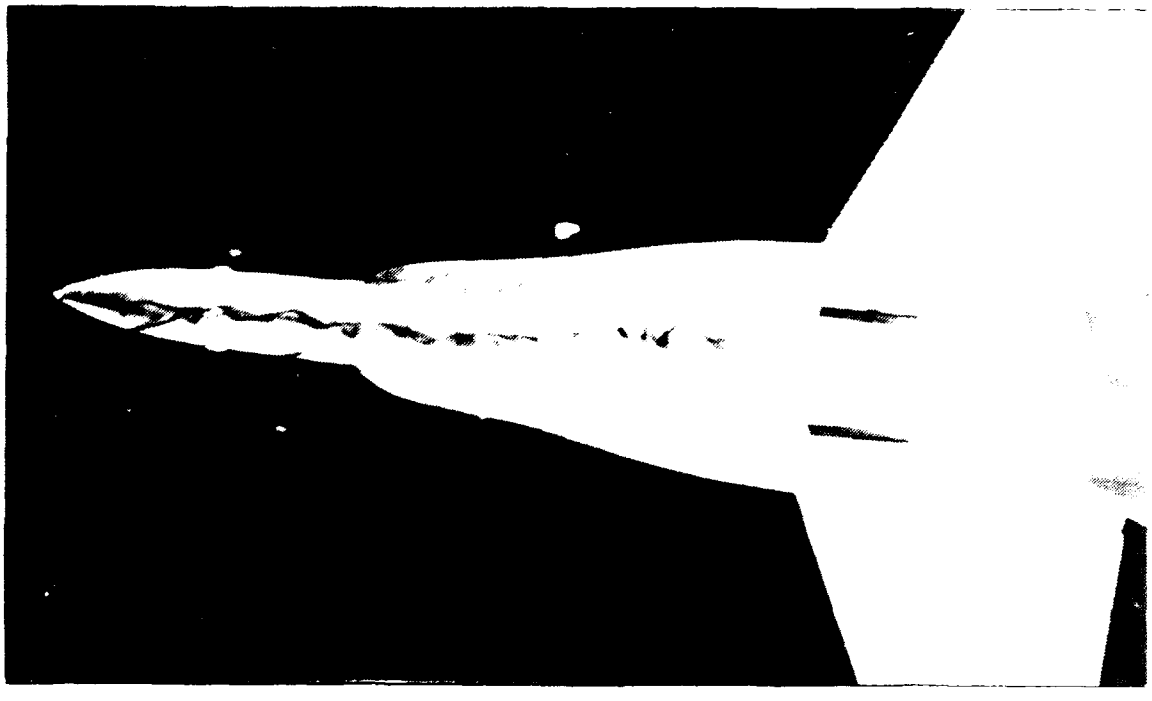

Figure 61. Forebody, High Pitch Down, AOA = 30 deg , YAW = 10 deg.

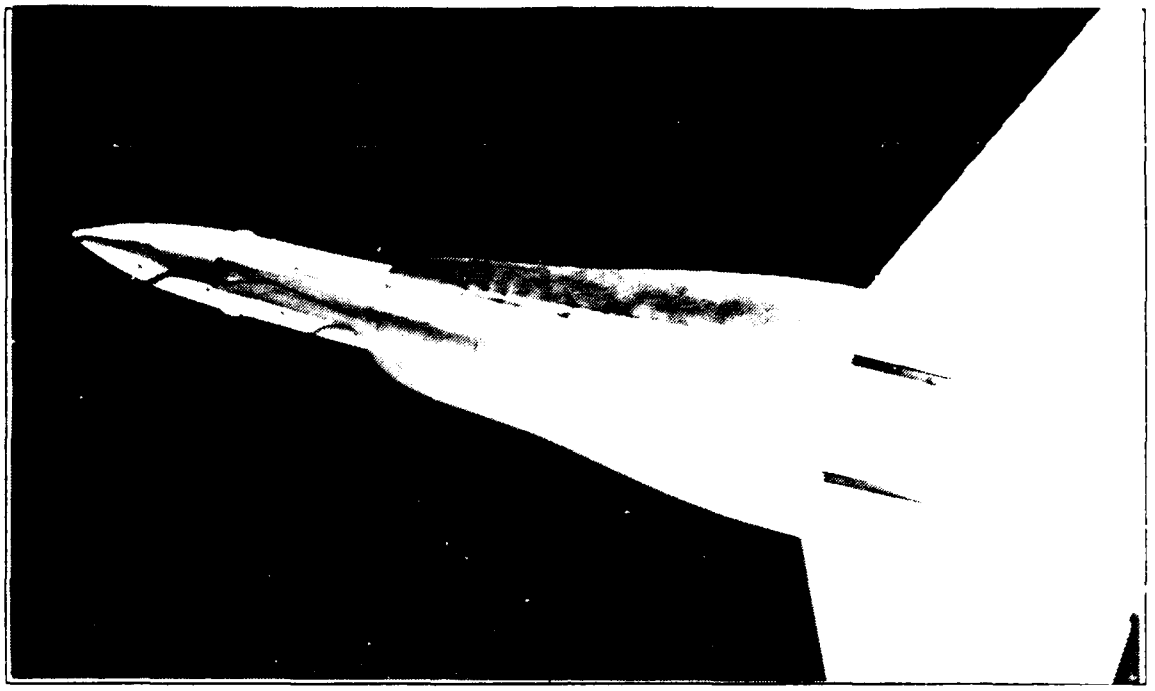

Figure 62. Forebody, Low Pitch Up, AOA = 30 deg , YAW = 20 deg.

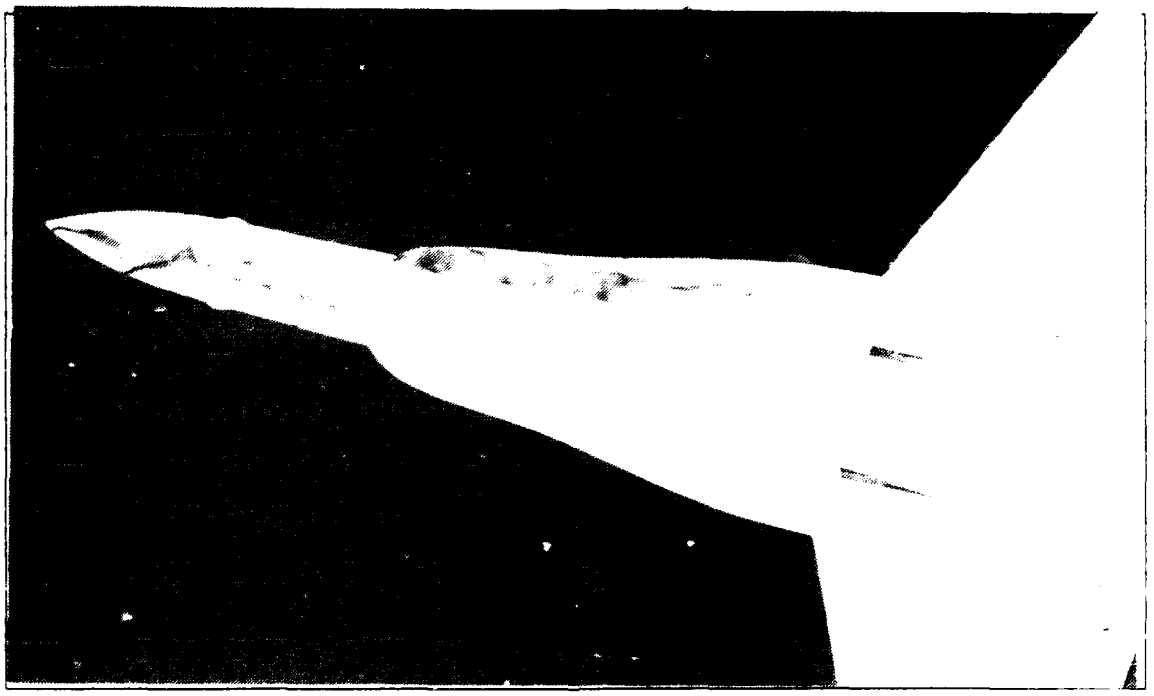

Figure 63. Forebody, Low Pitch Down, AOA = 30 deg , YAW = 20 deg.

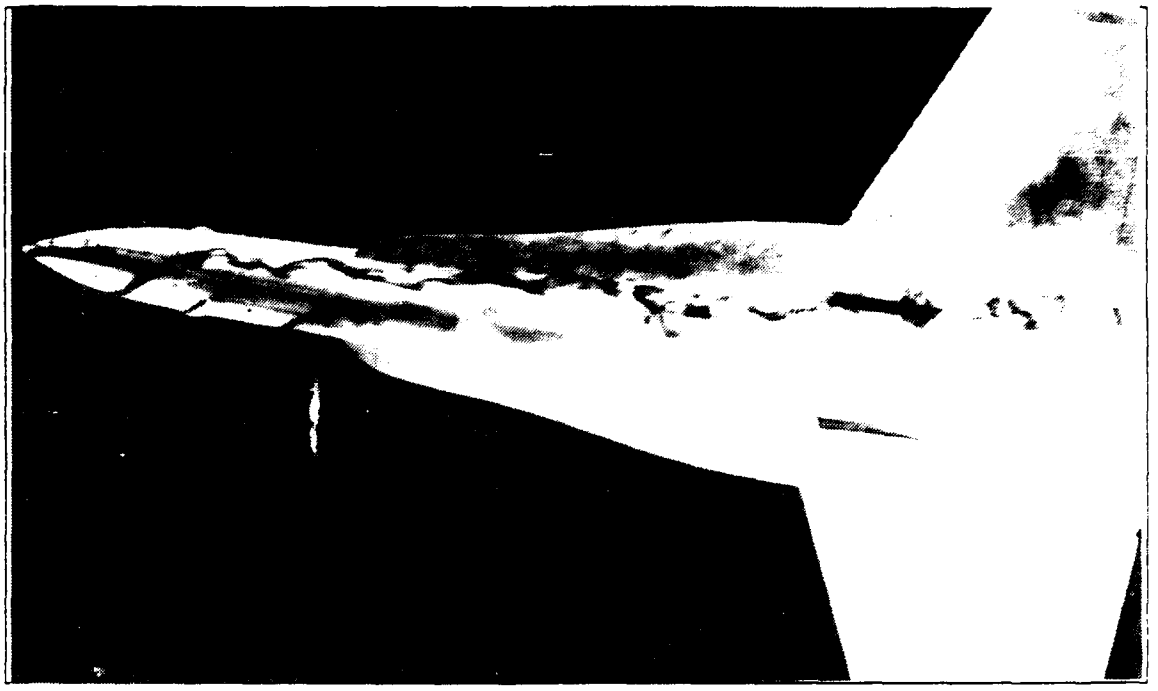

Figure 64. Forebody, High Pitch Up, AOA = 30 deg , YAW = 20 deg.

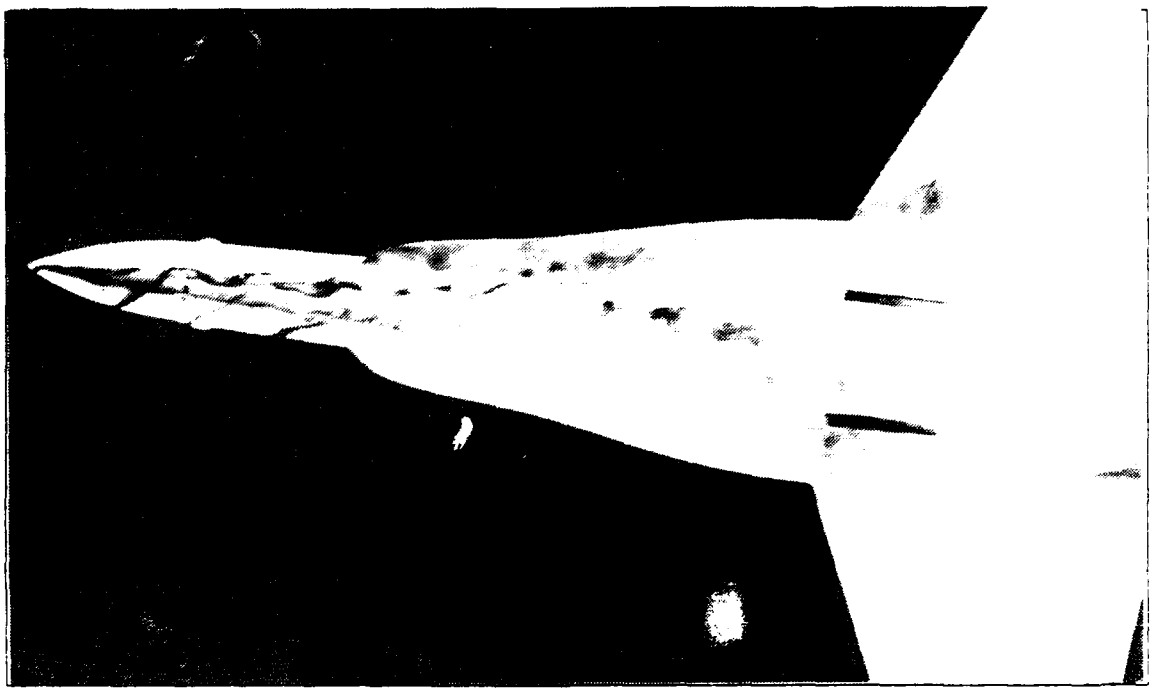

Figure 65. Forebody, High Pitch Down, AOA = 30 deg , YAW = 20 deg.

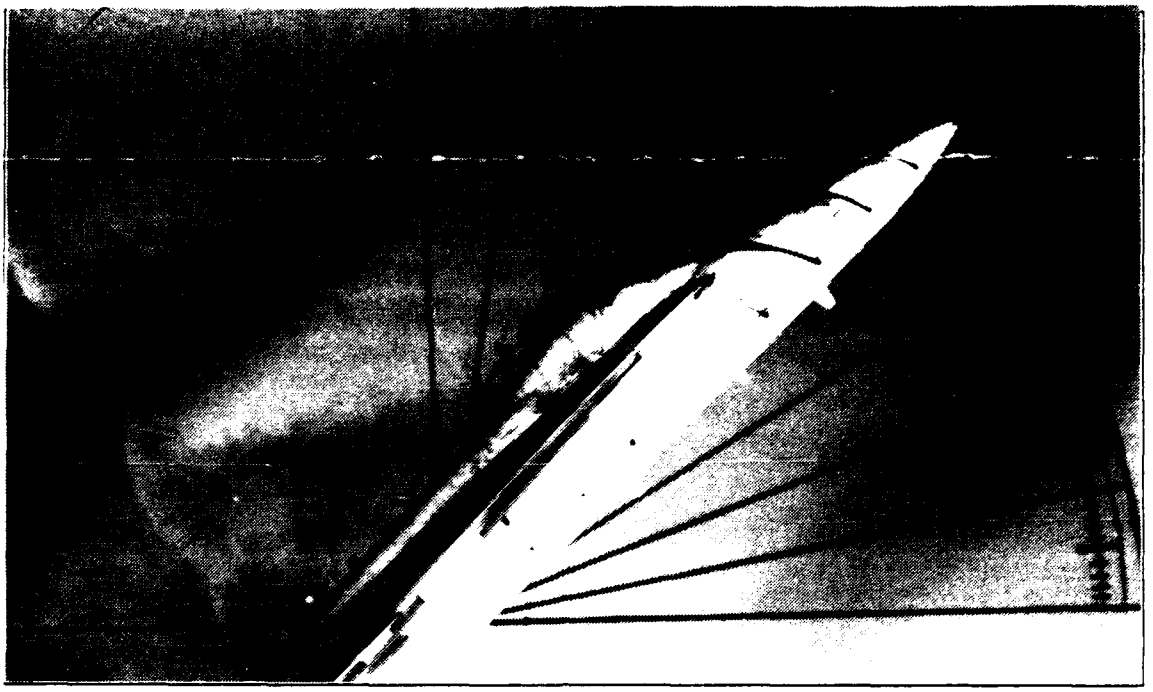

Figure 66. Forebody, Low Pitch Up, AOA = 40 deg , YAW = 0 deg.

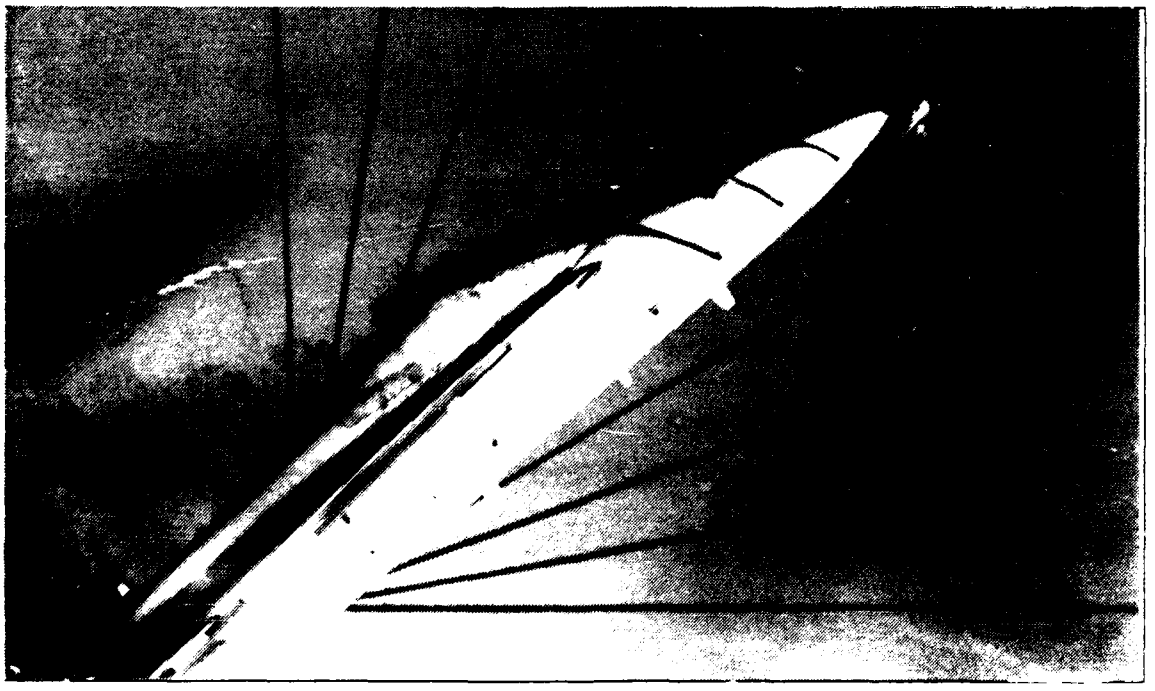

Figure 67. Forebody, Low Pitch Down, AOA = 40 deg , YAW = 0 deg.

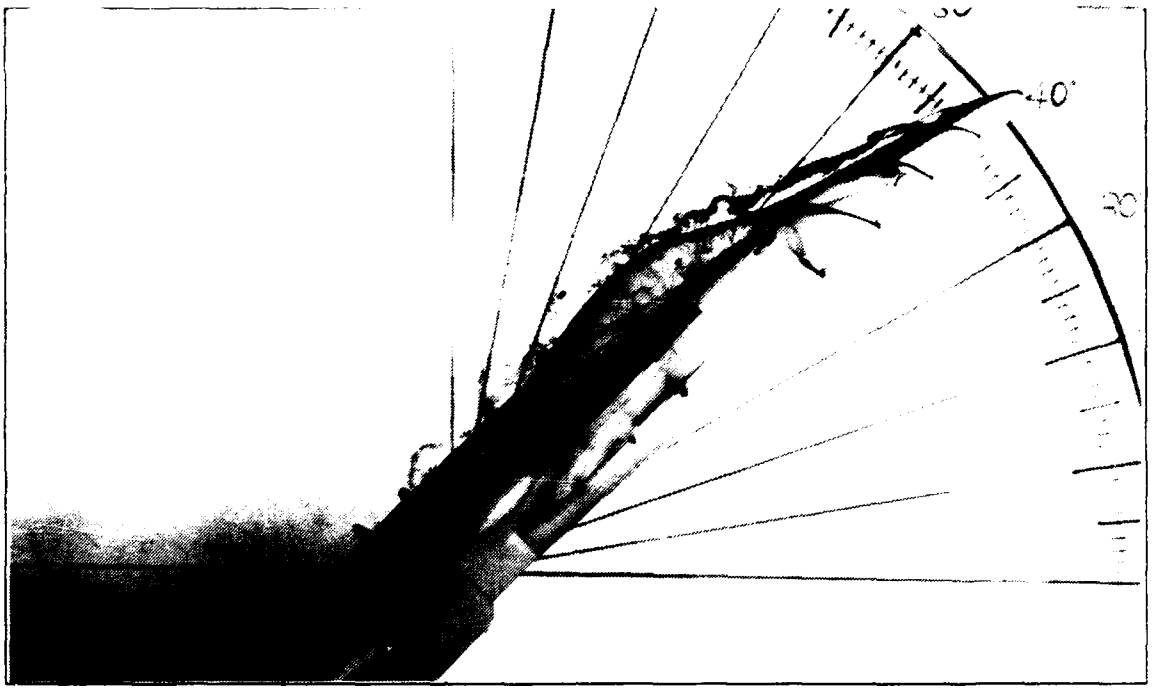

Figure 68. Forebody, High Pitch Up, AOA = 40 deg , YAW = 0 deg.

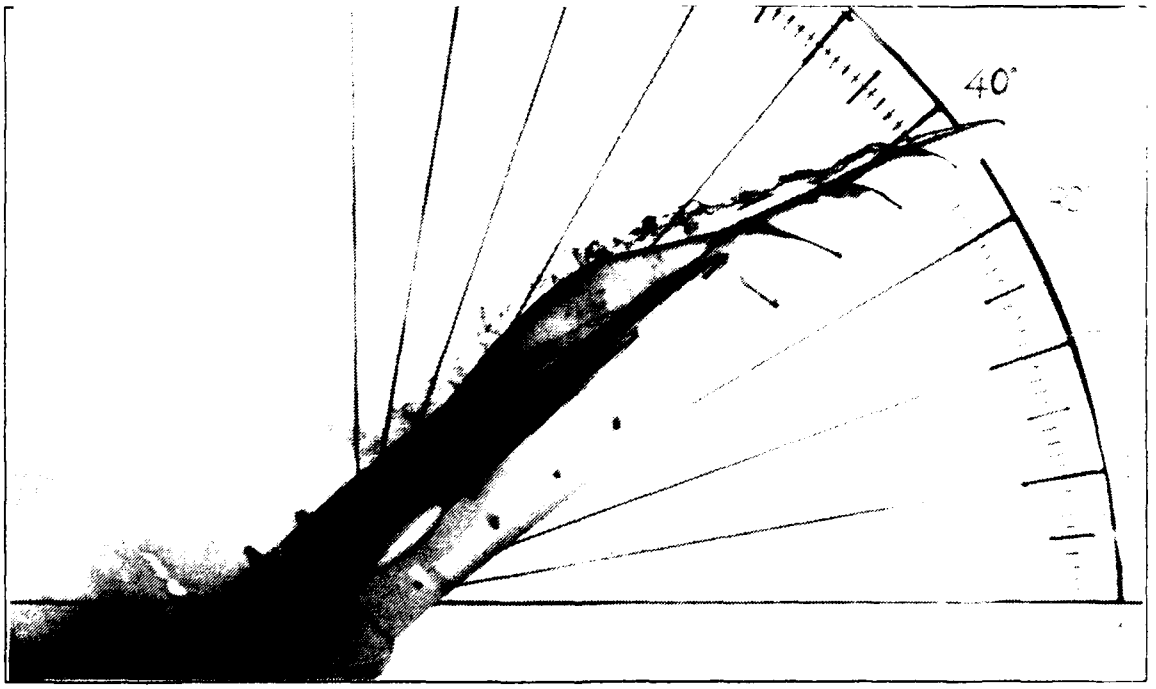

Figure 69. Forebody, High Pitch Down, AOA = 40 deg , YAW = 0 deg.

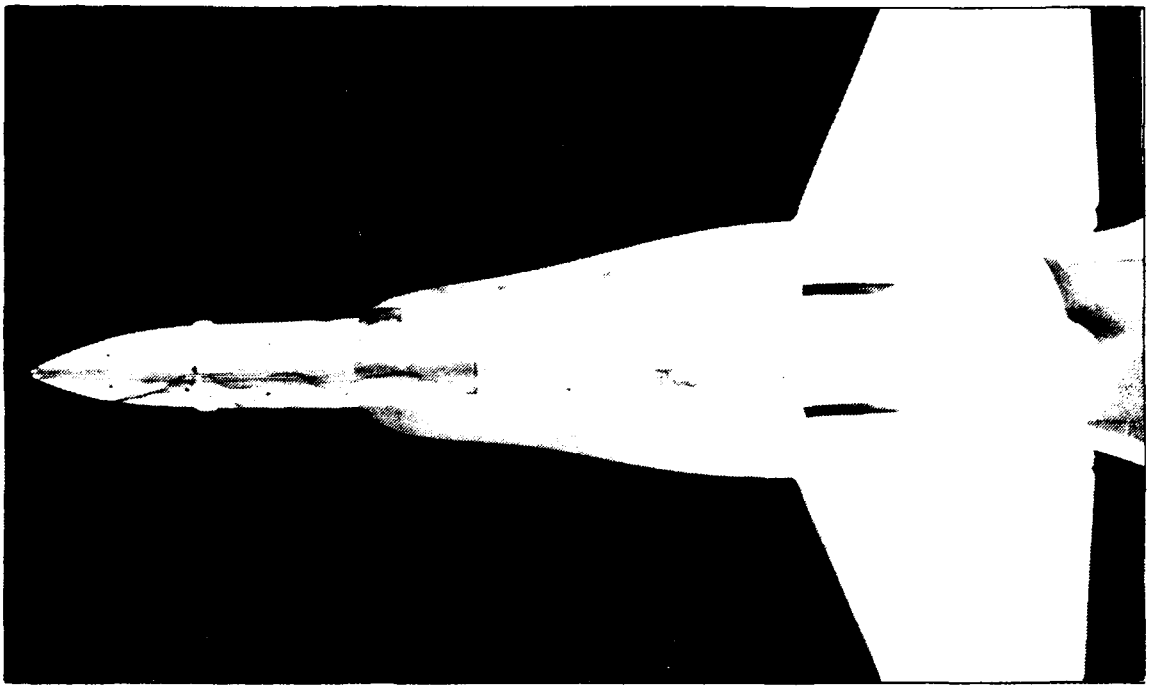

Figure 70. Forebody, Low Pitch Up, AOA = 40 deg , YAW = 5 deg.

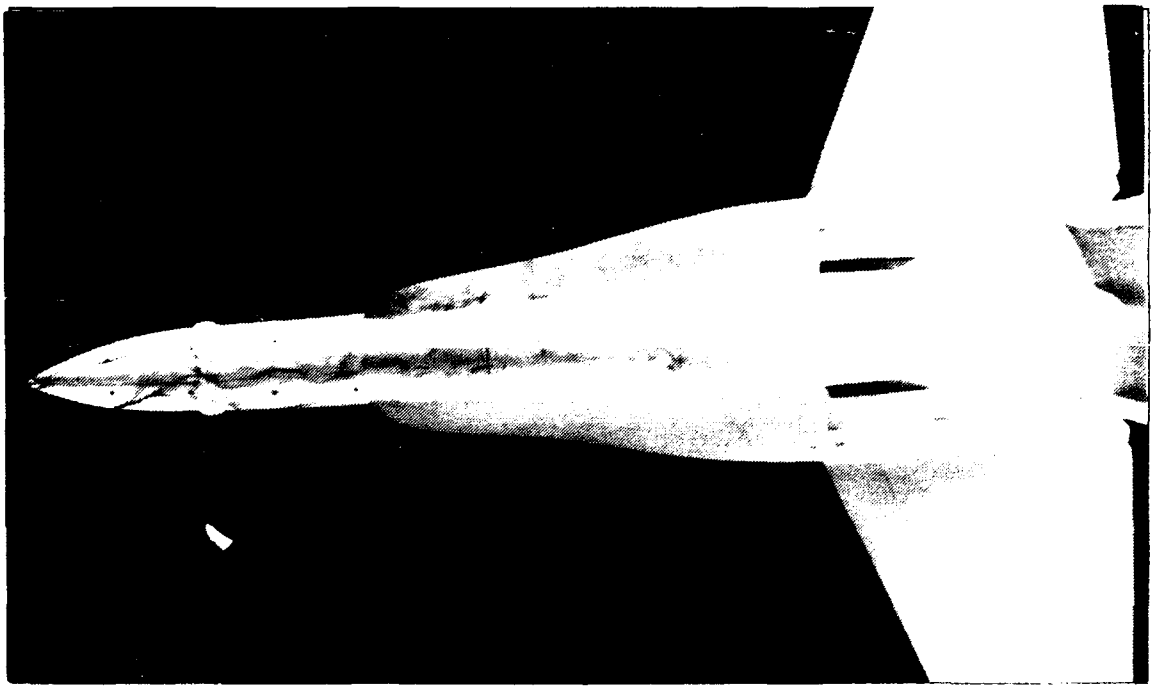

Figure 71. Forebody, Low Pitch Down, AOA = 40 deg , YAW = 5 deg.

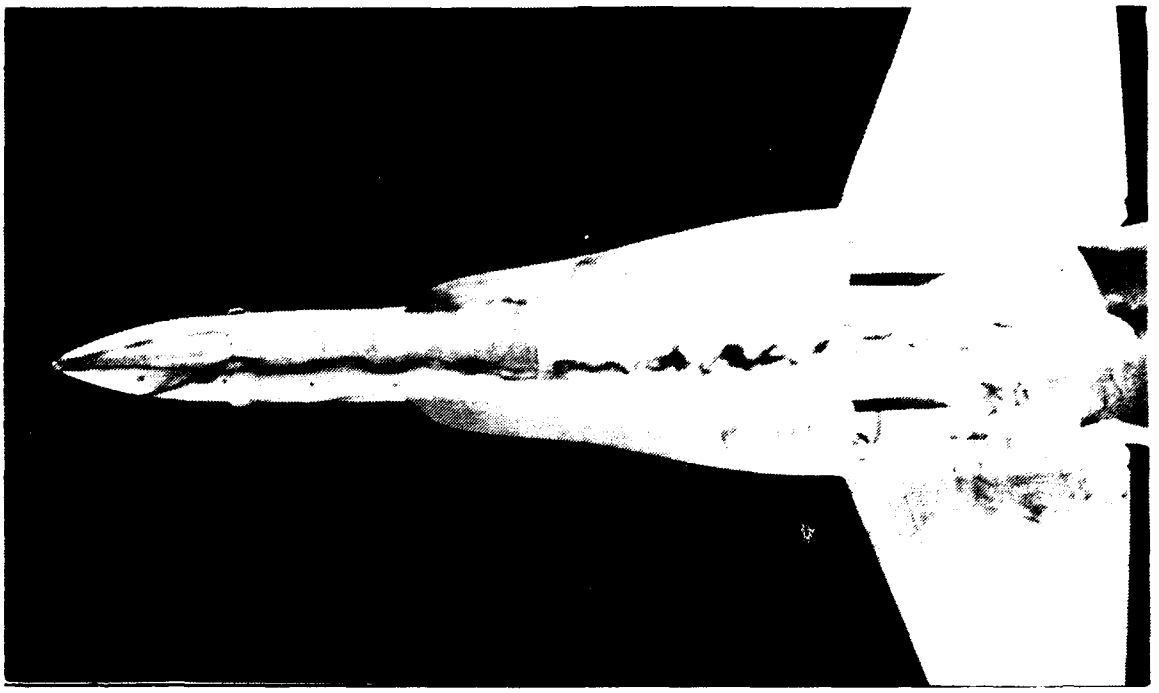

Figure 72. Forebody, High Pitch Up, AOA = 40 deg , YAW = 5 deg.

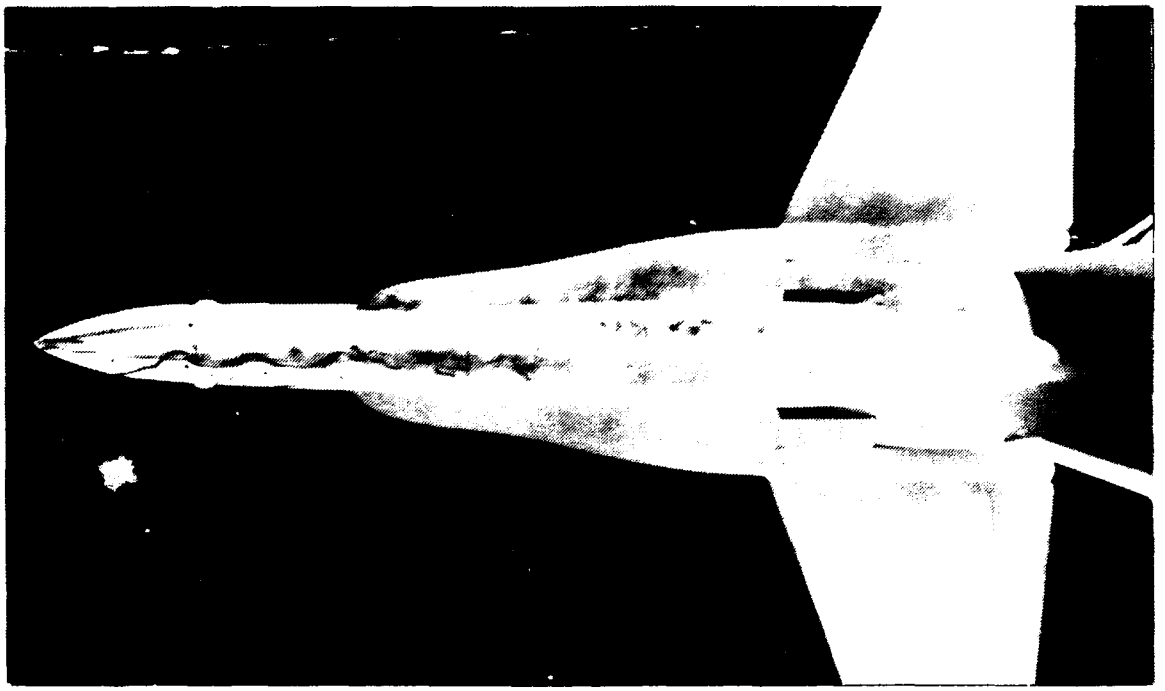

Figure 73. Forebody, High Pitch Down, AOA = 40 deg , YAW = 5 deg.

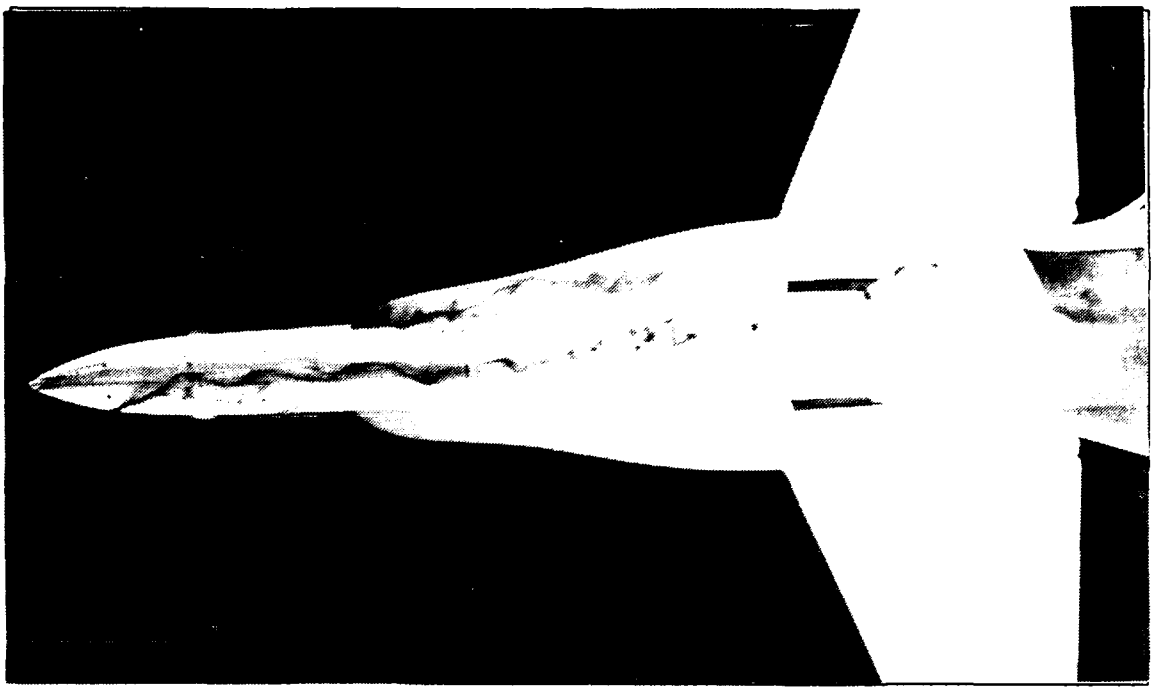

Figure 74. Forebody, Low Pitch Up, AOA = 40 deg , YAW = 10 deg.

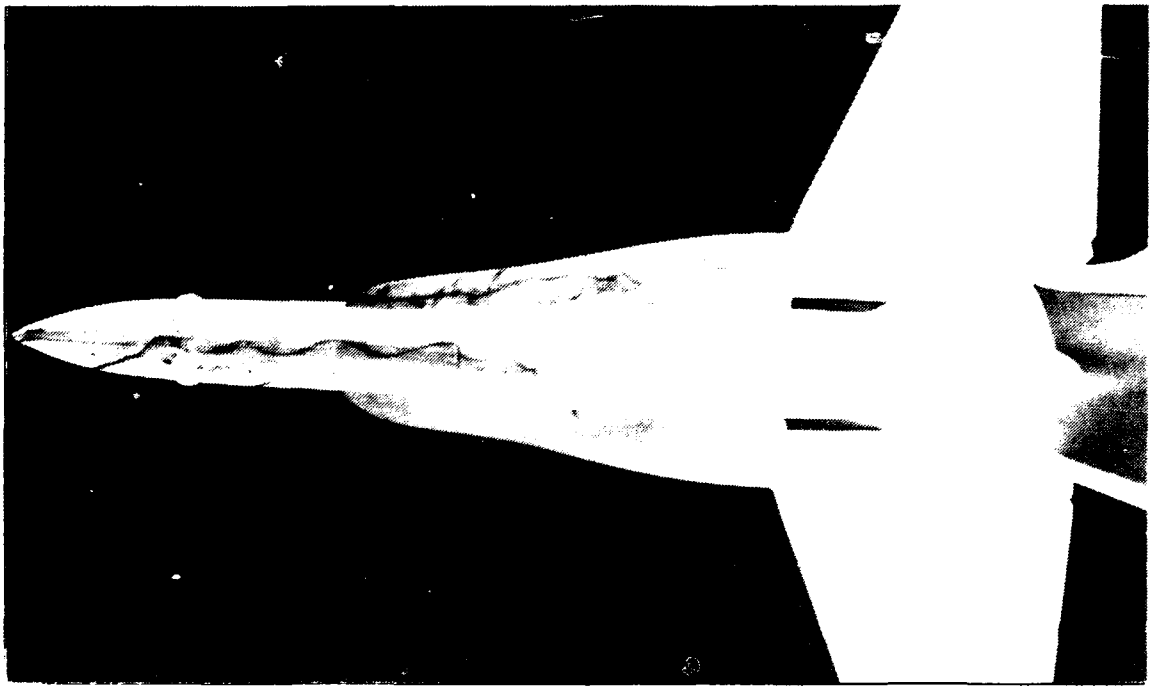

Figure 75. Forebody Low Pitch Down, AOA = 40 deg , YAW = 10 deg.

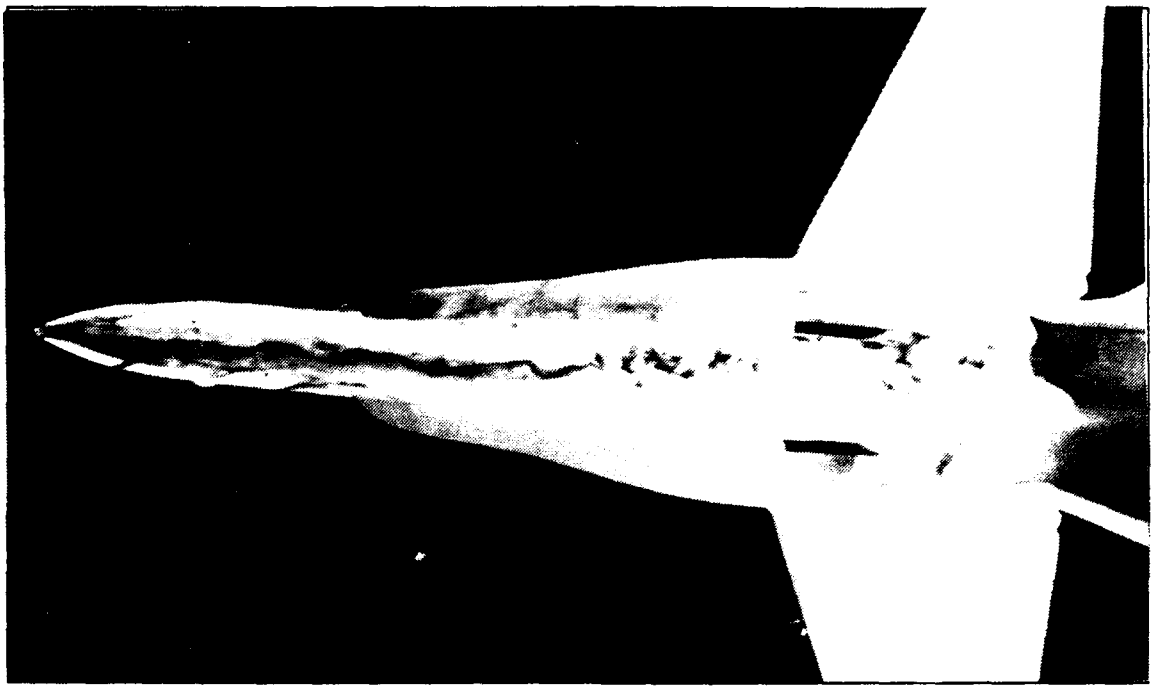

Figure 76. Forebody, High Pitch Up, AOA = 40 deg , YAW = 10 deg.

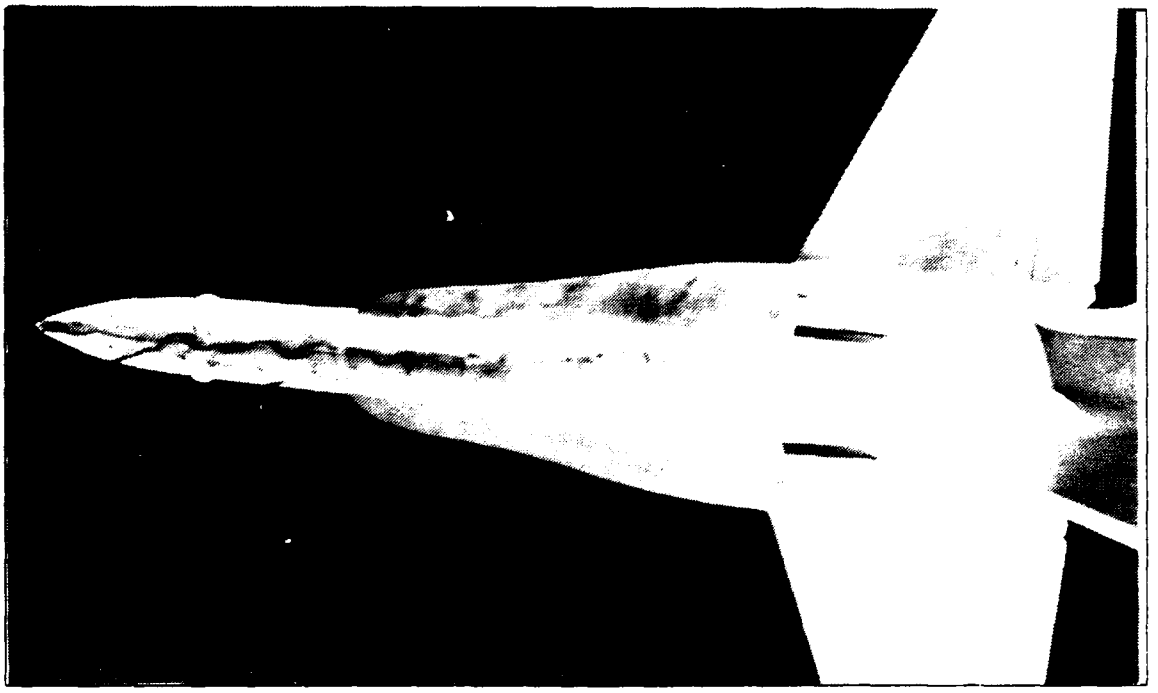

Figure 77. Forebody, High Pitch Down, AOA = 40 deg , YAW = 10 deg.

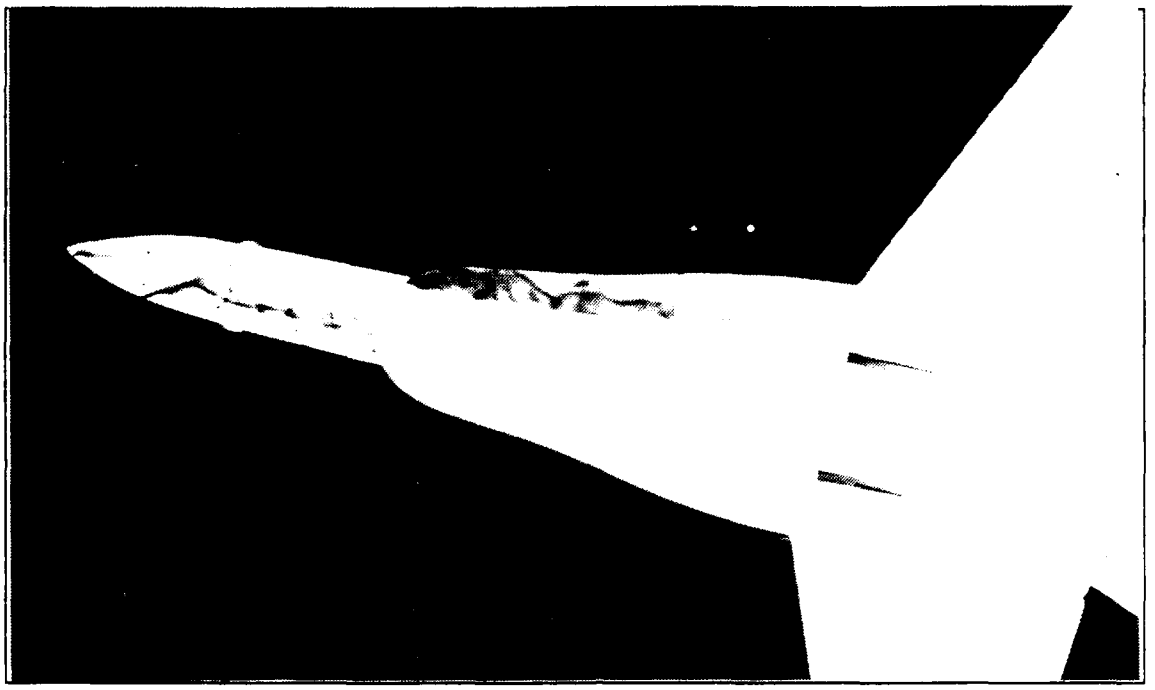

Figure 78. Forebody, Low Pitch Up, AOA = 40 deg , YAW = 20 deg.

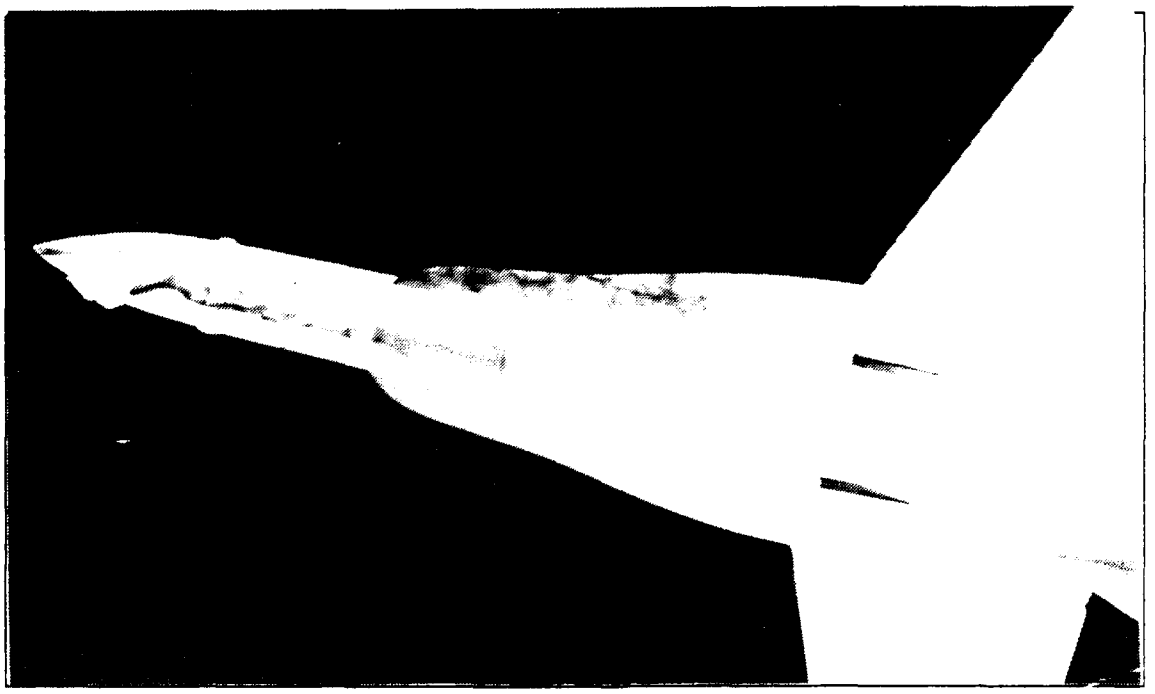

Figure 79. Forebody, Low Pitch Down, AOA = 40 deg , YAW = 20 deg.

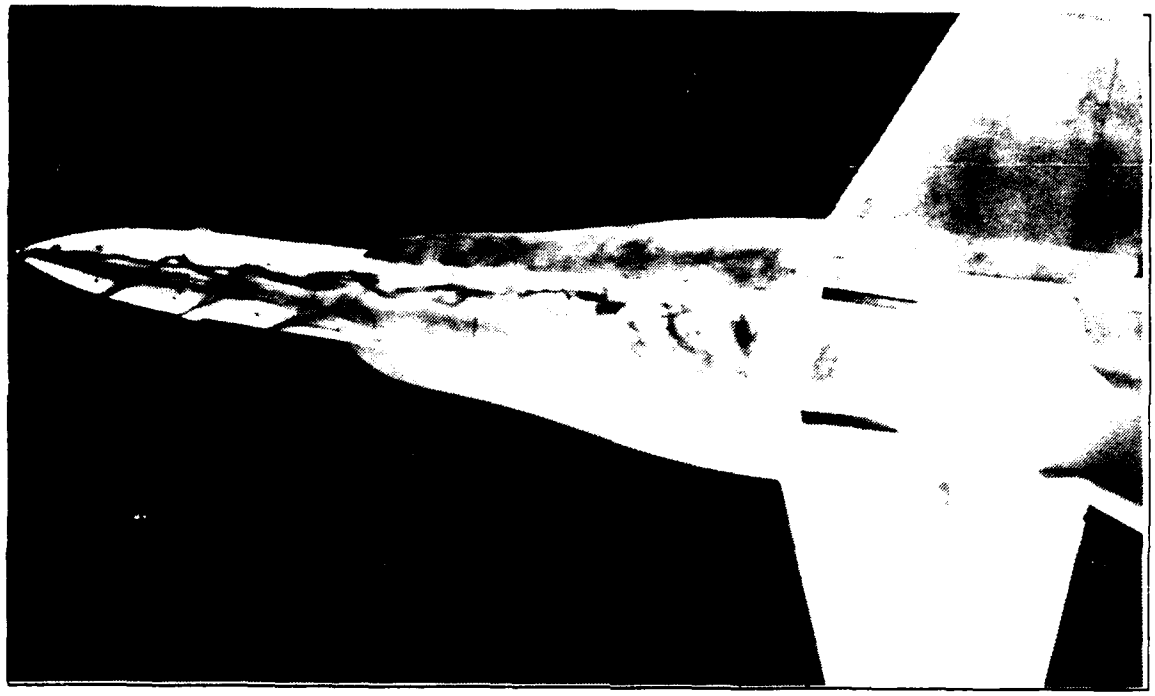

Figure 80. Forebody, High Pitch Up, AOA = 40 deg , YAW = 20 deg.

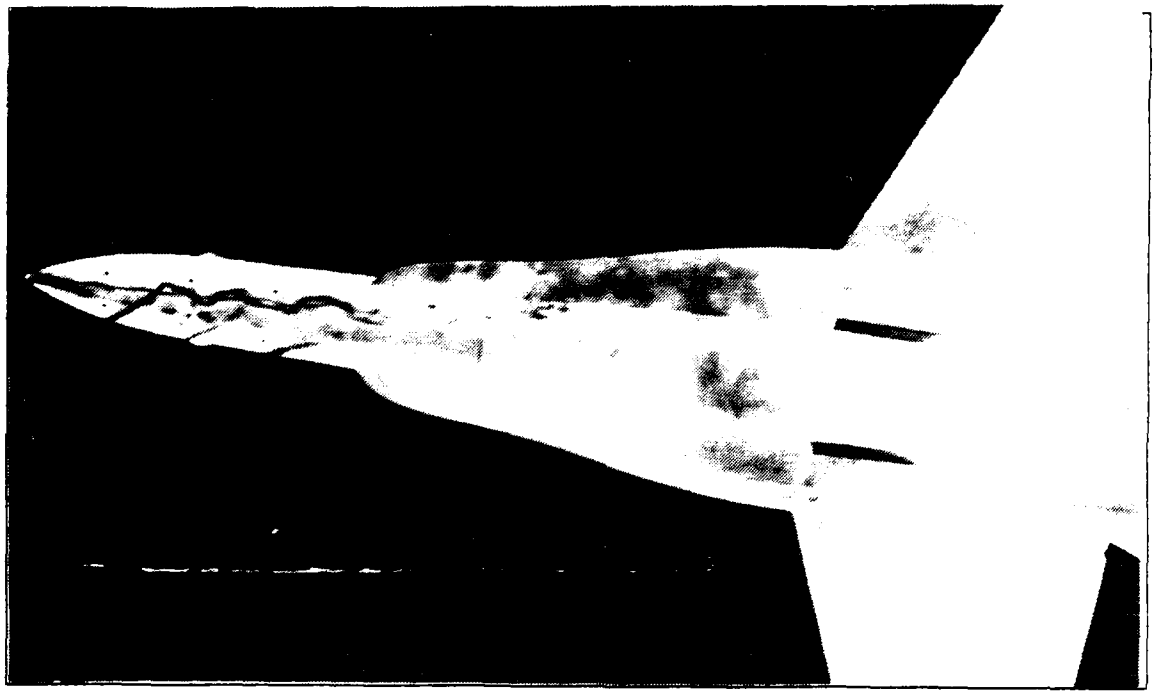

Figure 81. Forebody, High Pitch Down, AOA = 40 deg , YAW = 20 deg.

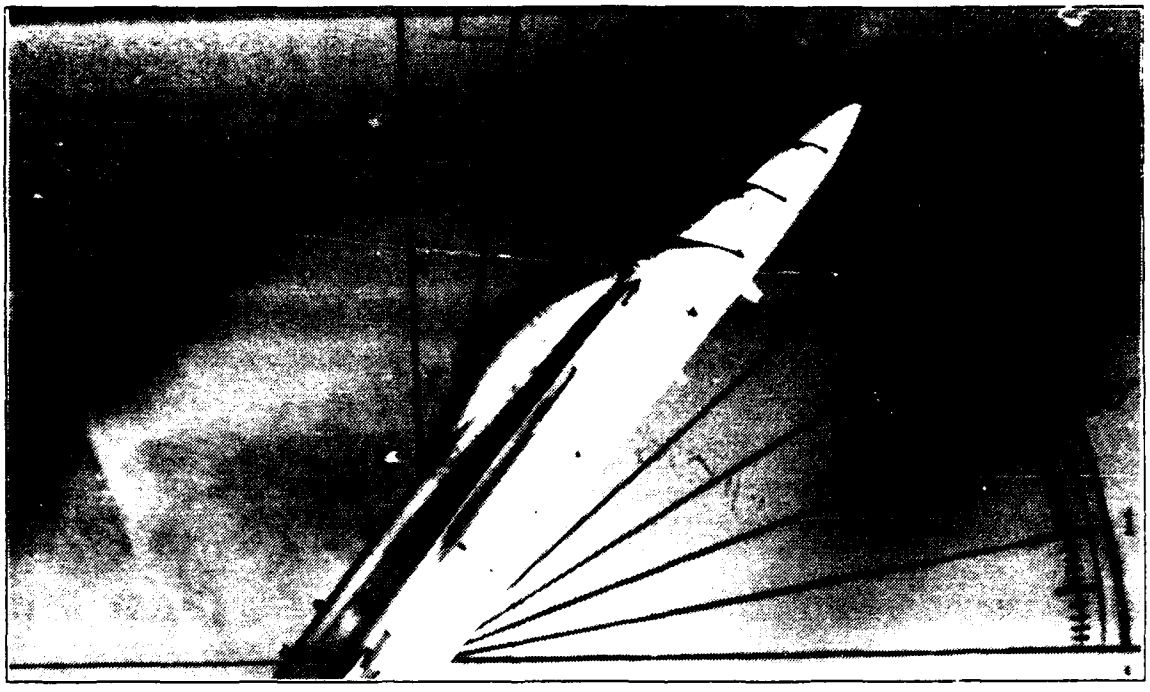

Figure 82. Forebody, Low Pitch Up, AOA = 50 deg , YAW = 0 deg.

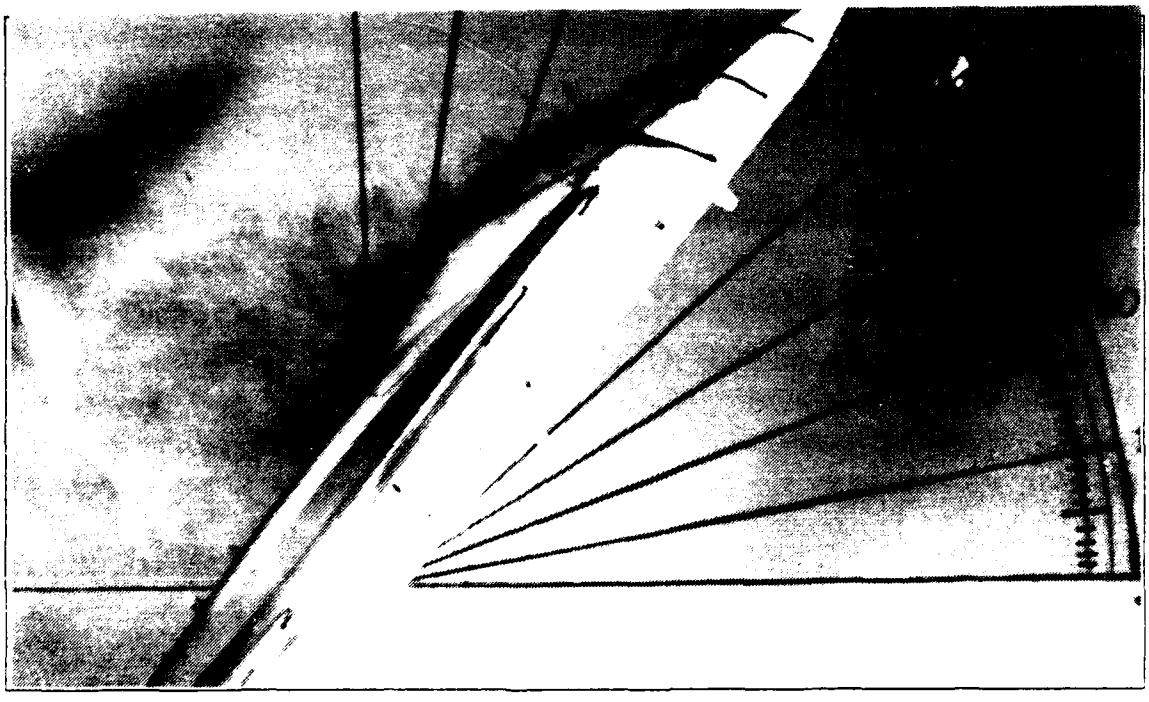

Figure 83. Forebody, Low Pitch Down, AOA = 50 deg , YAW = 0 deg.

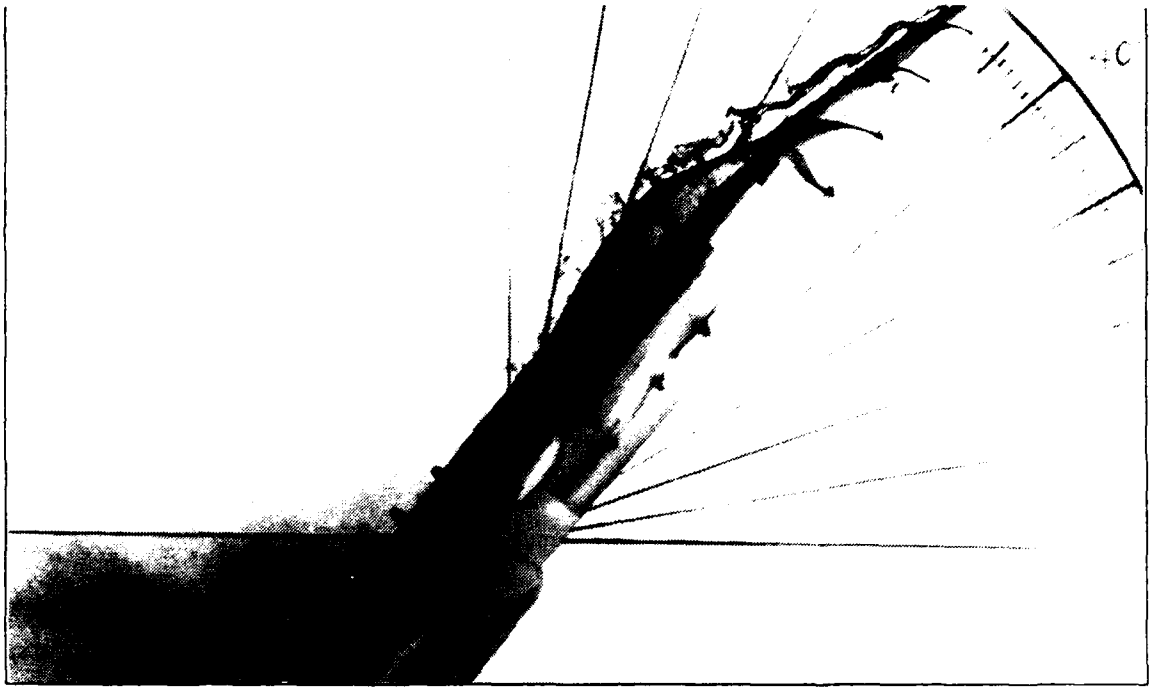

Figure 84. Forebody, High Pitch Up, AOA = 50 deg , YAW = 0 deg.

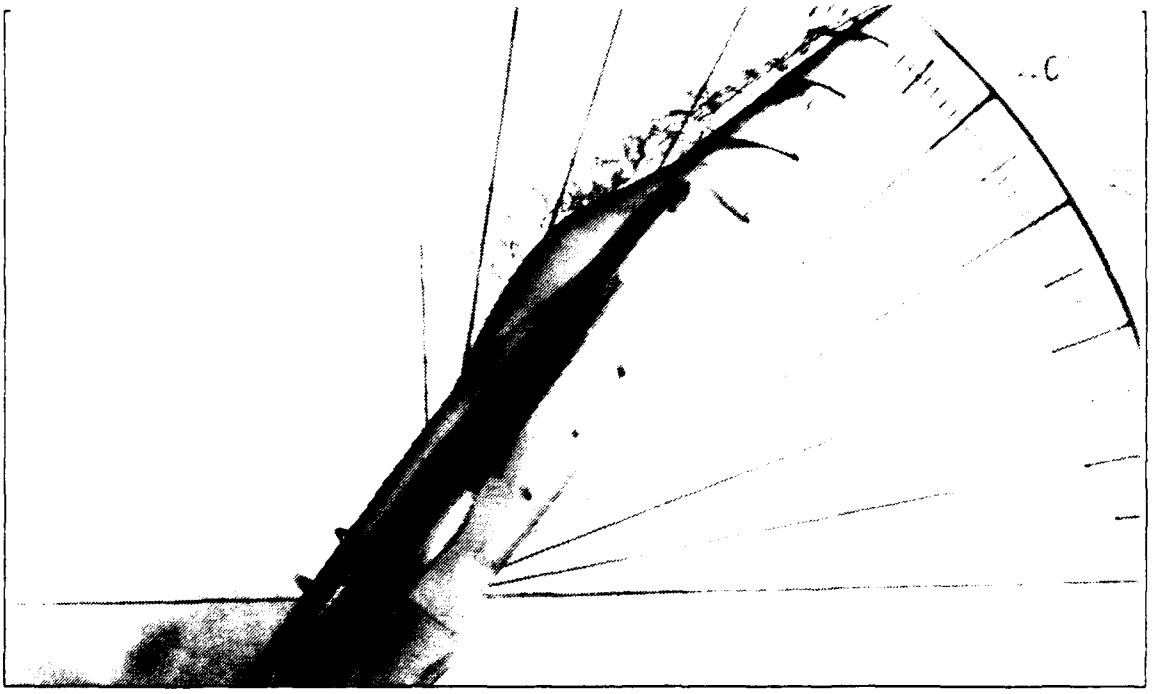

Figure 85. Forebody, High Pitch Down, AOA = 50 deg , YAW = 0 deg.

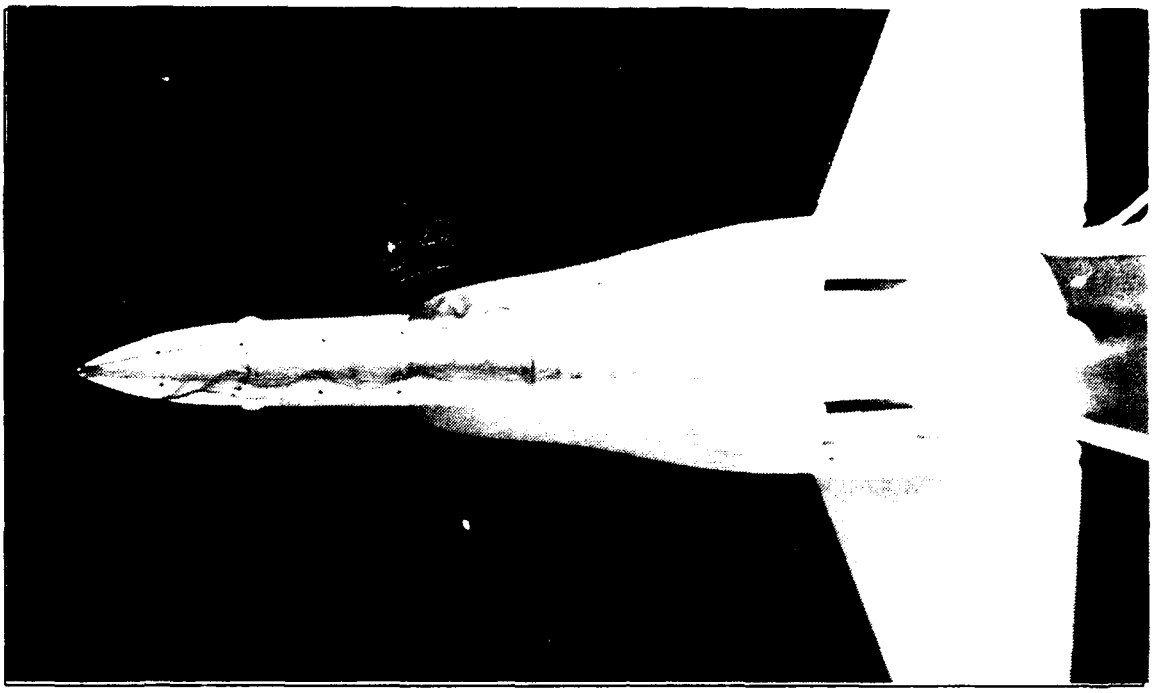

Figure 86. Forebody, Low Pitch Up, AOA = 50 deg , YAW = 5 deg.

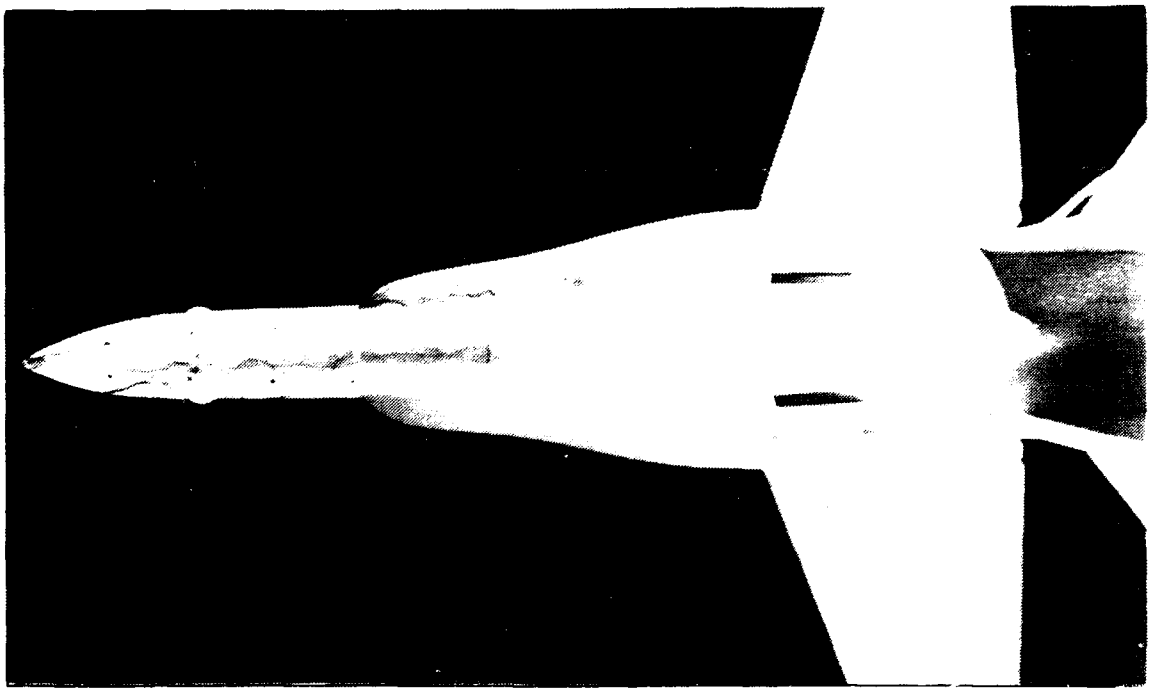

Figure 87. Forebody, Low Pitch Down, AOA = 50 deg , YAW = 5 deg.

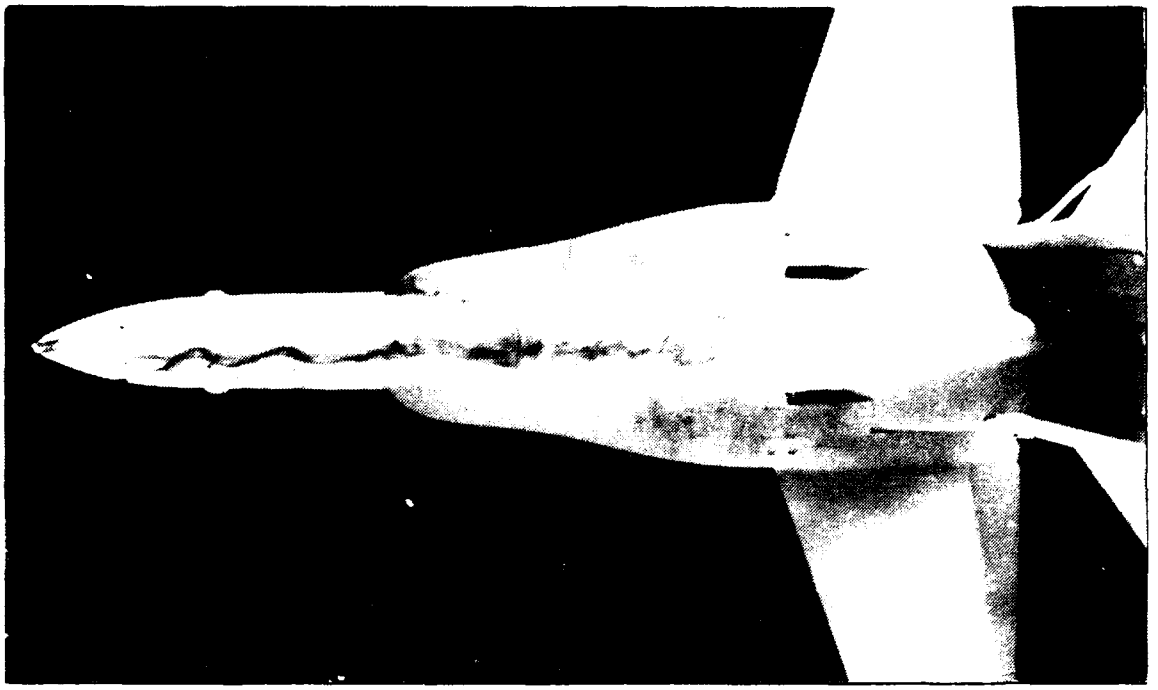

Figure 88. Forebody, High Pitch Up. AOA = 50 deg , YAW = 5 deg.

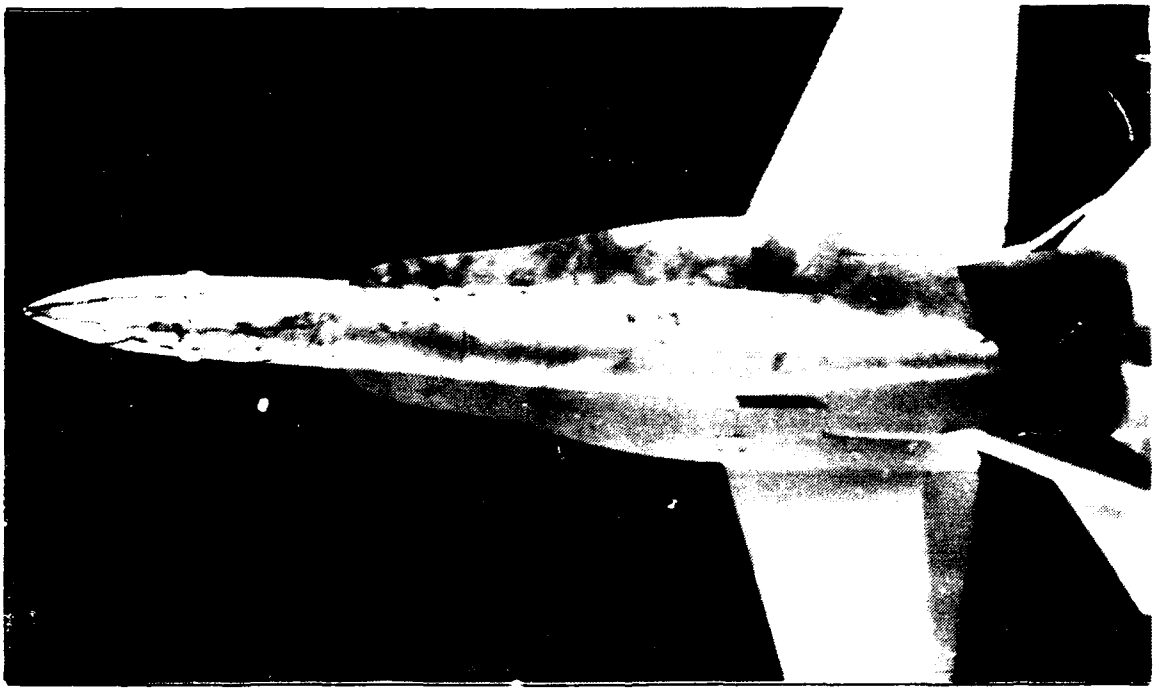

Figure 89. Forebody, High Pitch Down. AOA = 50 deg , YAW = 5 deg.

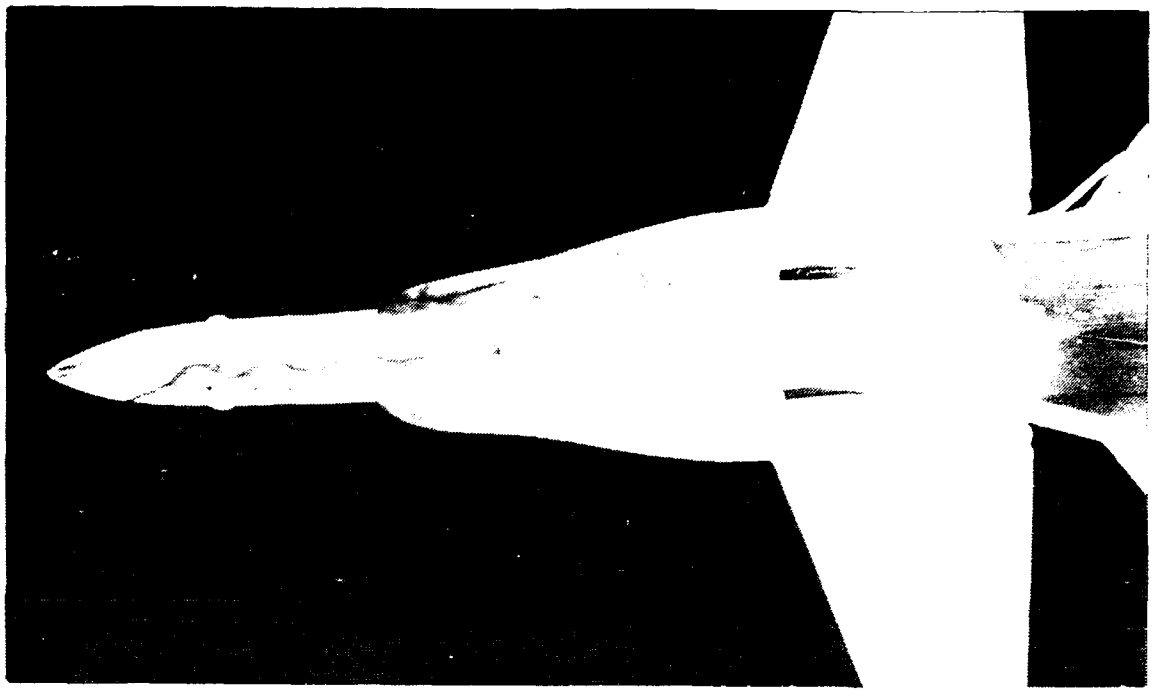

Figure 90. Forebody, Low Pitch Up, AOA = 50 deg, YAW = 10 deg.

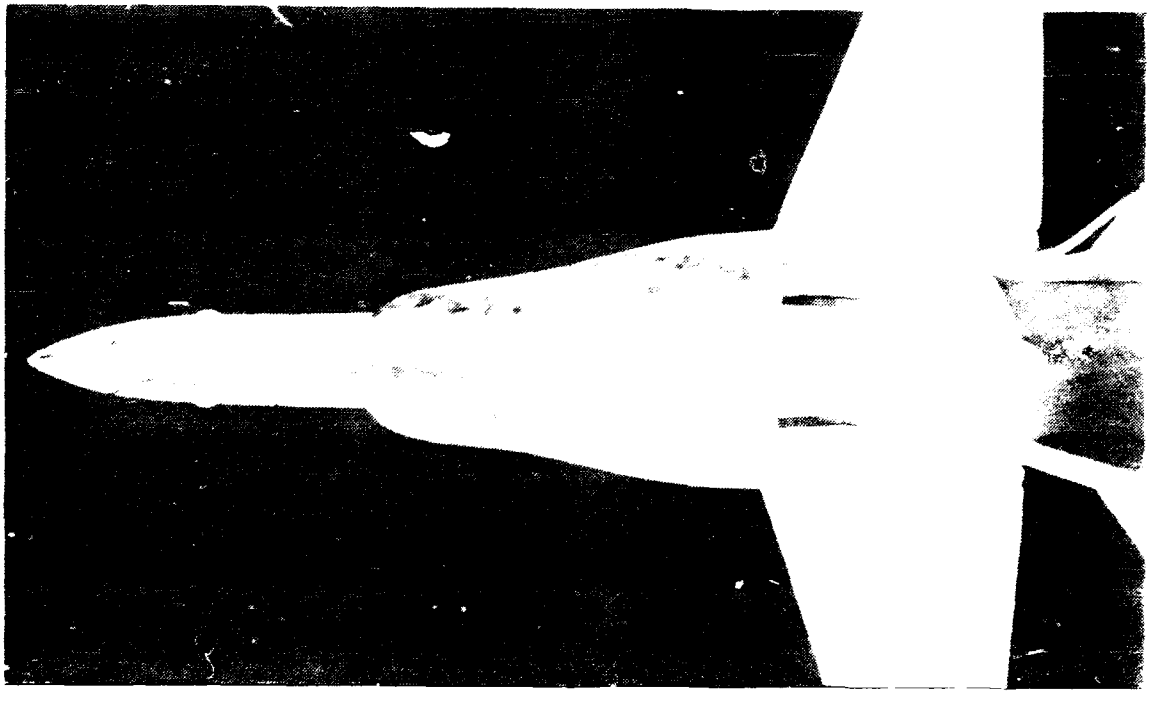

Figure 91. Forebody, Low Pitch Down, AOA = 50 deg, YAW = 10 deg.

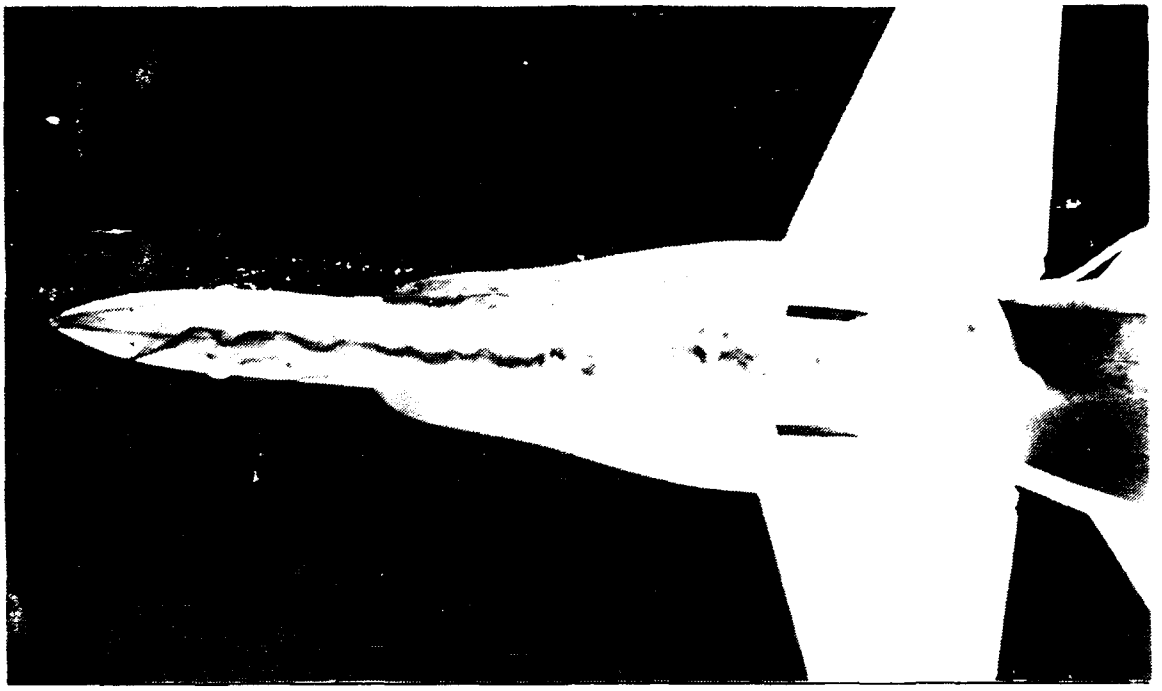

Figure 92. Forebody, High Pitch Up, AOA = 50 deg , YAW = 10 deg.

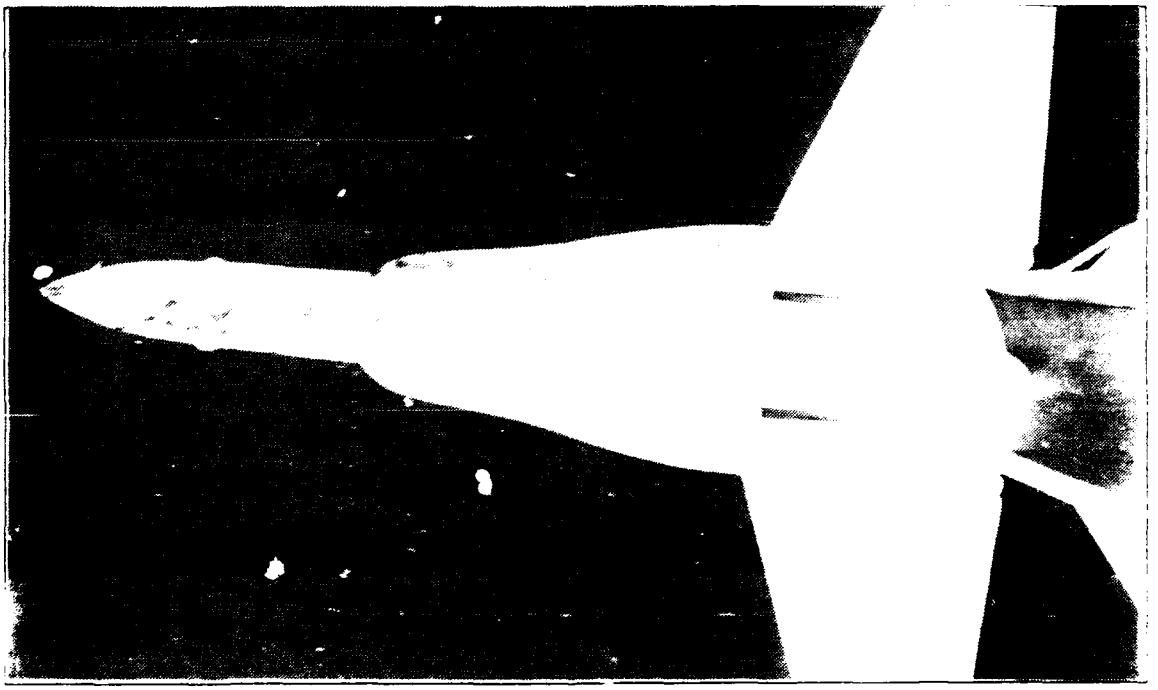

Figure 93. Forebody, High Pitch Down, AOA = 50 deg , YAW = 10 deg.

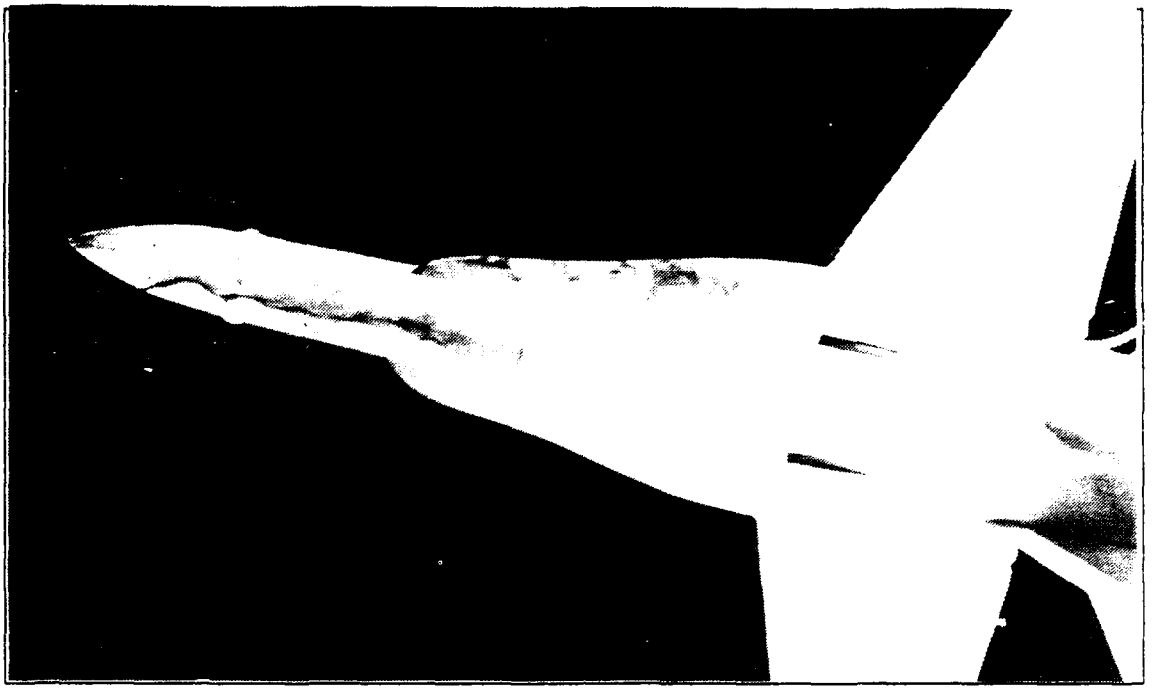

Figure 94. Forebody, Low Pitch Up, AOA = 50 deg , YAW = 20 deg.

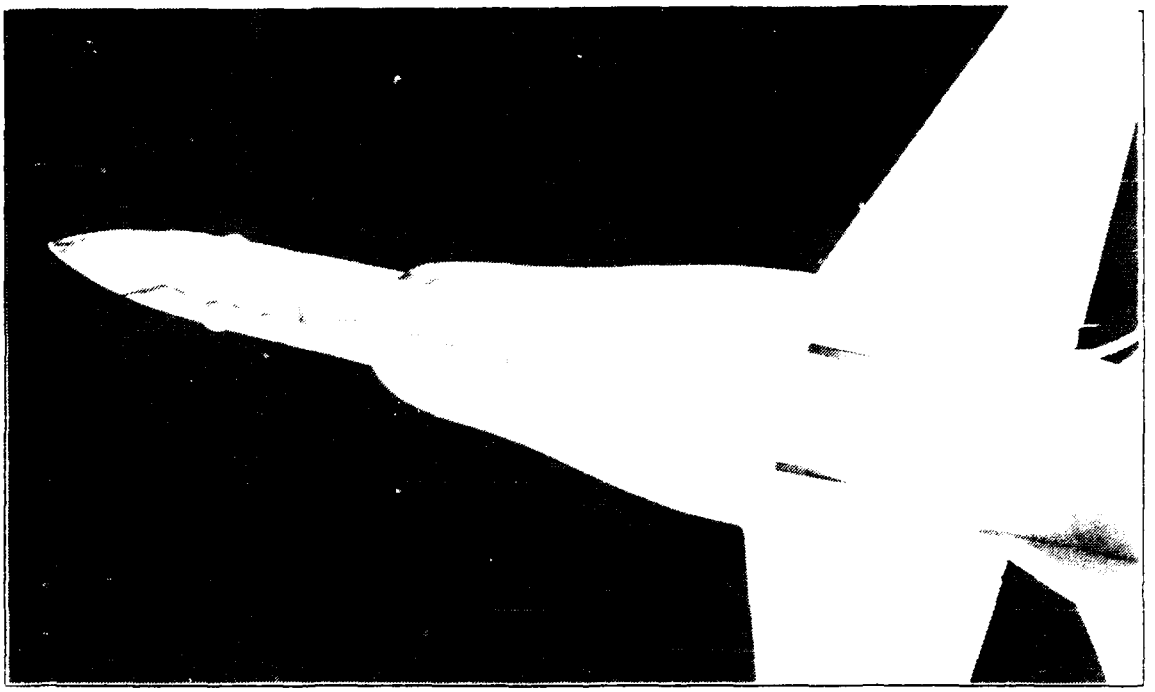

Figure 95. Forebody, Low Pitch Down, AOA = 50 deg , YAW = 20 deg.

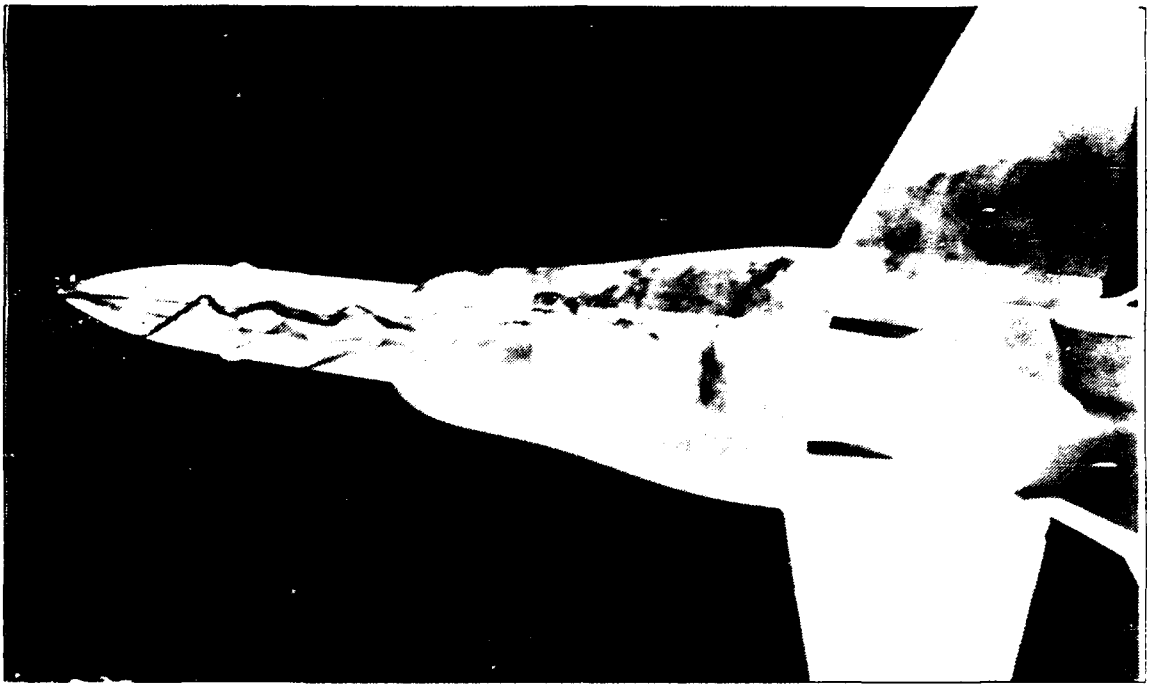

Figure 96. Forebody, High Pitch Up, AOA = 50 deg , YAW = 20 deg.

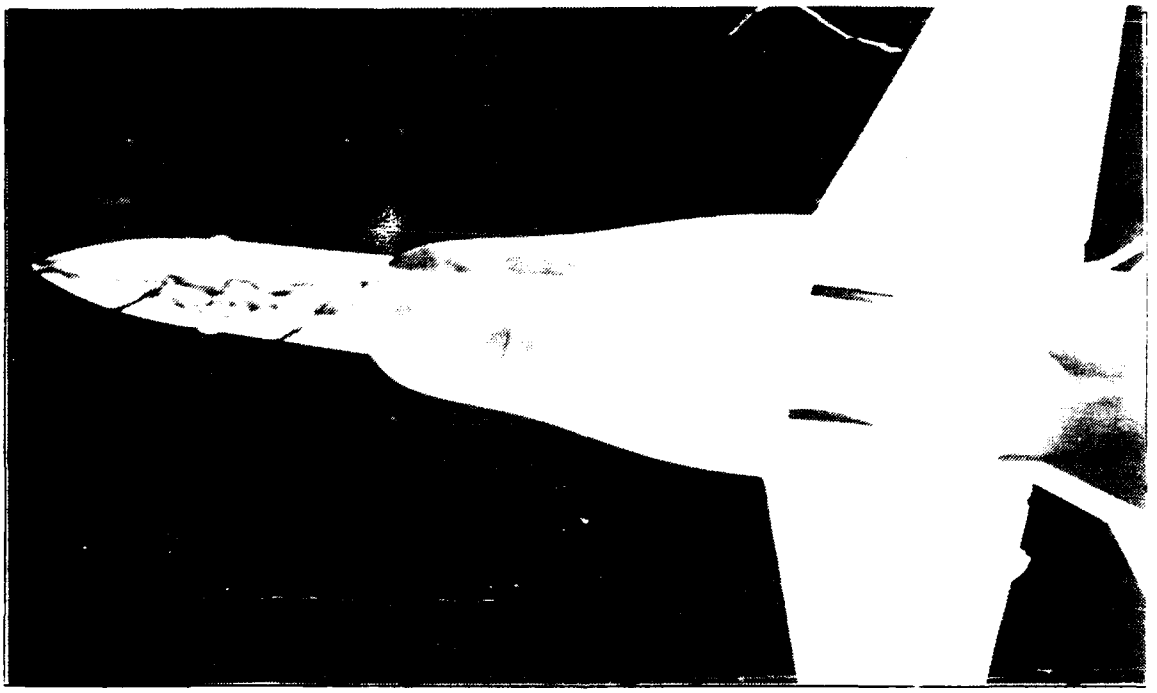

Figure 97. Forebody, High Pitch Down, AOA = 50 deg , YAW = 20 deg.

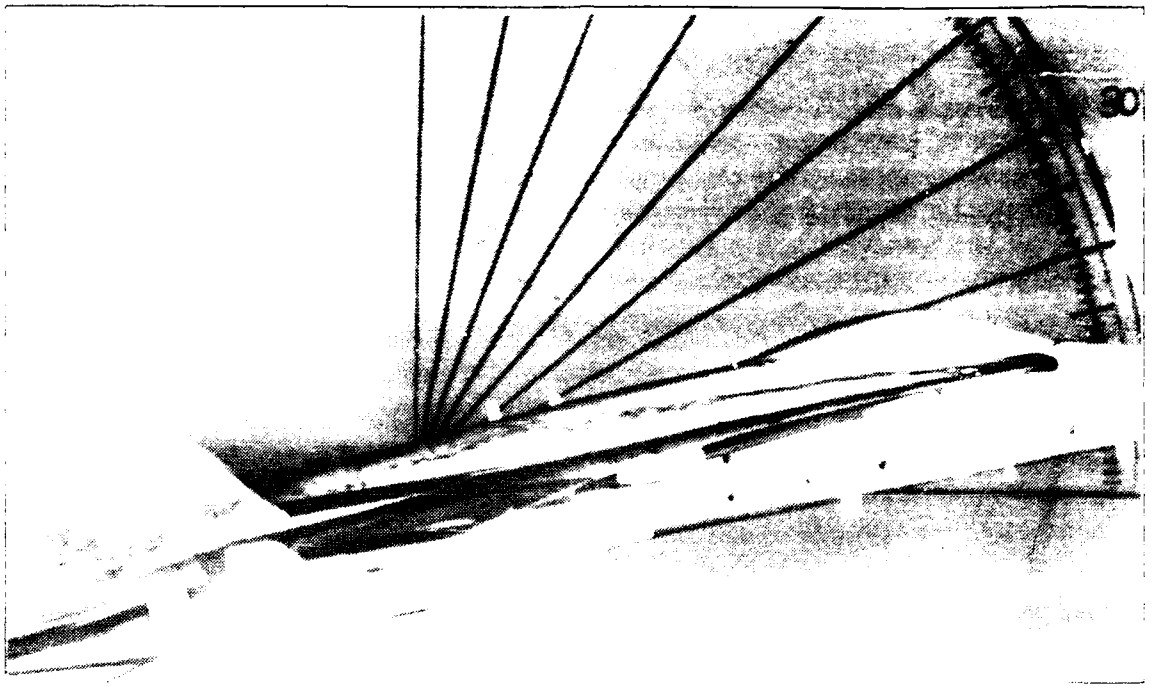

Figure 98. LEX, Static, AOA = 10 deg , YAW = 0 deg.

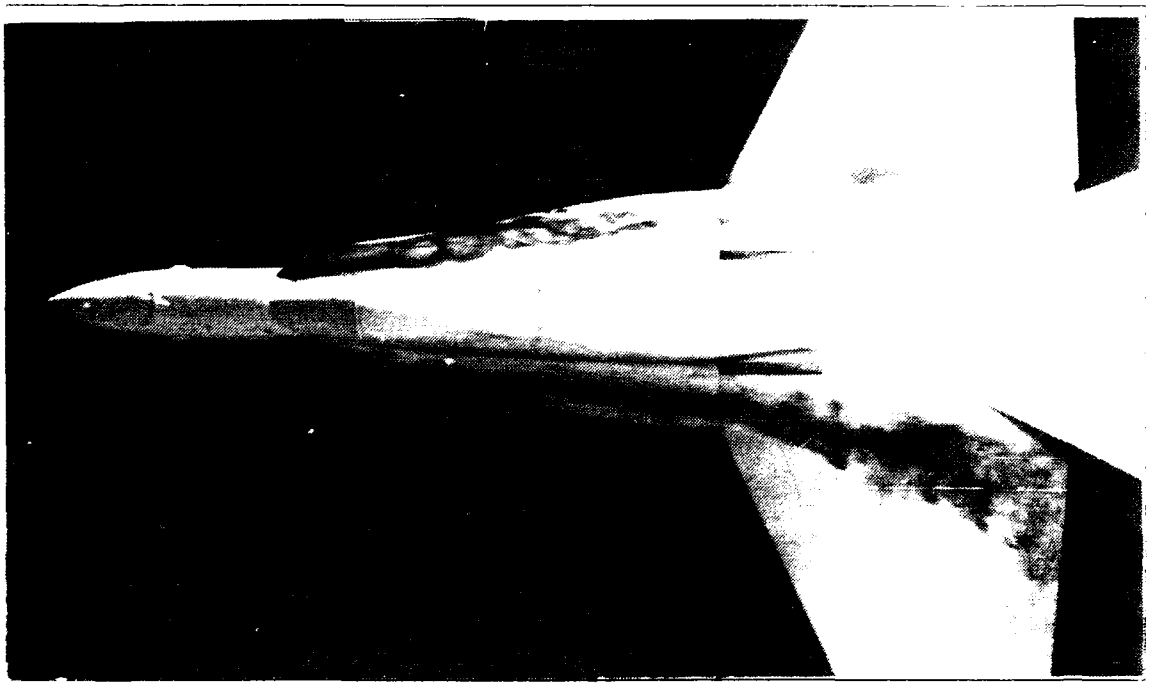

Figure 99. LEX, Low Pitch Up, AOA = 10 deg , YAW = 0 deg.

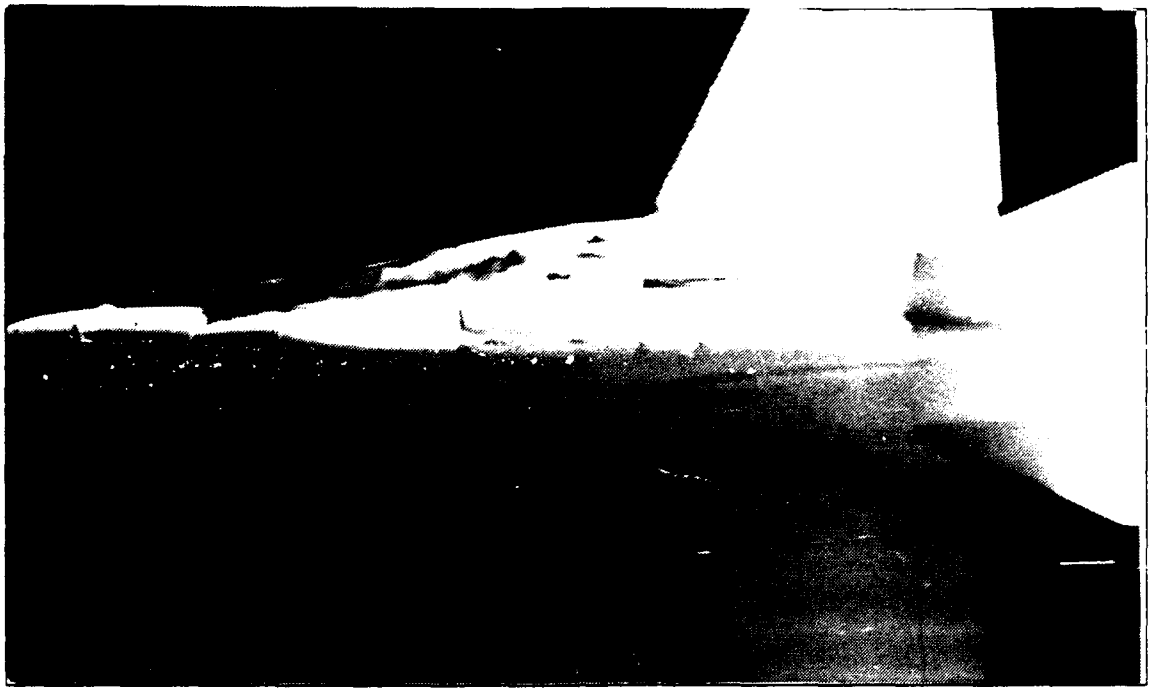

Figure 100. LEX, Low Pitch Down, AOA = 10 deg , YAW = 0 deg.

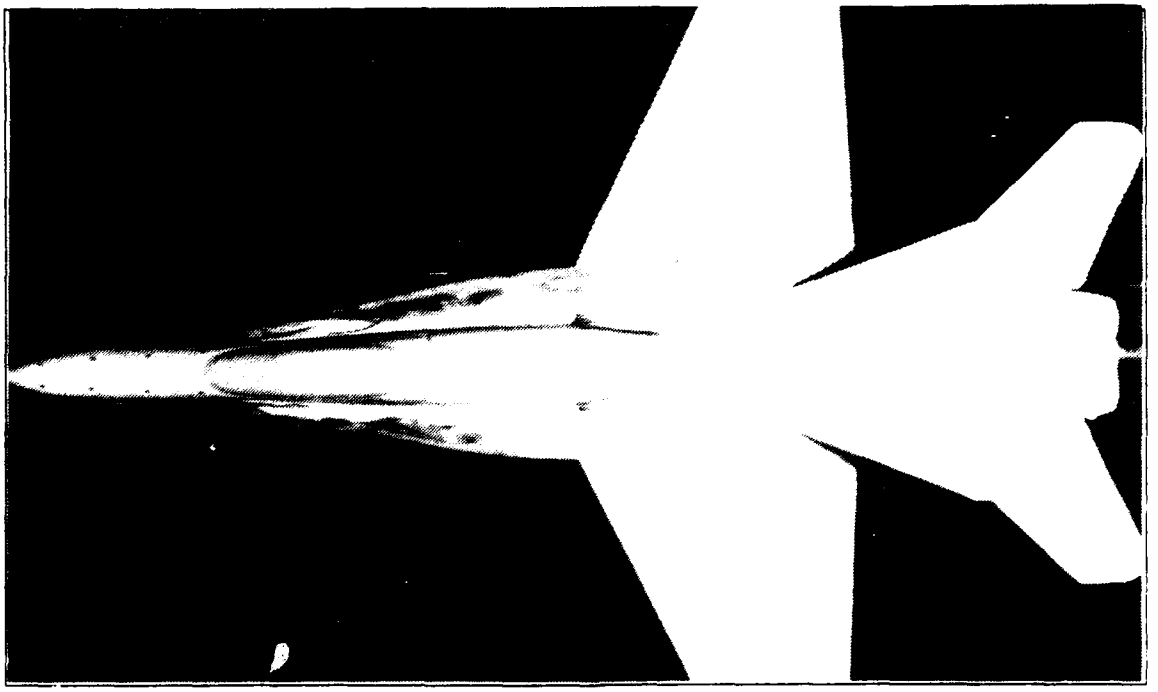

Figure 101. LEX, High Pitch Up, AOA = 10 deg , YAW = 0 deg.

Figure 102. LEX, Low Pitch Up, AOA = 20 deg , YAW = 0 deg.

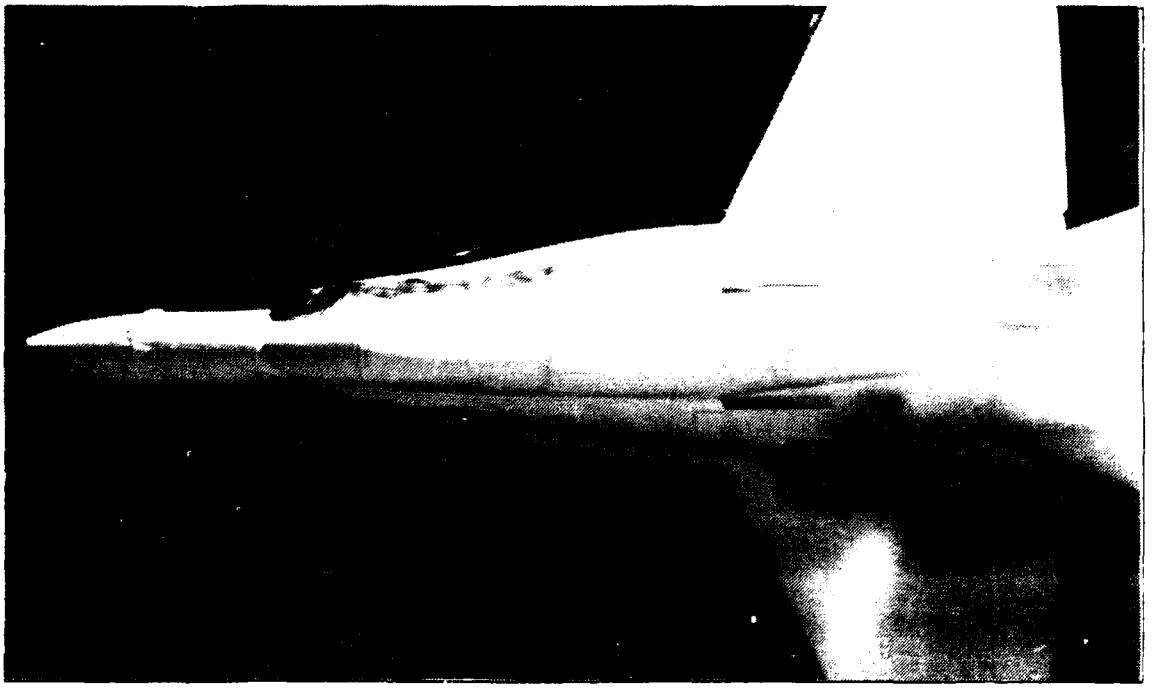

Figure 103. LEX, Low Pitch Down, AOA = 20 deg , YAW = 0 deg.

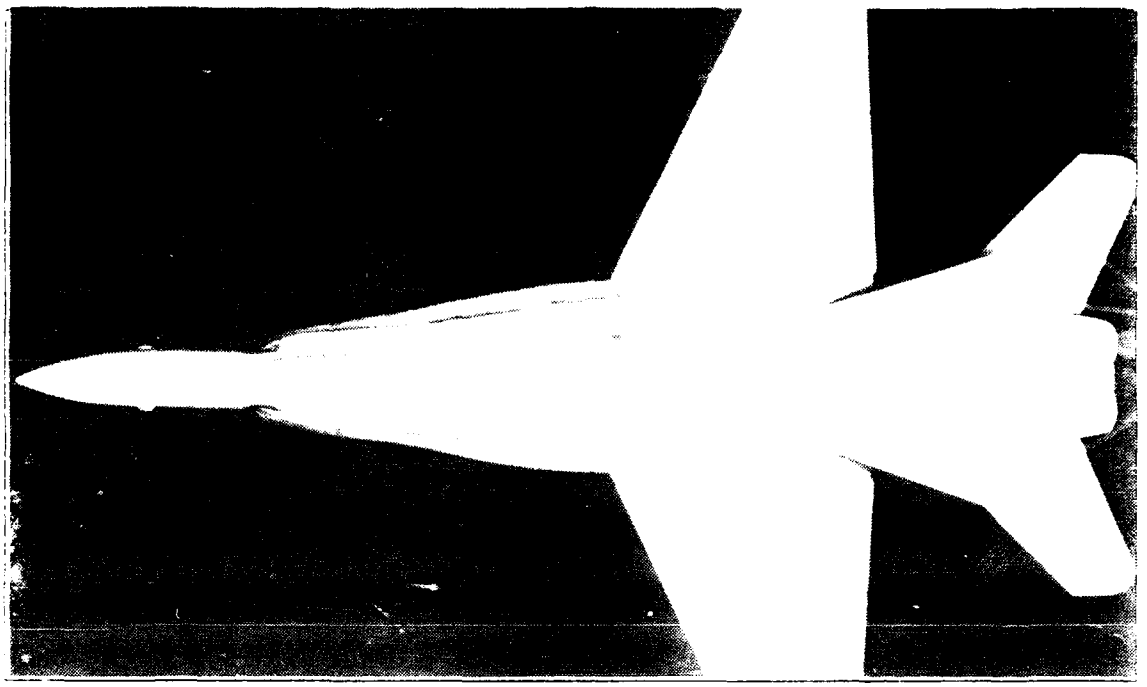

Figure 104. LEX, High Pitch Up, AOA = 20 deg, YAW = 0 deg.

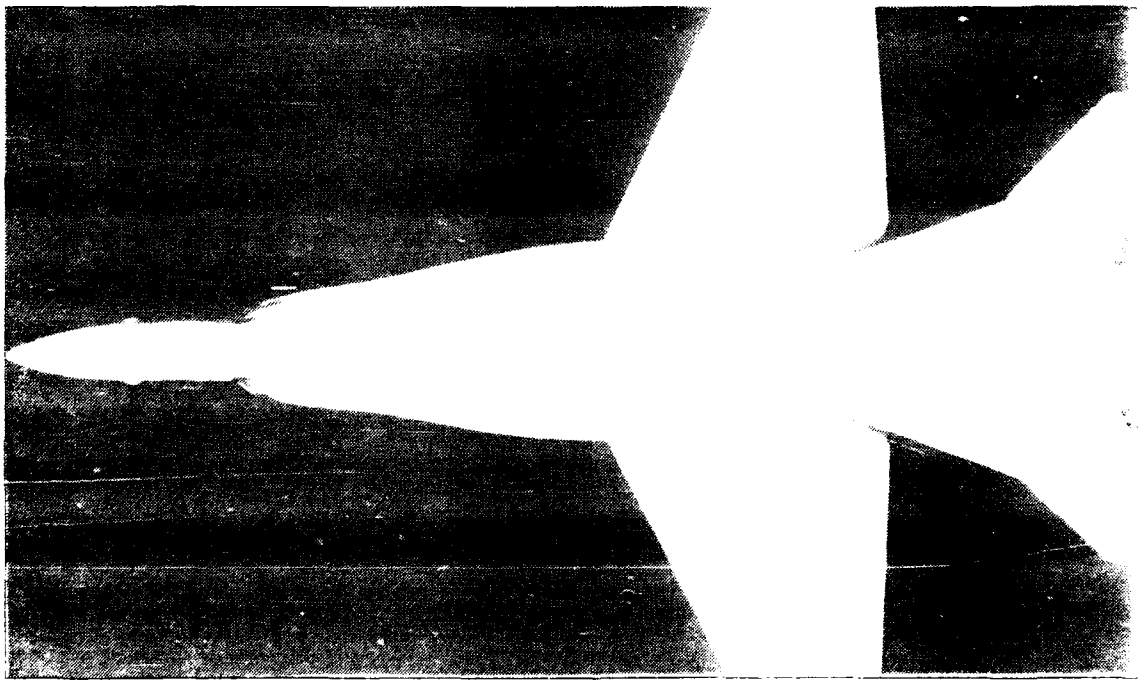

Figure 105. LEX, High Pitch Down, AOA = 20 deg, YAW = 0 deg.

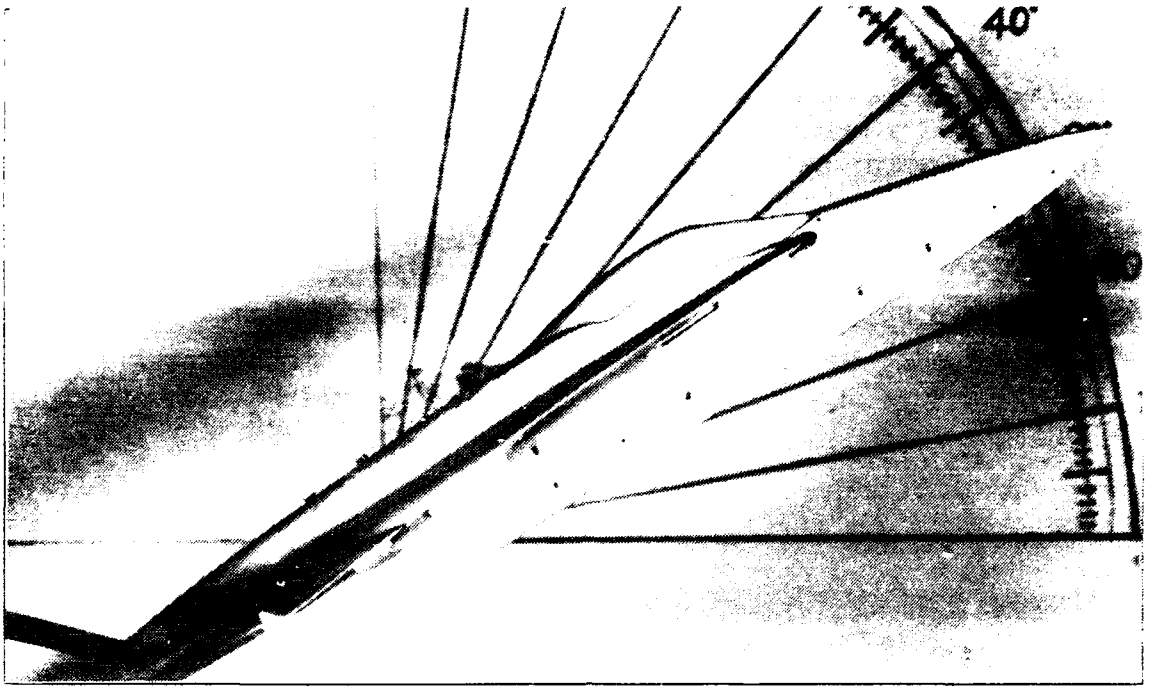

Figure 106. LEX, Static, AOA = 30 deg , YAW = 0 deg.

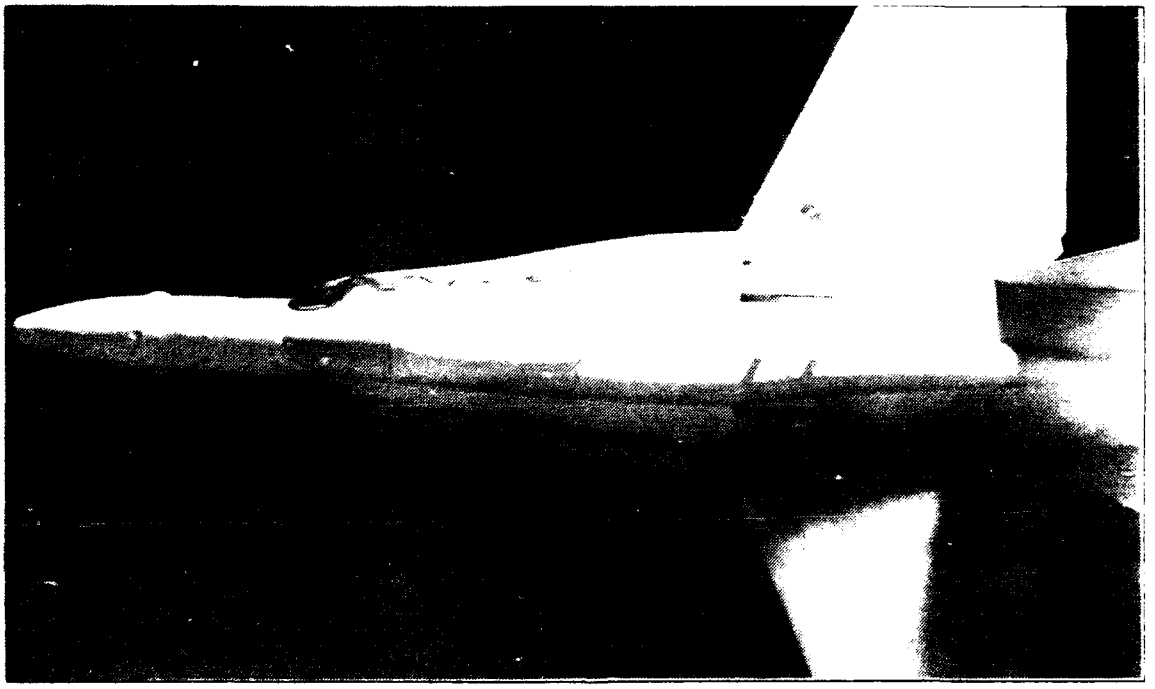

Figure 107. LEX, Low Pitch Up, AOA = 30 deg , YAW = 0 deg.

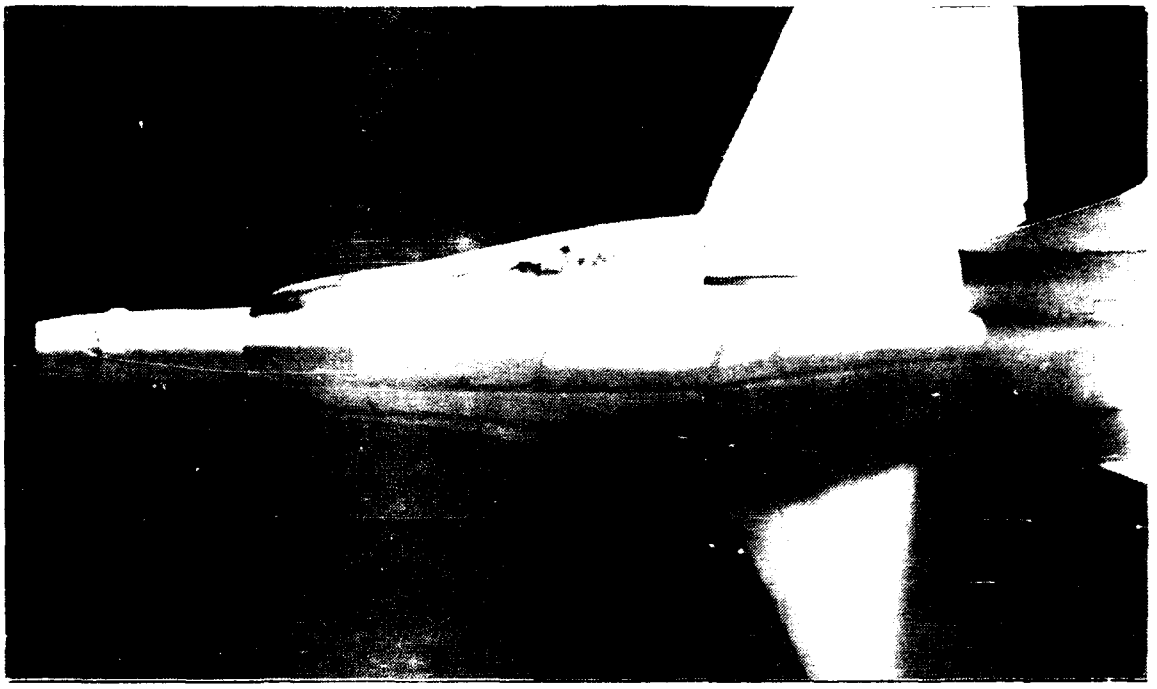

Figure 108. LEX, Low Pitch Down, AOA = 30 deg , YAW = 0 deg.

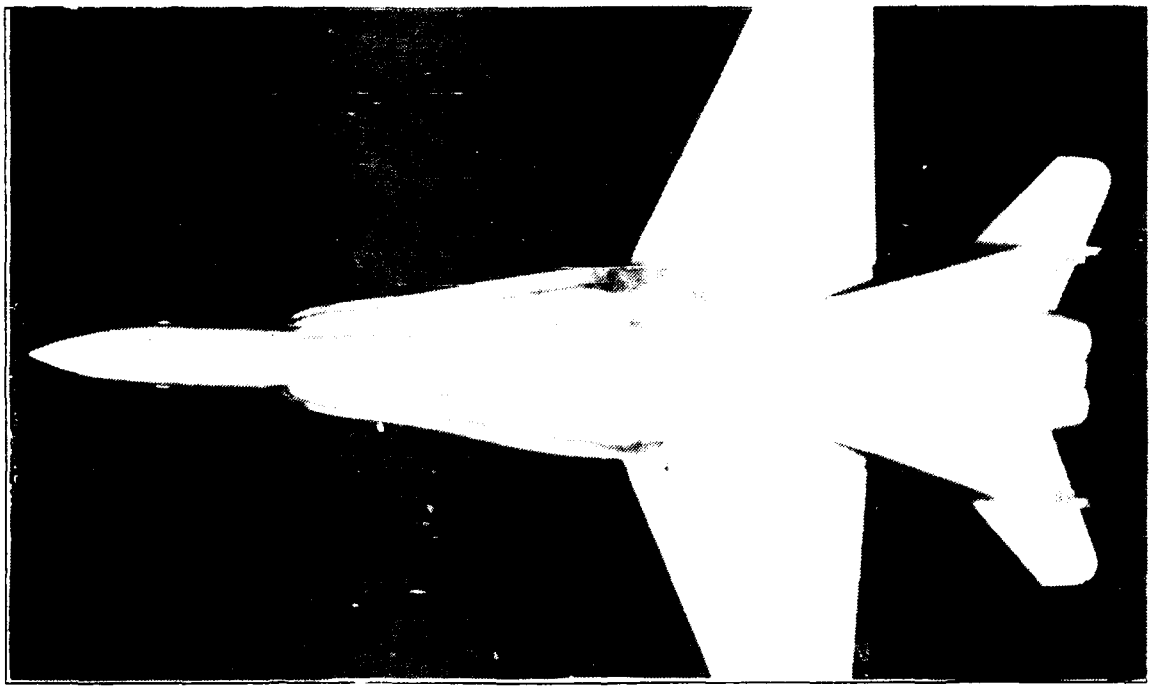

Figure 109. LEX, High Pitch Up, AOA = 30 deg , YAW = 0 deg.

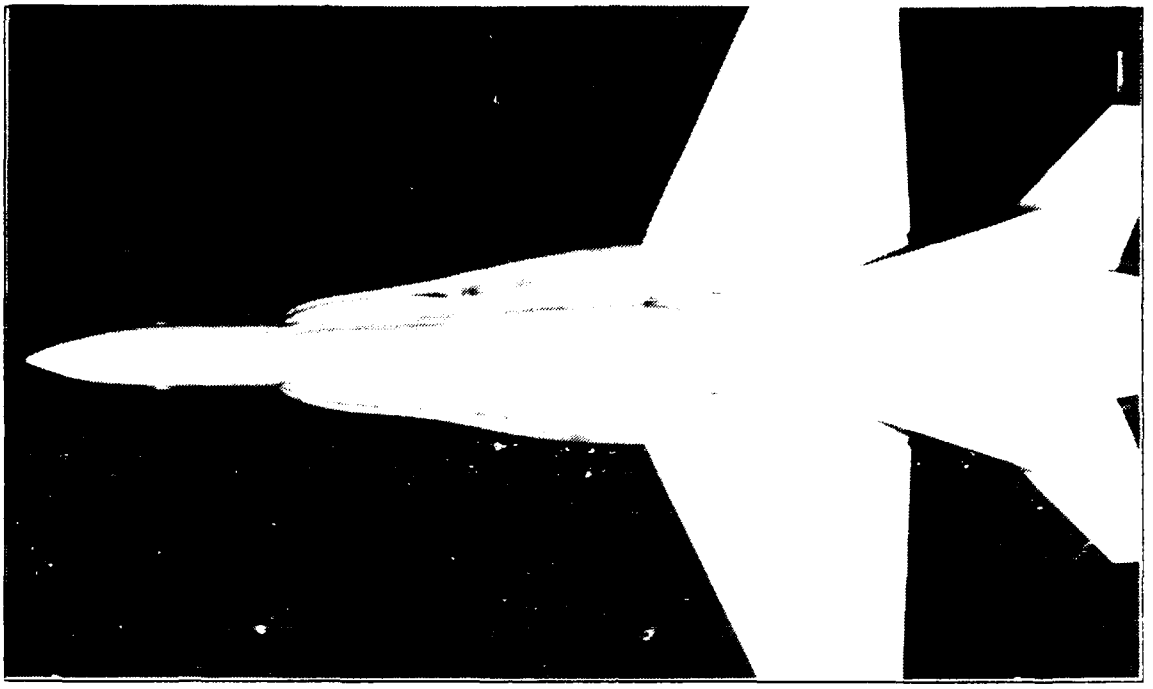

Figure 110. LEX, High Pitch Down, AOA = 30 deg , YAW = 0 deg.

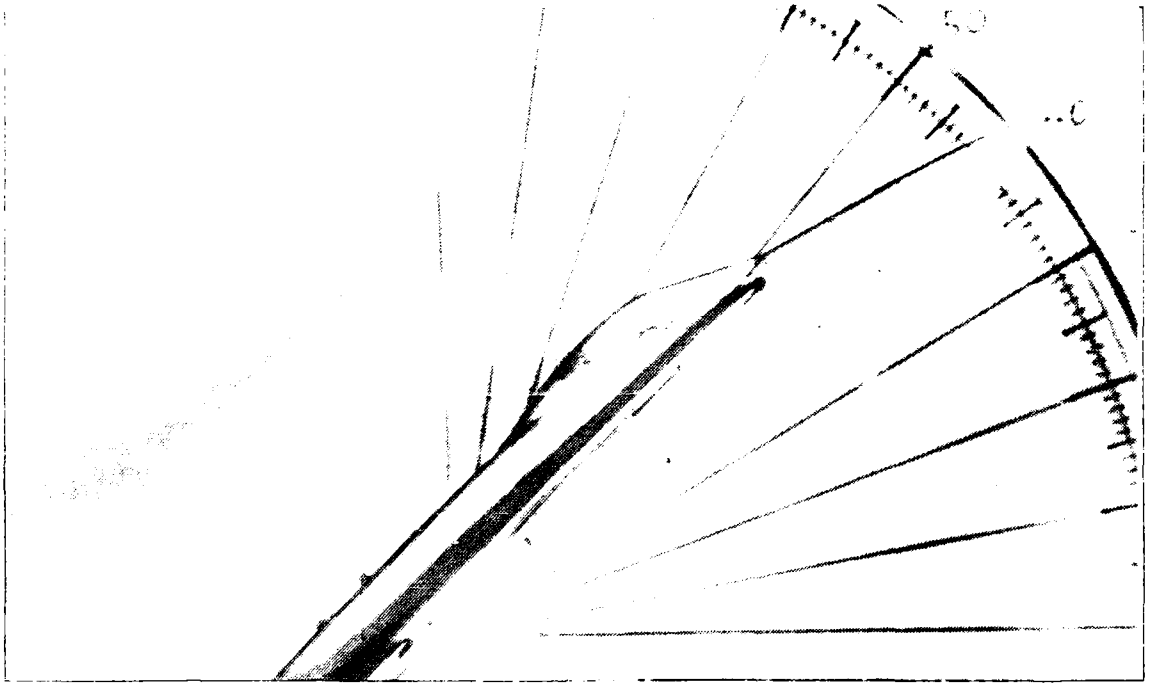

Figure 111. LEX, Static, AOA = 40 deg , YAW = 0 deg.

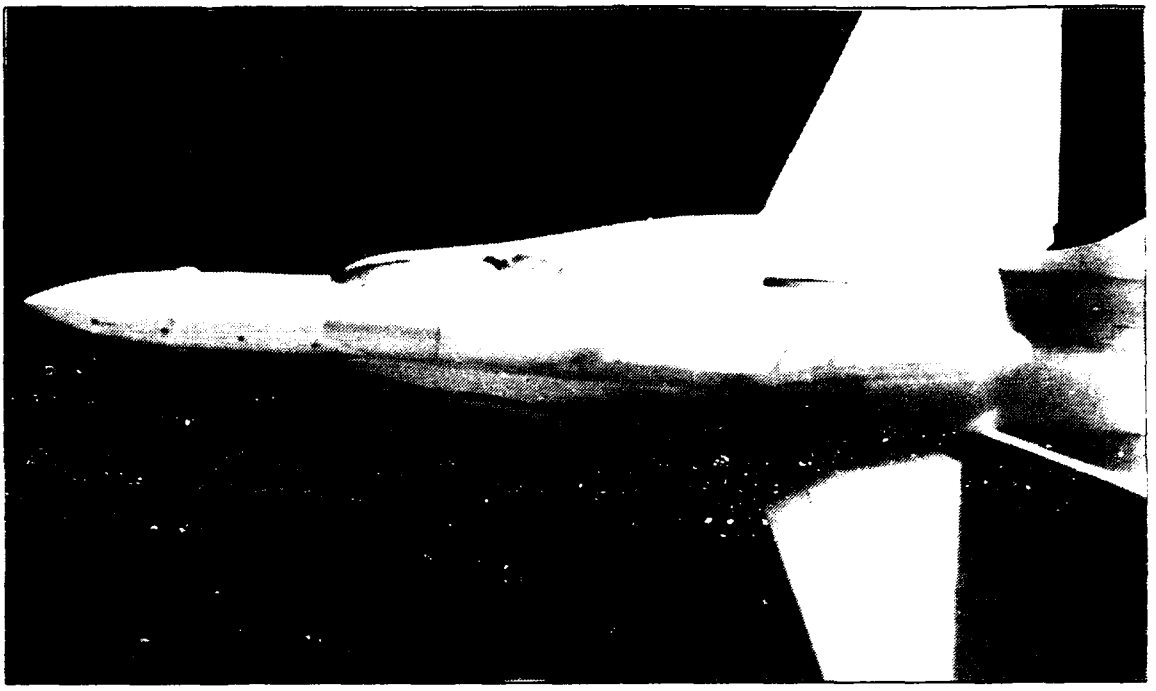

Figure 112. LEX, Low Pitch Up, AOA = 40 deg , YAW = 0 deg.

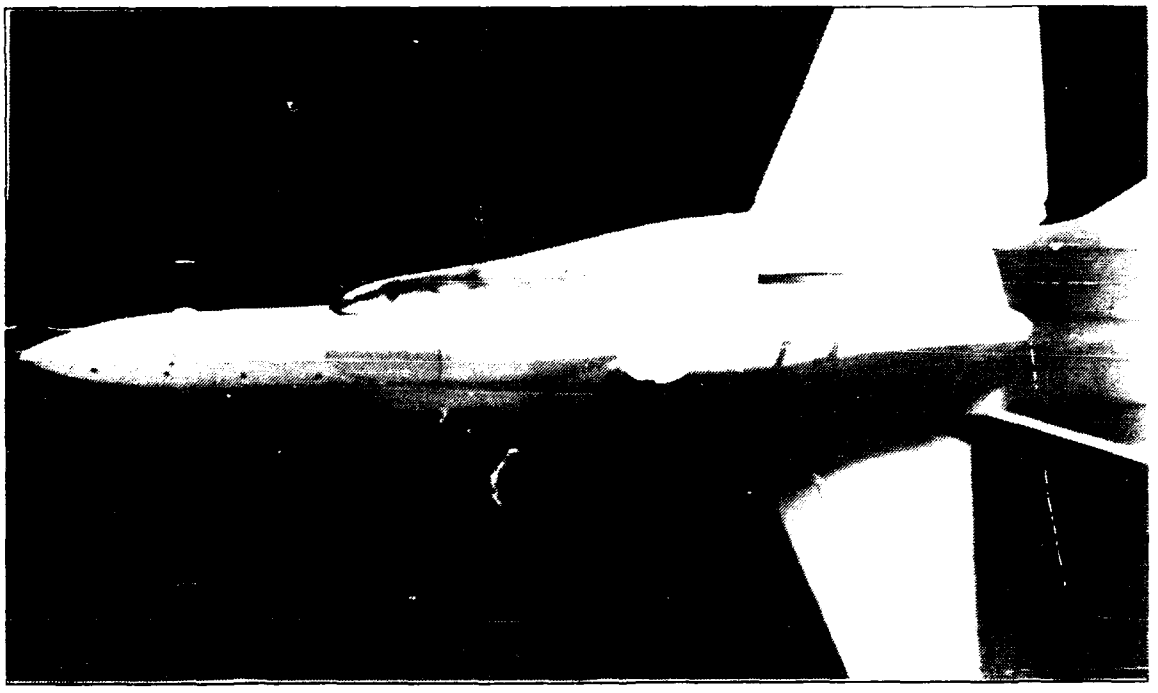

Figure 113. LEX, Low Pitch Down, AOA = 40 deg , YAW = 0 deg.

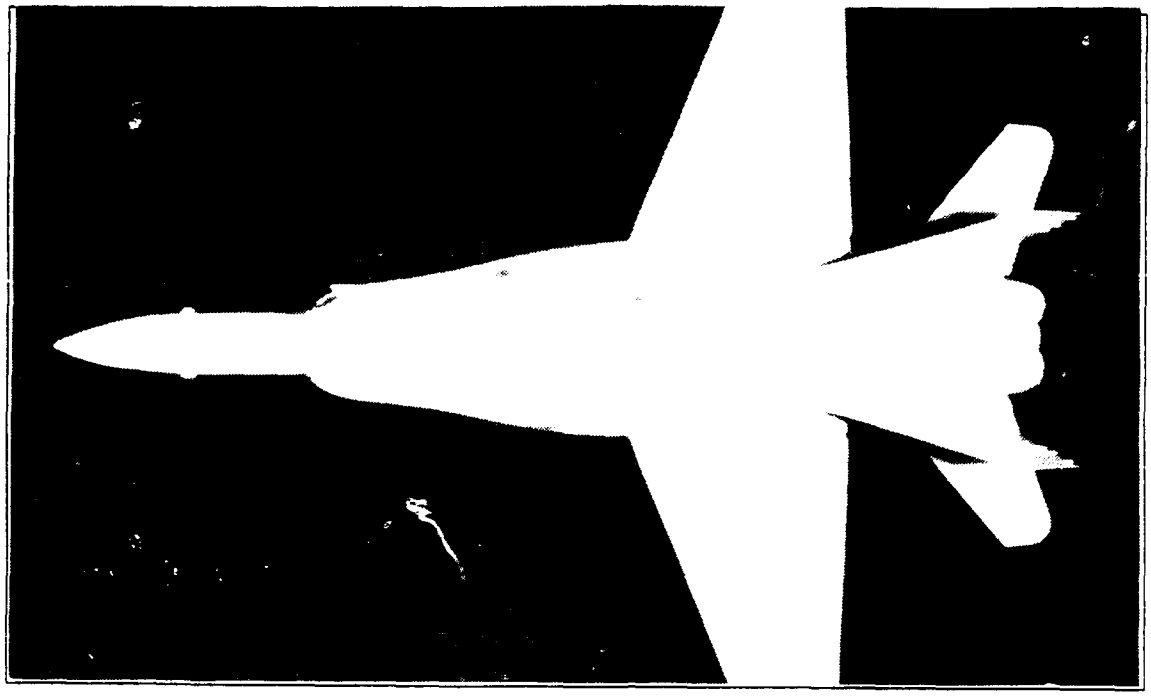

Figure 114. LEX, High Pitch Up, AOA = 40 deg, YAW = 0 deg.

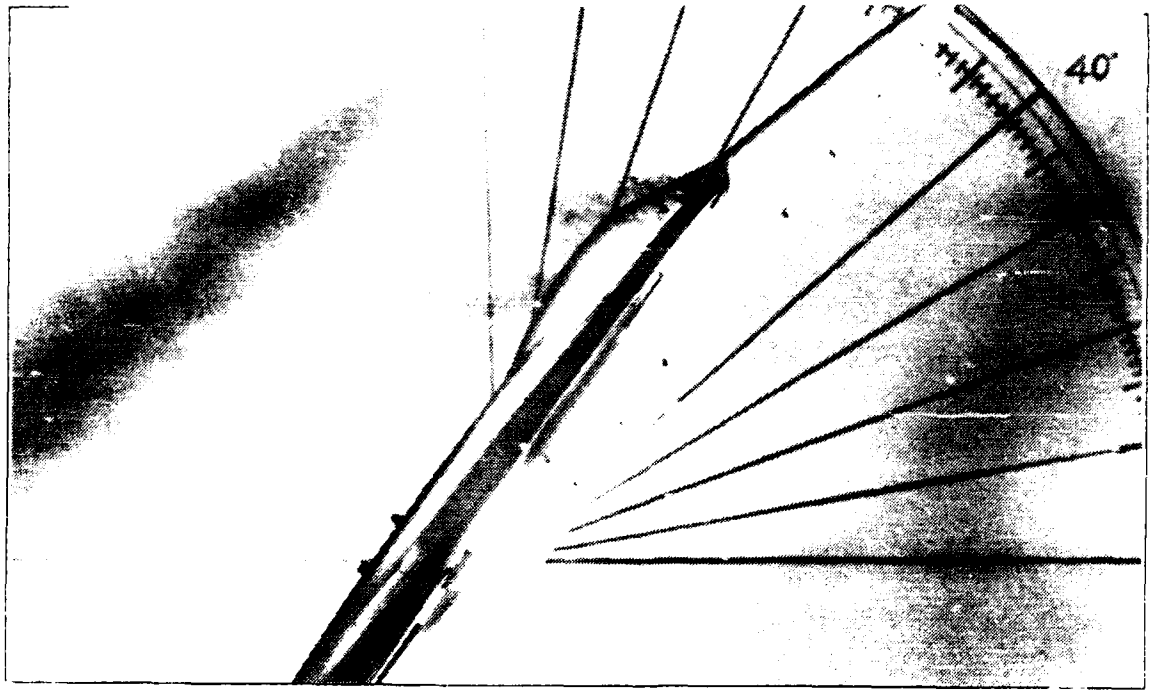

Figure 115. LEX, Static, AOA = 50 deg, YAW = 0 deg.

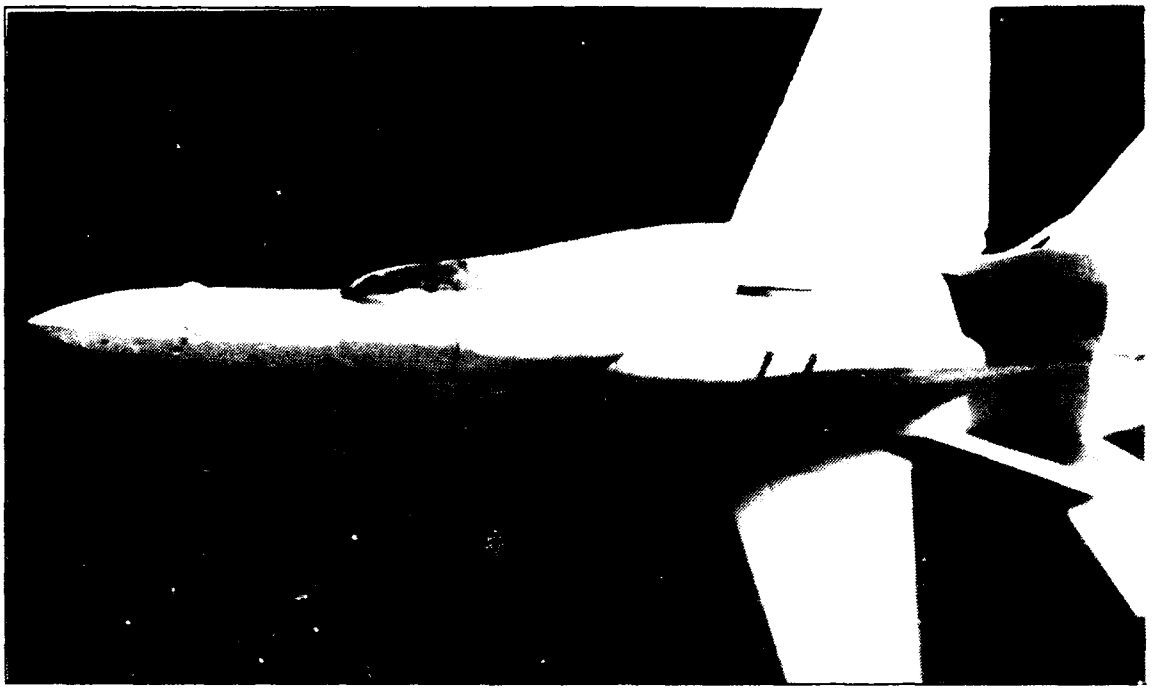

Figure 116. LEX, Low Pitch Up, AOA = 50 deg , YAW = 0 deg.

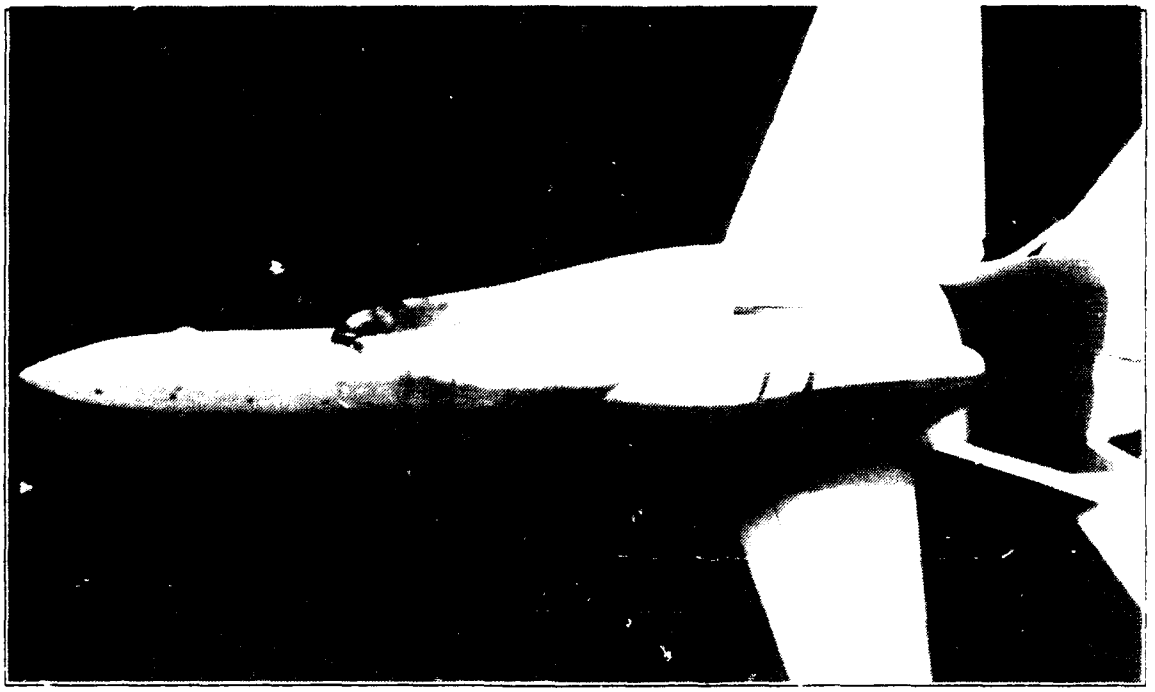

Figure 117. LEX, Low Pitch Down, AOA = 50 deg , YAW = 0 deg.

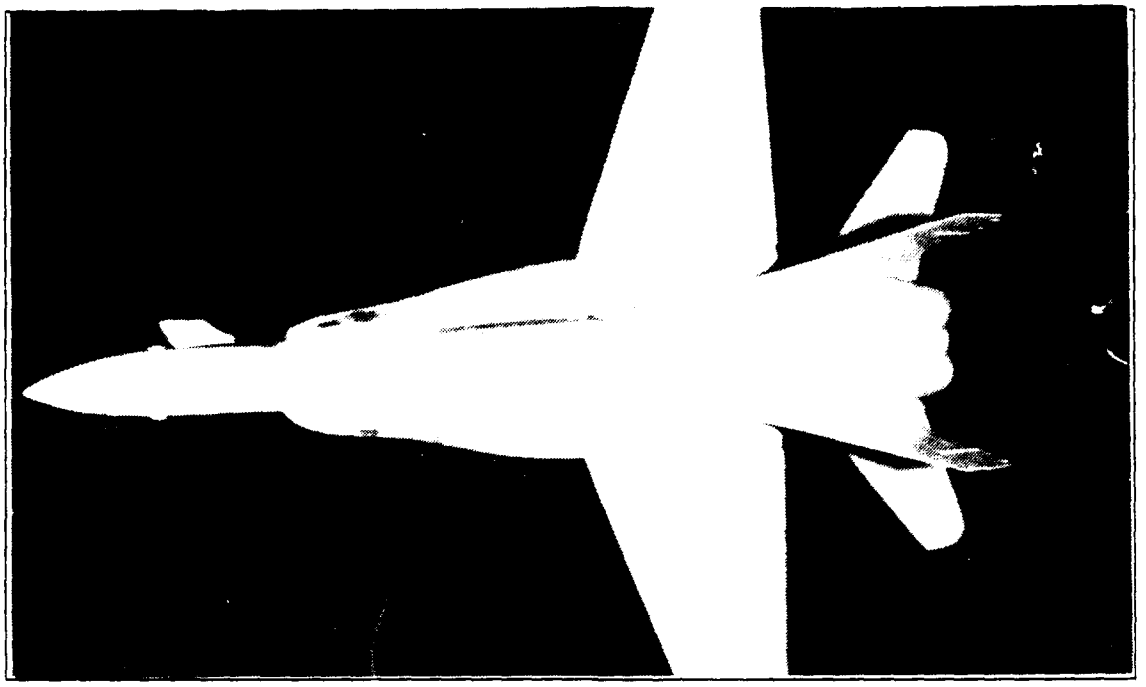

Figure 118. LEX, High Pitch Up, AOA = 50 deg , YAW = 0 deg.

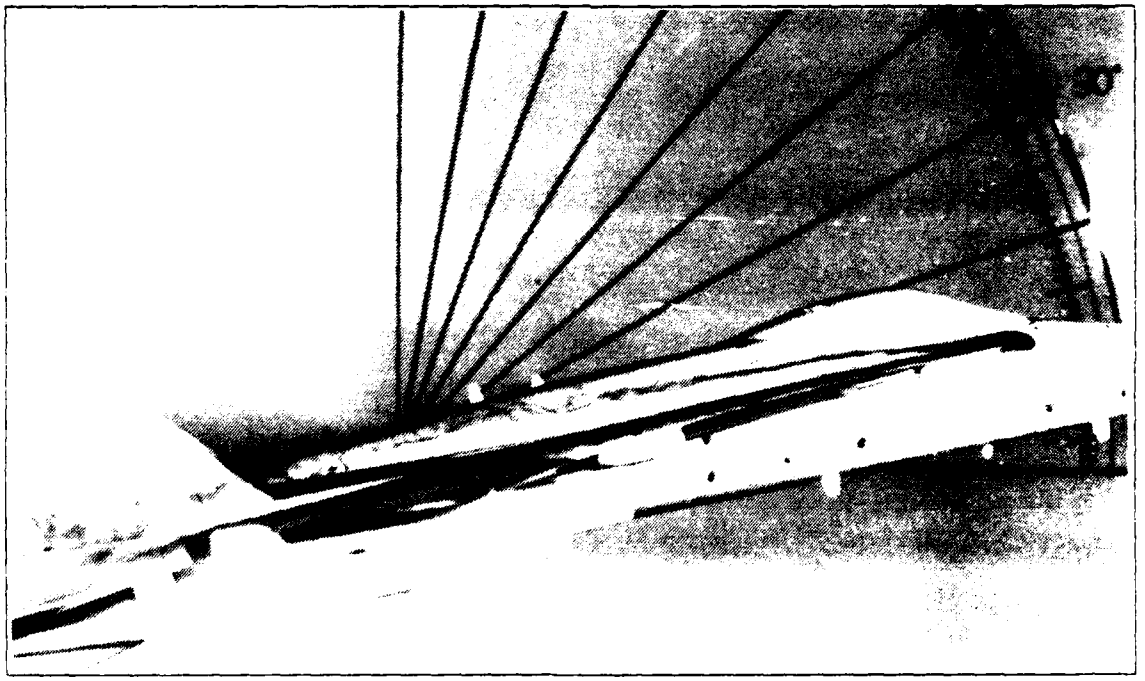

Figure 119. LEX, Static, AOA = 10 deg , YAW = 0 deg.

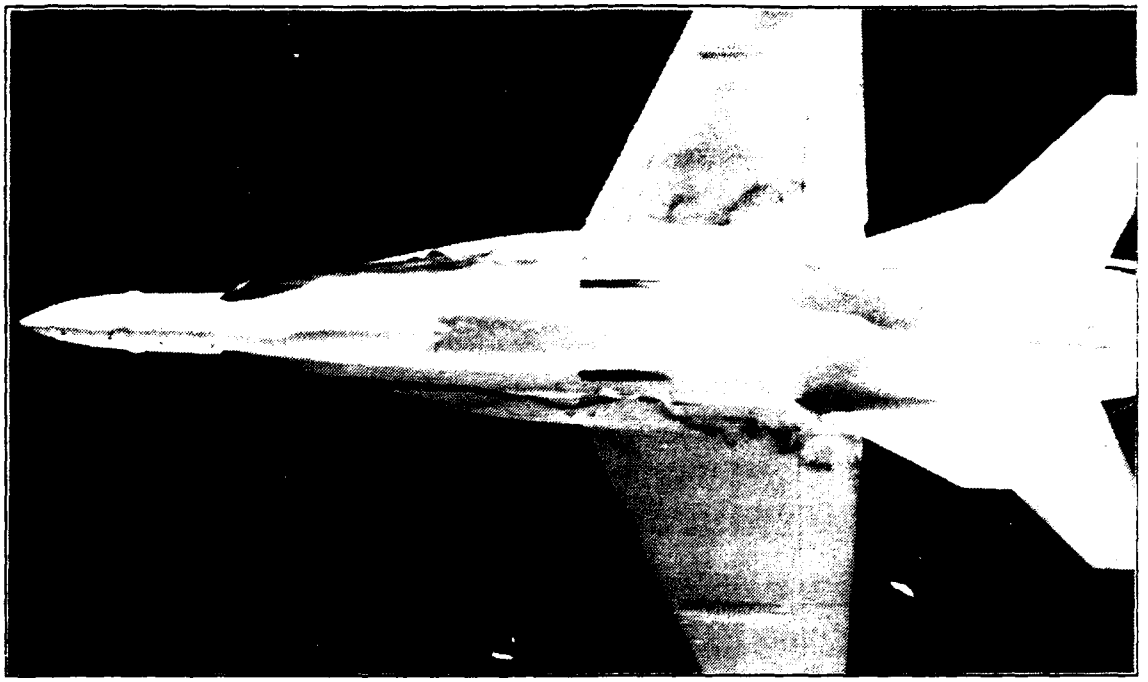

Figure 120. LEX, Static, AOA = 10 deg , YAW = 5 deg.

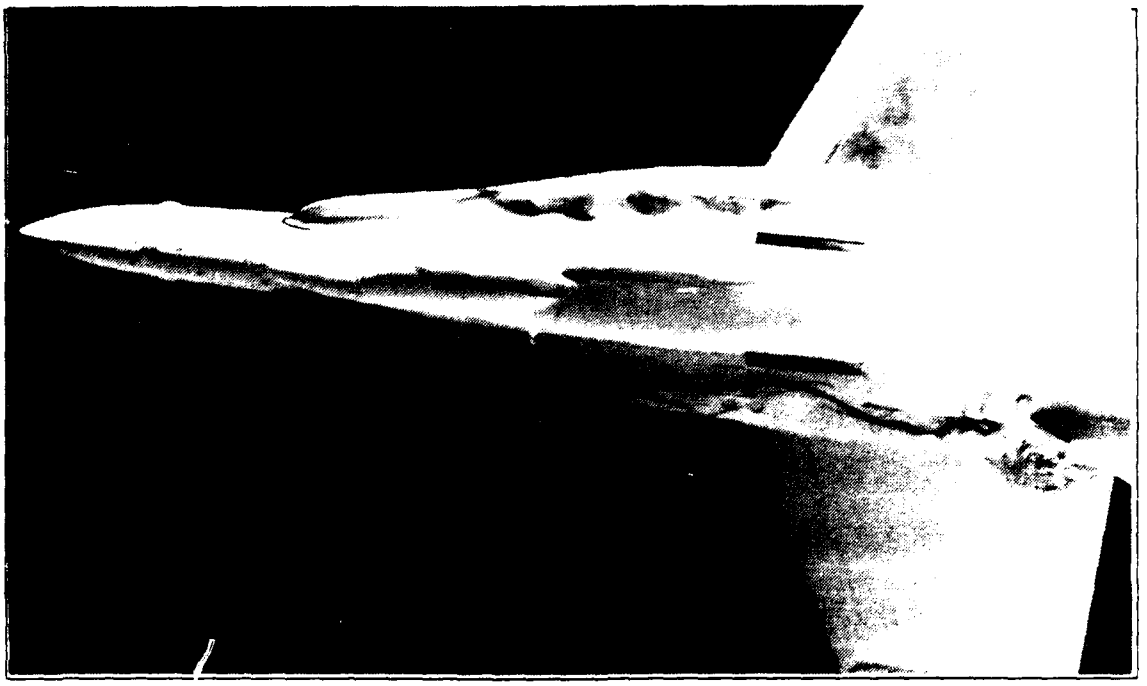

Figure 121. LEX, Static, AOA = 10 deg , YAW = 10 deg.

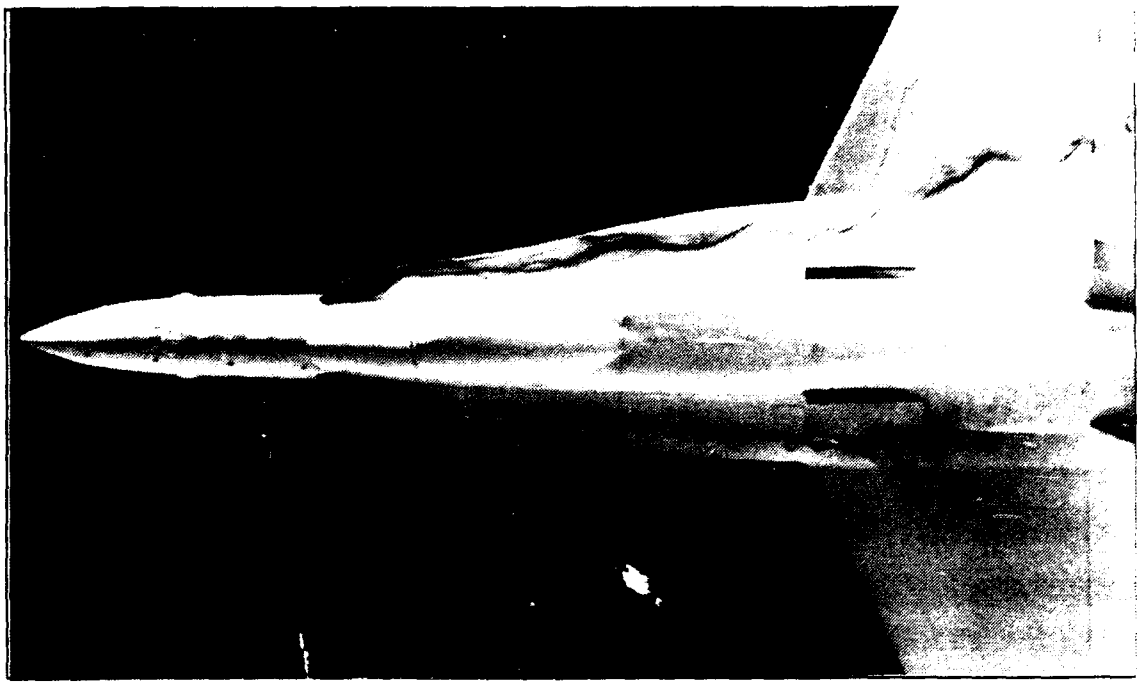

Figure 122. LEX, Static, AOA = 20 deg , YAW = 5 deg.

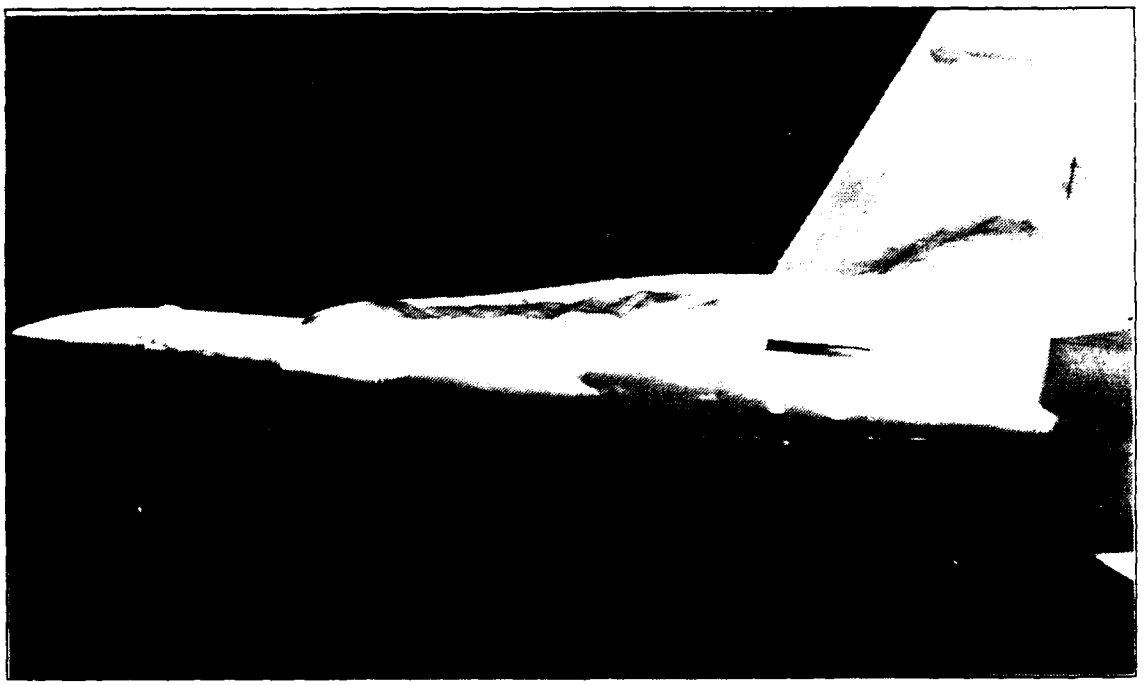

Figure 123. LEX, Static, AOA = 20 deg , YAW = 10 deg.

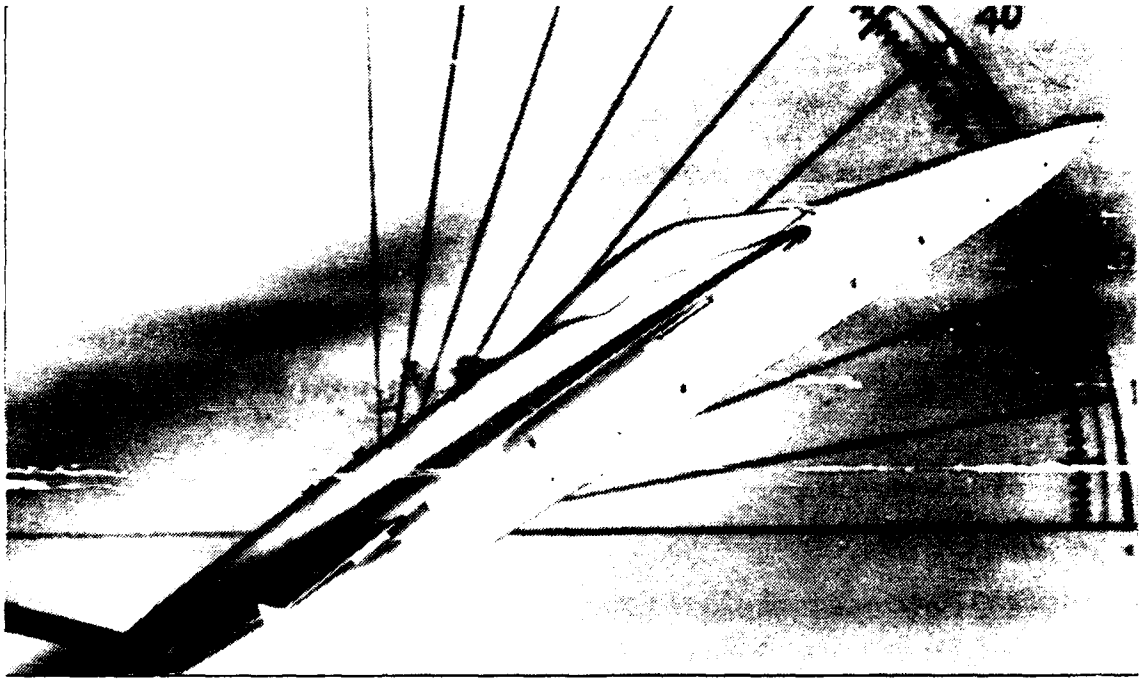

Figure 124. LEX, Static, AOA = 30 deg , YAW = 0 deg.

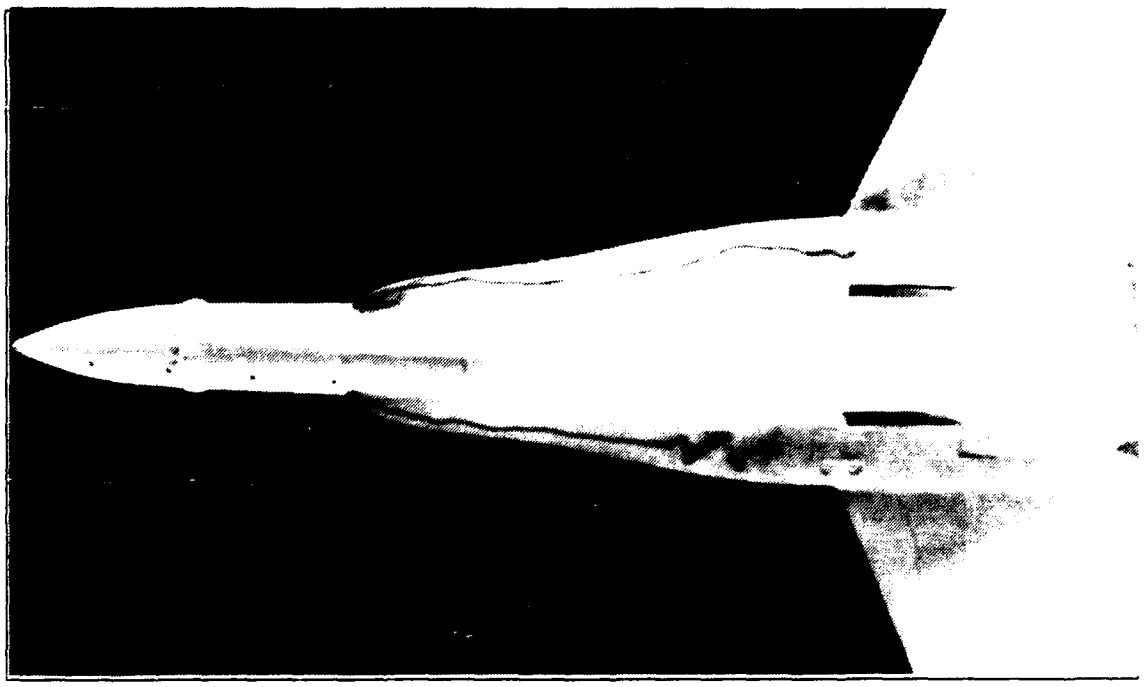

Figure 125. LEX, Static, AOA = 30 deg , YAW = 5 deg.

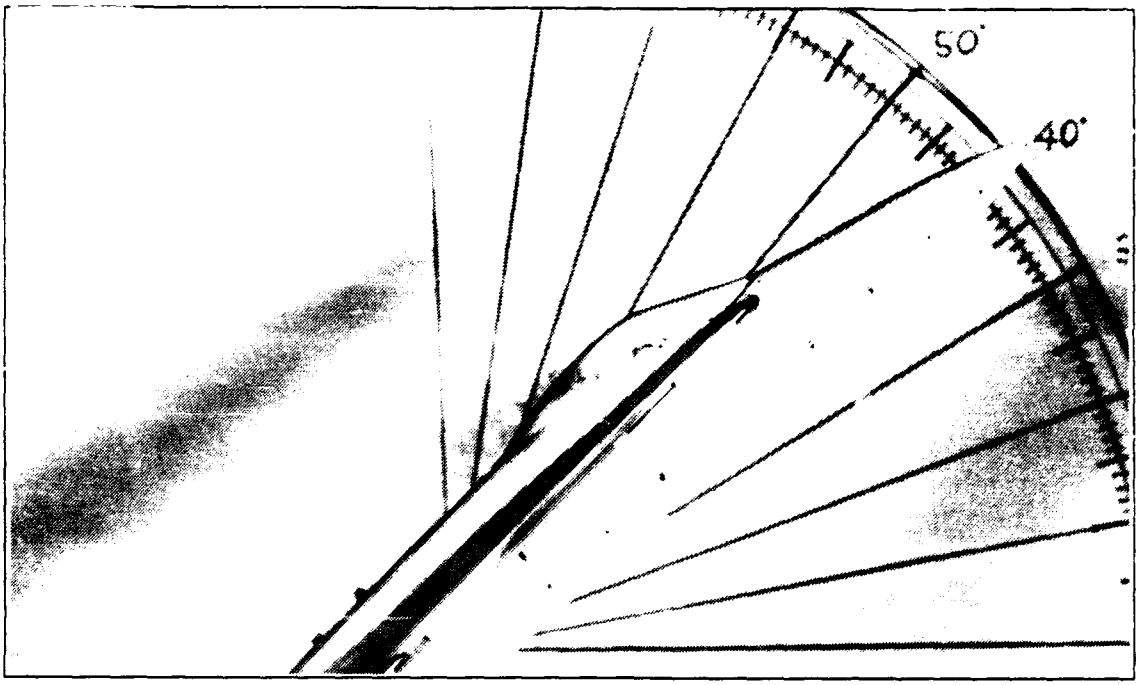

Figure 126. LEX, Static, AOA = 40 deg , YAW = 0 deg.

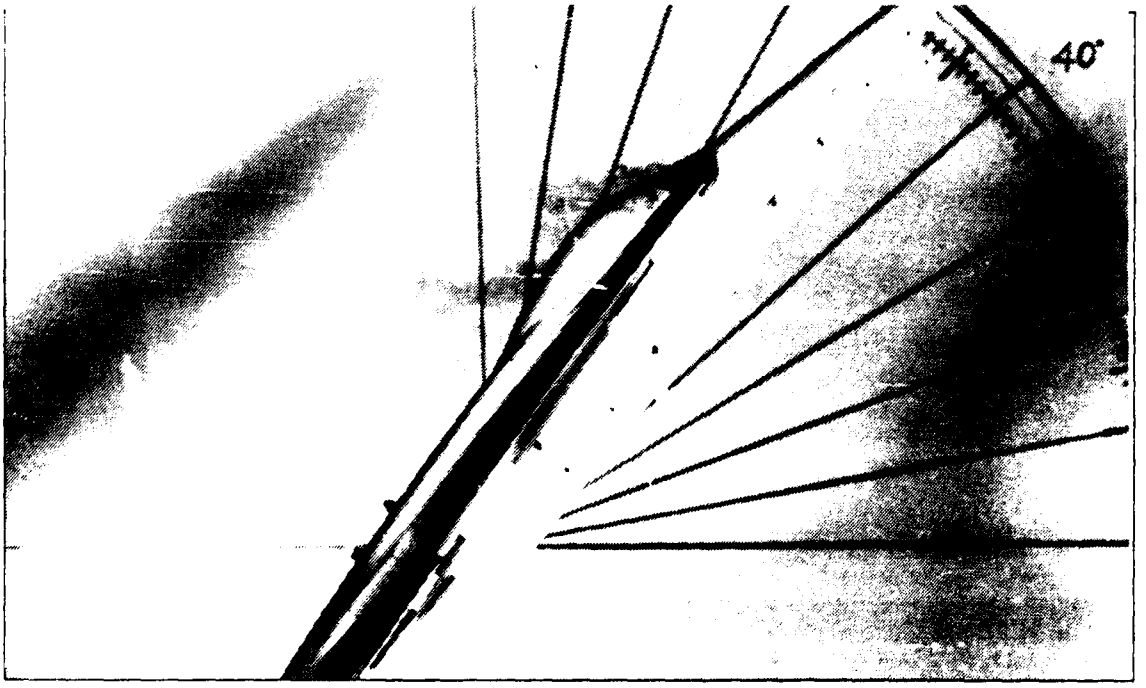

Figure 127. LEX, Static, AOA = 50 deg , YAW = 0 deg.

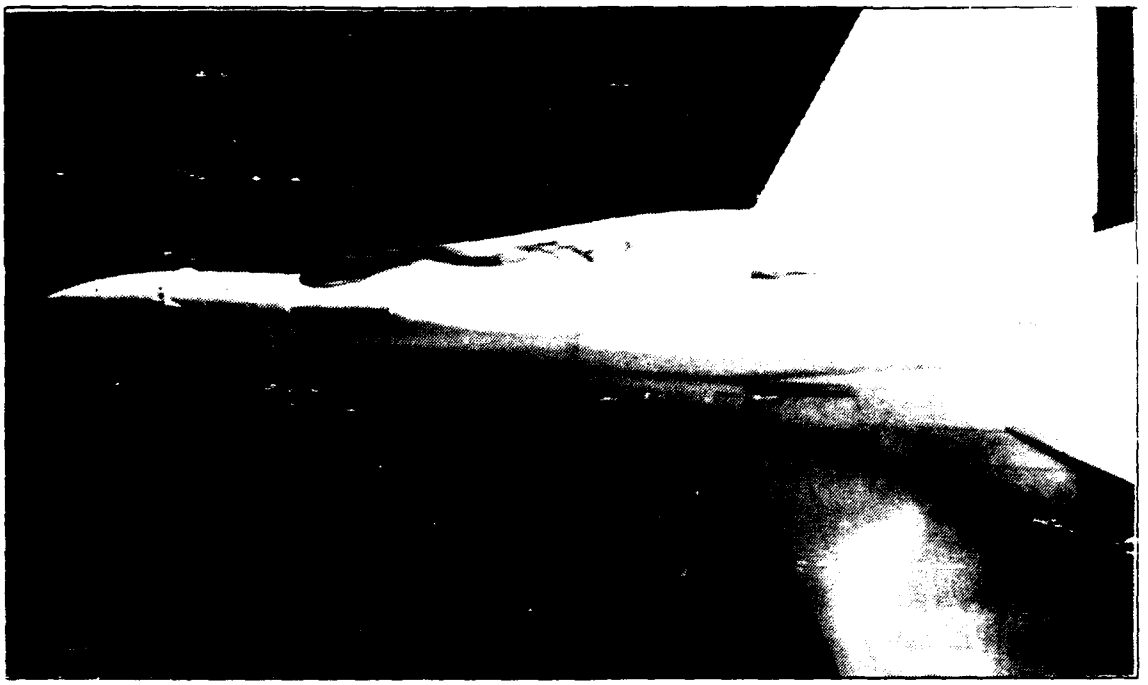

Figure 128. LEX, Low Pitch Up, AOA = 20 deg , YAW = 0 deg.

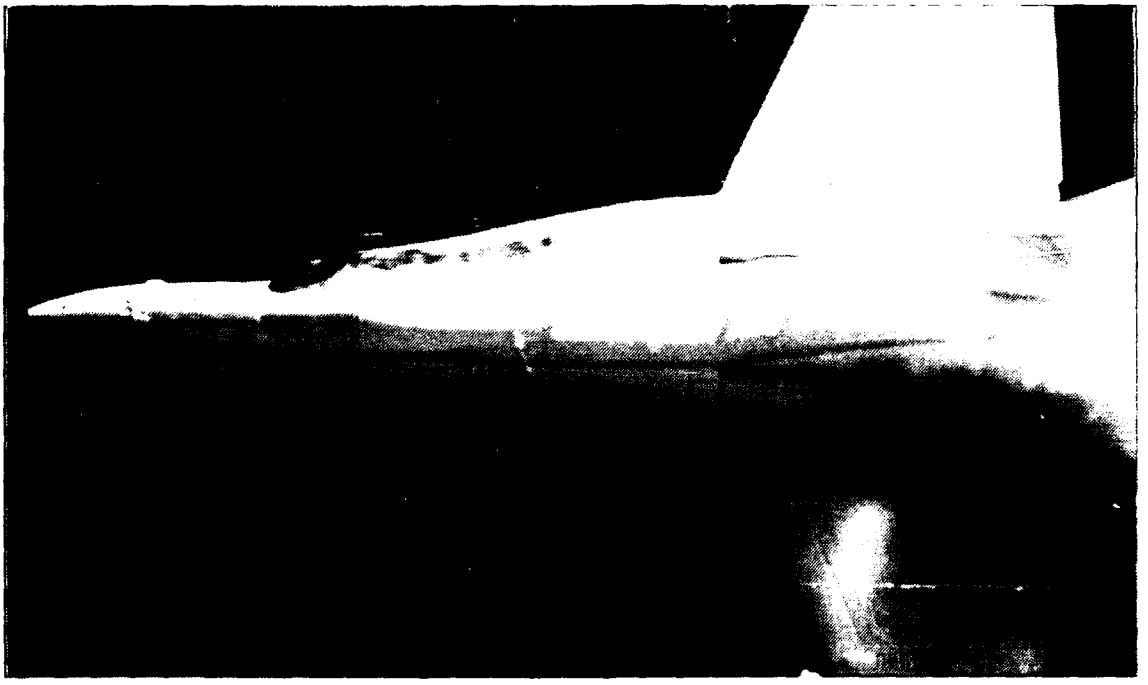

Figure 129. LEX, Low Pitch Down, AOA = 20 deg , YAW = 0 deg.

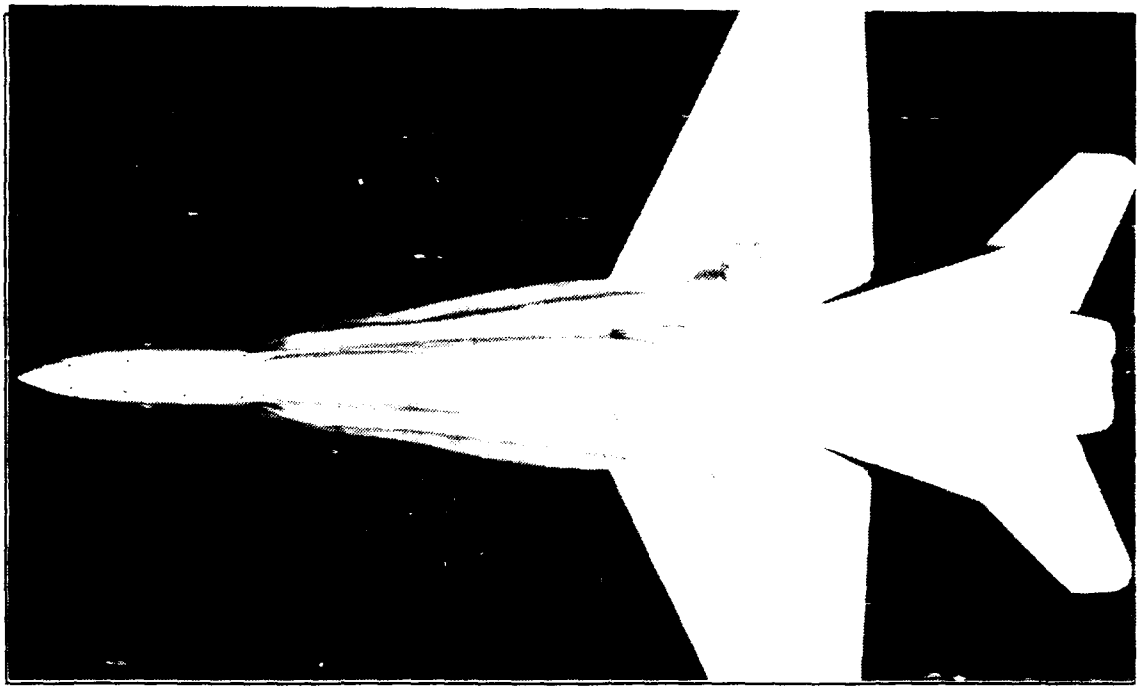

Figure 130. LEX, High Pitch Up, AOA = 20 deg , YAW = 0 deg.

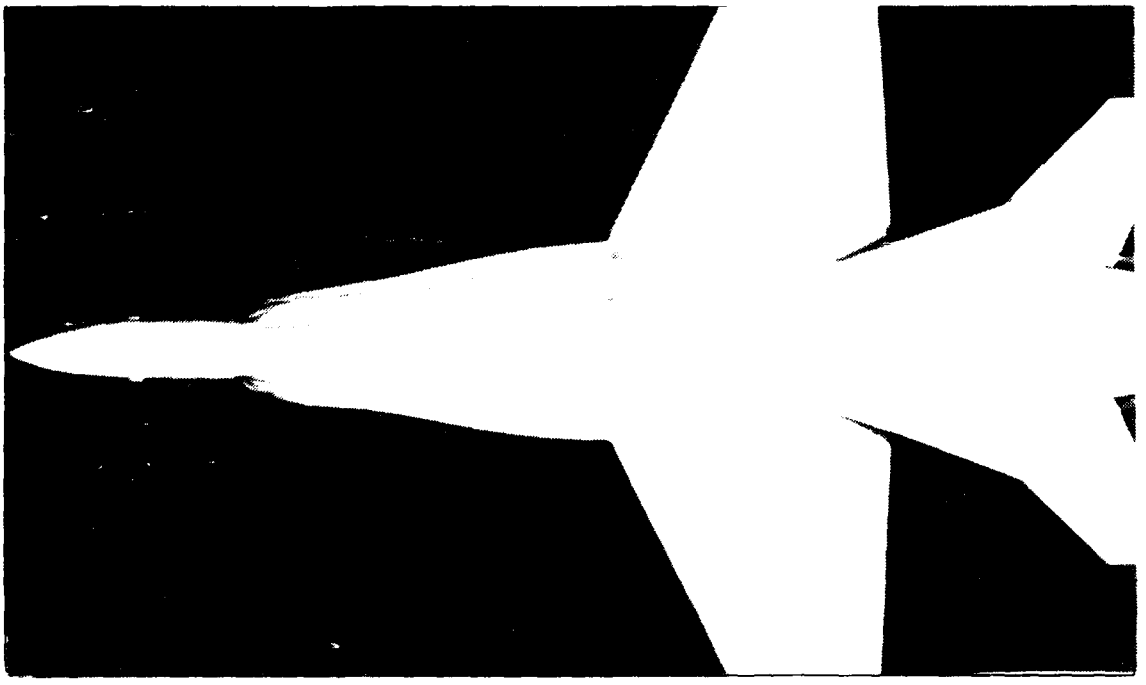

Figure 131. LEX, High Pitch Down, AOA = 20 deg , YAW = 0 deg.

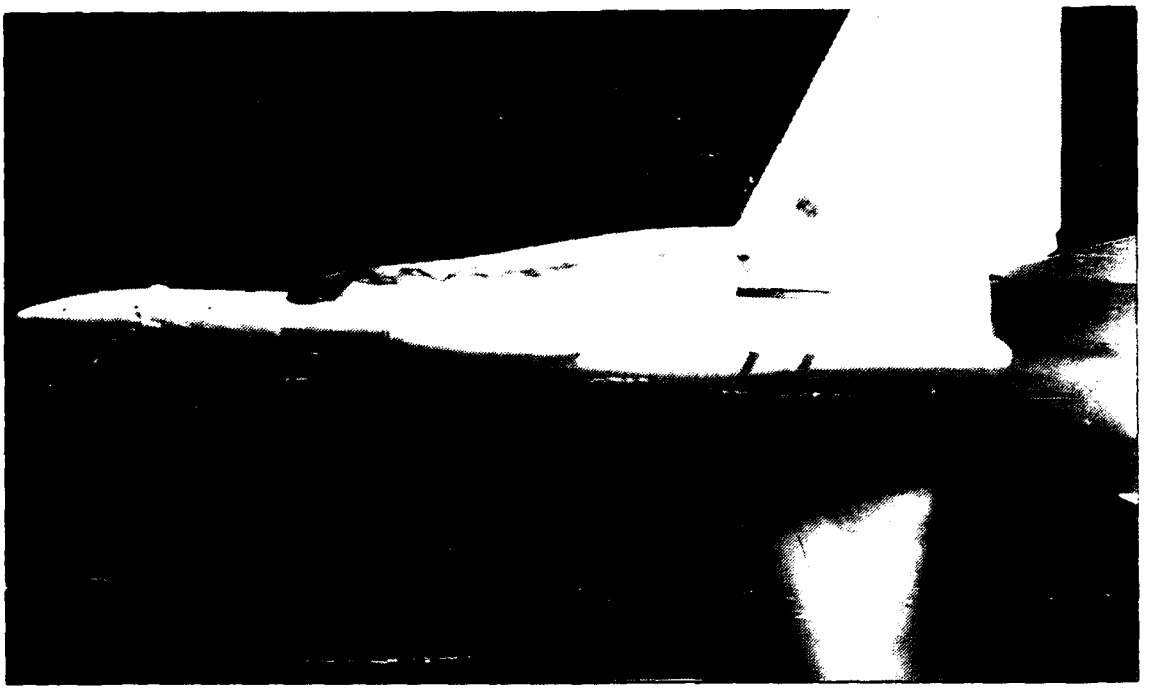

Figure 132. LEX, Low Pitch Up, AOA = 30 deg , YAW = 0 deg.

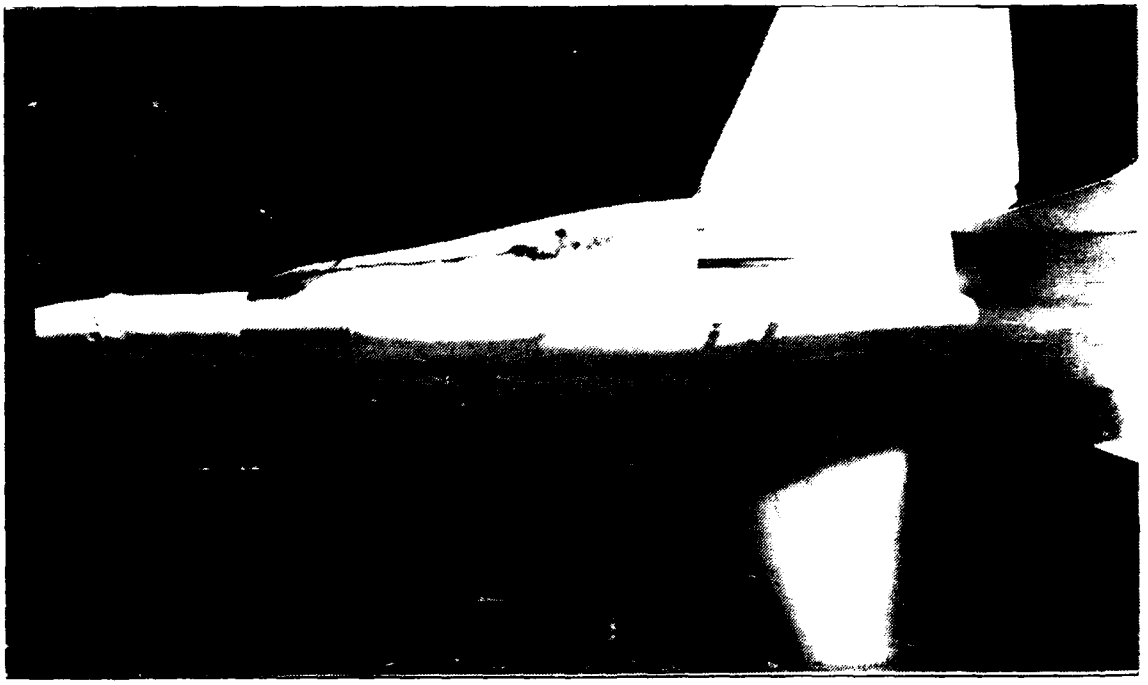

Figure 133. LEX, Low Pitch Down, AOA = 30 deg , YAW = 0 deg.

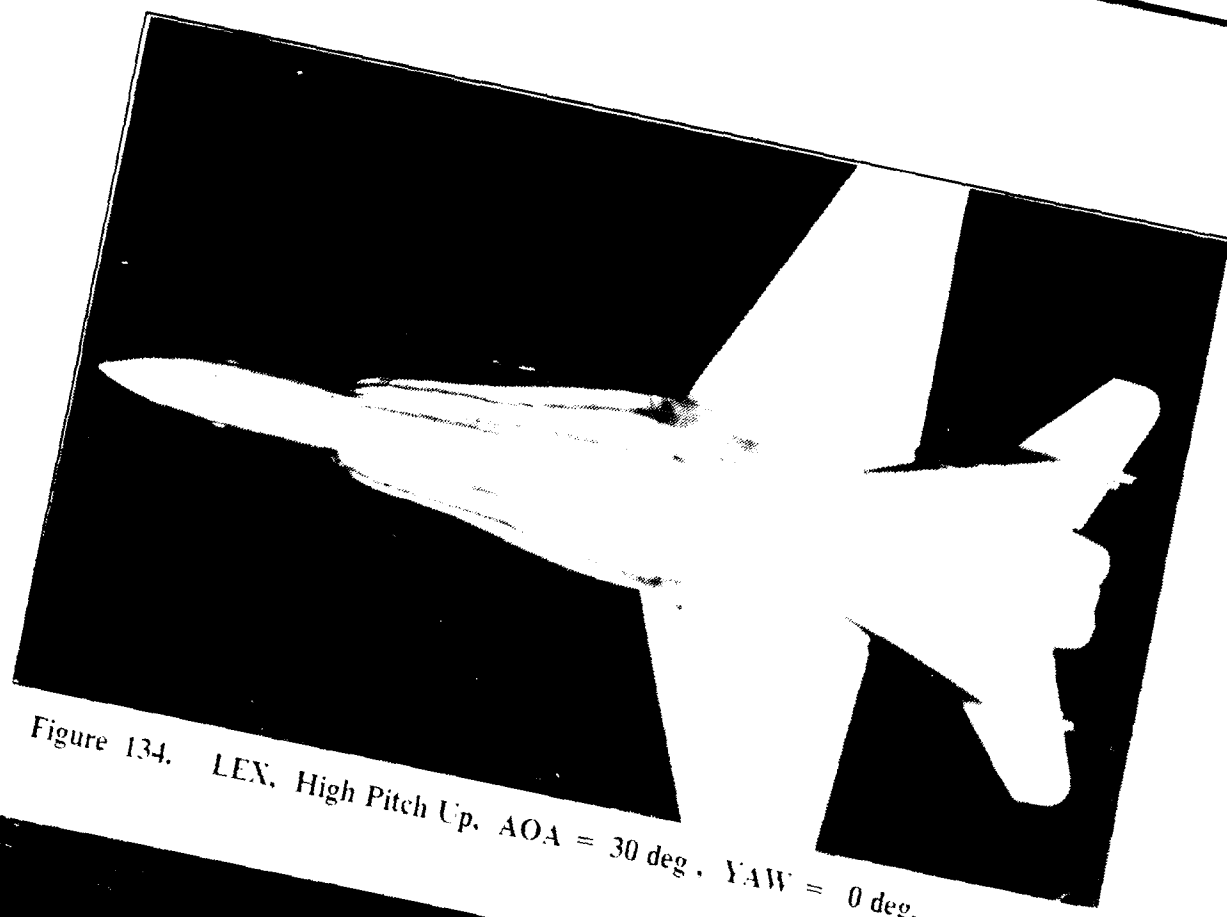

Figure 134. LEX, High Pitch Up, AOA = 30 deg, YAW = 0 deg.

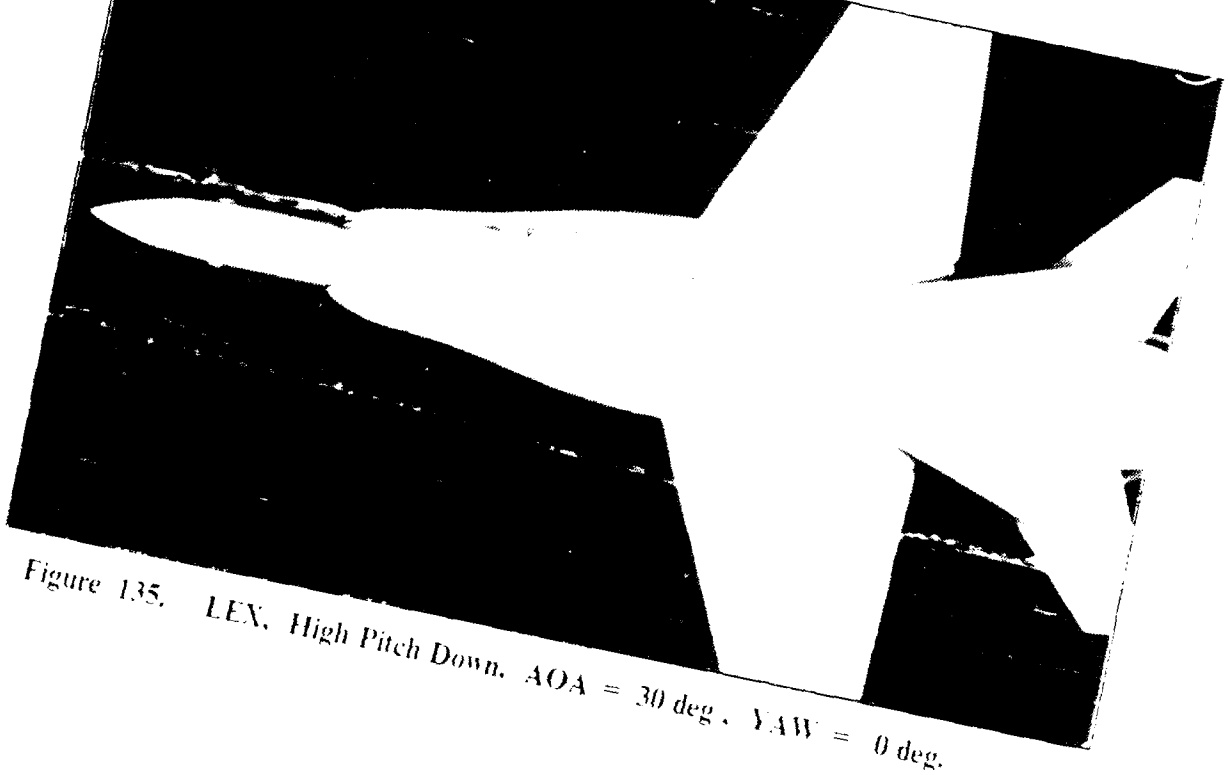

Figure 135. LEX, High Pitch Down, AOA = 30 deg, YAW = 0 deg.

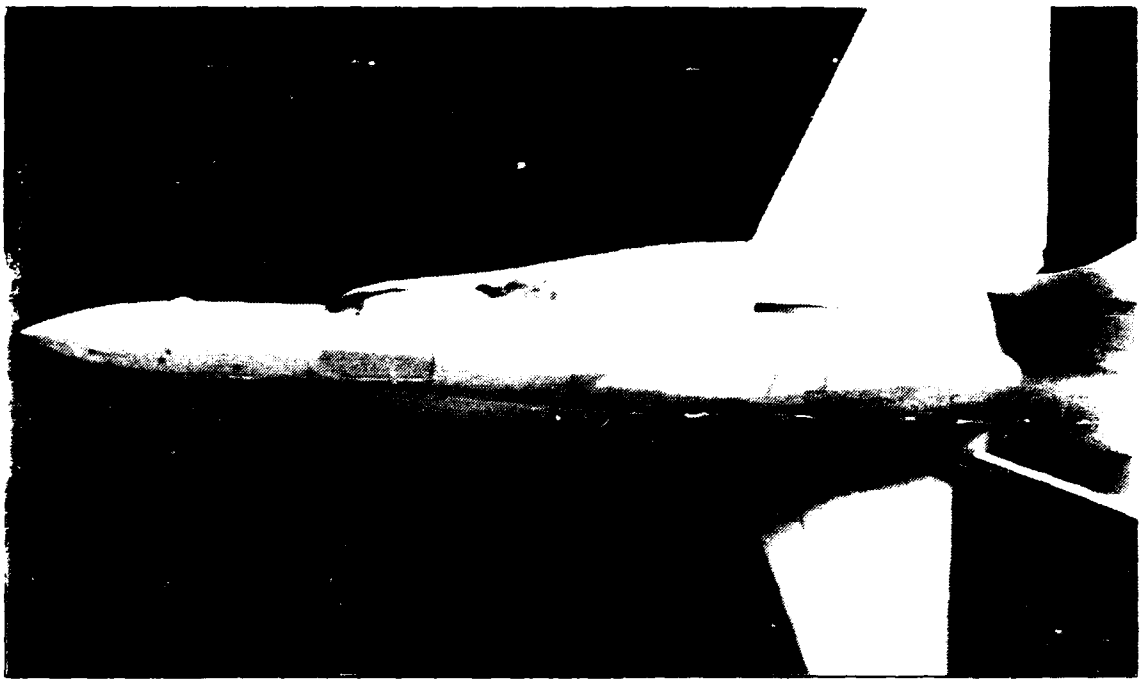

Figure 136. LEX, Low Pitch Up, AOA = 40 deg , YAW = 0 deg.

Figure 137. LEX, Low Pitch Down, AOA = 40 deg , YAW = 0 deg.

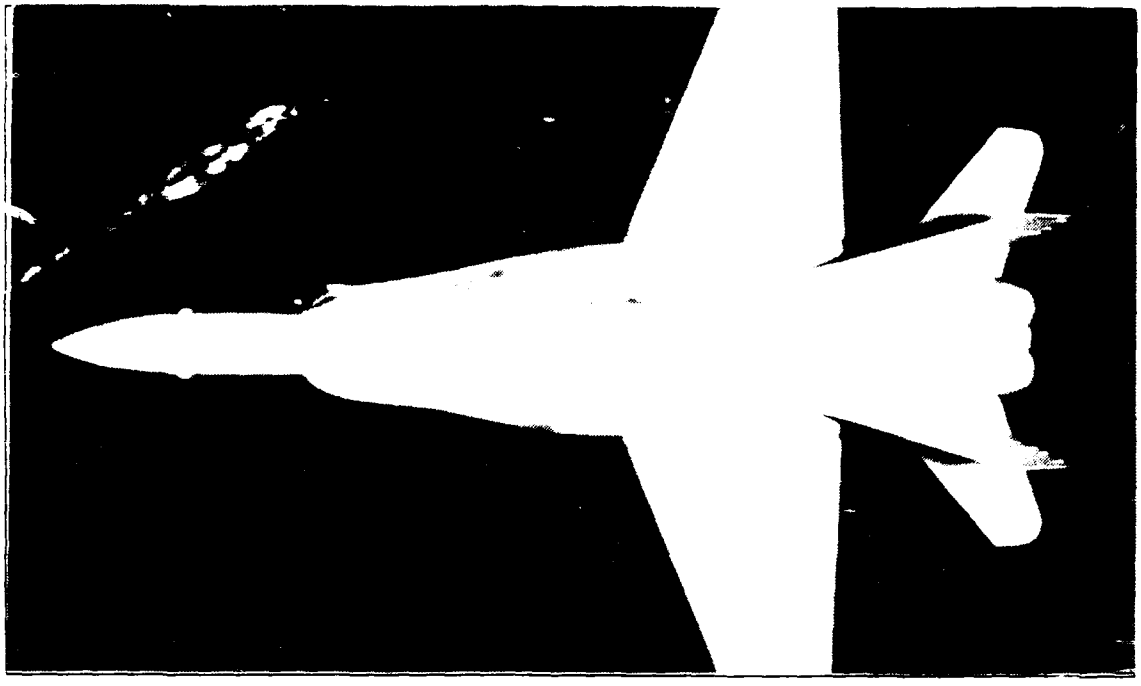

Figure 138. LEX, High Pitch Up, AOA = 40 deg , YAW = 0 deg.

Figure 139. LEX, Low Pitch Up, AOA = 50 deg , YAW 0 deg.

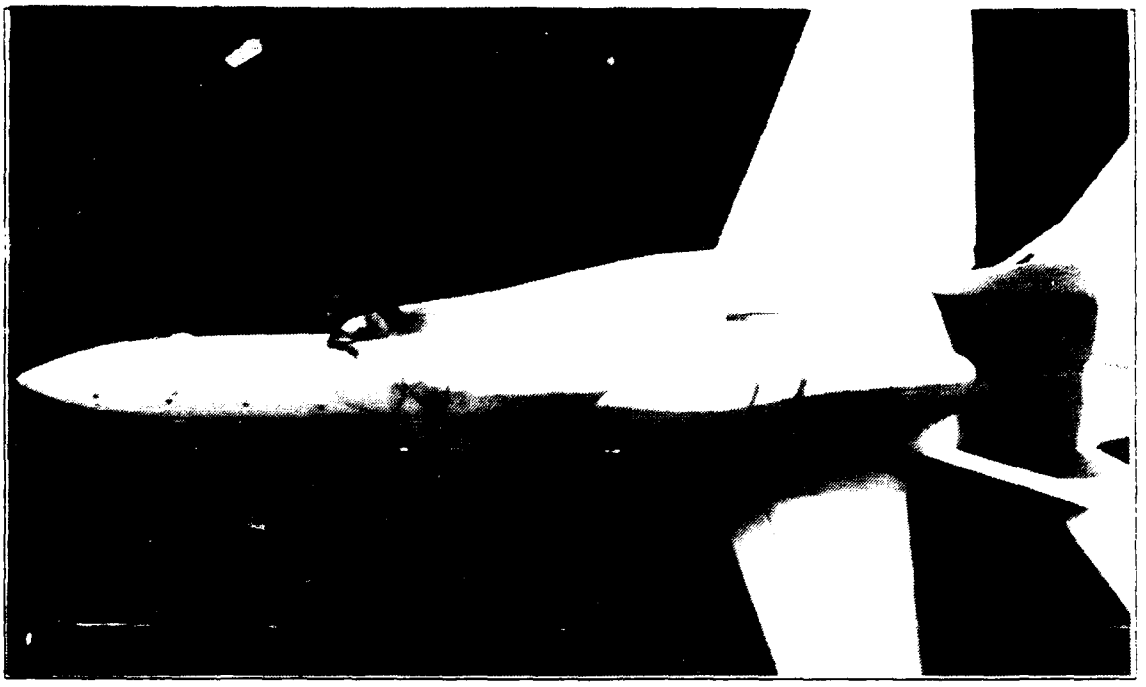

Figure 140. LEX, Low Pitch Down, AOA = 50 deg , YAW = 0 deg.

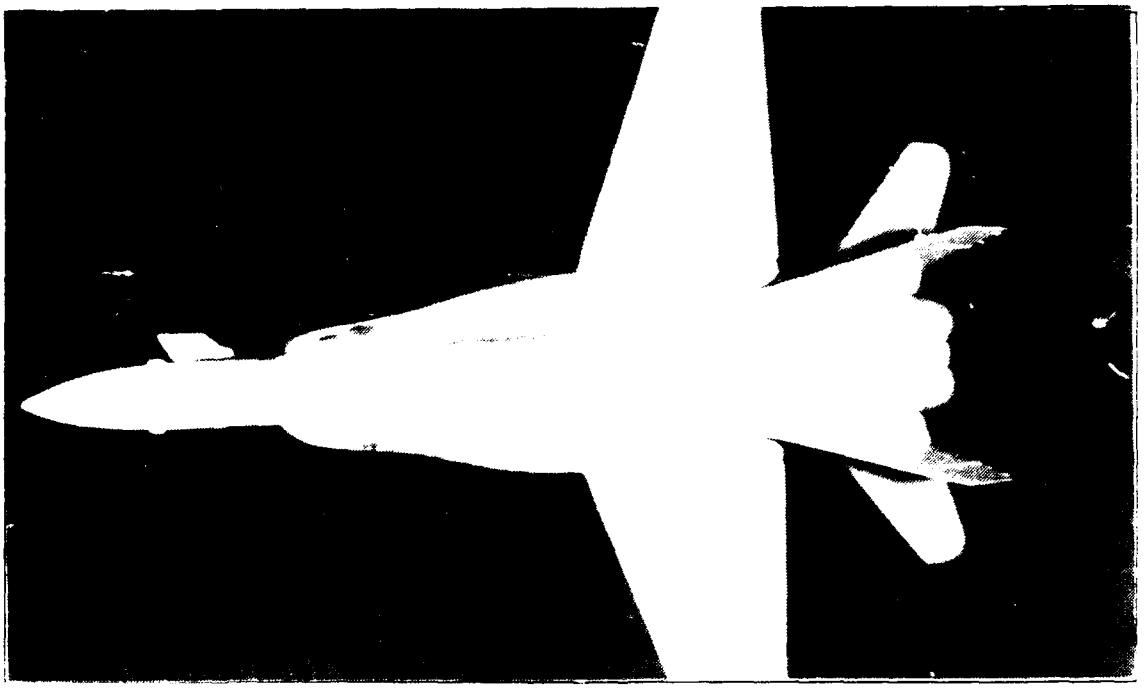

Figure 141. LEX, High pitch Up, AOA = 50 deg , YAW = 0 deg.

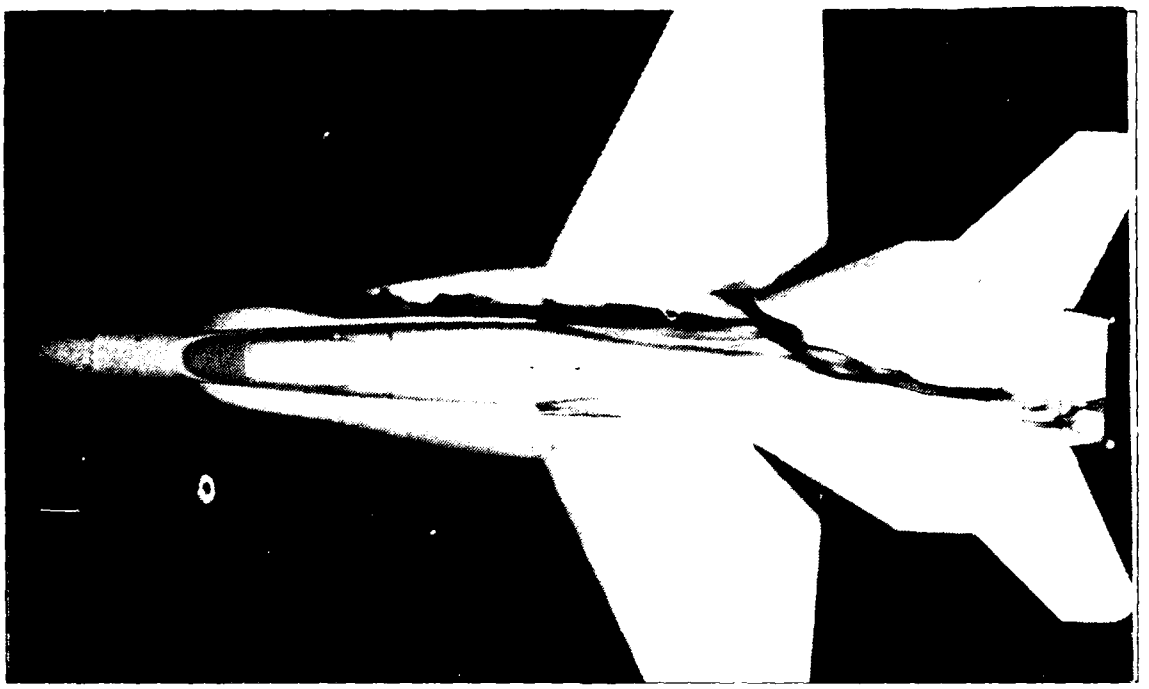

Figure 142. LEX Low Pitch Up. AOA = 0 deg , YAW = 5 deg.

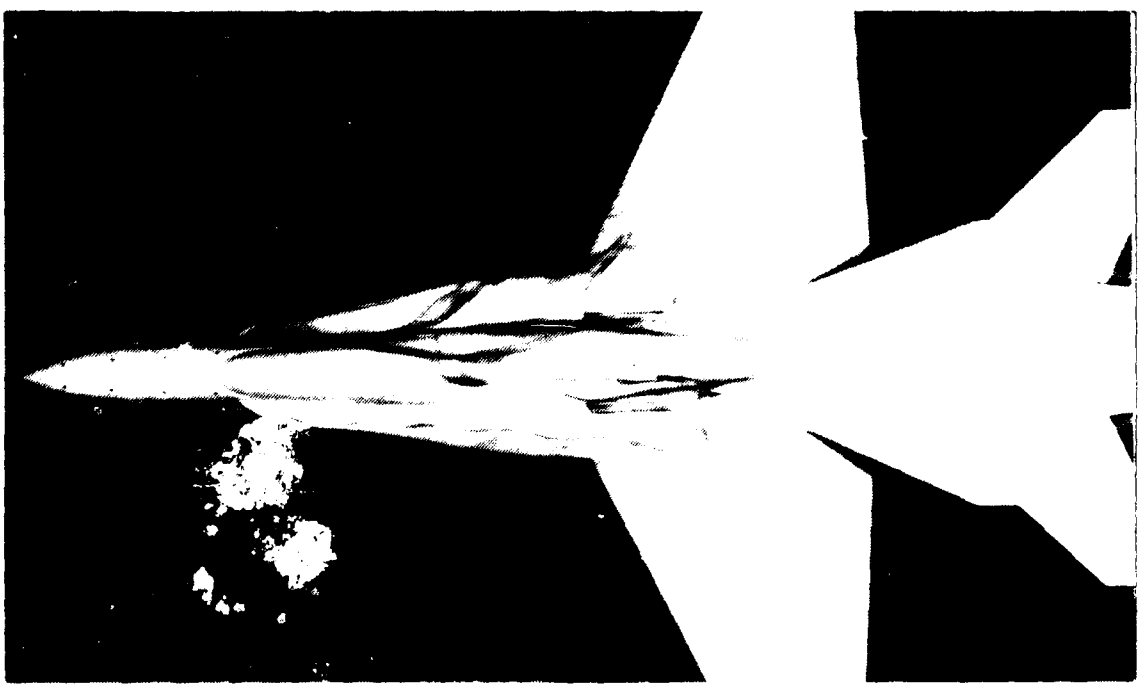

Figure 143. LEX, Low Pitch Up, AOA = 10 deg , YAW = 5 deg.

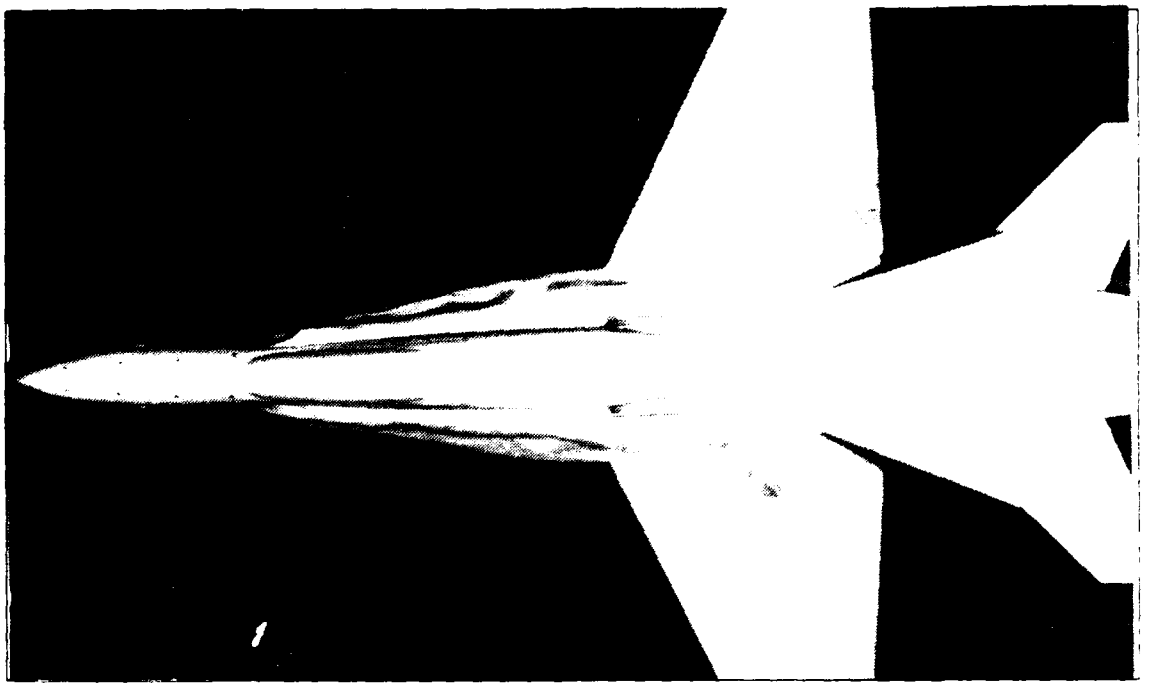

Figure 144. LEX, Low Pitch Up, AOA = 20 deg , YAW = 5 deg.

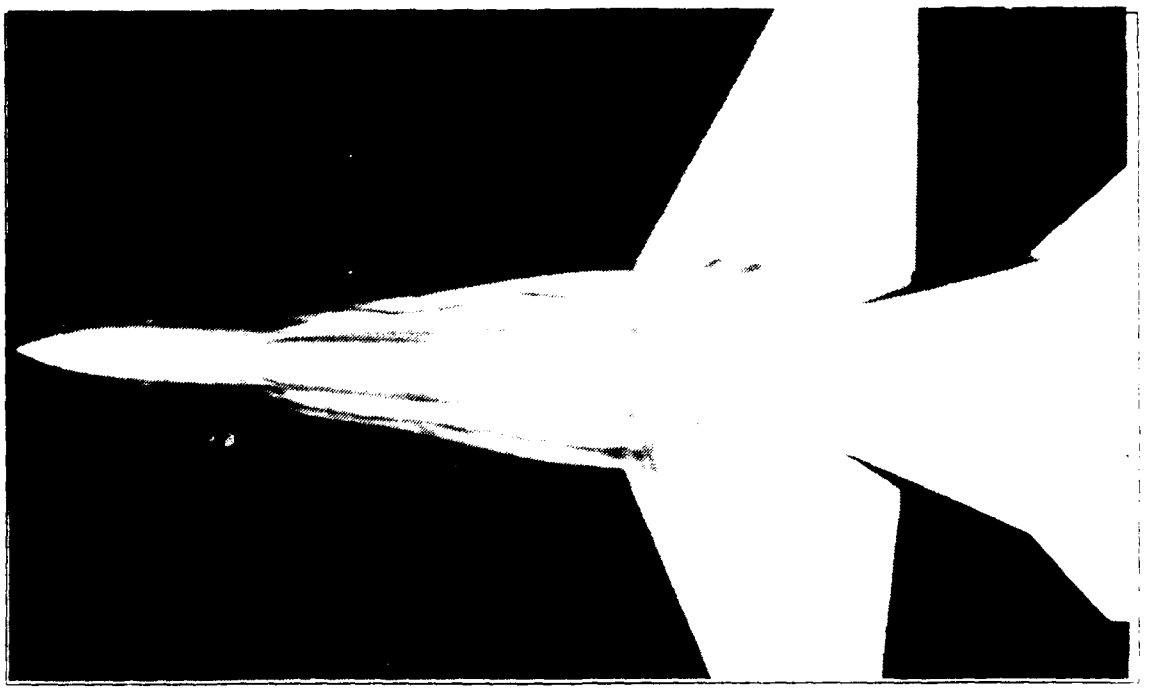

Figure 145. LEX, Low Pitch Down, AOA = 20 deg , YAW = 5 deg.

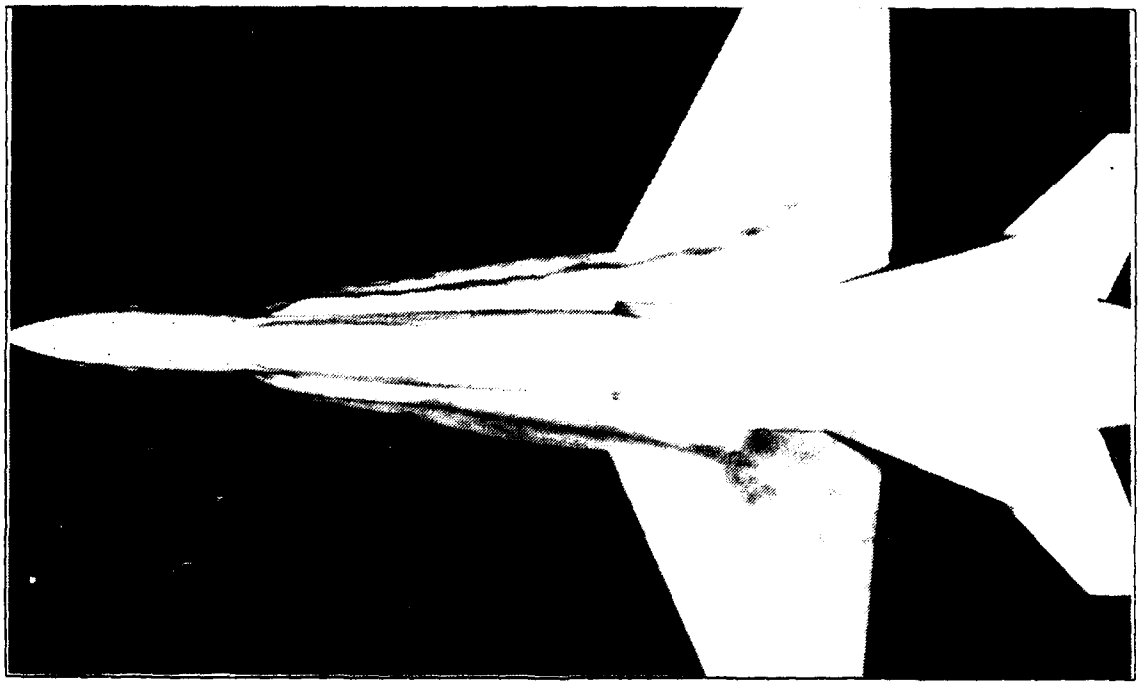

Figure 146. LEX, High Pitch Up, AOA = 20 deg , YAW = 5 deg.

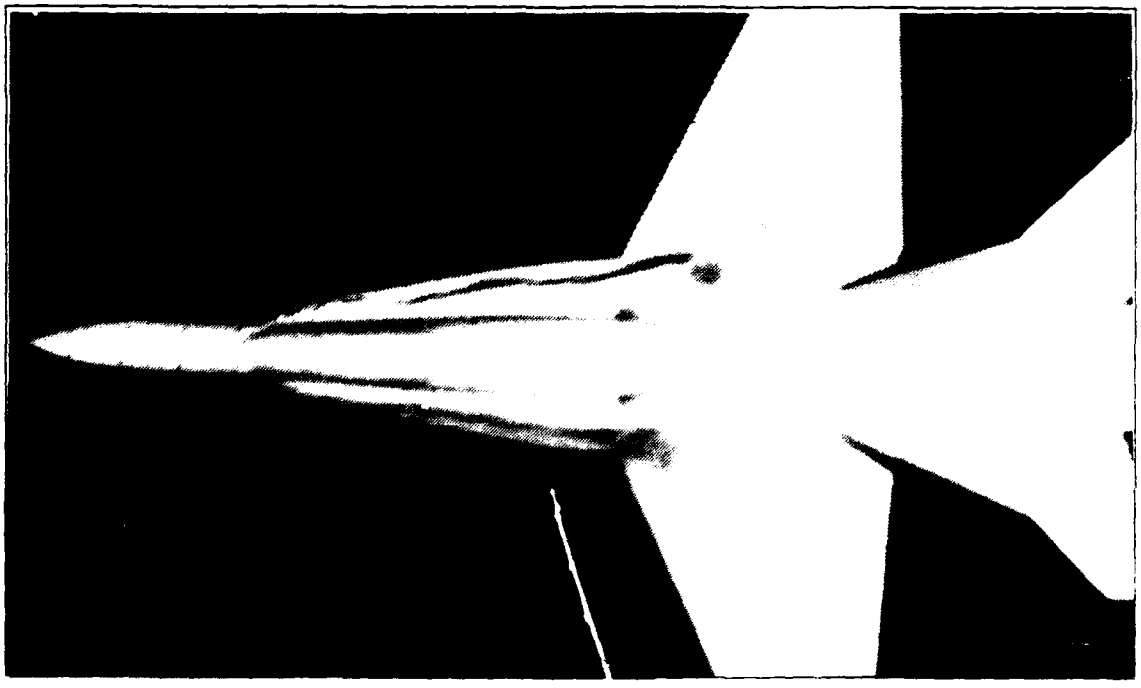

Figure 147. LEX, High Pitch Down, AOA = 20 deg , YAW = 5 deg.

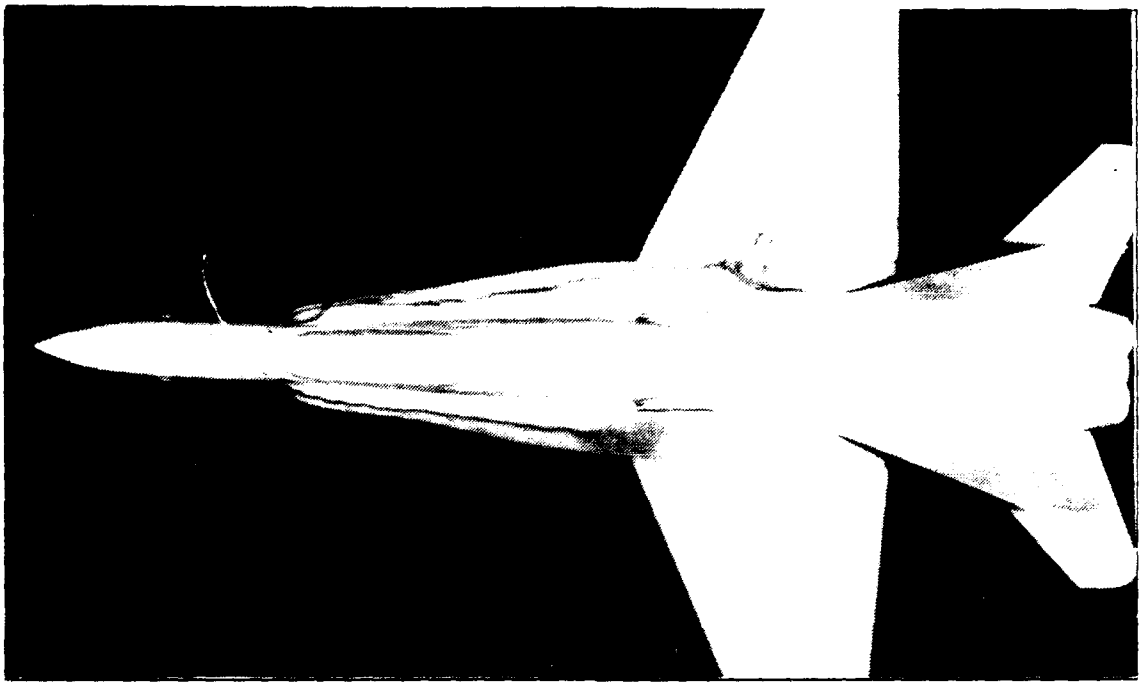

Figure 148. LEX, Low Pitch Up, AOA = 30 deg , YAW = 5 deg.

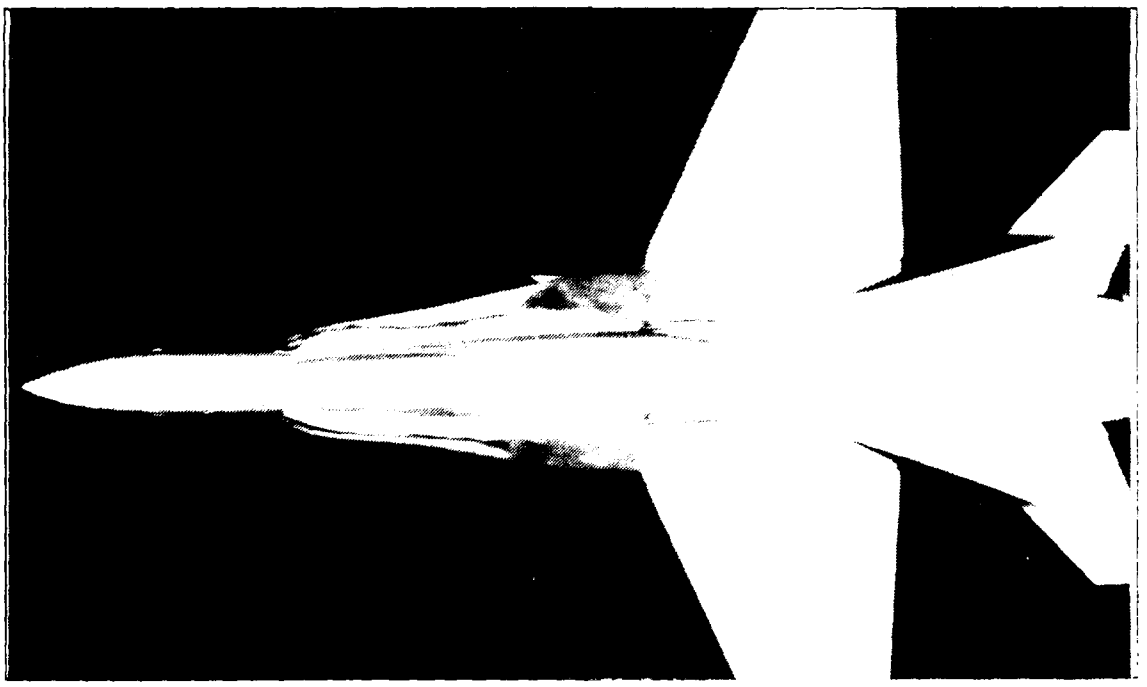

Figure 149. LEX, Low Pitch Down, AOA = 30 deg , YAW = 5 deg.

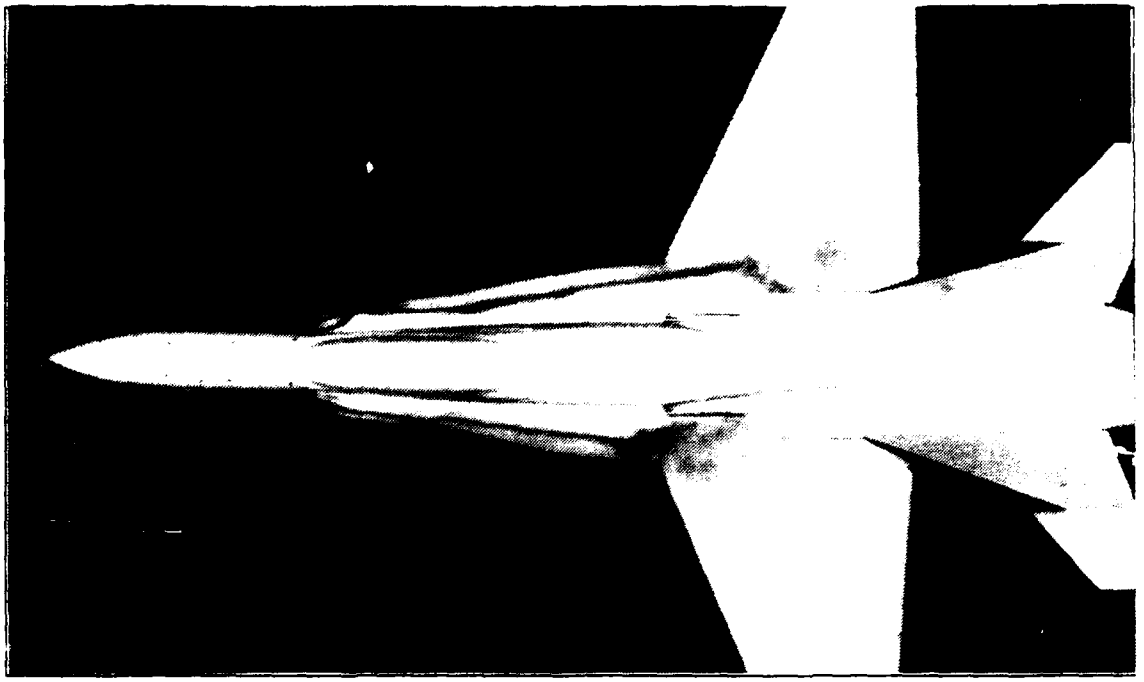

Figure 150. LEX, High Pitch Up, AOA = 30 deg , YAW = 5 deg.

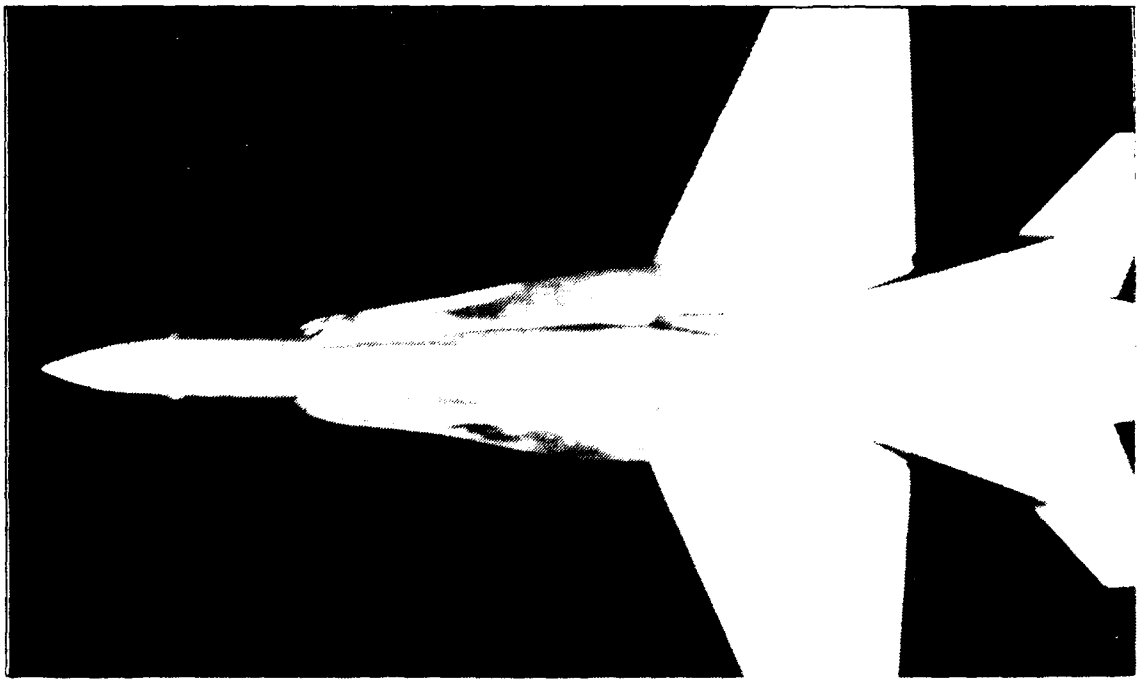

Figure 151. LEX, High Pitch Down, AOA = 30 deg , YAW = 5 deg.

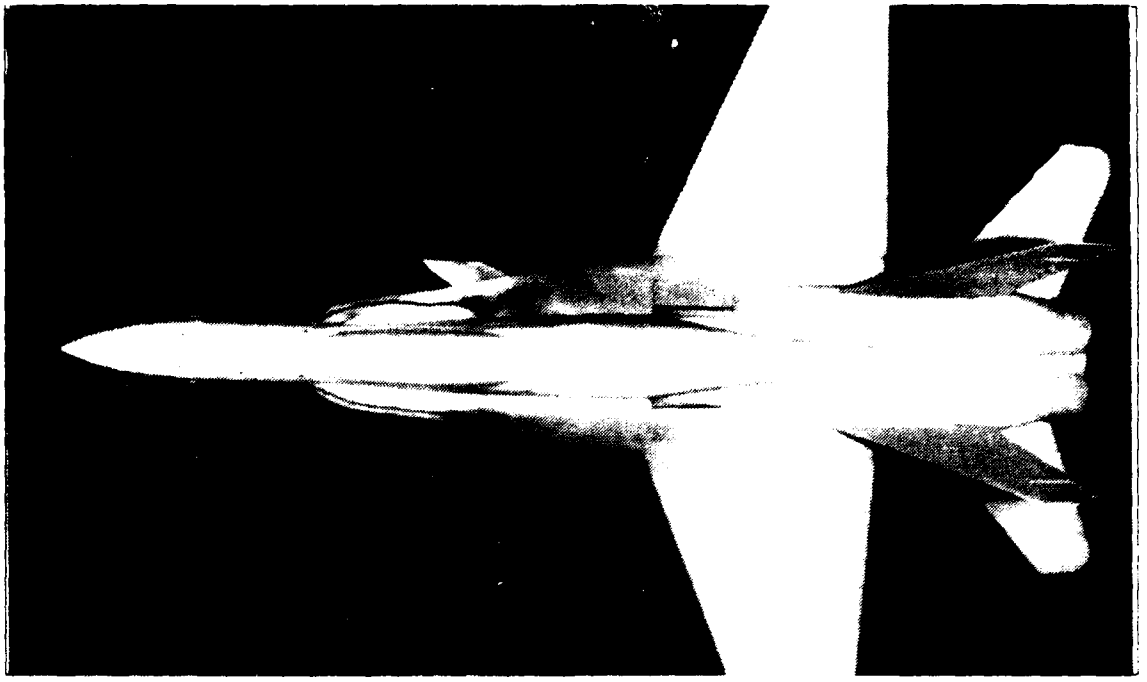

Figure 152. LEX, Low Pitch Up, AOA = 40 deg , YAW = 5 deg.

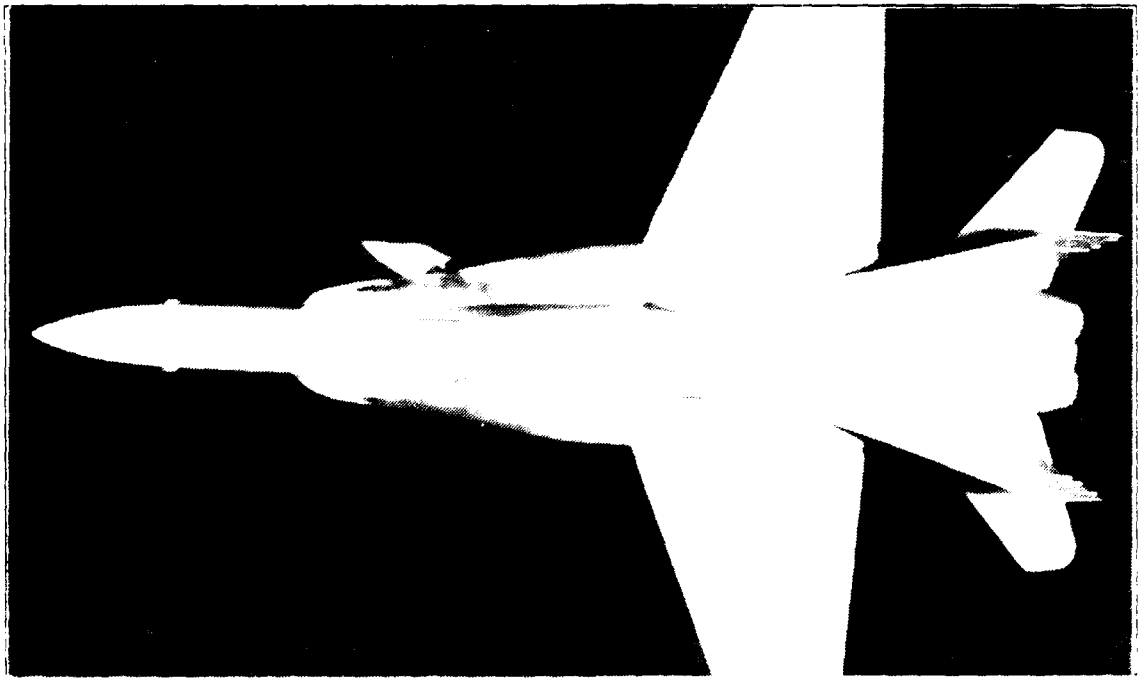

Figure 153. LEX, Low Pitch Down, AOA = 40 deg , YAW = 5 deg.

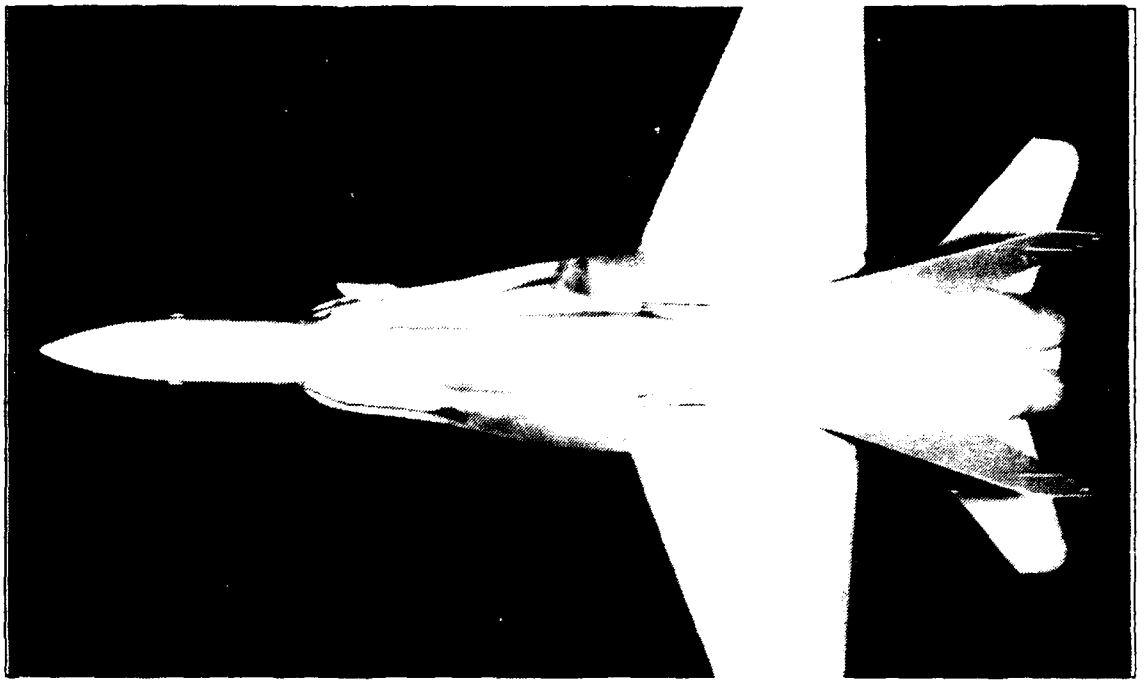

Figure 154. LEX, High Pitch Up, AOA = 40 deg , YAW = 5 deg.

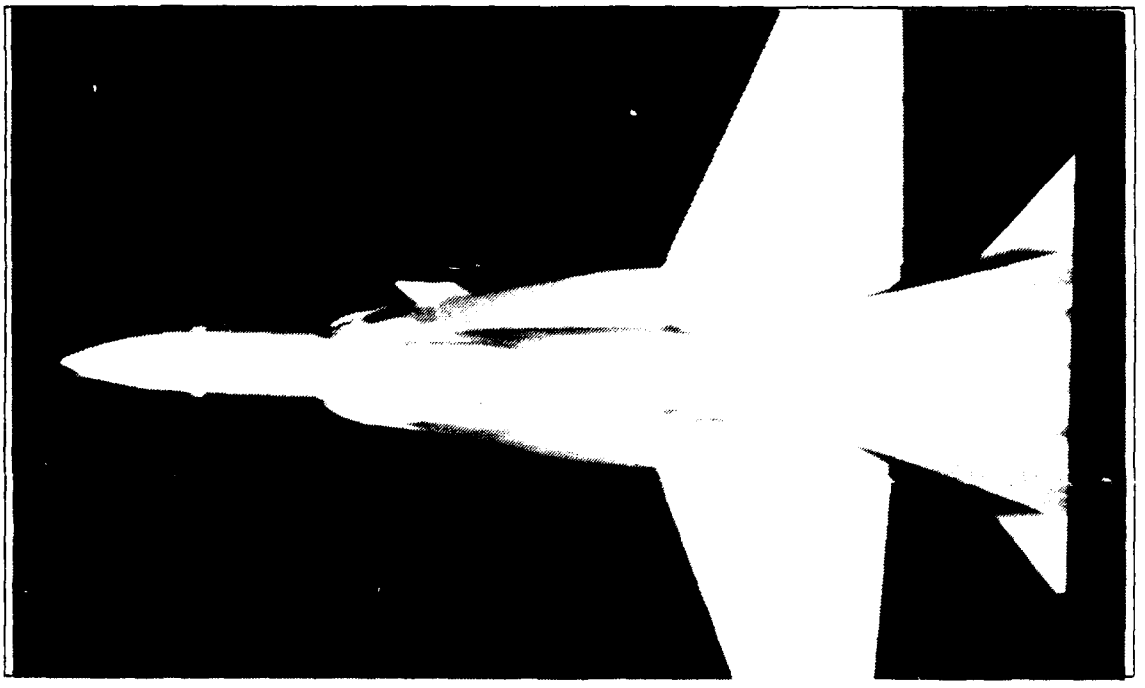

Figure 155. LEX, High Pitch Down, AOA = 40 deg , YAW = 5 deg.

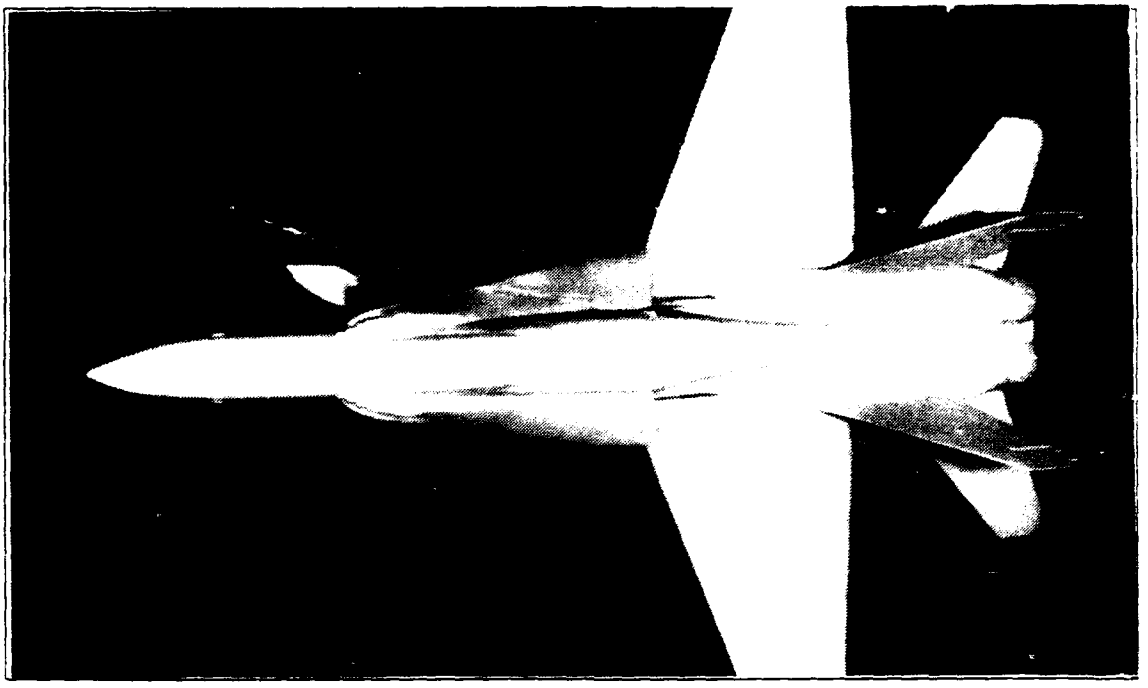

Figure 156. LEX, Low Pitch Up, AOA = 50 deg , YAW = 5 deg.

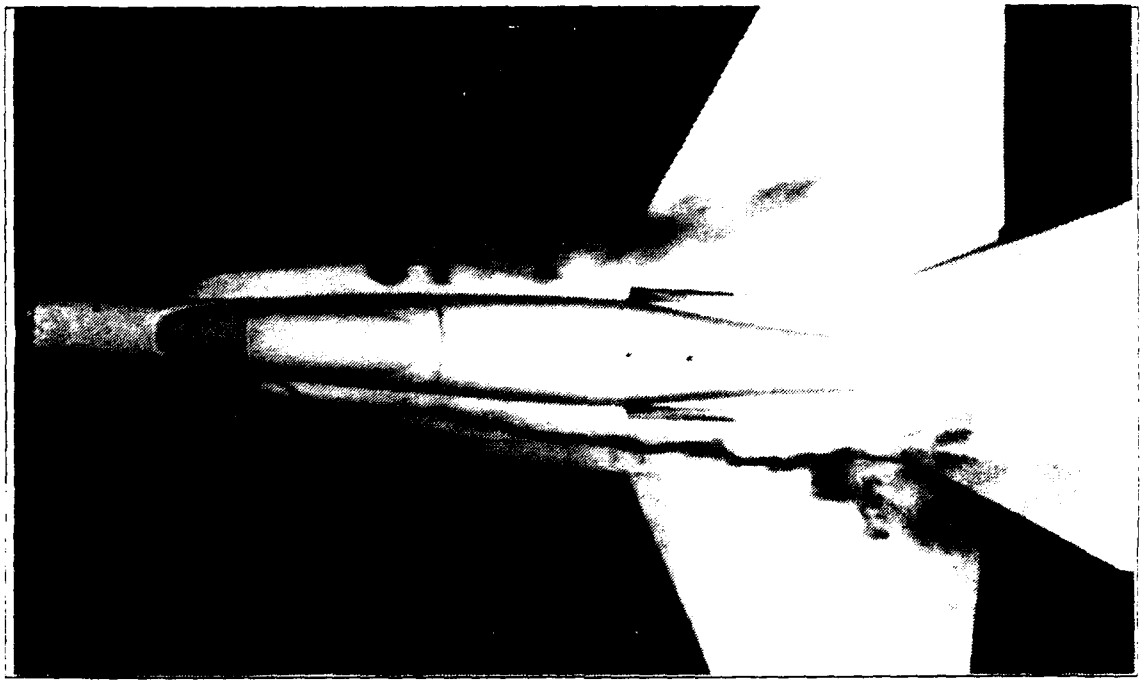

Figure 157. LEX, Low Pitch Down, AOA = 10 deg , YAW = 10 deg.

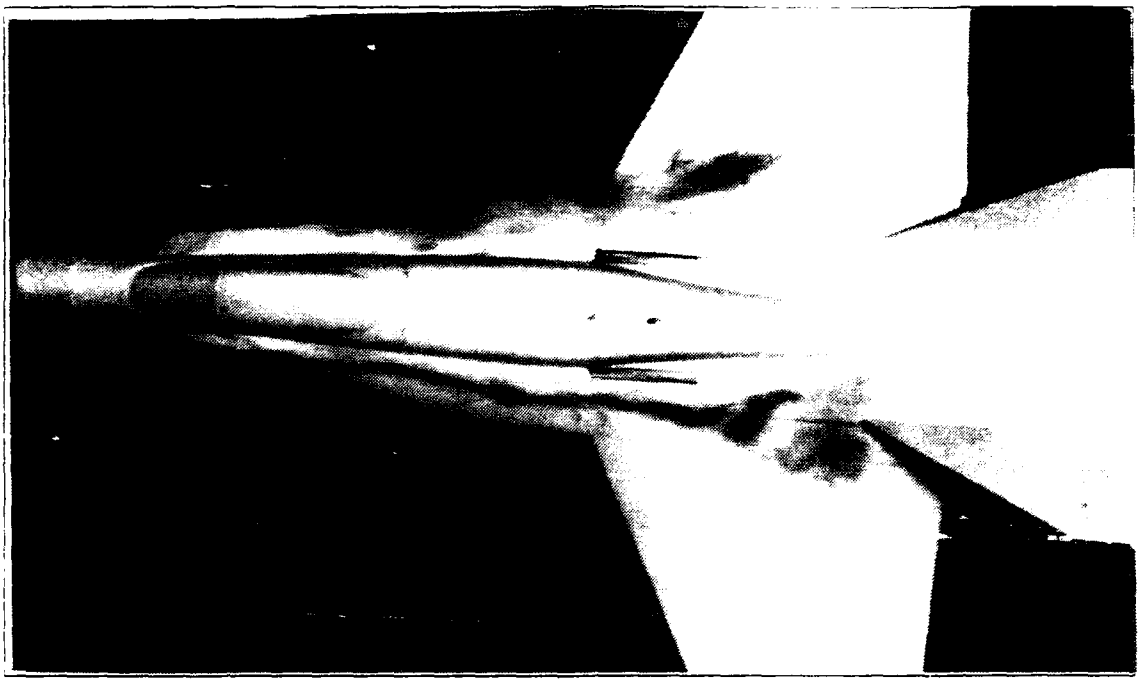

Figure 158. LEX, High Pitch Down, AOA = 10 deg , YAW = 10 deg.

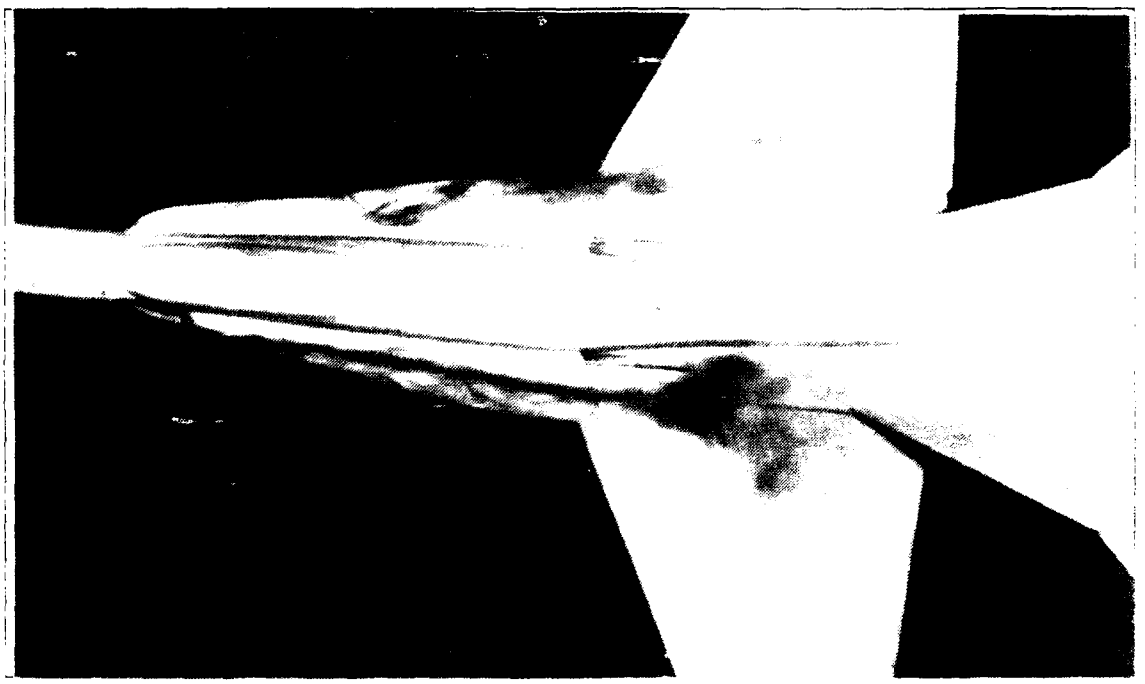

Figure 159. LEX, Low Pitch Up, AOA = 20 deg , YAW = 10 deg.

Figure 160. LEX, Low Pitch Down, AOA = 20 deg , YAW = 10 deg.

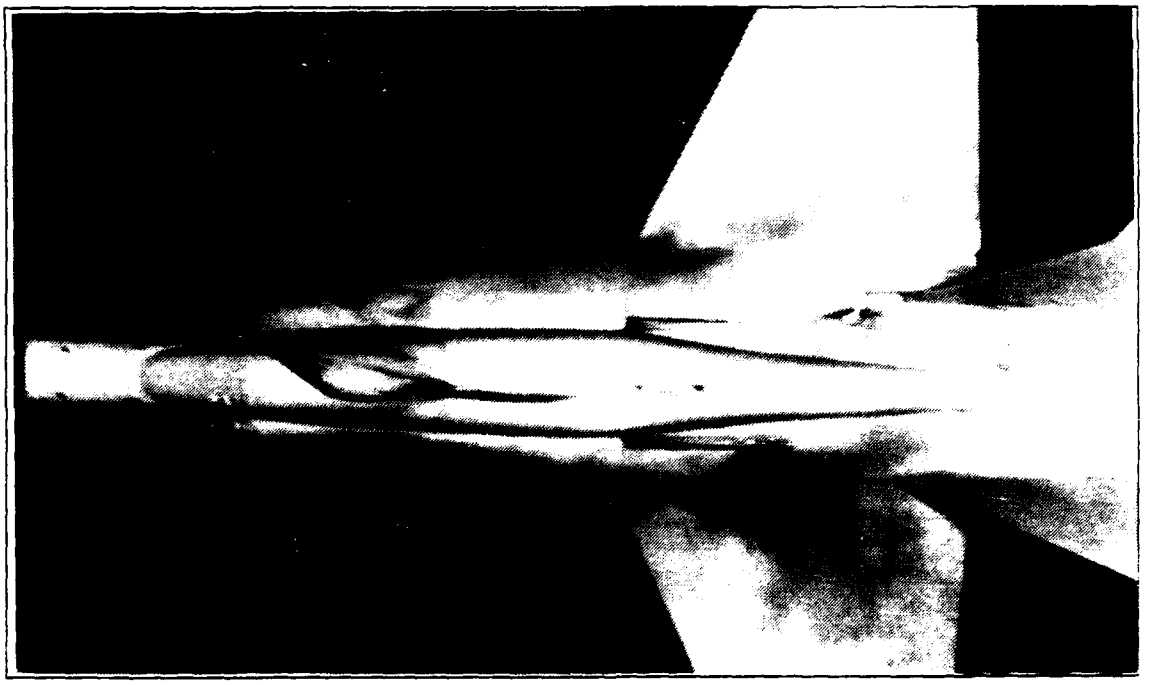

Figure 161. LEX, High Pitch Up, AOA = 20 deg , YAW = 10 deg.

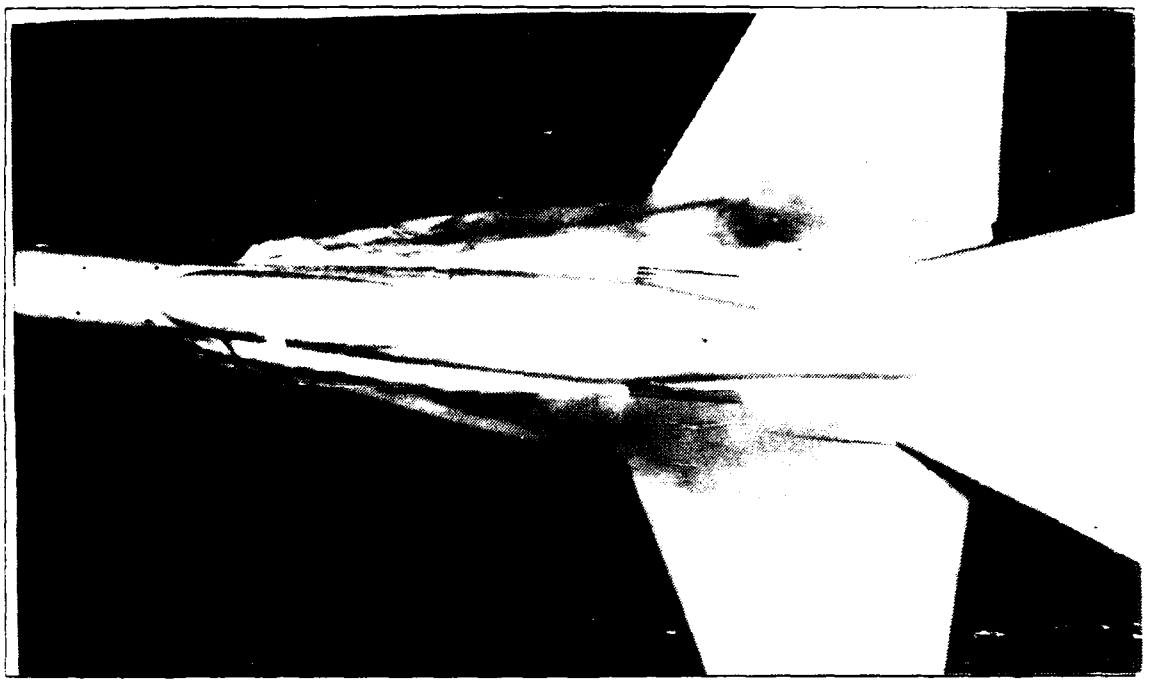

Figure 162. LEX, High Pitch Down, AOA = 20 deg , YAW = 10 deg.

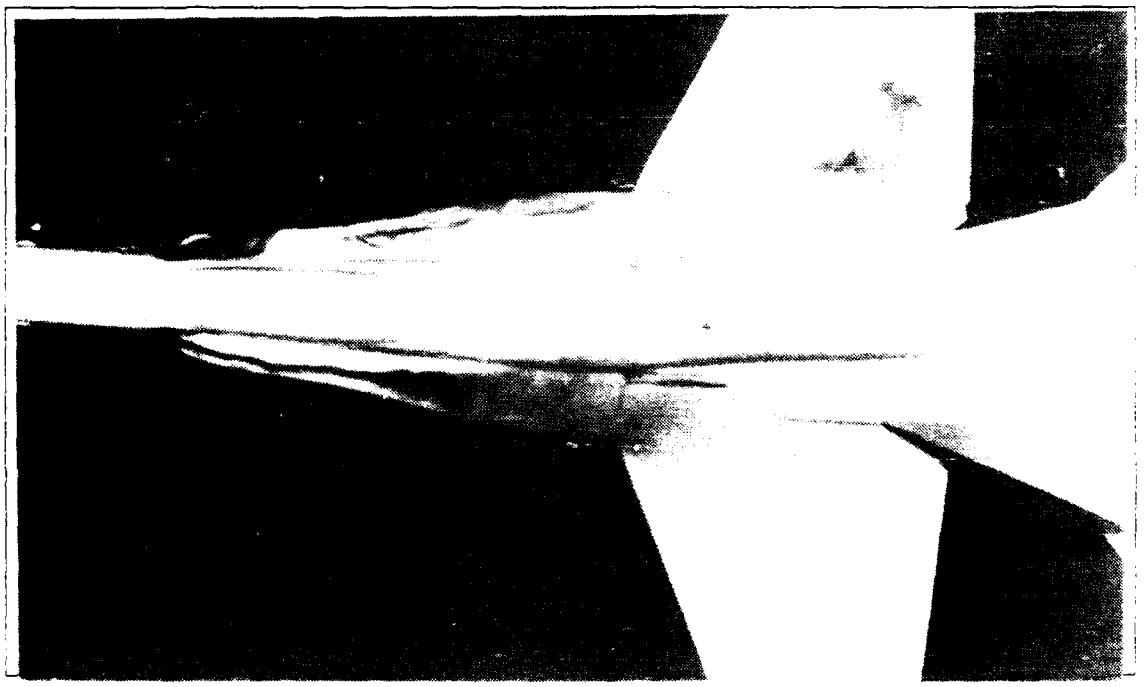

Figure 163. LEX, Low Pitch Up, AOA = 30 deg , YAW = 10 deg.

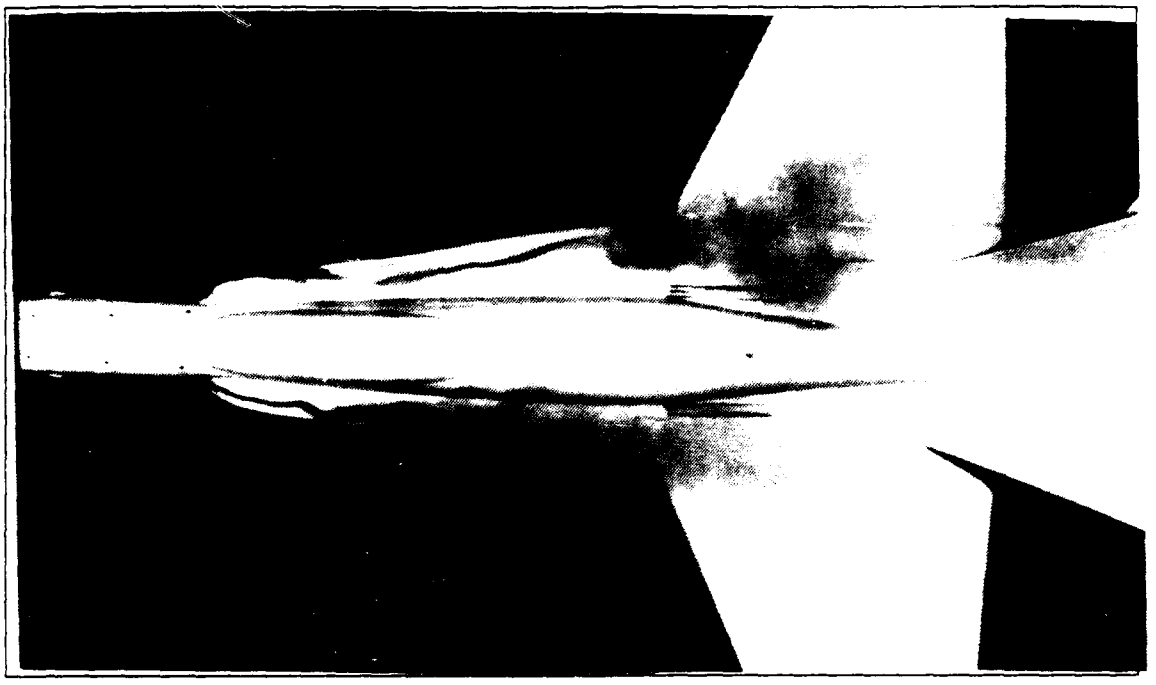

Figure 164. LEX, Low Pitch Down, AOA = 30 deg , YAW = 10 deg.

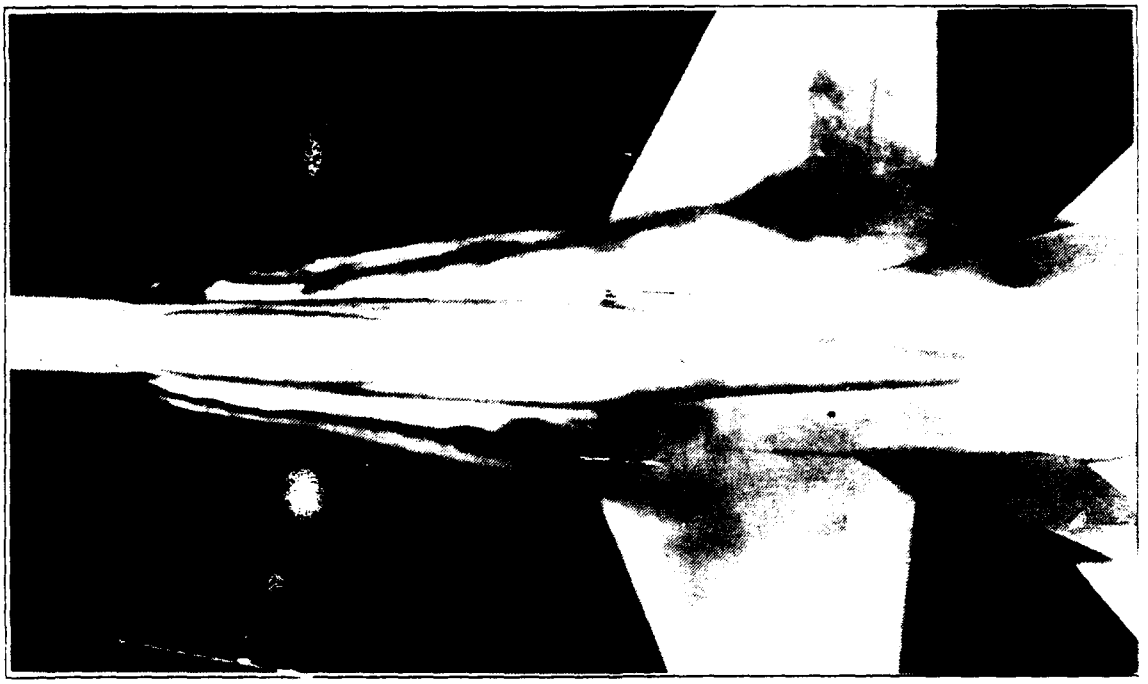

Figure 165. LEX, High Pitch Up, AOA = 30 deg , YAW = 10 deg.

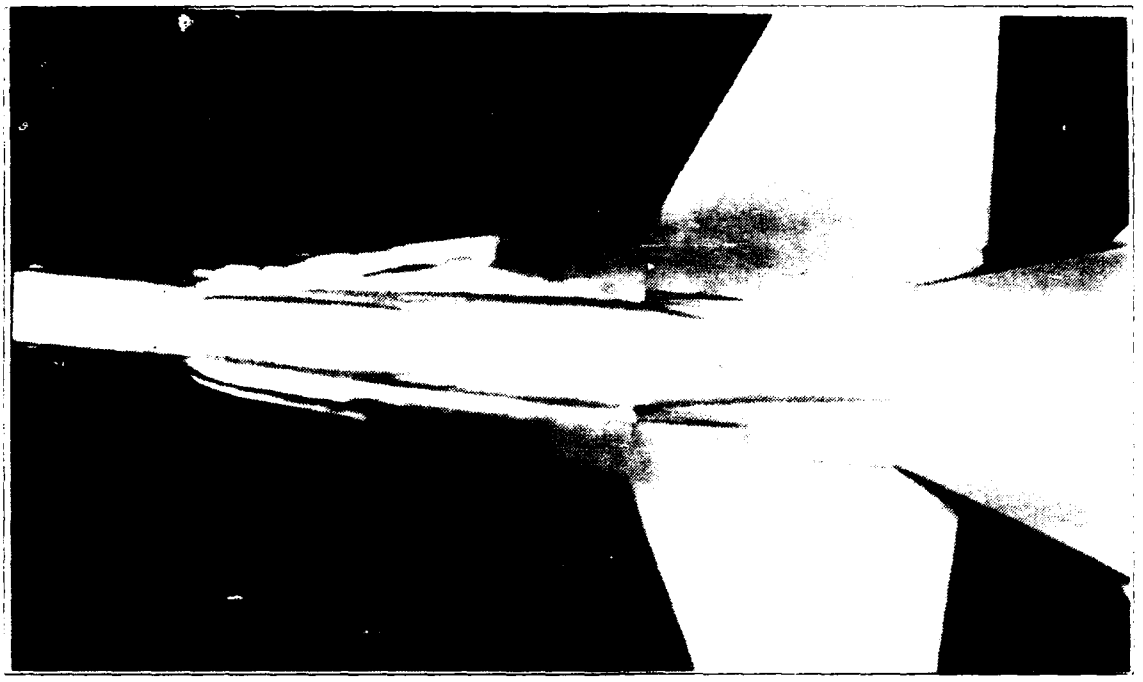

Figure 166. LEX, High Pitch Down, AOA = 30 deg, YAW = 10 deg.

Figure 167. LEX, Low Pitch Up, AOA = 40 deg, YAW = 10 deg.

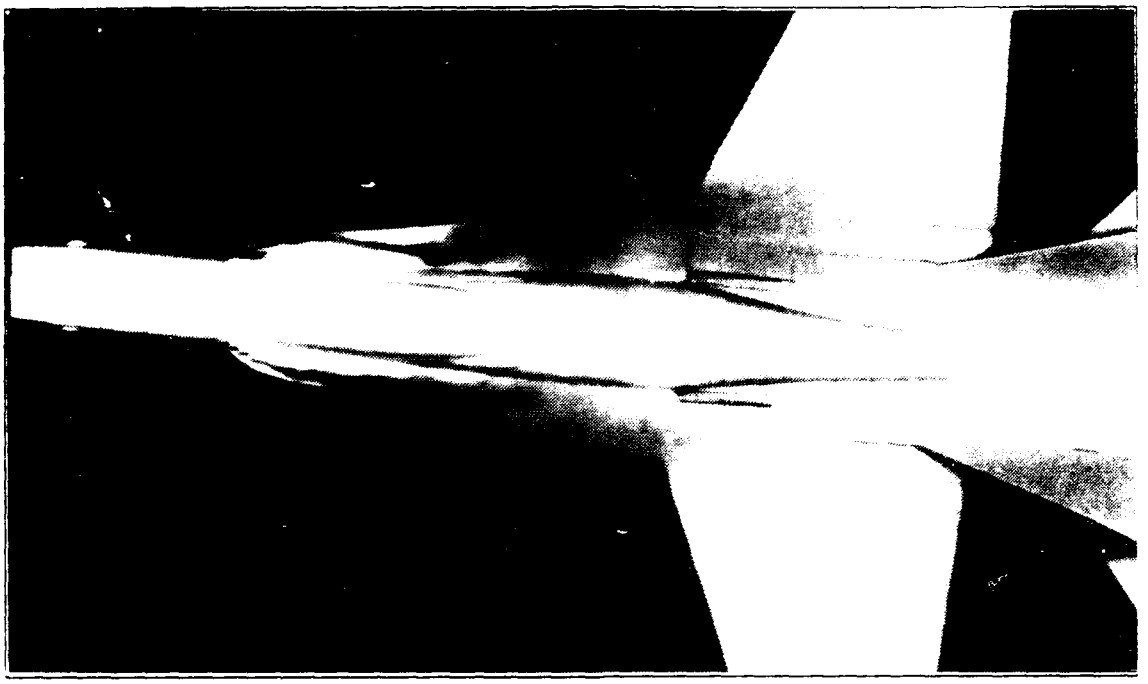

Figure 168. LEX, Low Pitch Down, AOA = 40 deg , YAW = 10 deg.

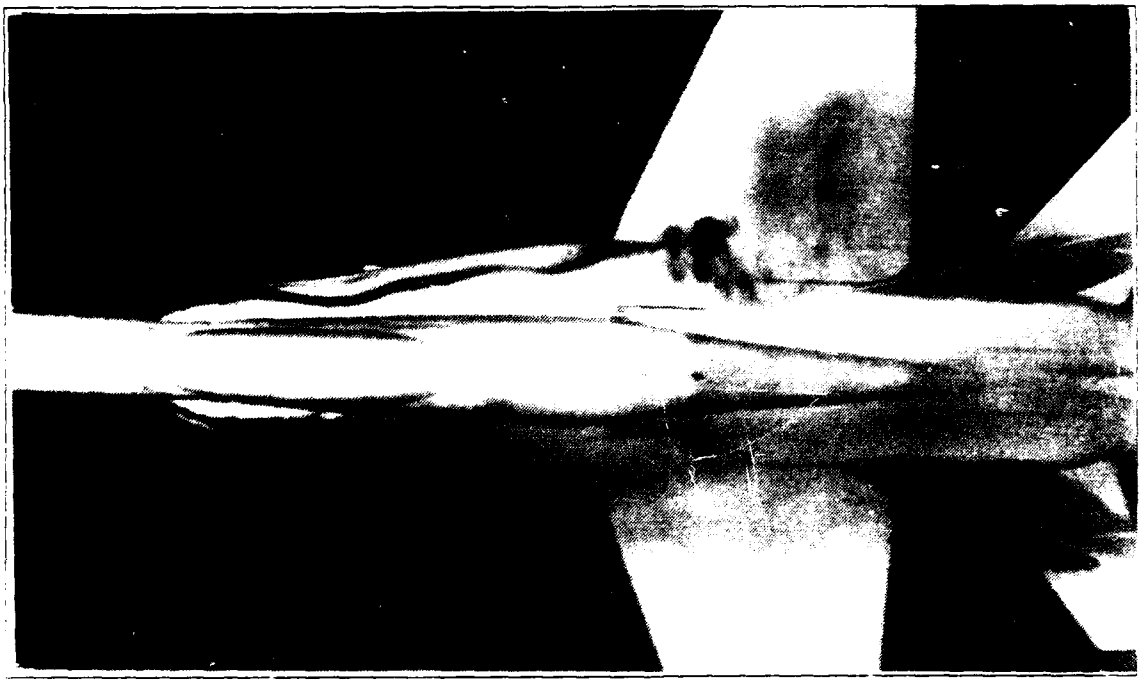

Figure 169. LEX, High Pitch Up, AOA = 40 deg , YAW = 10 deg.

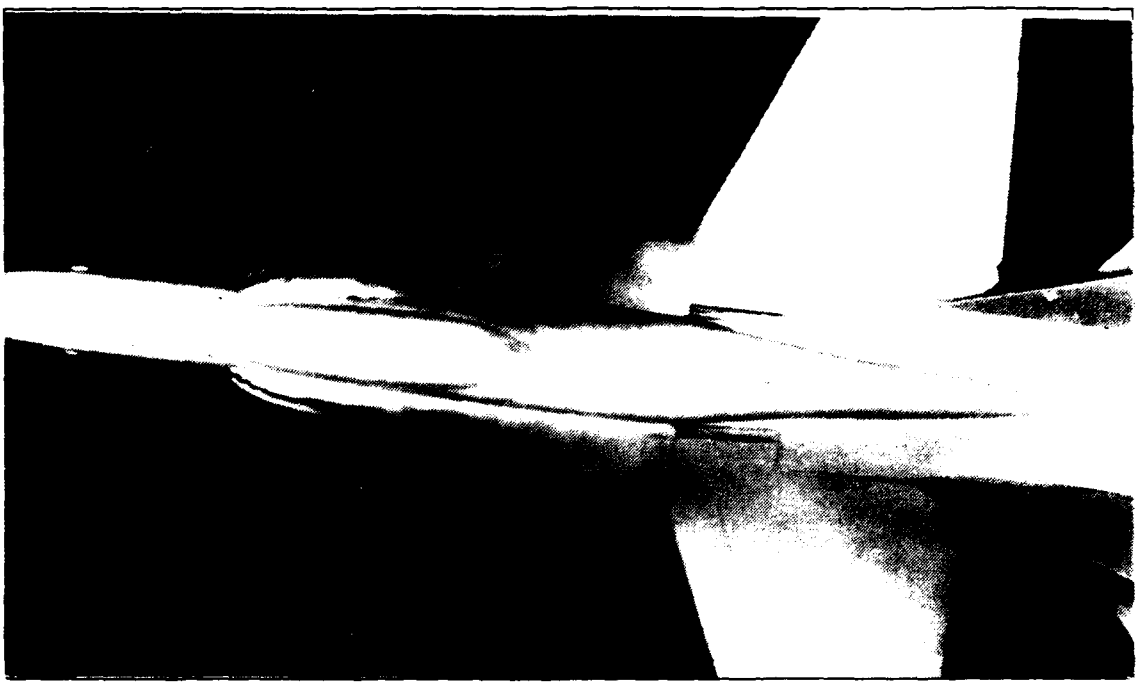

Figure 170. LEX, High Pitch Down, AOA = 40 deg , YAW = 10 deg.

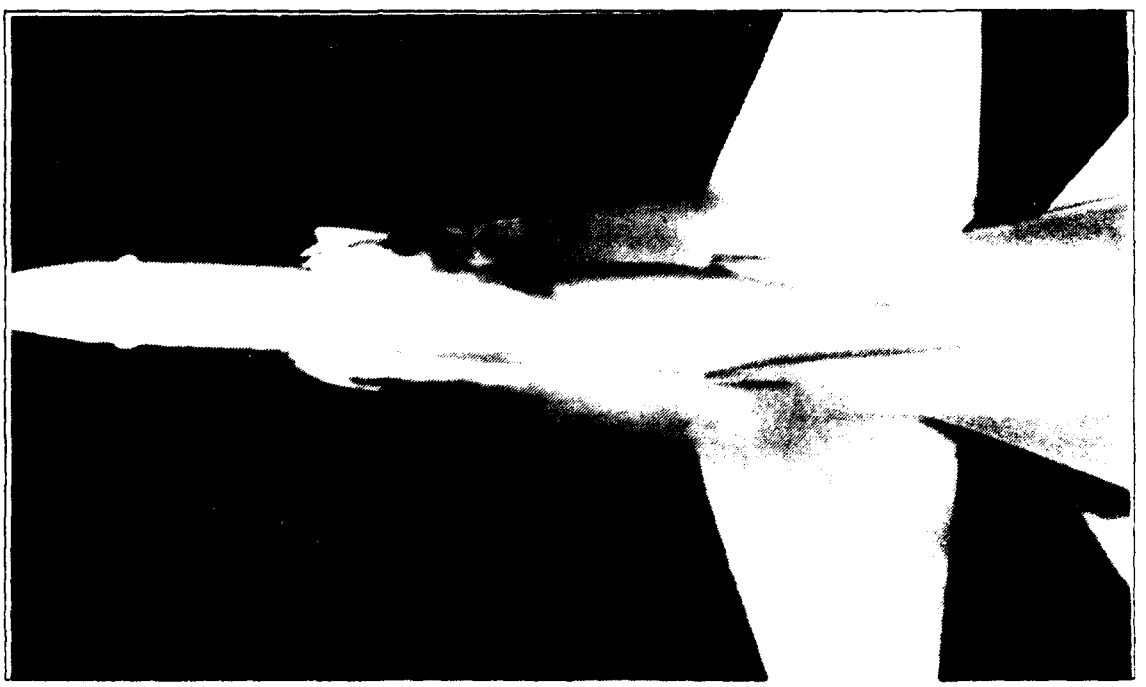

Figure 171. LEX, Low Pitch Up, AOA = 50 deg , YAW = 10 deg.

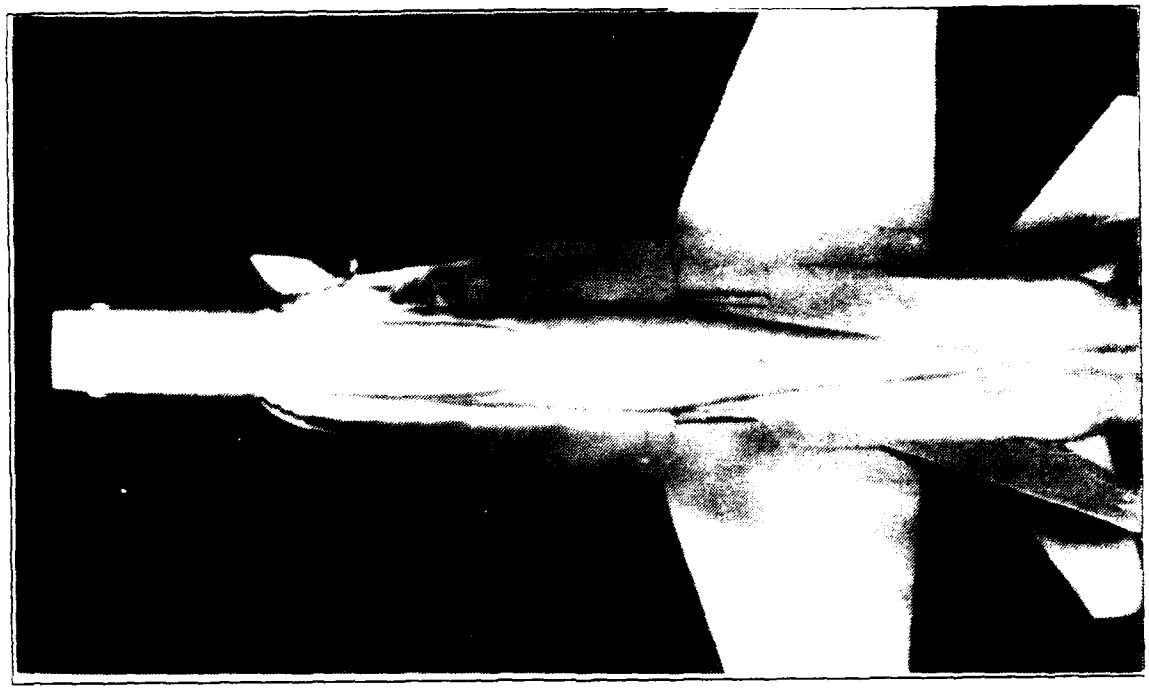

Figure 172. LEX, High Pitch Up, AOA = 50 deg , YAW = 10 deg.

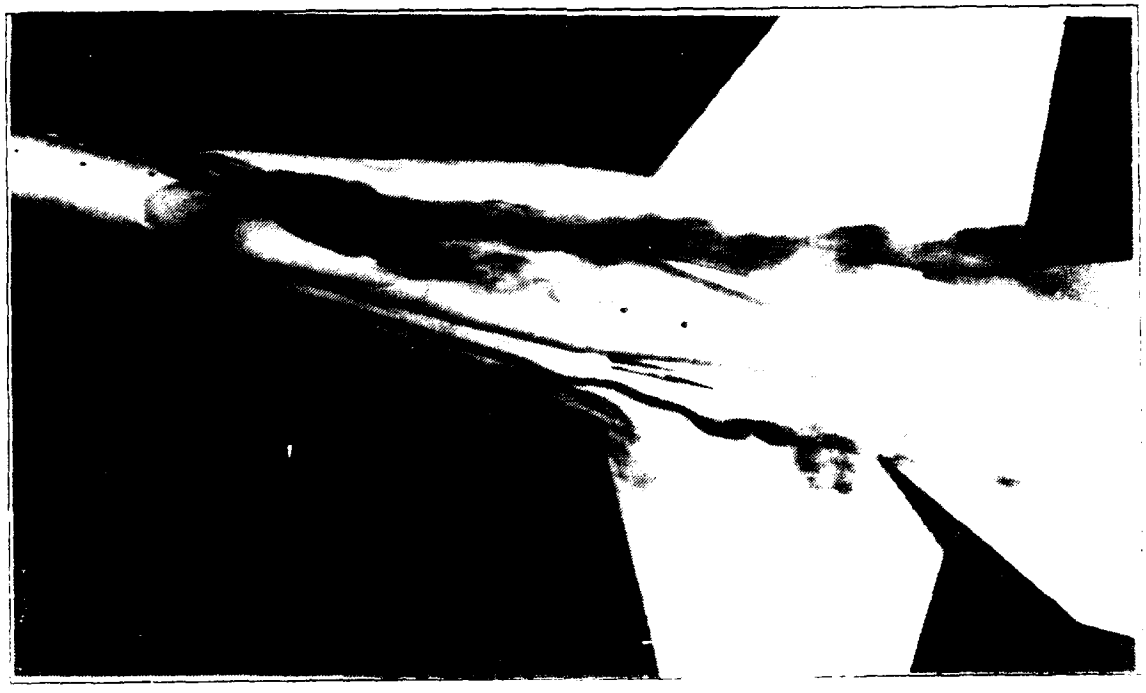

Figure 173. LEX, Low Pitch Up, AOA = 10 deg , YAW = 20 deg.

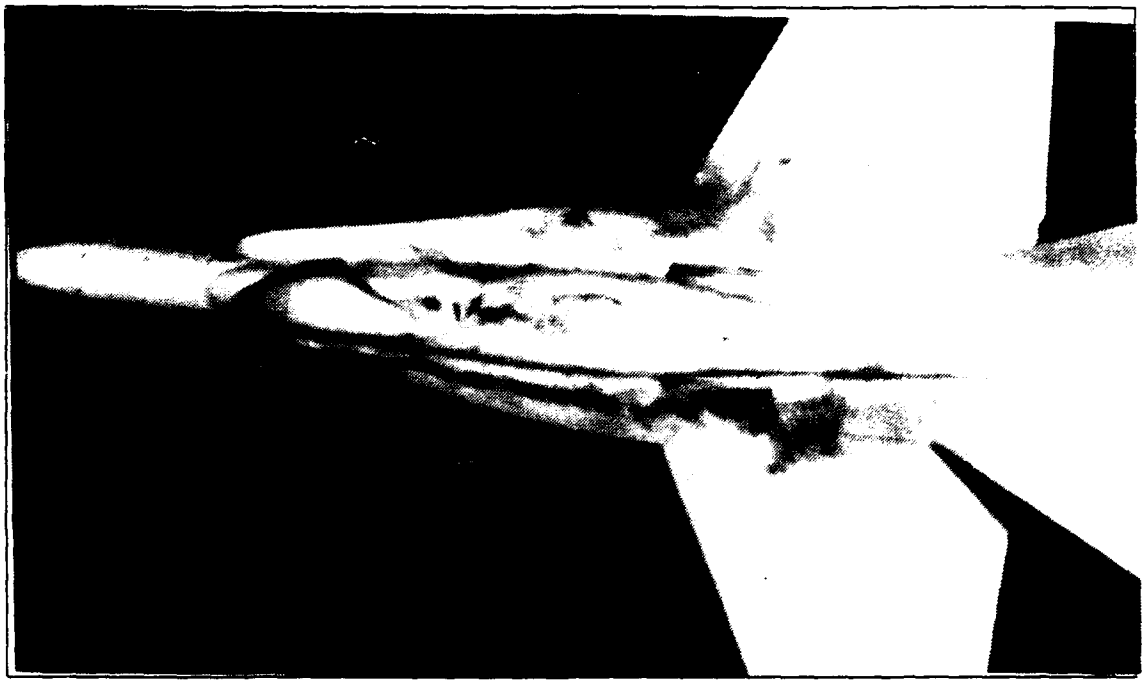

Figure 174. LEX, High Pitch Down, AOA = 10 deg , YAW = 20 deg.

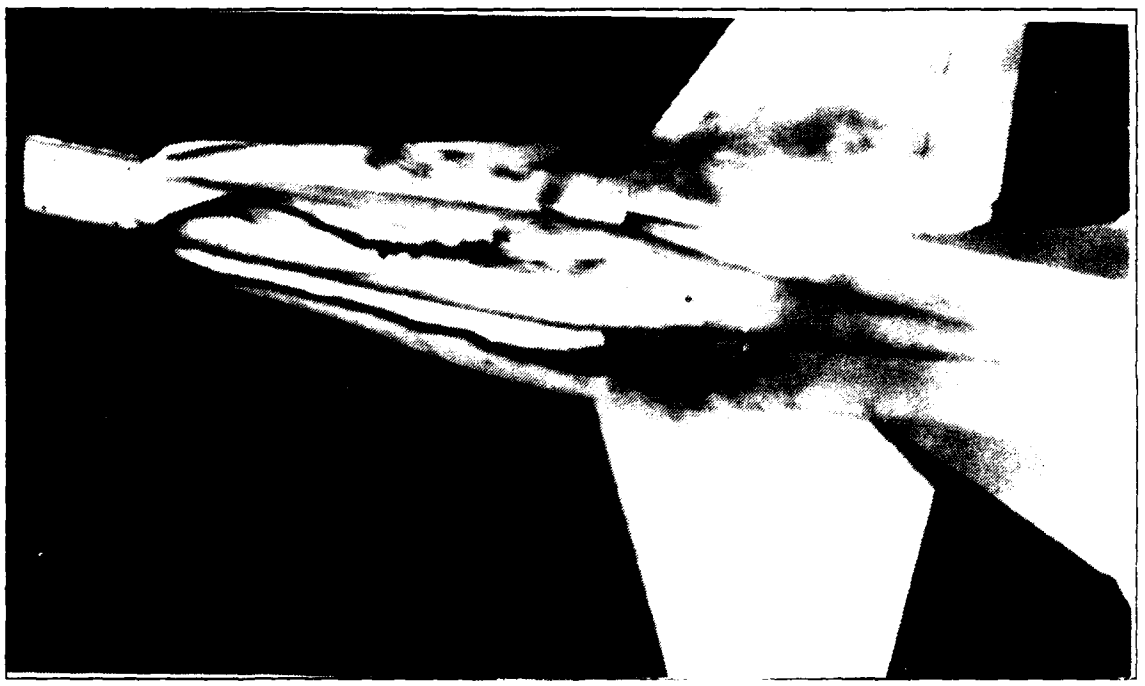

Figure 175. LEX, Low Pitch Up, AOA = 20 deg , YAW = 20 deg.

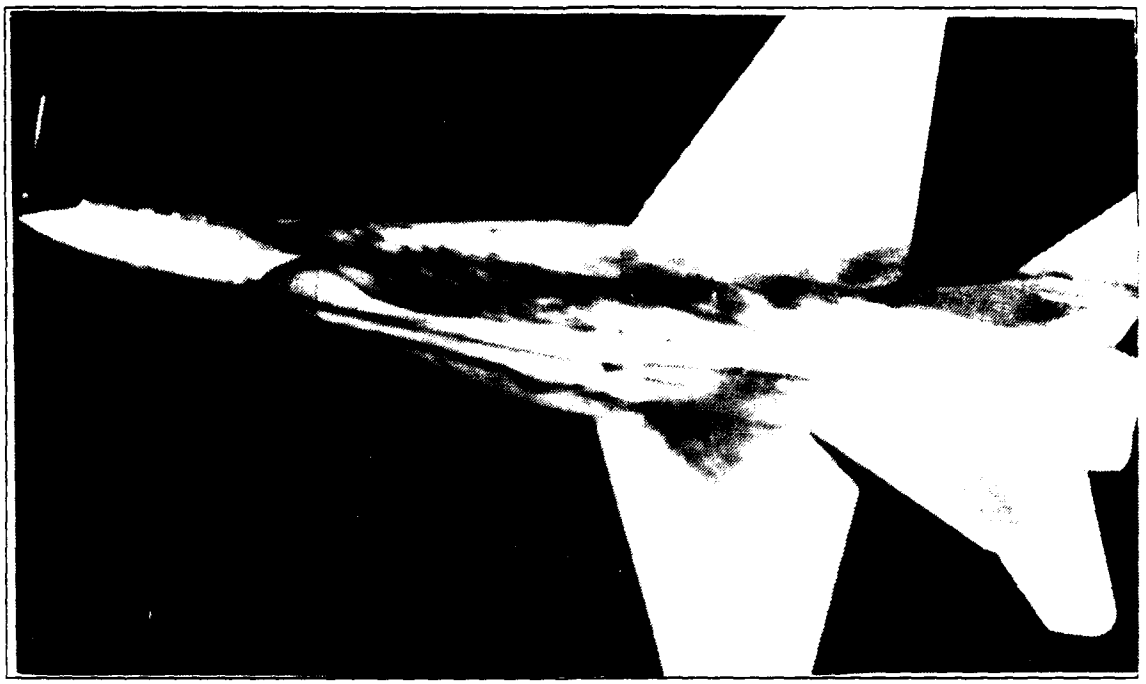

Figure 176. LEX, High Pitch Up, AOA = 20 deg , YAW = 20 deg.

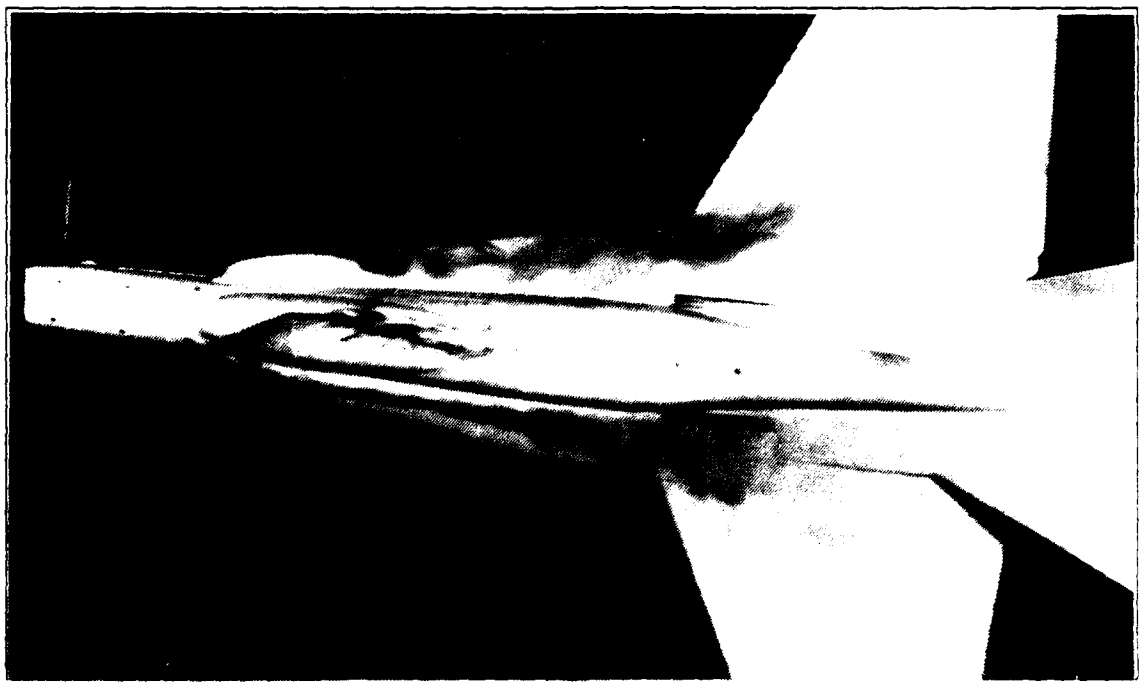

Figure 177. LEX, High Pitch Down, AOA = 20 deg , YAW = 20 deg.

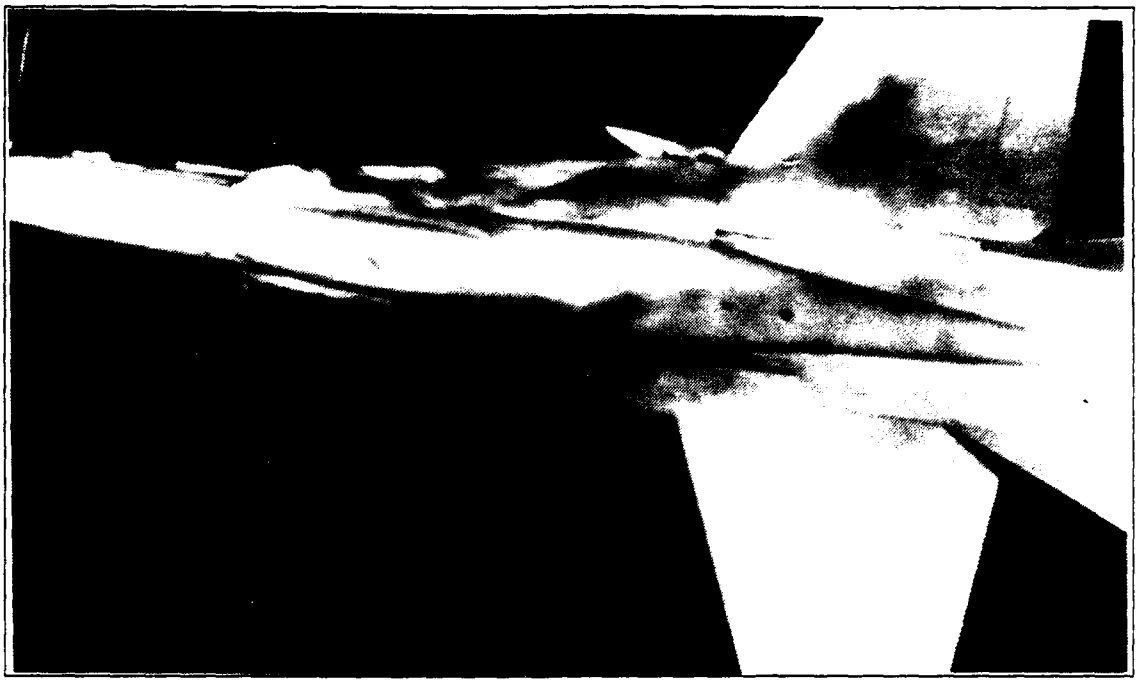

Figure 178. LEX, Low Pitch Up, AOA = 30 deg , YAW = 20 deg.

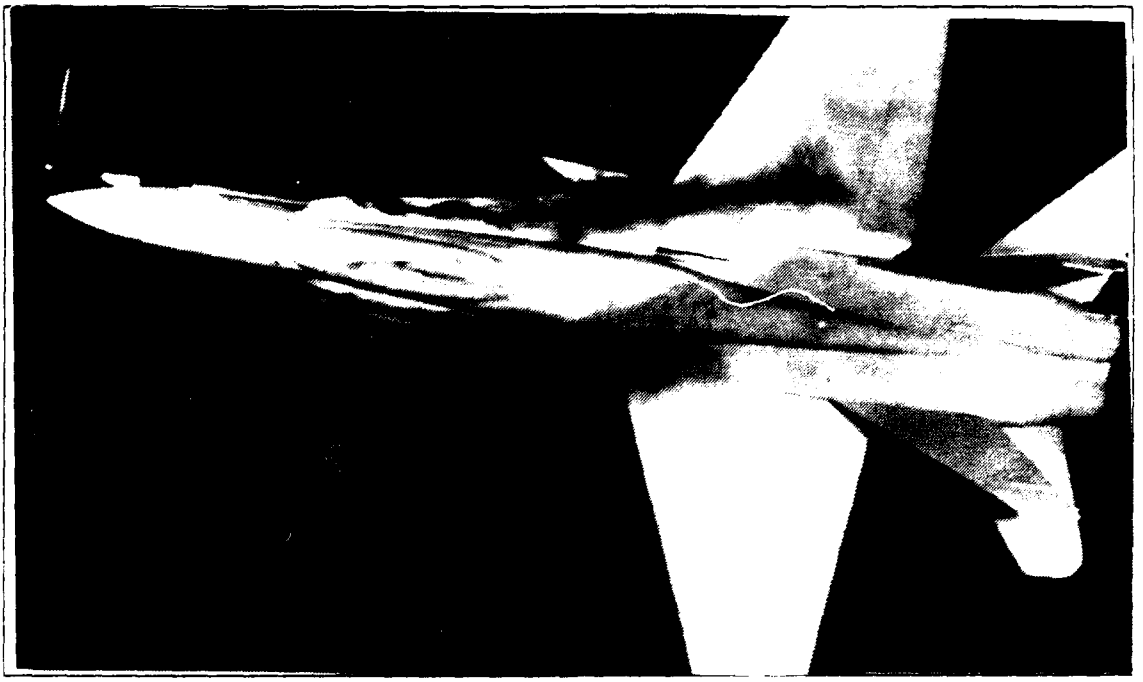

Figure 179. LEX, High Pitch Up, AOA = 30 deg , YAW = 20 deg.

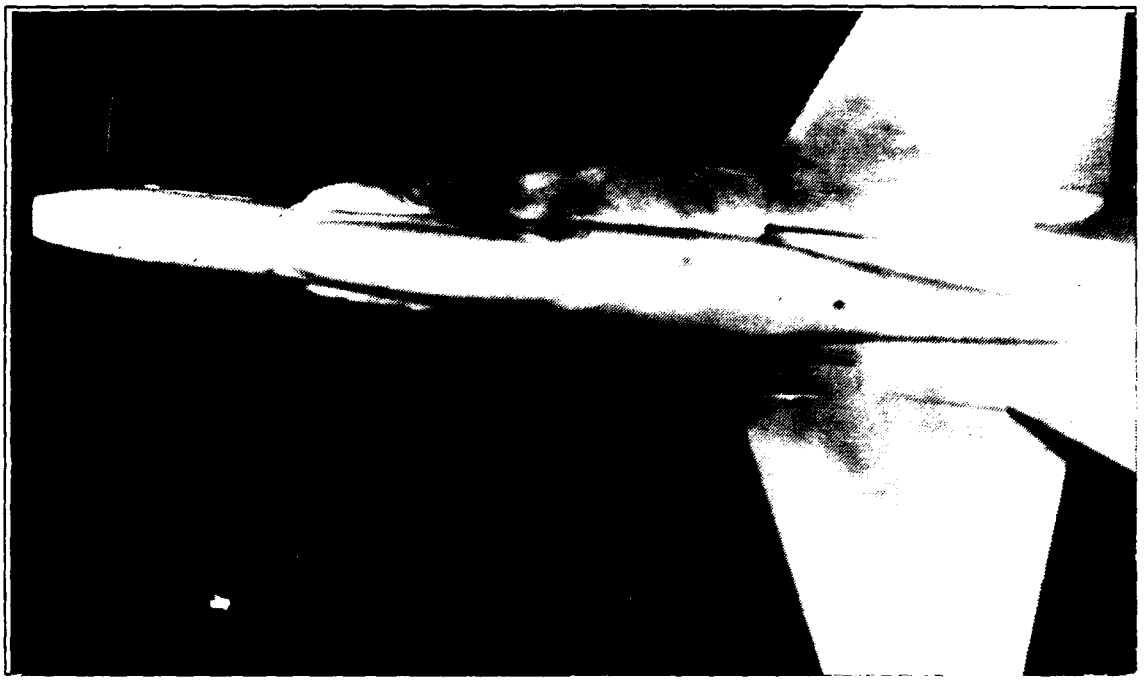

Figure 180. LEX, High Pitch Down, AOA = 30 deg , YAW = 20 deg.

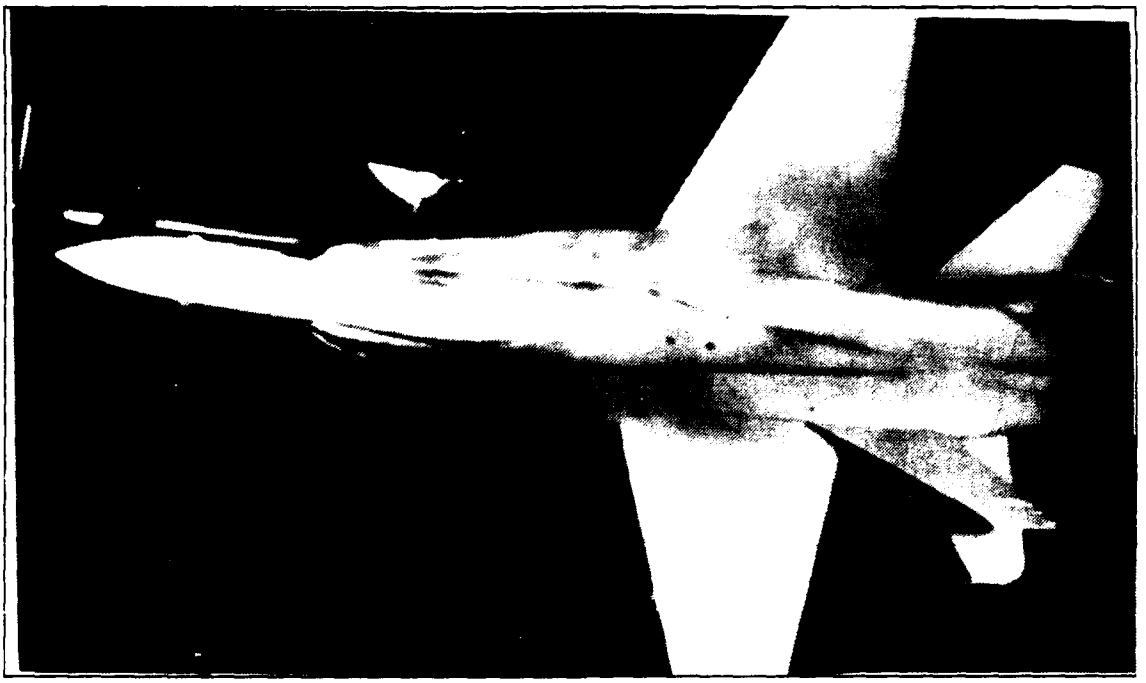

Figure 181. LEX, High Pitch Up, AOA = 40 deg , YAW = 20 deg.

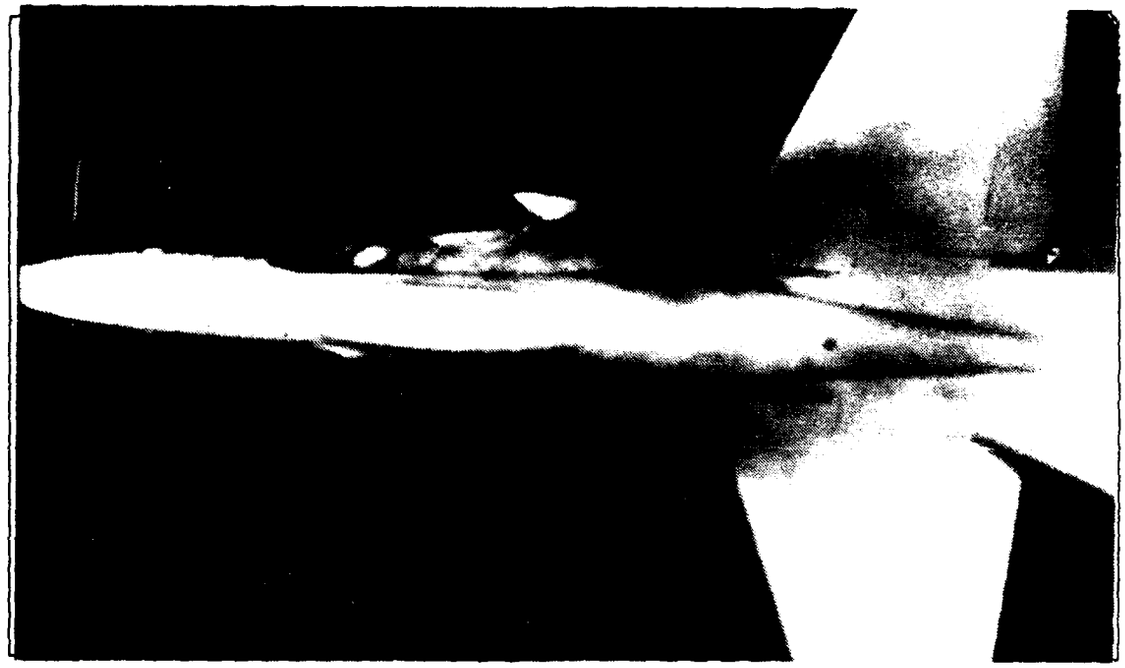

Figure 182. LEX, High Pitch Down, AOA = 40 deg , YAW = 20 deg.

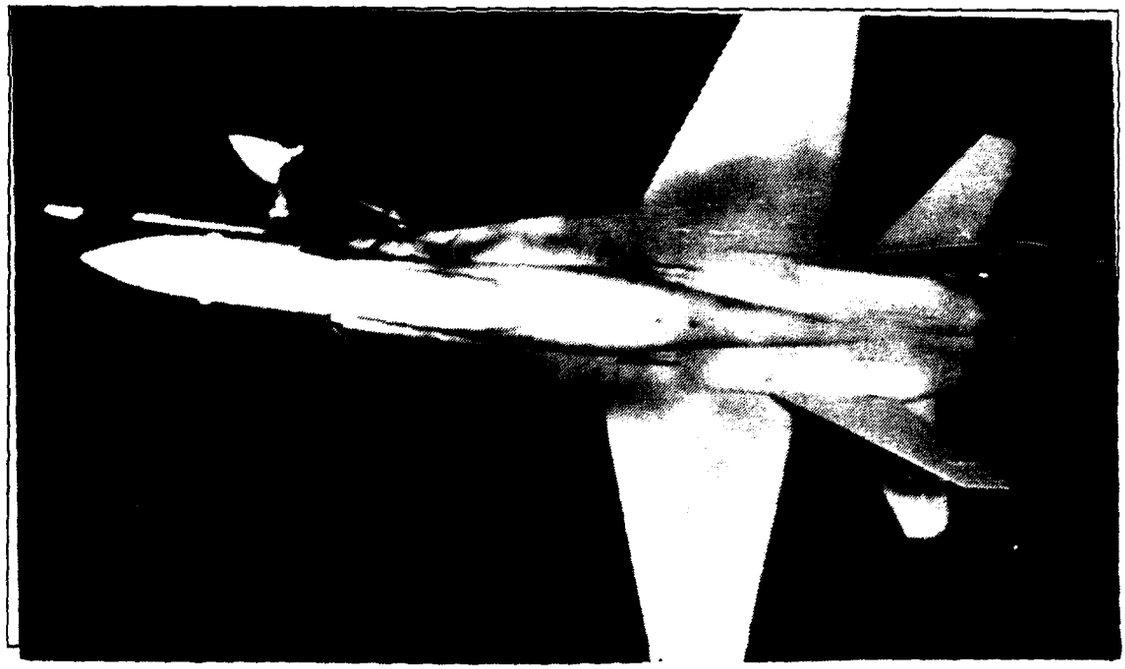

Figure 183. LEX, High Pitch Up, AOA = 50 deg , YAW = 20 deg.

APPENDIX B. EXPERIMENTAL RESULTS (GRAPHS)

FIGURES 184 THROUGH 195

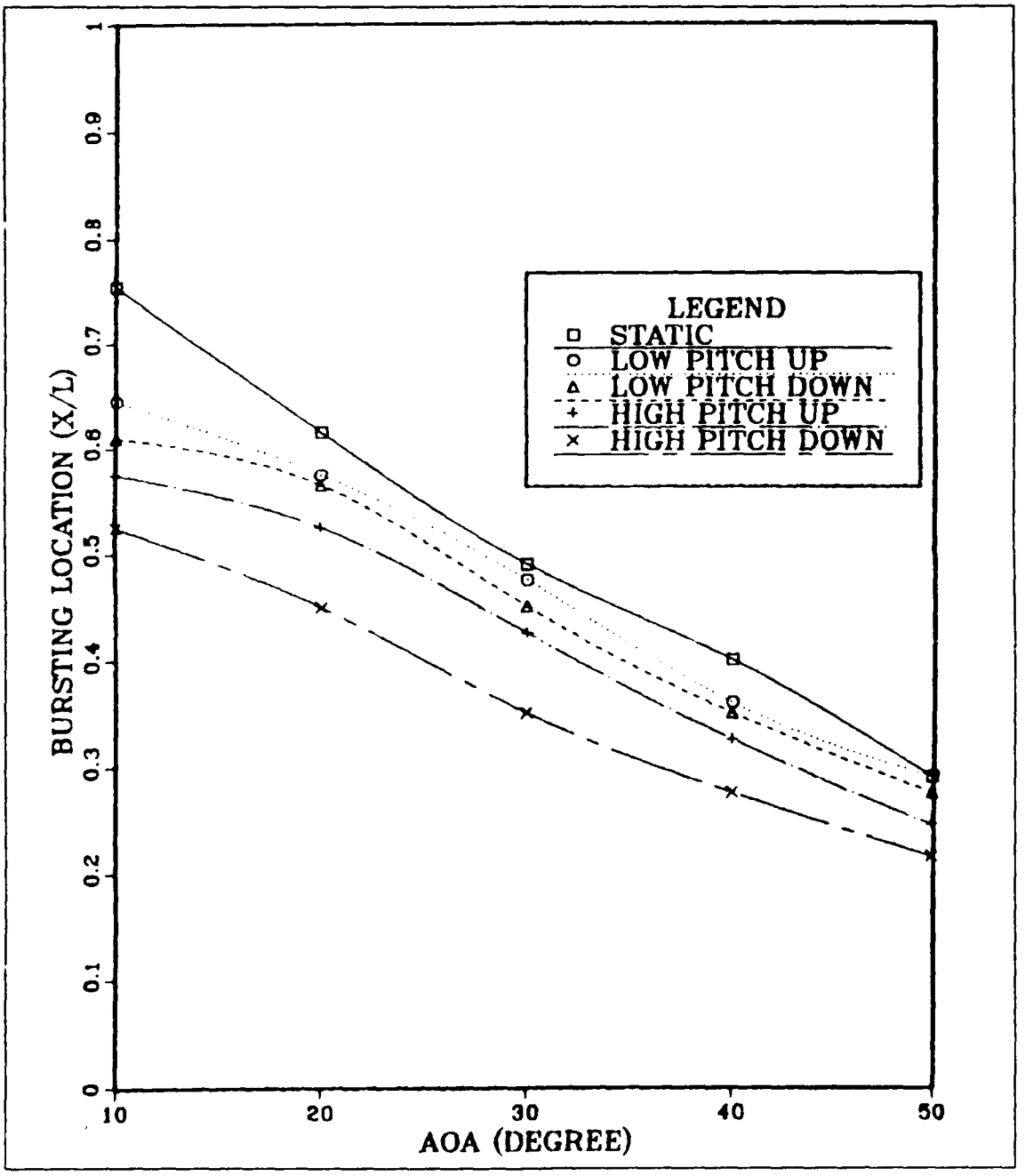

Figure 184. Forebody, Dynamic Effect (Yaw = 0)

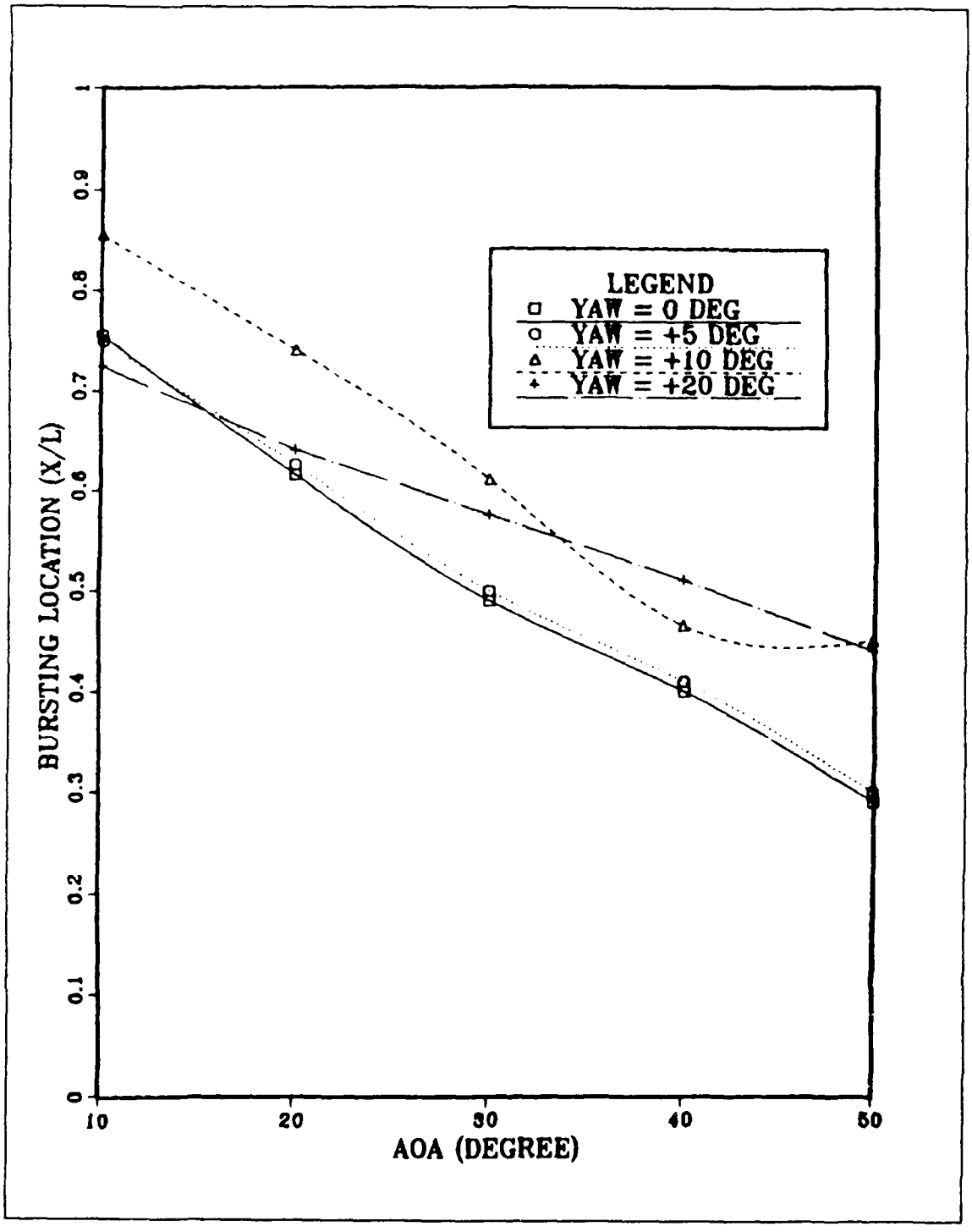

Figure 185. Forebody, Yaw Effect (Static)

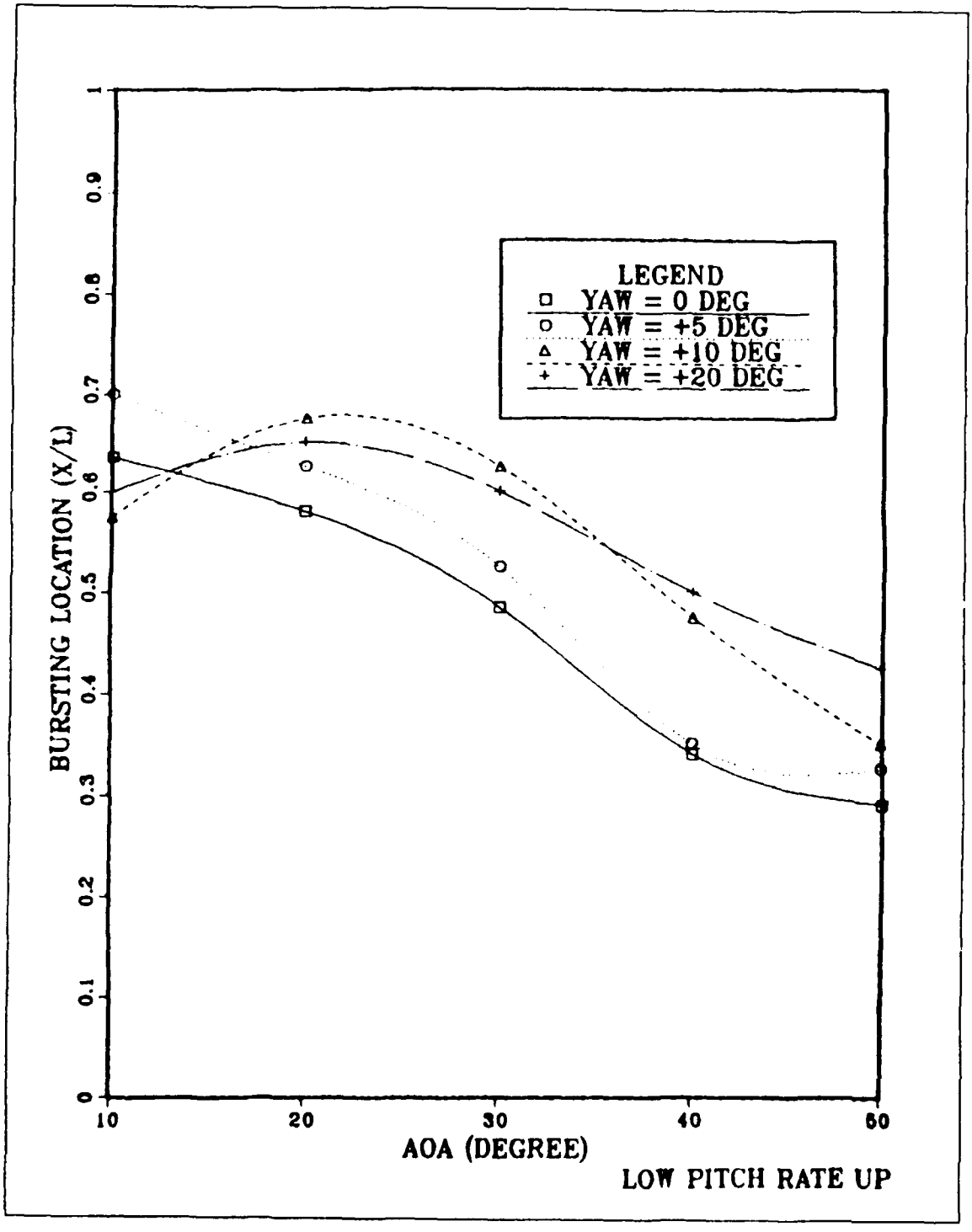

Figure 186. Forebody, Yaw Effect (Dynamic)

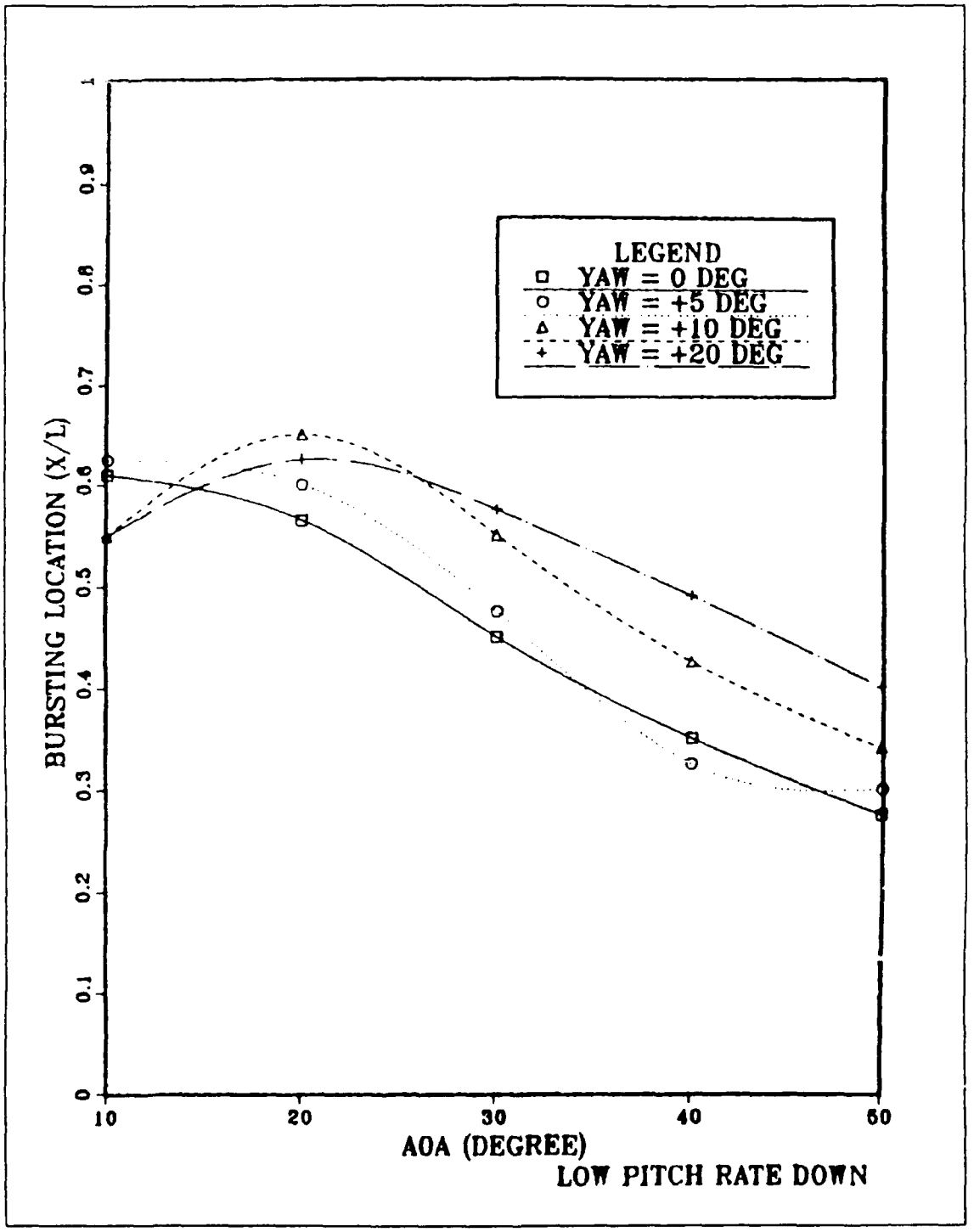

Figure 187. Forebody, Yaw Effect (Dynamic)

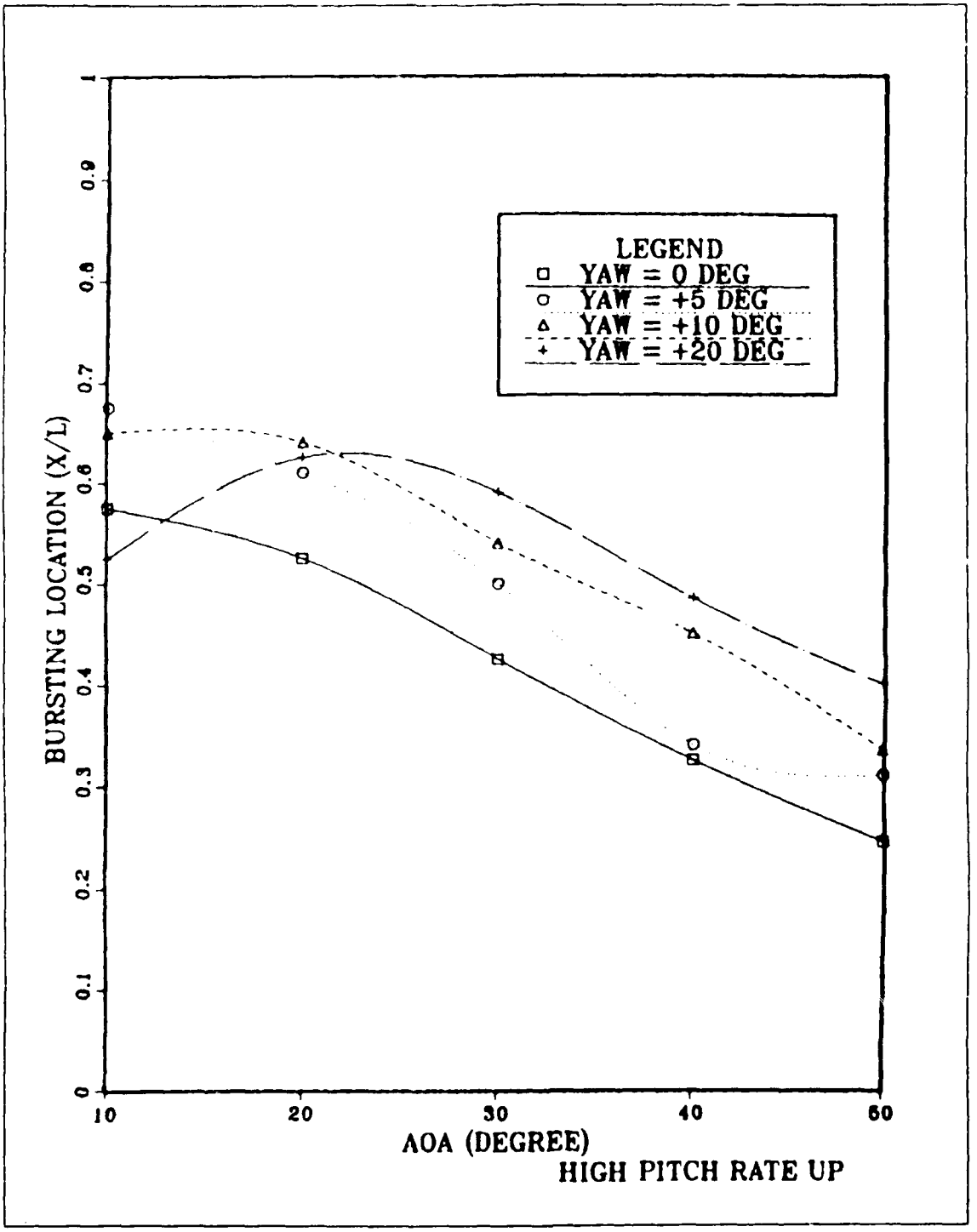

Figure 188. Forebody, Yaw Effect (Dynamic)

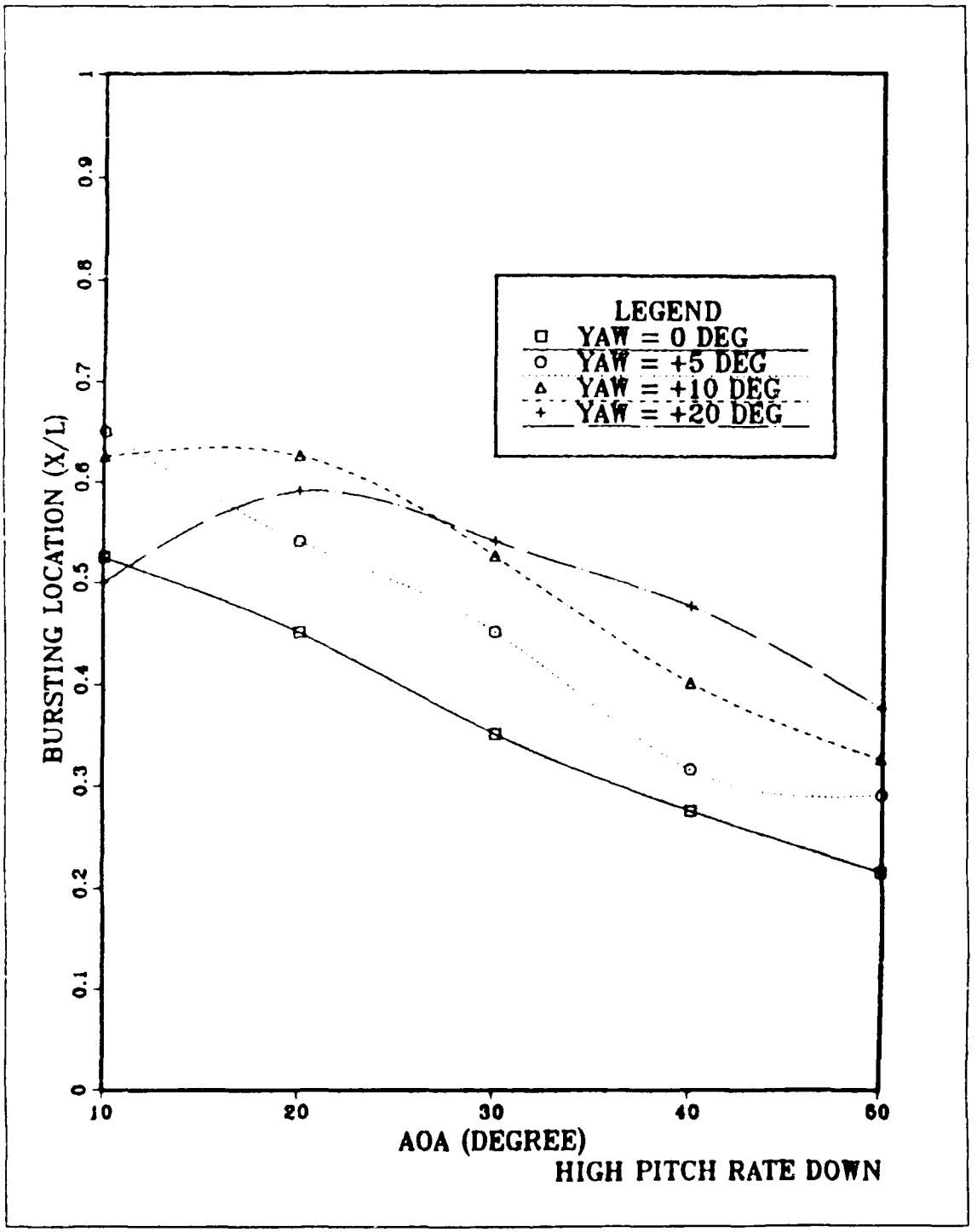

Figure 189. Forebody, Yaw Effect (Dynamic)

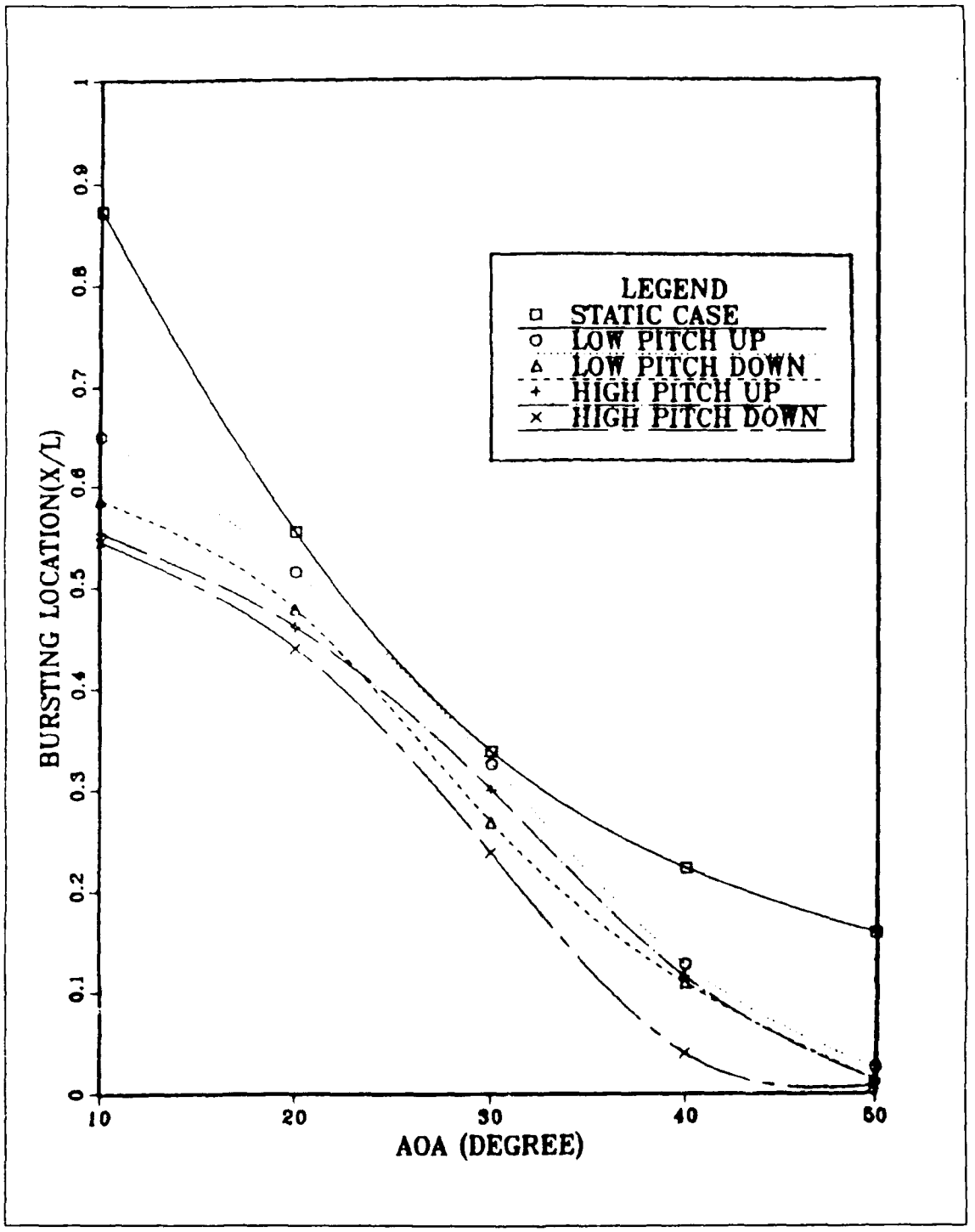

Figure 190. LEX, Dynamic Effect (Yaw = 0)

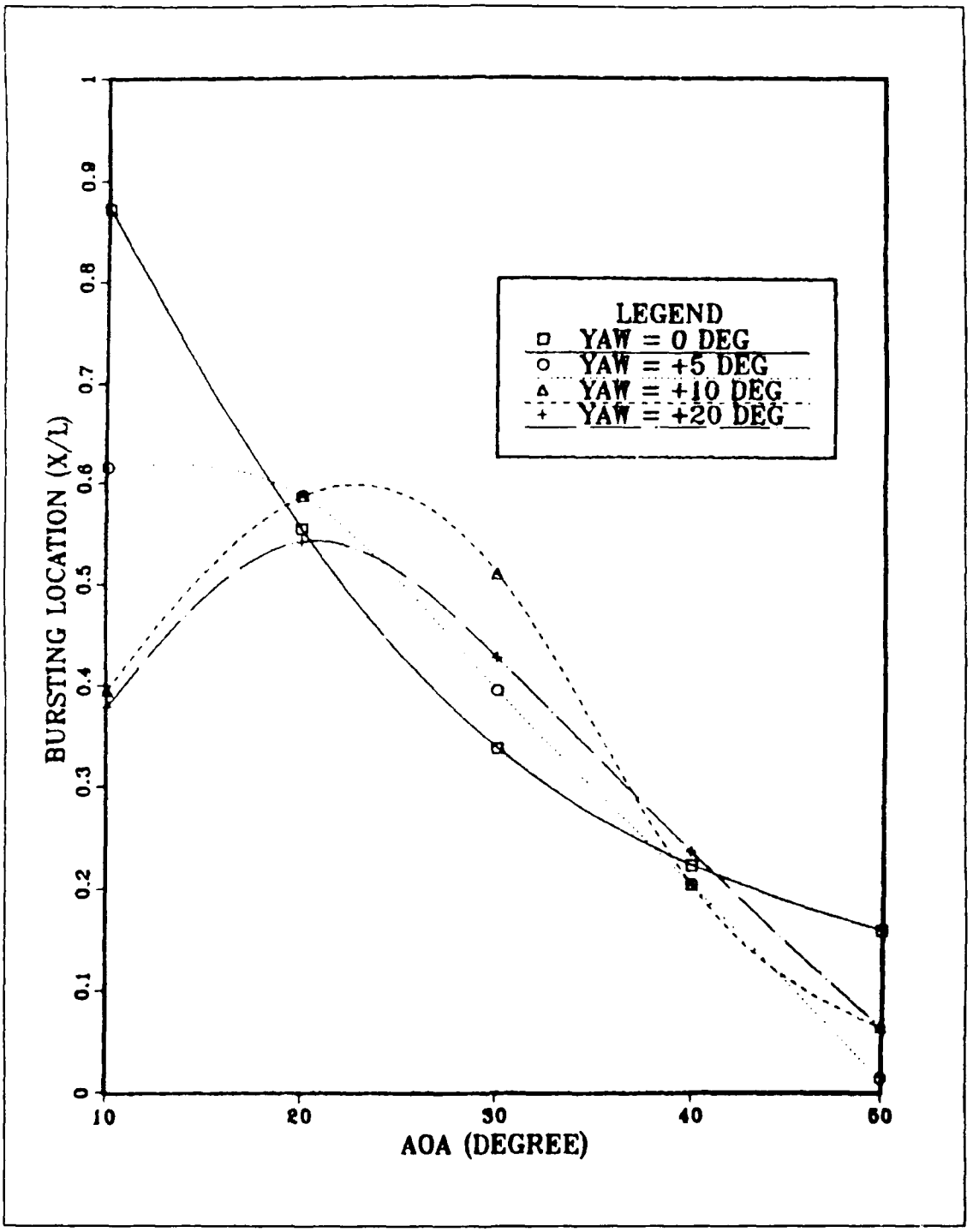

Figure 191. LEX, Yaw Effect (Static)

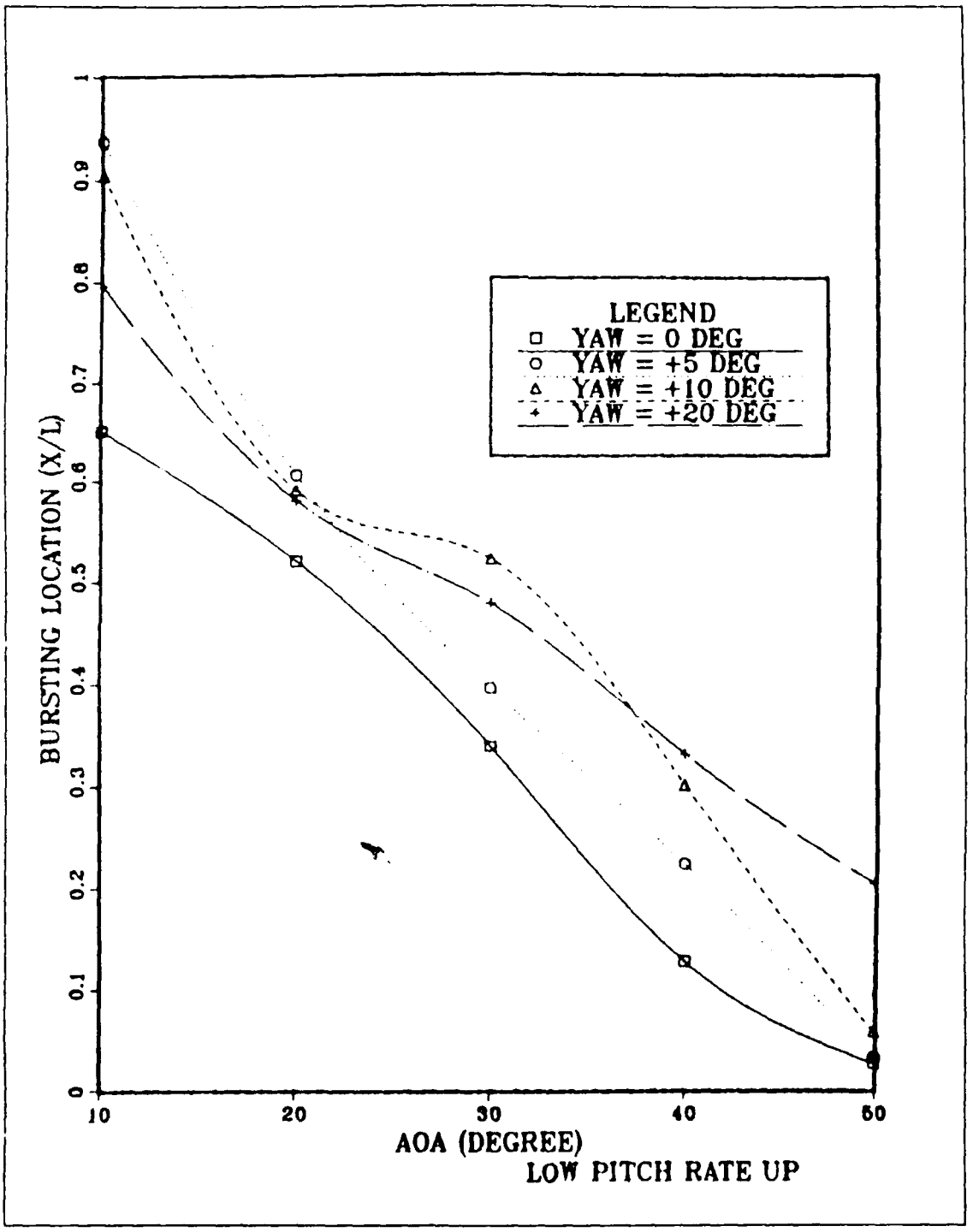

Figure 192. LEX, Yaw Effect (Dynamic)

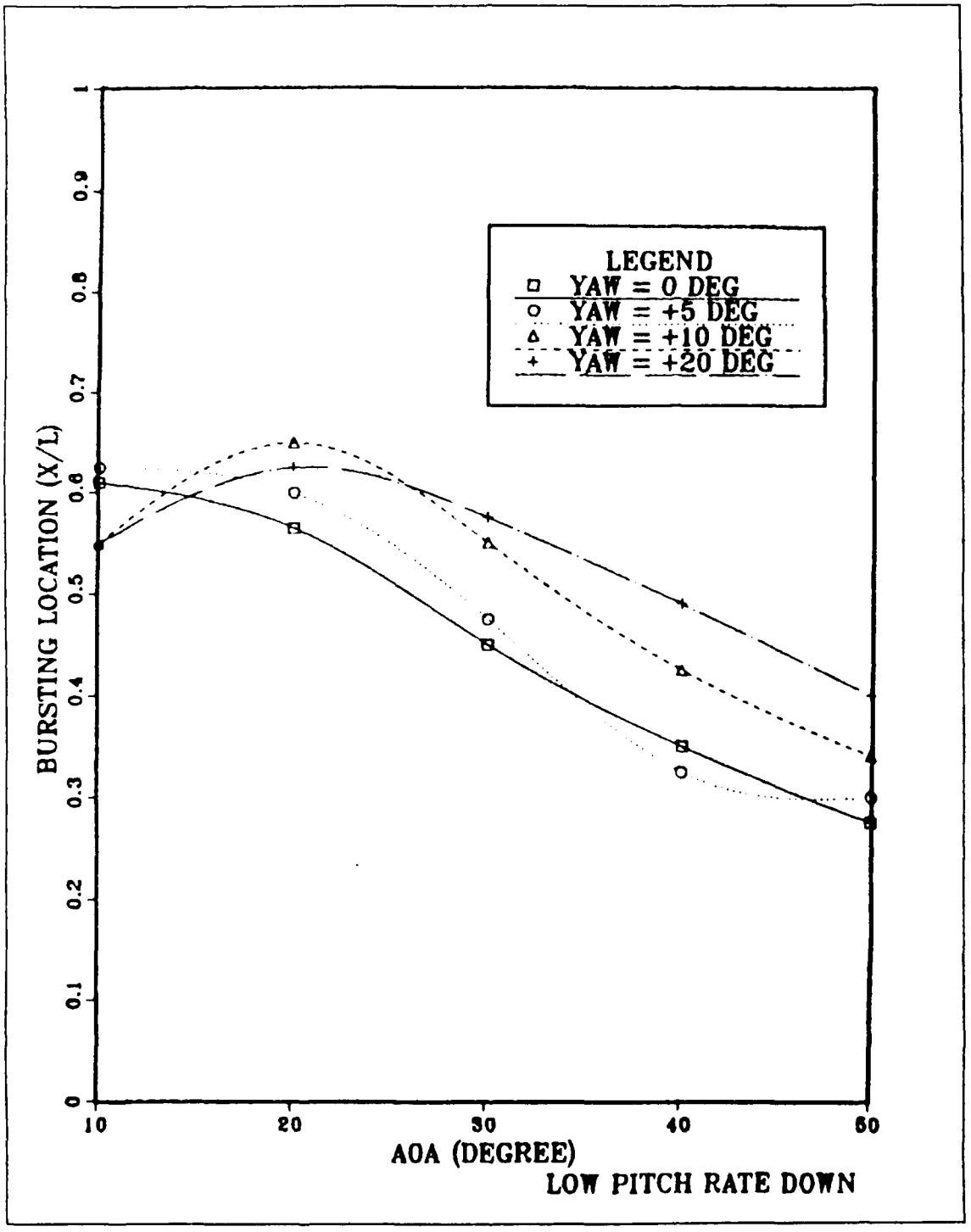

Figure 193. LEX, Yaw Effect (Dynamic)

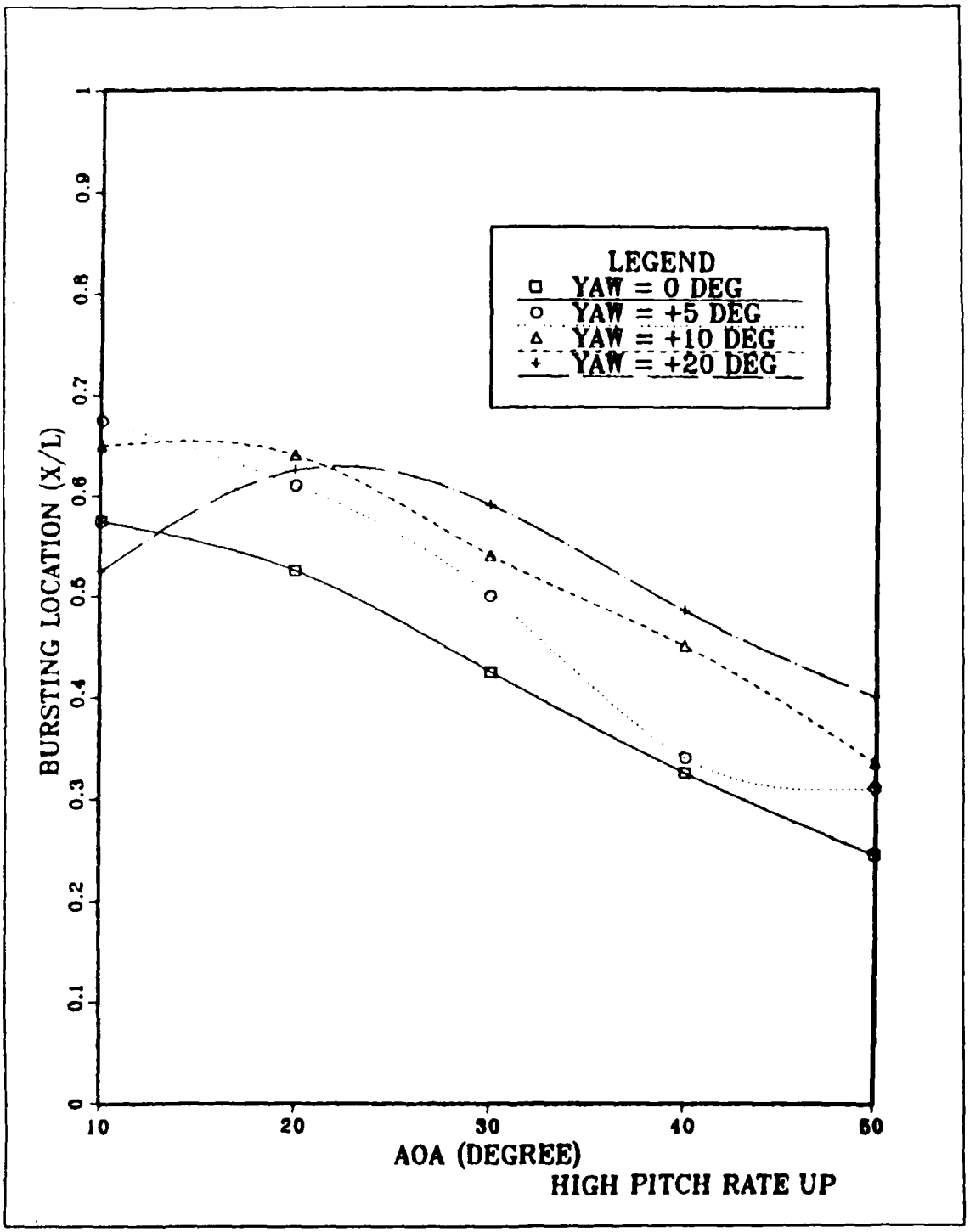

Figure 194. LEX, Yaw Effect (Dynamic)

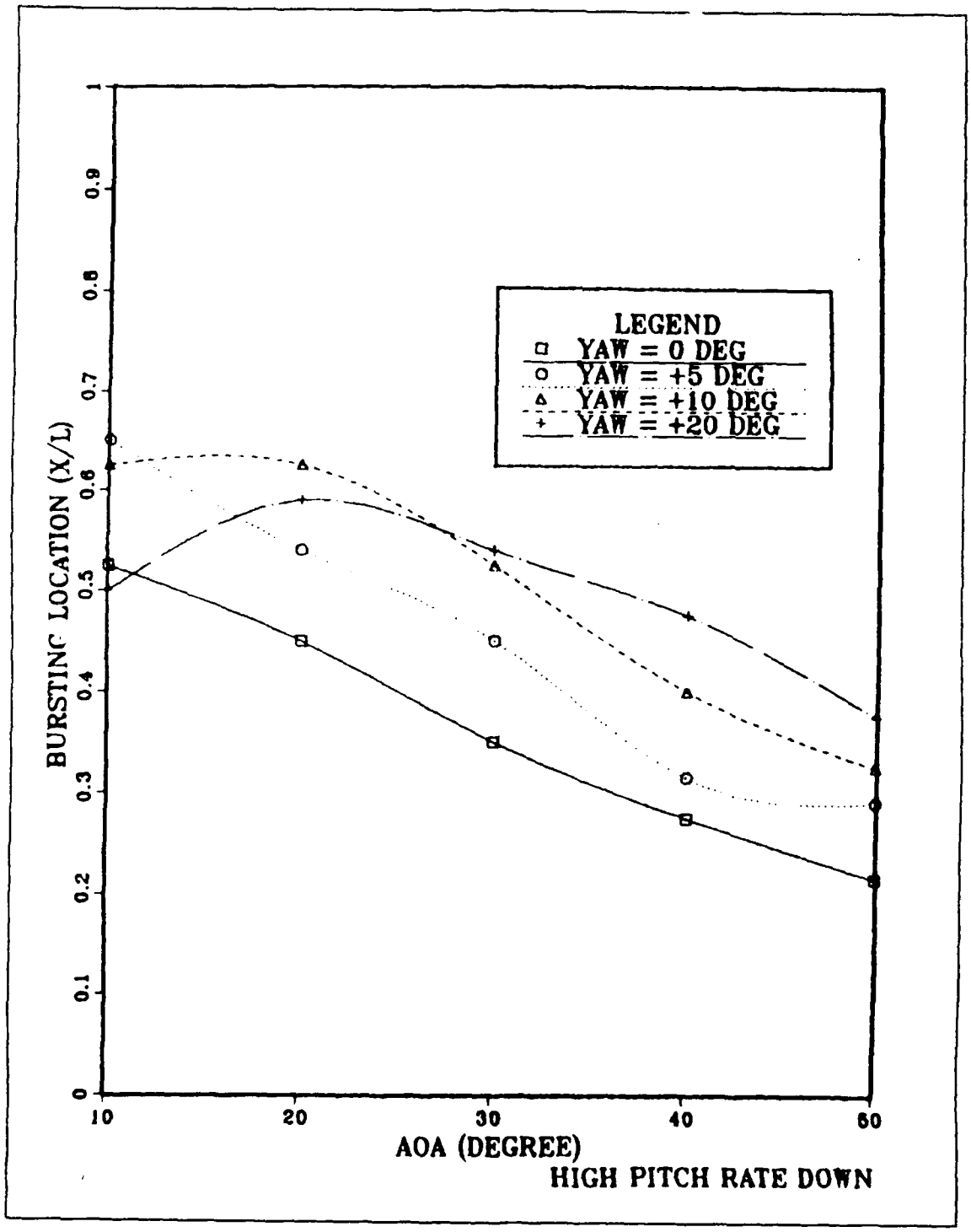

Figure 195. LEX, Yaw Effect (Dynamic)

LIST OF REFERENCES

1. Wedemeyer, E., *"Vortex Breakdown"*, AGARD Lecture Series No. 121, High Angle of Attack Aerodynamics, December, 1982. pp. 9-1 to 9-17.

2. Magness, C., Robinson, O., and Rockwell, D., *"Control of Leading-Edge Vortices on a Delta Wing"*, AIAA-89-0999, AIAA 2nd Shear Flow Conference, March 13-16, 1989.

3. Reynolds, G. A. and Abtahi, A. A., *"Instabilities in Leading-Edge Vortex Development"*,

4. Carr, L. W., *"Progress in Analysis and Prediction of Dynamic Stall"*, J. Aircraft, Vol. 25, Number 1, NASA, March, 1980.

5. McCroskey, W. J., *"The Phenomenon of Dynamic Stall"*, NASA. TM-81264, March, 1981.

6. Chandrasekhara, M. S., and Carr, L. W., *"Flow Visualization Studies of the Mach Number Effects on the Dynamic Stall of an Oscillating Airfoil"*, AIAA Paper No. 89-0023, AIAA 27th Aerospace Sciences Meeting January 9-12, 1989.

7. Lorber, P. F., and Carta, F. O., *"Unsteady Stall Penetration Experiments at High Reynolds Number"*, AFOSR TR-87-1202, UTRC Report R87-956939-3, April 1987.

8. Ekaterinaris, J. A., *"Compressible Studies on Dynamic Stall"*, AIAA Paper 89-0024, AIAA 27th Aerospace Sciences Meeting, Reno, NV, January 9-12, 1989.

9. Michael, T. Patterson., and Peter, F. Lorber., *"Computational and Experimental Studies of Compressible Dynamic Stall"*,Fourth Symposium on Numerical and Physical Aspects of Aerodynamic Flows, Califonia State University, Long Beach, Califonia, 16-19, January,1989.

10. Wolfgang, Merzkirch., *"Flow Visualization"*, Academic Press, Inc, Second Edition, 1987, pp 14-24.

11. User's manual, "Flow Visualization Water Tunnel Operations Manual for Model 1520", Eidetics International, Inc., Torrance, Califonia, 1988 (Prepared for Naval Postgraduate School, Monterey, Califonia).

INITIAL DISTRIBUTION LIST

		No. Copies
1.	Defense Technical Information Center Cameron Station Alexandria, VA 22304-6145	2
2.	Library, Code 0142 Naval Postgraduate School Monterey, CA 93943-5002	2
3.	Superintendent Naval Postgraduate School Monterey, Califonia 93943-5000	1
4.	Superintendent Naval Postgraduate School Attn: Chairman, Department of Aeronautics and Astronautics Code 67 Monterey, Califonia 93943-5000	1
5.	Superintendent Naval Postgraduate School Attn: Professor M. F. Platzer Code 67PL Monterey, Califonia 93943-5000	8
6.	Superintendent Naval Postgraduate School Attn: Professor S. K. Hebbar Code 67HB Monterey, Califonia 93943-5000	10
7.	Superintendent Naval Postgraduate School Attn: Dr Lee, Tae-Ho Code 67TI Monterey, Califonia 93943-5000	1
8.	Personnel Management Office Air Force Headquarters Sindaebang Dong. Kwanak Gu, Seoul, Republic of Korea	1
9.	Air Force Central Library Chongwon Gun, Chungcheong Bug Do Republic of Korea	2

10.	3rd Department of Air Force College Chongwon Gun, Chungcheong Bug Do Republic of Korea	1
11.	Library of Air Force Academy Chongwon Gun, Chungcheong Bug Do Republic of Korea	2
12	Park, Sung-Nam 168-1, Sangdo 2 Dong, Dongjak Gu, Seoul, Republic of Korea	10
13	Kwon, Hee-Man SMC 1375 Naval postgraduate School Monterey, Califonia 93943	1
14	Naval Air System Command Attn : Mr. Tom Momiyama, Director, Aircraft Division Code 931, Washington, D. C. 20361-9320	1
15	Ms. Lisa Cowles NADC Code 60 C Street Rd Warminster, PA 18974-5000	1
16	Mr. Larry Olson Acting Chief, Fixed Wing Aerodynamics Branch NASA Ames Research Center (M.S. 247-2) Moffet Field, CA 94035	1
17	Mr. Richard Margason Chief, Fixed Wing Aerodynamics Branch NASA Ames Research Center (M.S. 247-2) Moffet Field, CA 94035	1
18	Dr. Lewis Schiff Applied Computational Fluids Branch NASA Ames Research Center (M.S. 258-1) Moffet Field, CA 94035	1
19	Dr. Lawrence Carr Fluid Mechnics Laboratory NASA Ames Research Center (M.S. 260-1) Moffet Field, CA 94035	1
20	Dr. Tuncer Cebeci Proffessor and Chairman Department of Aerospace Engineering, CSULB Long Beach, CA 90840	1
21	Mr. Colin A. Martin Aeronautical Research Laboratories Box 4331 GPO Melbourne 3001, Australia.	1